

Georgia State University

ScholarWorks @ Georgia State University

Chemistry Dissertations

Department of Chemistry

8-4-2008

Rational Design of Calcium Biosensors

April L. Ellis

Follow this and additional works at: https://scholarworks.gsu.edu/chemistry_diss

 Part of the [Chemistry Commons](#)

Recommended Citation

Ellis, April L., "Rational Design of Calcium Biosensors." Dissertation, Georgia State University, 2008.
doi: <https://doi.org/10.57709/1059268>

This Dissertation is brought to you for free and open access by the Department of Chemistry at ScholarWorks @ Georgia State University. It has been accepted for inclusion in Chemistry Dissertations by an authorized administrator of ScholarWorks @ Georgia State University. For more information, please contact scholarworks@gsu.edu.

RATIONAL DESIGN OF CALCIUM BIOSENSORS

by

APRIL L. ELLIS

Under the Direction of Jenny J. Yang

ABSTRACT

Understanding the temporal and spatial changes in calcium concentration has been a difficult endeavor for many years due to the relatively small changes in calcium concentration during messaging events, the rapid changes upon physiological messaging, and the unavailability of fast, efficient, and sensitive sensors to detect calcium changes. In addition, the key factors in calcium binding have yet to be determined due to the metal-metal interactions, cooperativity, and conformational change involved in calcium binding to natural calcium-binding proteins. To overcome these obstacles and to engineer calcium sensors for in vivo studies of calcium signaling events, calcium binding sites have been engineered into Green Fluorescent Protein. The engineered binding sites demonstrate terbium binding affinity from 2-30 μM and calcium binding affinity from 50-100 μM . Site 177 demonstrates green fluorescence when expressed in mammalian cells and produces a response to calcium concentration changes when expressed in the cytosol. Addition of the cycle 3 mutations (M153T, V163A, F99S) to Site 177 allowed for increased brightness in the emission of the chromophore but still exhibited calcium response. The second generation Site 1

demonstrates fluorescence response to calcium concentration changes when expressed both in the cytosol and in the endoplasmic reticulum. Addition of M153T and V163A to Site 1 allowed for expression of fluorescent protein at 37 °C in HeLa cells and at 30 °C in bacteria. Site 1-M153T/V163A exhibits chromophore fluorescence response to calcium with a K_d of 100 μ M and competition with Rhodamine-5N produced a calcium K_d of 107 μ M. This designed sensor, Site 1-M153T/V163A is the first demonstration of a designed calcium binding GFP with calcium response measured both *in vivo* and *in vitro*.

INDEX WORDS: calcium, green fluorescent protein, protein design, metal binding, calcium sensor

RATIONAL DESIGN OF CALCIUM BIOSENSORS

by

APRIL L. ELLIS

A Dissertation Submitted in Partial Fulfillment of the Requirements for the Degree of

Doctor of Philosophy

in the College of Arts and Sciences

Georgia State University

2006

Copyright by

April Lee Ellis

2006

RATIONAL DESIGN OF CALCIUM BIOSENSORS

by

APRIL L. ELLIS

Major Professor:	Jenny J. Yang
Committee:	W. David Wilson
	Giovanni Gadda
	Vincent Rehder
	Charles Louis

Electronic Version Approved:

Office of Graduate Studies
College of Arts and Sciences
Georgia State University
May 2006

Dedication

This body of work has been a difficult endeavor for six years, but there have been many people who have cheered me along and lent me their support. First, I must dedicate this work to my mother, Linda Ellis, and my father, James A. Ellis, Jr., for without them I would never have made it through. They are the best people in the world and have always told me I could do anything I set my mind to do. They have never pushed and have been proud of me for every accomplishment. Mom, thanks for being my best friend in the world. Dad, thanks for not treating me like a girl and teaching me to drive a Bobcat. My friends have also helped me to get through by allowing me to vent my frustrations with this project, to lend a hand or advice for experiments and data analysis, and to just generally be “there”. Dr. Anna Wilkins Maniccia (grad school was the best because of you banana), John Maniccia (how do you put up with us?), Dr. Doyle J. Barrow, Jr. (“I’ve got the ways and means to New Orleans”....thanks for introducing me to experiences outside of science), Hsiau-Wei Lee (friends for so long, don’t forget me), and Katheryne Donald (the friend of my youth, may things be different in the future) have been the best a girl could ask for in support and help. My family has been wonderful and have each expressed their pride in my accomplishments. Thanks ya’ll. I must also thank my grandparents for their solid foundation of our family and for making sure I remember my roots even with all of my education. Lastly, my heart and my sweet pea, you have kept me at peace and with a tranquil state while reminding of the fun and spice of life, thank you.

Acknowledgements

Many people have assisted in the studies summarized in this work both directly and indirectly. First, my adviser Dr. Jenny J. Yang has pushed and prodded to make me into the researcher that I am today. She always backed us and took care of us. Dr. Yang's research group has my thanks for all of their help, especially Angela Holder and Yun Huang (Nancy). Their help with this project is immeasurable. Thank you to our summer student Dorinda Nelson for her help in expression of the GFP variants.

Our collaborators, Dr. Charles Louis and Dr. Monica Lurtz of UC Riverside, Dr. Vincent Rehder and Kristy Welshhans of GSU, and Dr. Aldebaran Hofer of Harvard University have provided studies of our sensors and experimental planning and discussion, which is all much appreciated. Dr. Myron Williams of Clark Atlanta University, Dr. Teryl Frey of GSU, and the late Dr. Alec Hodel of Emory University helped us to initiate this project and their assistance is much appreciated.

Technical support provided by Birgit Neuhaus (confocal facility) and Don Aiken (Zeiss International) is greatly appreciated.

My dissertation committee, Dr. Charles Louis, Dr. David Wilson, Dr. Giovanni Gadda, and Dr. Vincent Rehder are immensely thanked for their assistance in the completion of my degree requirements.

To all of the professors at GSU during my undergraduate and graduate career, thank you! You all made me appreciate and love science. Thanks to Dr. Jerry Smith for suggesting that I complete a PhD.

The American Heart Association and the Brain and Behavior program are much thanked for funding of my predoctoral fellowships. The NIH and NSF are thanked for funding.

TABLE OF CONTENTS

ACKNOWLEDGEMENTS	v
------------------	---

LIST OF TABLES	xii
----------------	-----

LIST OF FIGURES	xiv
-----------------	-----

CHAPTER

1 INTRODUCTION	1
1.1 Calcium Signaling and Homeostasis	1
1.2 Drugs and Agonists Involved in Calcium Signaling	3
1.3 Current Methods to Monitor Calcium Concentration	7
1.4 Criteria for an Ideal Sensor	17
1.5 Green Fluorescent Protein	19
1.6 Calcium-binding Proteins and Calcium-binding Sites	27
1.7 Our Design Approach and Previous Work in the Yang Lab	33
1.8 Our Approach to Engineer Calcium Sensors	34
1.9 The Objective of this Dissertation	37
1.10 The Significance of this Dissertation	38
2 MATERIALS AND METHODS	40
2.1 Near Infrared Calcium-binding Dye 15C5-774	40
2.2 Site-directed Mutagenesis	43
2.3 Competent Cell Preparation	44

2.4 Incorporating EGFP Gene in Different Vectors	48
2.5 Expression and Purification of Histidine tagged GFP	48
2.6 Hitrap Q Purification	53
2.7 Protein Refolding with Urea	53
2.8 Circular Dichroism of Variant Proteins	54
2.9 Thermal Denaturation of Designed Proteins by Circular Dichroism	54
2.10 GFP Fluorescence Spectroscopy	55
2.11 Measuring Metal Effects on Histidine Tagged Proteins	55
2.12 Metal Binding Analysis	56
2.13 Terbium Binding Affinities for the Variant Proteins	60
2.14 Protein-dye Calcium Competition	61
2.15 Protein-Terbium Metal Competition	62
2.16 pK _a Measurements of EGFP and EGFP Variants	63
2.17 Quantum Yield Measurements of EGFP, L194N, and L15N	65
2.18 Chromophore Reduction	66
2.19 Mammalian Cell Culture	66
2.20 Cryogenic Stock Preparation	68
2.21 Plate Preparation and Transfection of Sensor DNA	69
2.22 Fluorescence Imaging of Variant Proteins by Inverted Epifluorescence	69
2.23 Calcium Response by Inverted Epifluorescence Microscopy	70

2.24 Calcium Response by Confocal Microscopy	72
2.25 Transfection of 177c3 for Suspension Growth in HeLa Cells	73
2.26 Fluorescence of 177c3 after Expression in Suspension HeLa Cells	74
3 STUDY OF A CALCIUM-BINDING NEAR INFRARED DYE	75
3.1 Rationale for Development of Near Infrared Calcium Sensitive Dye	75
3.2 Design of 15C5-774	76
3.3 Solution properties of 15C5-774	78
3.4 Metal binding affinities and selectivity of 15C5-774	78
3.5 pH dependence	83
3.6 Comparison of 15C5-774 and commercially available dyes	85
3.7 Conclusions	86
4 DESIGN OF CALCIUM-BINDING SENSORS: the first generation	88
4.1 Rationale for Engineering Calcium Biosensors by Design	88
4.2 Design of Potential Calcium Binding Sites	89
4.3 Engineering a Calcium-binding Protein	105
4.4 Expression and Purification of EGFP and Calcium-binding Variants	108
4.5 Investigation of Histidine Tag Interference by Interactions with Metal Ions	123
4.6 Metal-binding of Designed Proteins	130
4.7 Optical Properties of EGFP and the Designed Proteins	157

4.8 Conformation Analysis of Secondary Structure by CD	168
4.9 Endeavoring to Understand Fluorescence Loss of the Designed Proteins	174
4.10 Disulfide Bonds and Chromophore Reduction	188
5 THE EVOLUTION OF SENSOR 177	196
5.1 Mammalian Screening of Designed Proteins	196
5.2 Expression of Designed Proteins in Mammalian Cells	199
5.3 Engineering a Brighter Sensor: incorporation of the cycle 3 mutations	212
5.4 Calcium response of 177 and 177c3 in the cytosol	224
5.5 Calcium Response of Sensors 177 and 177c3 when Expressed in the ER	239
5.6 Calcium response of 177c3 in vitro	247
5.7 Major Findings	254
6 SECOND GENERATION OF DESIGNED SENSORS	255
6.1 Lessons Learned: design of a second generation of sensors	255
6.2 Protein Engineering of Calcium Sensors	260
6.3 Mammalian Expression of the Second Generation	262
6.4 Site 1 Calcium Response <i>in Vivo</i>	268
6.5 Site 1 in Vitro Profile and Calcium Response	276
6.6 Creation of Site 1 cycle 3	282
6.7 Major Findings	295

7	CONCLUSIONS AND MAJOR FINDINGS	299
7.1	Major Findings of the Designed Calcium-binding Proteins	299
7.2	Expression of Designed Proteins in Mammalian Cells	301
7.3	Major Findings from In Vivo Imaging of Calcium Response	302
7.4	Major Findings of the Second Generation of Designed Proteins	304
7.5	Major Findings of the <i>in Vivo</i> Calcium Measurements of Site 1	305
	REFERENCES	306

LIST OF TABLES

1.1 Agonists to induce calcium change in the cell	6
1.2 Summary of GFP mutations	23-26
2.1 Primers for the first generation of designed proteins	45
2.2 Primers for the second generation of designed proteins	46
2.3 FPLC programs for the His tag purification	52
2.4 Example spreadsheet for input in Specfit/32	57
2.5 A list of the buffers utilized for pH dependence measurements	64
3.1 Binding affinities of 15C5-774 and the ionic radii of the metals studied	82
4.1 Solvent accessibility of GFP (1b9c) calculated by GetArea	92
4.2 The design sites engineered into Green Fluorescent Protein	101
4.3 Summary of the conditions tested to provide EGFP variant fluorescence	113
4.4 A list of the metals studied for interference with histidine tagged proteins with the ionic radius and coordination numbers	129
4.5 The binding affinities, ligands, and charge of the amino acids in the binding pocket of the designed proteins	137
4.6 A summary of the surrounding positive and negative charges for each studied binding pocket	155
4.7 A table of the partial sites studied with the final fluorescent mutations shown in green	175
4.8 The pK _a values of EGFP, L15N, and L194N as measured by absorbance and fluorescence in various buffers to maintain the pH at each desired value	180

4.9 A summary of the quantum yield and extinction coefficient measurements for EGFP, L15N, and 194N	189
5.1 A summary of the four mammalian cell lines utilized in the characterization of the designed GFP calcium-binding proteins	198
5.2 Primers to insert the ER signal tags into EGFP variants	240
6.1 The second generation designed proteins are detailed with the calcium-binding pocket ligands, the charges introduced by mutation to the binding ligands, and the similar first generation sites	256
6.2 The order of the mutagenesis performed for the second generation	261

LIST OF FIGURES

1.1 Calcium's role in the cell	2
1.2 Process to induce calcium change in the cell	4
1.3 BAPTA structure	8
1.4 TF-BAPTA spectra with calcium	8
1.5 Fura-2 structure	10
1.6 Rhodamine-5N structure	10
1.7 Structure of apo and calcium-loaded aequorin	14
1.8 Illustrations of Persechini's constructs	15
1.9 Structure and spectra of Green Fluorescent Protein	20
1.10 Chromophore formation of GFP	22
1.11 The two possibilities of fluorescence change caused by calcium binding to a designed fluorescent protein	28
1.12 Pentagonal bipyramidal geometry of calcium binding	30
1.13 Continuous calcium binding sequence of the EF hand and examples of natural calcium-binding proteins	31
1.14 Proteinase K with the calcium binding sites highlighted	32
1.15 Designed protein 7E15-CD2	35
2.1 A screen capture of Specfit/32 is shown to illustrate the program's use in calculating binding affinities	59
3.1 Synthesis of 15C5-774	77
3.2 Absorbance spectra of 19.52 μ M 15C5-774 with increasing concentrations of CaCl_2	79
3.3 Fractional change of the absorbance at 774 nm as a function of Ca^{2+} concentration	81

3.4. A comparison of the Ca^{2+} free and Ca^{2+} loaded spectra of 15C5-774 at pH 6, pH 7.4, and pH 8.7	84
4.1 The ideal pentagonal bipyramidal geometry of a calcium binding site with the oxygen-calcium-oxygen angles (ϕ_1), (ϕ_2), and (ϕ_3) illustrated	91
4.2 Illustrations of the models highlighting the locations of the designed proteins	102
4.3 DNA and protein sequence of the host EGFP	106
4.4 The vector map of pet28a	107
4.5 SDS-PAGE gel and room light and fluorescent images of the cell pellet after expression of EGFP	109
4.6 SDS-PAGE gel and cell growth curve of the expression of 120 and 177	110
4.7 A graph of the Fluostar microplate assay results for the expression of designed protein 194a and four of its variants, K85D, S86D, L194N/K85D, and L194N/S86D	112
4.8 Purification scheme for EGFP utilizing the Hitrap nickel chelating column	116
4.9 SDS-PAGE gel and room light and fluorescent images of the purification of EGFP	117
4.10 SDS-PAGE gel of purification fractions after FPLC of EGFP illustrating dimer formation of the protein	118
4.11 SDS-PAGE gels of site 120 purification	120
4.12 Emission spectra (excitation at 482 nm) of 10 μM GFP without and with 1 mM calcium	125
4.13 Fluorescence spectra and metal binding fit of the nickel titration of histidine tagged GFP-S65T	126

4.14 Overall fluorescence emission decrease at 510 nm when excited at 482 nm of GFP-S65T caused by interference of the histidine tag with metals	127
4.15 Structure of EGFP with the tyrosines and tryptophan highlighted	132
4.16 Fluorescence spectra with excitation at 280 nm and binding curve of terbium bound to a designed variant, 177	133
4.17 Fluorescence spectra with excitation at 280 nm and binding curve of terbium bound to a designed variant, 120	134
4.18 Fluorescence spectra with excitation at 280 nm and binding curve of terbium bound to a designed variant, 194a	135
4.19 Fluorescence spectra with excitation at 280 nm and binding curve of terbium bound to a designed variant, 194b	138
4.20 Fluorescence spectra of the binding competition of 177 with terbium for other metals	140
4.21 The decrease in terbium FRET enhancement observed when other metals compete for binding to site 120	141
4.22 The spectra of the titration of Rhodamine-5N with calcium	143
4.23 Fluorescence spectra and Specfit/32 fit of Rhod-5N in competition with Site 177 for calcium binding	145
4.24 Fluorescence spectra and Specfit/32 fit of Rhod-5N in competition with Site 194a for calcium binding	147
4.25 Specfit/32 global fit of the competition of 45 μ M L194N/S86D and 20 μ M Rhod-5N for calcium binding	149
4.26 Fit of the competition of 45 μ M L914N/S86D and 20 μ M Rhod-5N for calcium with a competition equation	150
4.27 Chromophore emission change of L194N/S86D upon addition of calcium	151

4.28 Illustrations of the three studied binding sites	154
4.29 Absorbance spectra and neutral and anionic states of the chromophore of EGFP	158
4.30 Absorbance spectra of EGFP at pH 4 and pH 7.4	160
4.31 Absorbance spectra of EGFP and the designed protein 177	161
4.32 Emission spectra of GFP with the water scattering peak evident as it changes emission wavelength along with a change in the excitation wavelength	163
4.33 Aromatic fluorescence emission with excitation at 280 nm of L194N/S86D	164
4.34 Emission of EGFP L194N/S86D with varying excitations to illustrate the energy transfer from the aromatics to the chromophore	165
4.35 Energy transfer of EGFP observed between the aromatics and the chromophore	166
4.36 Circular dichroism of EGFP	169
4.37 Circular dichroism of 120, 177, and 194a	170
4.38 CD spectra of designed protein 194a with calcium, lanthanum, and terbium	171
4.39 CD spectra of designed protein 120 at various pH values	173
4.40 Pymol picture of EGFP site 120 to illustrate the position of V120	177
4.41 An illustration of the 194 family of designed proteins	178
4.42 Absorbance spectra of EGFP at various pH	181
4.43 pK_a plots of the absorbance at 398 nm and 488 nm of EGFP at various pH	183
4.44 EGFP pH dependence by fluorescence with excitation at 398 nm and 482 nm	184

4.45 pK _a plots of the fluorescence at 510 nm and 450 nm with excitation at 398 nm EGFP	185
4.46 pK _a plot of the fluorescence at 510 nm with excitation at 482 nm EGFP at various pH	186
4.47 Absorbance and fluorescence spectra of EGFP at various concentrations to calculate the quantum yield	190
4.48 Absorbance and fluorescence spectra of L15N at various concentrations to calculate the quantum yield	191
4.49 Extinction coefficient calculation for EGFP at 488 nm	192
4.50 Extinction coefficient calculation for L15N at 280 nm	193
4.51 L194N/S86D in 10% β-mercaptoethanol with and without calcium	195
5.1 Vector map and details of the pcDNA3.1+ vector from Invitrogen	200
5.2 Images of site 120 in HeLa cells	201
5.3 Images of 194a in HeLa cells	201
5.4 Images of Site 120b in CHO cells	203
5.5 Images of Site 229 in HeLa cells	203
5.6 Images of L15N/R122D in CHO cells	204
5.7 Images of L194N/S86D in HeLa cells	205
5.8 Images of Site 177 expressed in HeLa cells	205
5.9 Site 177 with different amounts of DNA transfected into HeLa cells	208
5.10 Images of EGFP transfected into Vero cells at different DNA:liposome ratios	209

5.11 Images of Site 177 expressed in Vero cells at different DNA concentrations	210
5.12 Images of Site 177 expressed in CHO cells	211
5.13 EGFP with Site 177 ligands and the cycle 3 mutations	214
5.14 Images of 120c3 and 194a-c3 in HeLa cells	216
5.15 Images of site 177 in HeLa cells	218
5.16 Images of Site 177 in CHO cells	219
5.17 Expression of 177 and 177c3 in HeLa cells at 30 °C	220
5.18 Images of 177c3 expressed in HeLa cells at 30 °C and 37 °C	222
5.19 Imaging on the inverted Nikon microscope of EGFP expressed in HeLa cells with induction of calcium concentration change	226
5.20 Calcium response of Sensor 177 expressed in the cytosol of HeLa cells	227
5.21 Averaged and normalized data of Sensor 177's <i>in vivo</i> calcium response	228
5.22 Statistical evaluation of the calcium response imaging of cytosolically expressed 177 in HeLa cells	229
5.23 Imaging of cytosolically expressed 177 in HeLa cells with addition of 50 μ M ATP	231
5.24 Imaging of cytosolically expressed 177 in HeLa cells with addition of thapsigargin and calmidazolium	232
5.25 Imaging of cytosolically expressed EGFP in HeLa cells on the Zeiss Axiovert 200 microscope	233
5.26 <i>In vivo</i> calcium response of 177 as imaged by the Zeiss Axiovert 200	234

5.27 <i>In vivo</i> calcium response of 177c3	237
5.28 <i>In vivo</i> calcium response of 177c3 in HeLa cells imaged on the Zeiss Axiovert 200	238
5.29 Confocal images of Sensor 177-ER cotransfected with DsRed2-ER in HeLa cells	242
5.30 Colocalization of 177c3-ER and DsRed2-eR in HeLa cells	243
5.31 Calcium response of 177-ER with the addition of ATP	245
5.32 Response of 177c3-ER as imaged by confocal microscopy	246
5.33 Excitation and emission spectra of 177c3 in cell supernatant	249
5.34 Emission spectra of 177c3 lysate with increasing calcium concentration	250
5.35 Excitation and emission spectra of EGFP with and without calcium	253
6.1 Models of the second generation of designed calcium-binding proteins	258
6.2 Images of the first round of mutations for Site 1, L194E/S86D, expressed in HeLa cells	264
6.3 Images of Site 1 expressed in HeLa cells with all three mutations	265
6.4 Site 2 partial mutations of R122E/V120S expressed in HeLa cells	265
6.5 Site 5 with mutations L7D/V12N expressed in HeLa cells	267
6.6 Site 1 calcium response in HeLa cells	270
6.7 Calcium response of Site 1 expressed in HeLa cells obtained on the Nikon inverted epifluorescence microscope	271
6.8 ER targeted Site 1 cotransfected with DsRed2-ER and calcium response of Site 1-ER by confocal microscopy	273
6.9 Control experiments of EGFP-ER expressed in HeLa cells	274

6.10 Fluorescence imaging for calcium response of Site1-ER expressed in HeLa cells	275
6.11 SDS-PAGE gels of the purification of Site 1-His/pcDNA	278
6.12 SDS-PAGE gel of the partitioning by molecular weight of Site 1 expressed in HeLa cells	279
6.13 Excitation and emission spectra for Site 1 cell lysate	281
6.14 Excitation and emission spectra for Site 1 cell lysate with increasing calcium concentration	283
6.15 Images of Site 1 expressed in HeLa cells at 30 °C and 37 °C for 48 hr	285
6.16 Images of Site 1-M153T/V163A expressed in HeLa cells at 30 °C and 37 °C for 48 hr	286
6.17 Images of Site 1 expressed in HeLa cells at 30 °C and 37 °C for 72 hr	287
6.18 Images of Site 1-M153T/V163A expressed in HeLa cells at 30 °C and 37 °C for 72 hr	288
6.19 Fluostar microarray results of the expression of Site 1-M153T/V163A in bacteria	290
6.20 SDS-PAGE gel of the expression of Site 1-M153T/V163A in E. coli	291
6.21 Excitation and emission with excitation at 398 nm spectra of Site 1-M153T/V163A with calcium after expression in E. coli	293
6.22 Calcium induced chromophore emission change for Site 1-M153T/V163A expressed in E. coli with excitation at 482 nm	294
6.23 Rhodamine-5N competition with Site 1-M153T/V163A for calcium binding	296
6.24 The Specfit results of the competition between Site 1-M153T/V163A and Rhodamine-5N	297

Chapter 1 Introduction

1.1 Calcium Signaling and Homeostasis

As a secondary messenger, calcium regulates many biological processes in various intracellular compartments (Fig 1.1) (1, 2). First isolated by Sir Humphrey Davy in 1808, calcium was named for the latin calx, meaning lime. Further studies in the last two centuries have revealed that calcium is involved in muscle contraction (including heartbeat), is the major component of bones and teeth, and is involved in vision and in neuronal signaling (3-7). Normally, during rest conditions, the intracellular calcium concentration is ~ 0.1 to $1.0 \mu\text{M}$ (8). When the cell is excited, its intracellular calcium concentration can rise up to $\sim 10 \mu\text{M}$ by release from internal calcium stores in the endoplasmic reticulum (ER) or by entering the cell from the extracellular matrix through the action of calcium pumps (9). The cellular compartments are also involved in calcium signaling. In the ER, calcium is stored in its free form and in complex with proteins, such as calsequestrin, and is thought to range in concentration from $100 \mu\text{M}$ to 1 mM (1). Calcium is released from the ER in response to IP3 (inositol 1,4,5-triphosphate) binding to IP3 receptors, which is an element of numerous signal cascades, such as in response to histamine. In the mitochondria, calcium has been observed to play a role in metabolism. When mitochondrial calcium is decreased, the rate of metabolism is decreased and, therefore, the rate of ATP production is decreased (10). In addition, mitochondrial uptake of calcium regulates the calcium wave induced by ER release of calcium by decreasing the amount of calcium in the cytosol available

for sensitizing the IP3 receptors. The sensitization of the IP3 receptors allows for calcium induced calcium release from the ER, promoting a calcium wave across the cell and turning on other signals. When the mitochondria uptakes calcium, it slows this wave and, in turn, controls other signaling events (12).

Both overloading and depleting the calcium concentration inside cells is directly related to different disease states in human health, such as Marfan's Syndrome and Osteoporosis (13, 14). Mishandling of calcium, such as inappropriate protein binding or release can turn on or off many signals that could lead to disease states or death, such as malignant hyperthermia (15-19). Calcium's prevalence throughout the biological system is well-known and some of its actions have been well-studied, but the temporal and spatial changes of calcium in response to various processes is not well understood. As shown in figure 1.1, many proteins are calcium ion dependent for their function, including calmodulin, a signaling protein whose functions in the regulation of more than 100 biological processes are controlled by calcium binding, which allows calmodulin to bind to target molecules (20-25). The troponin family of proteins confer calcium sensitivity to muscle cells, allowing for contraction and relaxation as the calcium concentration changes (26). Monitoring the effects of calcium on the abundant cellular processes has, thus far, been a difficult endeavor due to numerous factors, such as lack of sensitive and fast sensors.

1.2 Drugs and Agonists Involved in Calcium Signaling

There are abundant agonists that bind to receptors on the cell surface or on the ER membrane that induce calcium response. Figure 1.2 illustrates a few of those

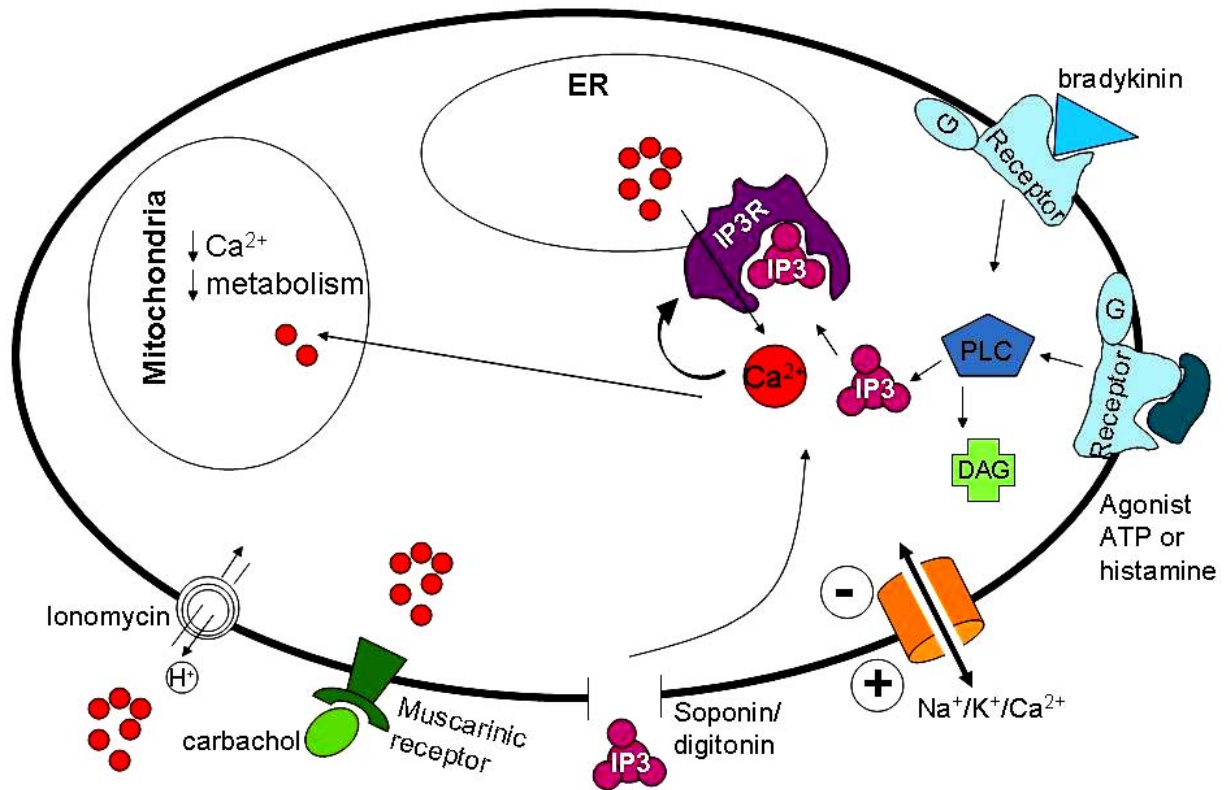


Fig 1.2 Examples of the various means to modify calcium concentration in the cell are illustrated.

pathways. As shown in table 1.1, the most noted response is the binding of an agonist, such as ATP or histamine, to G-protein coupled receptors. This binding induces IP3 release by breakdown of phosphatidylinositol-4,5-bisphosphate into IP3 and diacylglycerol (DAG) by phospholipase C. The released IP3 then binds to IP3 receptors on the ER membrane, stimulating calcium release from the ER and, in turn, increasing cytosolic calcium. Calcium can then bind to calcium binding proteins, such as calmodulin, to signal other processes to occur. Bradykinin, a small peptide, also stimulates this pathway by binding to G-protein coupled receptors. DAG produced during this process increases the affinity of protein kinase C for calcium, thereby stimulating its action.

Another process utilized by neuroscientists is the binding of carbachol, an acetylcholine analog that does not hydrolyze, to muscarinic receptors expressed by neural cells and smooth muscle cells. Carbachol binding induces calcium oscillations in the cytosol, again invoking other signal pathways (27).

Calcium is, quite often, its own agonist. Calcium Induced Calcium Release (CICR) causes Ryanodine Receptors to release calcium, which triggers other events. Ryanodine Receptors are located on the ER membrane in certain cell types and can completely empty the ER of calcium (8, 9).

Sphingosine-1-phosphate, when present in the extracellular matrix, can trigger calcium release from the ER when the ceramide production pathway is induced. Sphingolipids are involved in many processes and are known to regulate cell growth

Table 1.1 A table of the most common agonists to induce intracellular calcium change.

Drug/Agonist	Use	Cell Type
Ionomycin	H ⁺ /Ca ²⁺ Exchanger	HeLa
	Forms channels shuttling Ca ²⁺ into the cell	HEK293
	At low concentrations, cytosolic calcium increase	Cos7
	At high concentrations, said to act on ER as well	
Carbachol	Binds to muscarinic receptors (acetylcholine receptors) and causes Ca ²⁺ oscillations in the cytosol	HEK293 Neurons
ATP	Ca ²⁺ release from ER due to IP3 activation	Any
Histamine	Ca ²⁺ release from ER by acting as an IP3 agonist	Any
Cyproheptadine	Histamine inhibitor used to reverse or stop Ca ²⁺ release by histamine action	Any
Soponin/digitonin	Detergents that create pores in the cell membrane allowing calcium entry or other drugs	Any epithelial
Bradykinin	Ca ²⁺ release from the ER by stimulating production of phospholipase C, which makes IP3 and triggers the IP3 pathway	Fibroblasts Vascular endothelial
IP3 or InsP3 Inositol 1,4,5-triphosphate	With addition of a detergent, IP3 entering the cell binds to the IP3 receptor on the ER causing a Ca ²⁺ release from the ER	Any epithelial
Thapsigargin	Block Ca ²⁺ reuptake pumps in ER allowing slow Ca ²⁺ leak	Any

and death. Calcium's involvement in this process is not yet well understood, but investigations are currently underway (28, 29).

In *Calcium Signalling*, Hofer details the use of TPEN (tetrakis-(2-pyridylmethyl) ethylenediamine) to decrease ER calcium to a large extent (30). TPEN has been used as a heavy metal scavenger, but has also been found to be permeable to the cell membrane. After entering cells, TPEN binds calcium and becomes trapped so it does not leak out of the cells. In addition, since TPEN is membrane permeable, there is no need to permeabilize the cells with detergent.

1.3 Current Methods to Monitor Calcium Concentration

1.3.1 Small molecules to monitor calcium

Currently, many approaches are taken to study calcium including calcium-binding dyes and protein-based sensors. Commercially available dyes are obtainable in a wide variety of colors, spectroscopic properties, and binding affinities. Many of the dyes are cell permeable esters and are loaded into mammalian cells through simple incubation. Molecular Probes offers numerous calcium binding indicators with spectra ranging from the ultraviolet to the red (31). The binding affinities range from 60 nM to hundreds of micromolar. Largely, the dyes are BAPTA-based indicators with different functional groups to change the binding affinities and the colors. BAPTA (1,2-bis(o-aminophenoxy)ethane-N,N,N',N'-tetraacetic acid) is a strong calcium chelator ($K_d = 60$ nM) based on EGTA that functions by binding calcium with the four acetic acid moieties in the structure (Figs 1.3 and 1.4). The absorbance of BAPTA is calcium dependent with a decrease evident at 250 nm as calcium is increased (31-33).

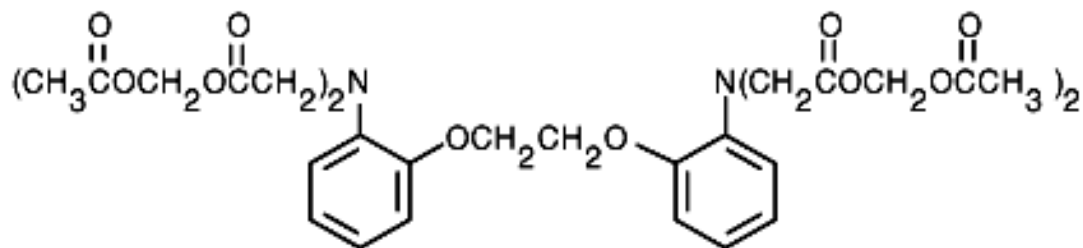


Fig 1.3 The structure of BAPTA, a calcium chelator whose absorbance changes upon calcium binding (Molecular Probes, Inc.).

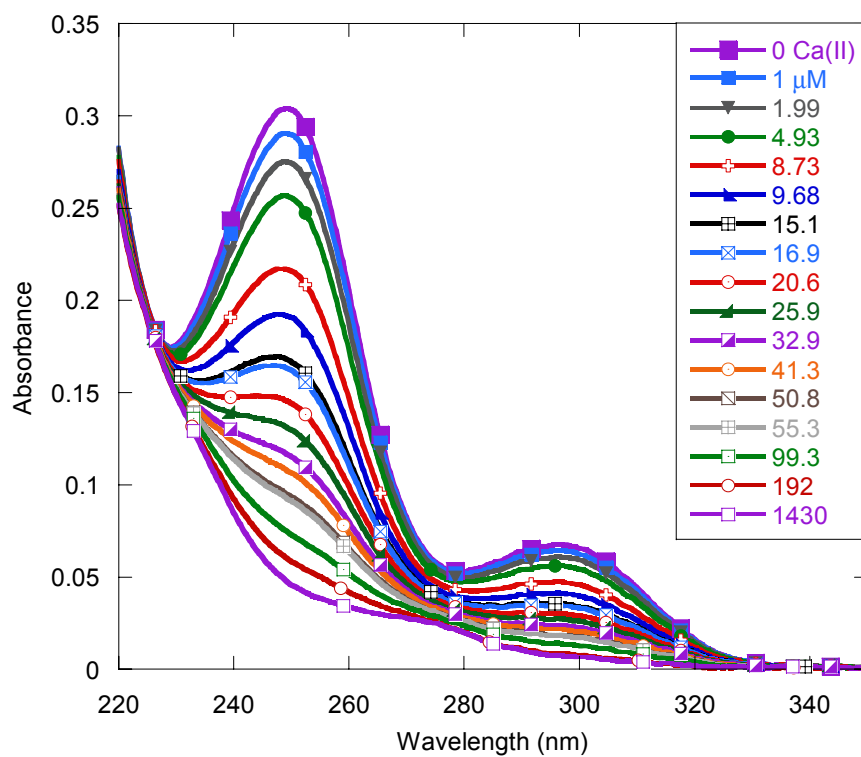


Fig 1.4 The spectra of TF-BAPTA in 10 mM Tris with increasing calcium shown to illustrate the absorbance change of BAPTA dyes upon binding calcium. The binding affinity for this particular dye was measured to be 13 μM in our laboratory.

Fura-2, a popular calcium indicator shown in figure 1.5, is BAPTA based with a more conjugated system to allow for fluorescence at 510 nm when excited at 340 or 380 nm. The excitation spectrum of Fura-2 is calcium dependent with an increase observed at 340 nm upon increasing calcium concomitant with a decrease at 380 nm. During the measurements of Fura-2, the emission of the dye is measured with excitation at two wavelengths, and the emission increase with 340 nm excitation should correlate with an emission decrease with excitation at 380 nm. The ratiometric property of this indicator is highly valued in the study of calcium as they allow for better calibration of an experiment and for more reliable calcium measurements.

Another type of small molecule dye is Rhodamine-5N shown in Fig 1.6, which is also BAPTA based, but exhibits virtually no fluorescence in the calcium free state and increases in fluorescence as calcium is increased. The fluorescence of this molecule is red with maximum emission observed at 578 nm. The Rhodamine based dyes have been utilized in cell studies by direct injection of the dye or by incubating the cells with the AM ester derivative of the molecule, which can freely pass across the cell membrane, and imaging induced calcium changes in the cytosol (34, 35). The AM ester derivatives are not active until they pass into the cell and the cell machinery cleaves the ester portion. Once that portion is cleaved, the dye theoretically can not cross the cell membrane to leak back out of the cell. Most of the available dyes are also constructed as AM esters. Rhodamine-5N will be further discussed in Chapter 4 as a means to obtain calcium binding affinity of calcium binding proteins through competition.

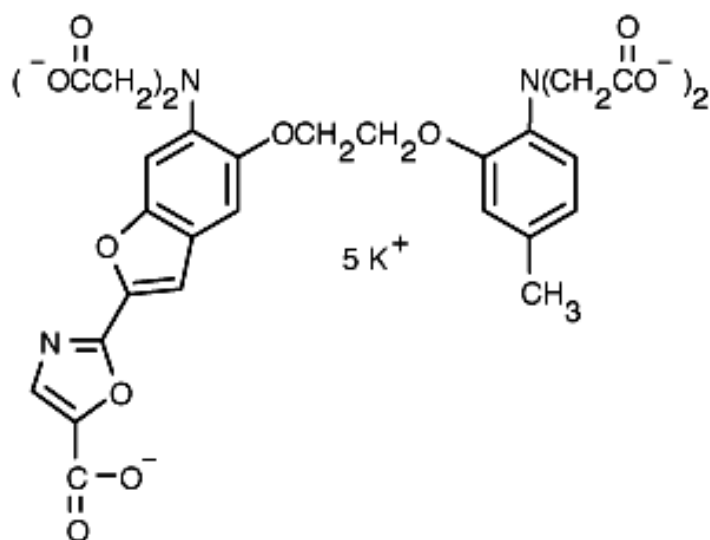


Fig 1.5 The structure of Fura-2, a BAPTA based calcium indicator (Molecular Probes, Inc.).

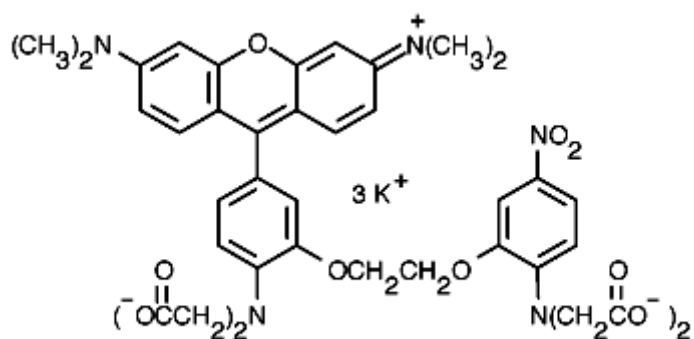


Fig 1.6 The structure of Rhodamine-5N from Molecular Probes. The spectral properties are illustrated in Chapter 4.

Derivatives of these dyes, such as Mag-Fura-2, have been utilized to study calcium in cell subcompartments. Hofer reports the use of Mag-Fura-2 as an ER calcium indicator, citing that Mag-Fura-2 will enter the ER of certain cell types (BHK fibroblasts, for example) and that removal of the dye from the cytosol allows one to measure the ER calcium change in response to a variety of agonists (30). The weaker binding affinity of Mag-Fura-2, as compared to Fura-2, allows for measurement in the ER.

Although many dyes with different desirable properties are available, small molecule indicators also contain their own set of disadvantages. Dyes may be loaded into cell subcompartments by varying temperature or extracellular medium or buffer to induce the cells to shuffle the dye to different compartments, but dyes can not be targeted to specific cell compartments nor is it quick or easy to verify which compartment is loaded. The small molecules often enter more than one compartment with no straightforward way to separate and identify the compartments. Also, dyes will localize in intracellular organelles to an unpredictable extent, causing difficulty in accurately determining the dye concentration and monitoring calcium concentration. The synthesis of ratiometric dyes have helped reduce this problem, but many applications need particular properties not available with the ratiometric dyes. In addition, Fura-2 is ratiometric but must be excited by UV light, which may damage the tissue under study. At increased temperatures, small molecule dyes tend to leak out of the cells causing a disruption in experimental procedures. Some of the small molecule indicators have been observed to be sequestered into vesicles due to their

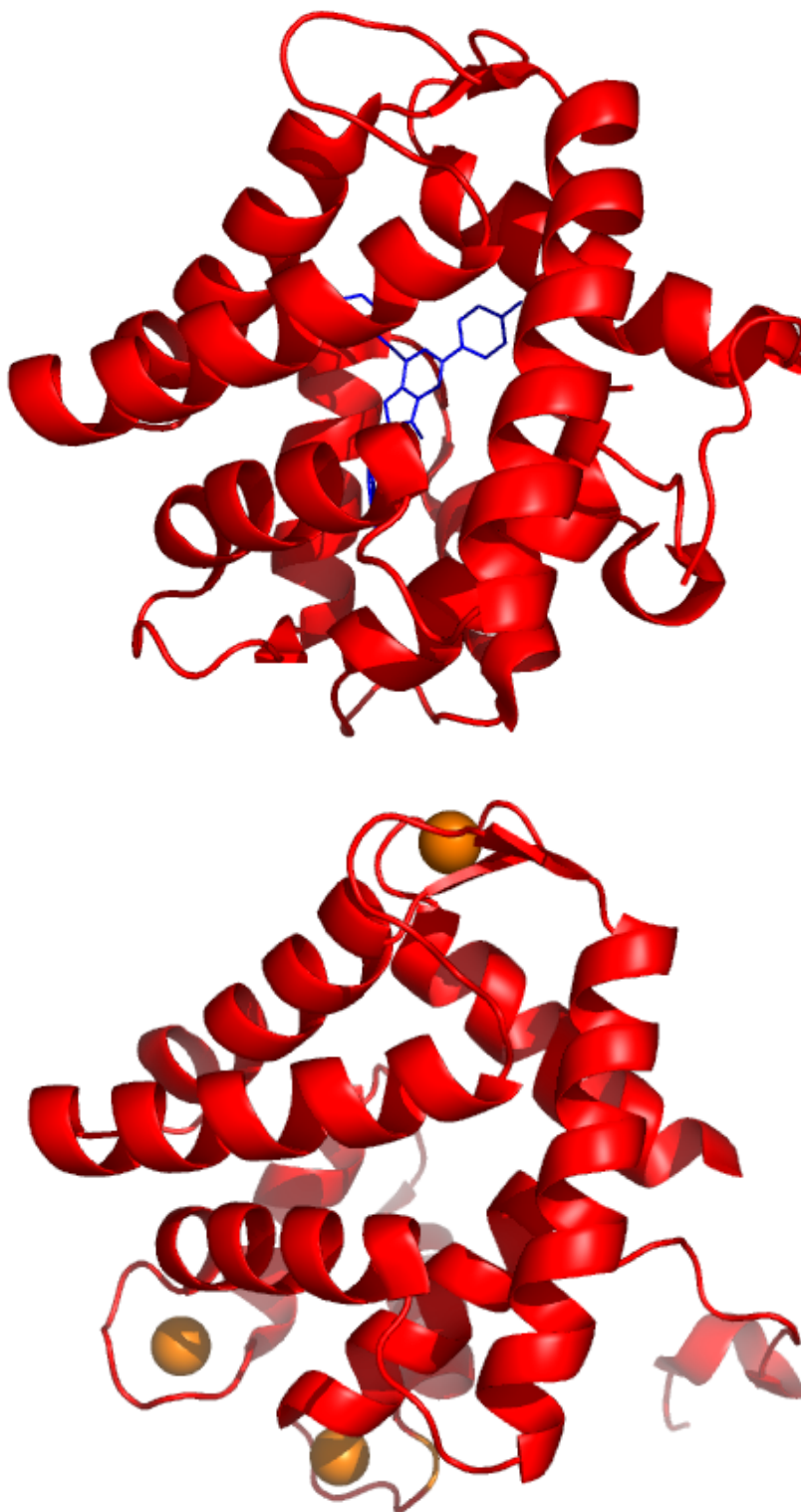
hydrophobicity. Many of these dyes have such strong calcium affinities that they have been observed to cause a buffering effect in cells so that the calcium signaling is not correctly observed and calcium is not correctly handled. Hofer reports that the buffering effect of BAPTA-AM can mimic the uptake of calcium by the mitochondria, which modulates the rate of ER store refilling (36). Wang et. al. observed deleterious effects on the intercellular calcium waves induced by mechanical stimulation when the cells were loaded with the high affinity BAPTA (37). Many of these dyes are perturbed by cellular components, such as pH, ATP, and salt. Environmental factors, i.e. temperature, may also have an effect on the dyes' ability to report cellular calcium changes. Lastly, small molecule indicators do not provide the necessary sensitivity for thick tissues, intact organisms, or non mammalian cells and are subject to interference by autofluorescence. To overcome this problem, we have explored the synthesis and design of a calcium binding dye based on a near infrared absorbing moiety and the metal binding properties of a 15-crown-5 moiety (Chapter 3).

1.3.2 Protein based calcium sensors

An alternative to small molecule dyes are calcium-sensitive proteins. Proteins can be directly expressed by the cells to be studied and can be targeted to specific subcompartments with the addition of signal peptides, small amino acid chains that direct an expressed protein to various cell compartments (i.e. the calreticulin sequence that directs to the ER). Proteins do not leak out of cells due to their larger size. Protein sensors can also be used in a wide variety of cell types, including mammalian and bacteria. A desirable protein sensor will not be perturbed by cellular components and

will not be vesicularized. Currently, there are four classes of protein based calcium sensors developed in the past several years. The first is aequorin (Fig 1.7), a natural calcium-dependent protein from jellyfish, which is known as the companion protein to green fluorescent protein (38). The protein contains 4 high affinity EF hand calcium binding motifs and a fluorescent cofactor, coelenterazine, which fluoresces upon calcium binding. Aequorin has been utilized to great extent in the study of intracellular calcium dynamics and homeostasis due to its inherent calcium sensitivity and the ability to target the protein to particular intracellular compartments with signal peptides (39-42). In addition, aequorin's coupling of calcium binding and light emission falls in the perfect range for intracellular calcium study with low micromolar concentrations of calcium necessary to cause light emission (43, 44). However, aequorin requires the constant addition of coelenterazine, which is consumed after each reaction (45), further complicating the imaging measurements. A second approach was directed by Persechini and coworkers by engineering a calmodulin binding peptide from smooth muscle light chain kinase between two differently colored fluorescent proteins, blue and red mutants of green fluorescent protein (46-48), as shown in figure 1.8. This approach measures calcium by reduction in FRET between the two fluorescent molecules caused when the peptide binds calmodulin and separates the two fluorophores. The initial constructs indicated inefficient FRET due to the far separation of the excitations and emissions of the blue and red fluorophores. Further work revealed that the use of blue and yellow constructs increased the FRET efficiency. In addition, to further increase the efficiency and to allow for "direct" monitoring of calcium, the C-terminal of one of the

Fig 1.7 The structures of aequorin from jellyfish in the apo and calcium loaded forms. The fluorescent cofactor, coelenterazine, is shown in blue in the top illustration. Calcium is shown in orange in the bottom illustration. The structure of aequorin undergoes a conformational change upon calcium binding. The structures were visualized by Pymol (49) using the pdb 1EJ3 (top) and 1SL8 (bottom).



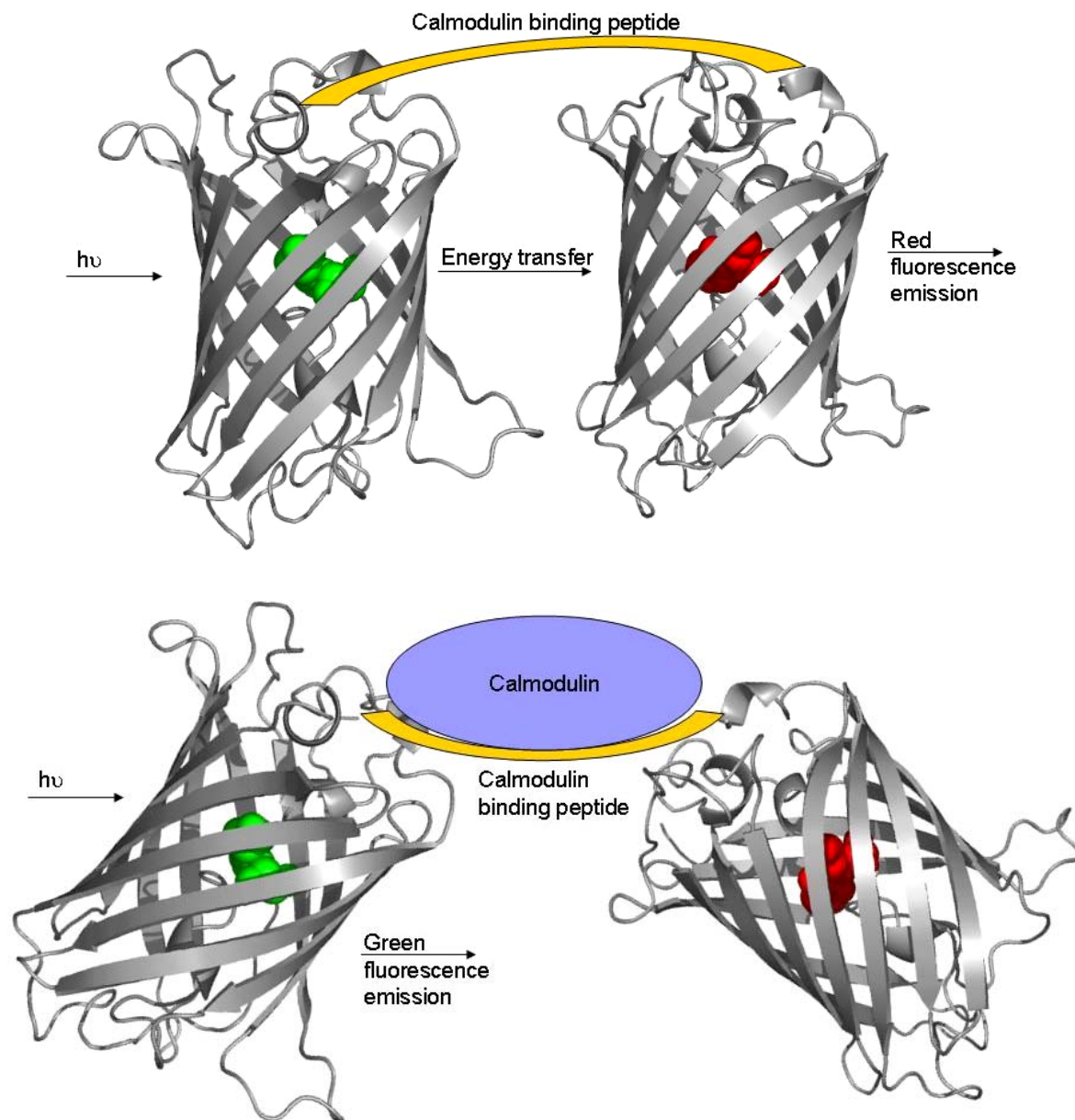


Fig 1.8 Illustrations of Persechini's constructs, which allows for monitoring of calcium through calmodulin (blue) binding to the calmodulin binding peptide (shown in orange) through the use of energy transfer. When the peptide is not bound to calmodulin, energy transfer occurs between the green and red mutants of GFP. The distance is increased between the two fluorophores upon calmodulin binding so that no energy transfer is observed, only green fluorescence. The GFP proteins are visualized using Pymol (49).

fluorescent proteins was amended to include calmodulin so that binding of the small peptide to the C-term calmodulin would separate the fluorophores and decrease FRET. Persechini's constructs better indicate calcium changes, but the constructs suffer from interference from endogenous proteins, i.e. calmodulin and calcium binding peptides, so that the true spatial and temporal changes in calcium can not be accurately measured. In addition, the constructs with only the binding peptide rely on the availability of calmodulin in the cell and truly measures the calmodulin change, not the calcium change. Tsien, Miyawaki and coworkers furthered this approach by engineering constructs with calmodulin between two fluorescent proteins so that calcium binding to calmodulin would separate the two fluorophores and decrease FRET (50). They created numerous constructs by varying the color of the fluorescent pairs, varying the calmodulin mutant used, adding the binding peptide to the construct so both calmodulin and the peptide were contained in one molecule, and circularly permutating the fluorescent molecules for more desirable properties (50-54). These sensors more directly monitored calcium changes than Persechini's constructs, but they all utilize calmodulin as their target molecule, causing interference from endogenous proteins. With FRET, the ability to monitor multiple wavelengths provides ratiometric measurements so that data can be normalized. However, energy transfer is distance and orientation dependent, is not as efficient as direct fluorescence change, and requires more convoluted microscopy set ups than single fluorophores. One of the newer approaches, developed by Heim and Griesbeck, utilizes Troponin C (TnC) as the calcium binding moiety, which would encounter less interference in cell types that do not

produce TnC than the calmodulin based sensors. This construct was able to monitor the calcium oscillations produced by carbachol addition and indicated an 80% increase in fluorescence upon ionomycin and calcium addition. To date, this is the best published calcium sensor, but the construct can not be used in skeletal or cardiac muscle cells that produce TnC, limiting the use of the sensor (27). Cardiac mishandling of calcium has been reported to be a large problem in cardiac disease, and the study of cardiac calcium could lead to prevention or cessation of heart disease (55-58). This limits the use of the TnC sensor, and an ideal sensor should be of use in all mammalian cell types. Protein-based calcium sensors have many advantages, but the currently available protein-based sensors are not as sensitive to small calcium changes as small molecule dyes. The sensors based on natural calcium-binding proteins, as most of them are, contain numerous calcium binding sites causing difficulty in data deconvolution, and they can not be tuned to different affinities because they employ natural calcium binding sites. To overcome these difficulties, we have designed a calcium-binding protein with an intrinsic ability to report calcium changes.

1.4 Criteria for an Ideal Sensor

The ideal calcium sensor to monitor real time calcium alterations requires many features that have not been found in a single sensor up to this point. First, the sensor must exhibit a large change in optical signal, preferably fluorescence with minimized background interference, such as autofluorescence. A near infrared signal would be ideal because all background interference would be eliminated. A signal increase in intensity upon calcium binding would be the most useful. A wavelength change would

only be acceptable if the calcium free and calcium bound wavelengths were far separated as most imaging is performed on microscopes with filters that allow a certain band of wavelengths through without distinguishing small wavelength shifts. Ideally, a sensor should contain the means to measure both a calcium sensitive signal and a calcium insensitive signal so that the data could be normalized and the concentration of the sensor could be easily calculated. This would eliminate any interference in calcium measurements due to cell shape change or swelling. Second, the binding of the sensor should be selective for calcium as magnesium and other ions are in much greater abundance in the cell. The binding site should be tunable to obtain a large range of binding affinities so the correct affinity could be utilized for each subcompartment to be studied as well as the cytosol. Third, fast off rates to allow the signal to truly reflect calcium changes are necessary. The off rates of the currently available sensors are too slow to monitor the fast calcium dynamics that occur in the cell. Schuhmeier and coworkers measured the k_{off} of EGTA in cells to be 2.73 s^{-1} (59). Linse and Forsen report the off rate for calcium of regulatory proteins, i.e. calmodulin, to be $10 - 10^3 \text{ s}^{-1}$ while the off rates of non-regulatory proteins, such as calbindin D_{9k} , to be $1 \text{ to } 3 \text{ s}^{-1}$, in the range of EGTA (60). Linse and Forsen also report the off rates of calbindin mutants measured by ^{45}Ca NMR to be $<10 \text{ s}^{-1}$ for the first site (61). The off rates of current protein based calcium sensors are generally much slower ($\sim 1 \text{ s}^{-1}$) with the exception of a recent report of 256 s^{-1} , described by Palmer and Tsien, for a sensor with “improved reaction kinetics” (62). The sensor should have fast off rates so that quick calcium signals can be monitored. Fourth, the sensor should not induce a buffer effect by

disrupting calcium signaling intra- or intercellularly. Fifth, the sensor should not exhibit pH sensitivity in the cellular pH flux range (6.0 to 8.5) or the pH sensitivity should be small enough to account for in the measurements. Sixth, an ideal sensor should have the ability to be targeted or delivered to any desired location. Protein sensors can be targeted with the addition of signal peptides to the ER, mitochondria, nucleus, and cell membrane. A protein based sensor must be engineered with a stable host protein, preferably with its own ability to report calcium binding. To monitor calcium variations in the ER, mitochondria, and extracellular environment requires a sensor with a binding affinity in the proper range for the range of calcium concentration in each of those locations. The ER, as a calcium store, contains ~0.5 mM calcium at rest. The mitochondria contains less calcium at rest, but the calcium concentration increases when calcium waves are induced in the cell. The extracellular matrix contains 1.8 mM calcium at rest with large local changes as signals are propagated. Each of these locations requires sensors with different affinities, which have not been available to date due to the reliance on natural calcium binding proteins as the binding moiety of the sensors.

1.5 Green Fluorescent Protein

Green fluorescent protein has been chosen for the initial design process (Fig 1.9) due to the abundant literature information and previous mutational work. Green fluorescent protein from *Aequorea victoria*, or jellyfish, is a bioluminescent protein that is a companion to aequorin, a calcium binding protein discussed in section 1.3.2. The blue emission from aequorin is used by GFP to create a green glow in the cell, hence

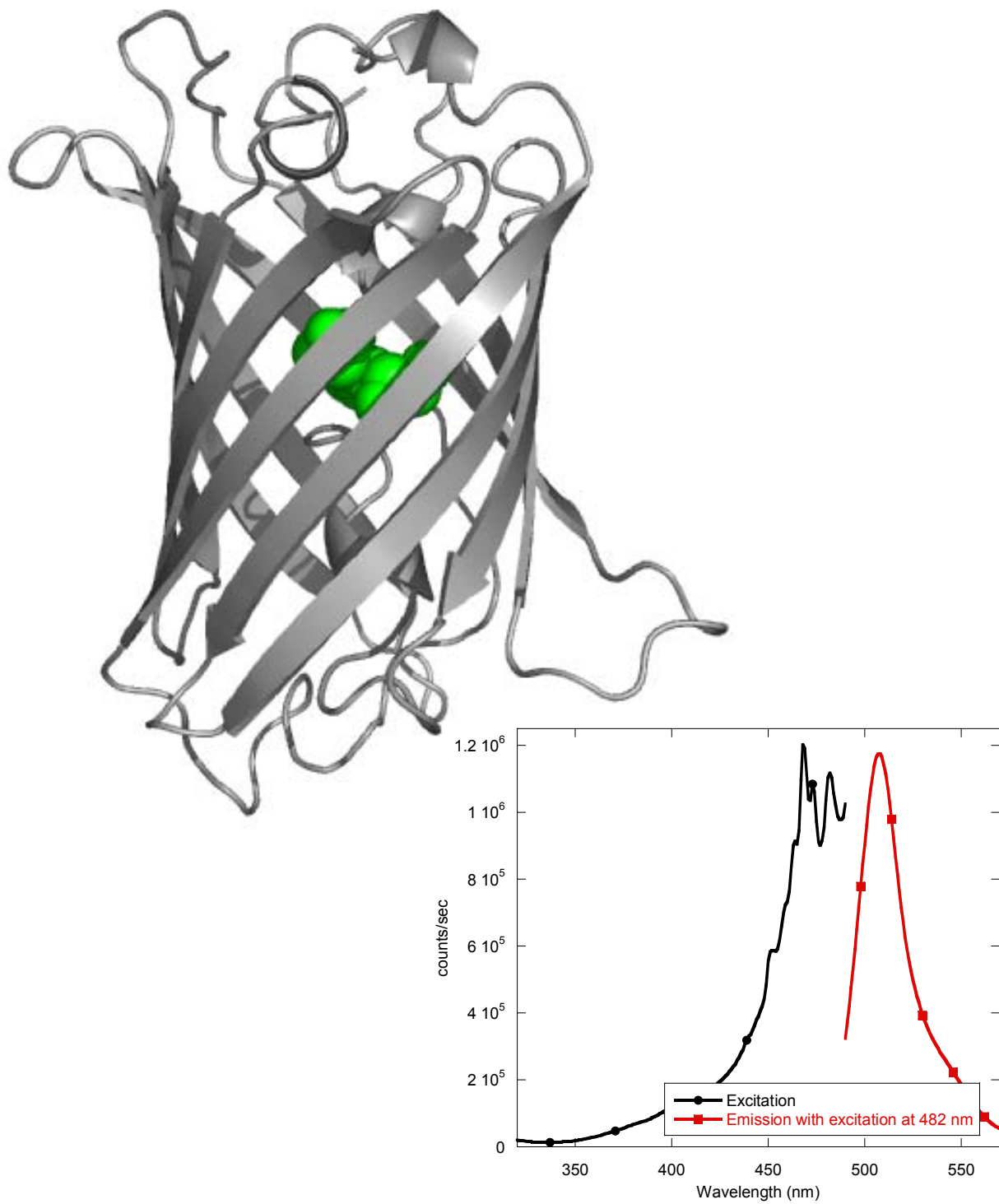


Figure 1.9 β -barrel structure of green fluorescent protein visualized with Pymol (1b9c) with the chromophore shown in green. The excitation and emission spectra of EGFP are shown on the bottom.

the reason jellyfish glow (63). The structure of GFP is an 11 stranded β -barrel with an α -helix running through the middle of the barrel and several loops and short helices capping the barrel on each end. The chromophore in GFP, consisting of residues 65-67 (Ser, Tyr, and Gly), is attached to the α -helix and almost completely buried in the center of the barrel (64). The proposed formation of the chromophore is illustrated in Fig 1.10. Wavelength shifts of the absorbance of the chromophore occur with a change in protonation. The anionic form has an excitation maximum at 475 nm whereas the protonated or neutral forms exhibit a maximum at 395 nm. The emission of the wild type protein has a λ_{max} at 504 nm (65). Generally, both forms exist in solution in a 6:1 neutral:anionic ratio (63). Wild type green fluorescent protein is ~28 kDa and contains 238 residues (63).

Many mutations have been investigated as a means of changing the wavelengths of the chromophore, the folding properties, and the temperature sensitivity, as detailed in table 1.2. Tsien divided GFP mutations into several classes according to the changes in the chromophore. With all of the mutations, GFP's intrinsic ability to fold properly has been established. In aerobic conditions, the chromophore forms despite the mutations. So called "folding mutants" have been made to help GFP to fold and form the chromophore in higher temperatures (37 °C vs. 25 °C) and with quicker maturation rates, such as the cycle3 derivative. In addition, many mutations have been performed on this protein to shift the chromophore's optical activity (63, 66, 67), to form metal binding sites (68, 69), and to attach metal sensitive proteins for design of

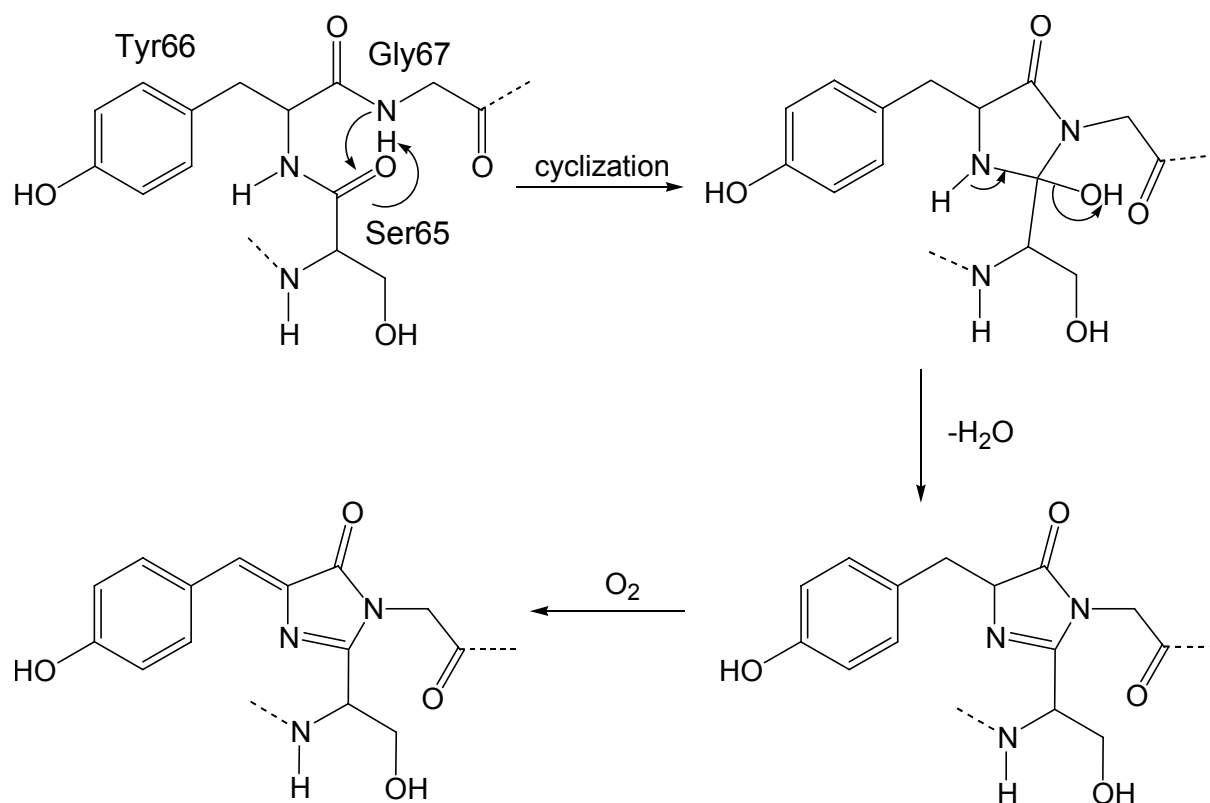


Fig 1.10 Chromophore formation of GFP modified after that proposed by Tsien in his 1998 review (63) is shown. This is the generally accepted formation reaction although the true formation has not yet been elucidated.

Table 1.2 A summary of the mutations made to GFP with various affects. The information was gleaned from Tsien's review (63) unless otherwise noted.

Name	Mutation (s)	λ_{exc}	ϵ ($M^{-1} cm^{-1}$)	λ_{em}	Effects	Ref
H9	T203I	400		512		
	T203I/S202F	398		511		
H9-40	T203I/S72A/Y145F	399	29,000	511	chromophore considered neutral phenol; bright as cycle 3	
5B, 9B	T203H/S65T	512	19,400	524		
	T203H/S65G/S72A	508	48,500	518	phenolate anion with stacked π -electron system (yellow)	
	T203F/S65G/S72A	512	65,500	522	phenolate anion with stacked π -electron system (yellow)	
6C	T203Y/S65T	513	14,500	525		
10B	T203Y/F64L/S65G/S72A	513	30,800	525		
10C	T203Y/S65G/V68L/S72A	513	36,500 (83,400)	527	phenolate anion with stacked π -electron system (yellow)	
10C Q69K	T203Y/S65G/V68L/Q69K/S72A	516	62,000	529	phenolate anion with stacked π -electron system (yellow)	(70)
	T203Y/S65G/V68L/S72A/S147H/Q204H				Cu^{2+} binding mutant	(68)
	T203Y/S65G/V68L/S72A/E95H/Q184H				Cu^{2+} binding mutant	(68)
11	T203W/S65G/S72A	502	33,000	512		
Topaz	T203Y/S65G/S72A/K79R	514	94,500	527	phenolate anion with stacked π -electron system (yellow)	
	S65 to R, N, D, F, W				weak or no fluorescence	
	S65A	471		503, 504		
EGFP mut2	S65A/V68L/S72A	481		507	19-fold fluorescence intensity increase	

Name	Mutation (s)	λ_{exc}	ϵ ($M^{-1} cm^{-1}$)	λ_{em}	Effects	Ref
	S65T	489, 488	39,200 or 52,900	509- 511	2 different trials by same investigator; 6-fold greater peak amplitude of E. coli expressed protein relative to WT; 18-fold brighter than WT by FACS; 4-fold faster oxidation; no photo-isomerization; very slow photo-bleaching when excited at 280 nm	
EGFP	S65C	479	47,400	507		
mut1	S65T/F64L	488		507	35-fold fluorescence intensity increase	
	F64L/S65T/V163A	488	42,000	511	chromophore considered phenolate anion	
ECFP	F64L/S65T/Y66W/ N146I/M153T/ V163A/N164H				Calmodulin--M13 Ca^{2+} binding mutant	(70)
EYFP	S65G/S72A/T203Y				yellow mutant, used by Tsien as CaM fusion for Ca^{2+} binding	(70)
RSGFP4	F64M/S65G/Q69L	490		505	24-fold brighter than WT by FACS	
EGFP	S65G/S72A	501		511	21-fold fluorescence intensity increase relative to WT	
mut3					solubility changes, S65T mutant background	
smRS-GFP	S65T/F99S/M153T/ V163A	489		511		
P4-1	S65T/K238E/ M153A	504 (396)		514		
Emerald	S65T/S72A/N149K/ M153T/I167T	487	57,500	509	chromophore considered phenolate anion; bright as cycle 3	

Name	Mutation (s)	λ_{exc}	ϵ ($M^{-1} cm^{-1}$)	λ_{em}	Effects	Ref
P11	I167T	471 (396)		502 (507)		
cycle 3	E222G	481		506		
	F99S/M153T/ V163A	395 (475)	30,000 (6500- 8500)	508 (540)	45-fold brighter whole cell fluorescence relative to WT GFP when excited by UV light; 4-fold less bright whole E. coli cell fluorescence relative to EGFPmut1 when excited at 488 nm	
P4 or BFP	Y66H	382	21,000	448	blue fluorescent	
P4-3	Y66H/Y145F	381	22,300	445	blue fluorescent; imidazole in chromophore	
smBFP	Y66H/F99S/M153T/ V163A	382		448	blue fluorescent; solubility changes; Y66H mutant background	
W	Y66W	458		480	blue fluorescent	
W2	Y66W/I123V/ Y145H/H148R /M153T/V163A/ N212K	432 (453)		480	blue fluorescent	
W7	Y66W/N146I/ M153T/V163A/ N212K	433 (453)		475 (501)	blue fluorescent	
W1B	Y66W/F64L/S65T/N1 46I/M153T/V163A	434 (452)	32,500	476 (505)		
W1C	Y66W/S65A/S72A/N 146I/M153T/V163A Y66F	435 360	21,200	495 442	blue fluorescent; less bright than WT; shortest wavelength excitation and emission peaks	

Name	Mutation (s)	λ_{exc}	ϵ ($M^{-1} cm^{-1}$)	λ_{em}	Effects	Ref
EBFP	F64L/S65T/Y66H/ Y145F	380		440	blue fluorescent; brighter signal;	
	F64L/S65T				improves expression	
	F64L/T203Y				improves ϵ	
	V68L/ S65A				improves expression	
	V68L/ T203Y				improves ϵ	
	S72A/ S65G				improves expression	
	S72A/ S65A				improves ϵ	
	S72A/ T203Y				improves expression	
	F99S				improves ϵ and brightness	
	Y145F/ Y66H				improves ϵ and brightness	
	N146I/ Y66W				improves ϵ and brightness	
	M153T/ Y66W				improves expression	
	M153T				improves ϵ and brightness	
	V163A/ Y66W				improves expression and thermo- tolerance	
	V163A/ Y66H				improves brightness	
	V163A				improves thermo- tolerance	
	I167T/ V163A/S175G/ S65T				improves ϵ and brightness	

biosensors (70-72). Although much of this work has been successful, the end results generally contain very large proteins that are difficult to work with and may not be usable for intracellular study due to the disadvantages stated in section 1.4. Also, the utilization of Fluorescence Resonance Energy Transfer in detecting calcium does not provide the necessary sensitivity in cellular work. The design of a calcium binding site within the frame of GFP that would cause an emission increase upon binding of calcium would make a smaller protein that is easier to study with faster kinetics and eliminates the conformational changes that accompany the currently available protein sensors. Fig 1.11 illustrates two hypothetical responses that could be observed upon calcium binding to a designed calcium-binding fluorescent protein. A fluorescence increase would be most preferred for microscope imaging of live cells since microscopes employ filters with 20 to 30 nm band passes. A wavelength shift would be preferred for *in vitro* studies so that small concentration changes would not impair the study.

1.6 Calcium-binding Proteins and Calcium-binding Sites

Oxygen is the preferred ligand for calcium binding, commonly from the amino acid sidechains of Glu, Asp, Gln, and Asn, the mainchain carbonyl and water, but also from Ser and Thr in some proteins. Calcium binding to small molecules can occur with 4 to 12 ligands with water as an available ligand. In proteins, generally calcium binding occurs with 5 to 8 ligands with water binding in one or two positions. Although the pentagonal bipyramidal geometry is the most often observed, some proteins also bind in an octahedral geometry. EF hands, with a helix-loop-helix calcium binding motif, bind calcium in a pentagonal bipyramidal geometry with one ligand, aspartate or glutamate,

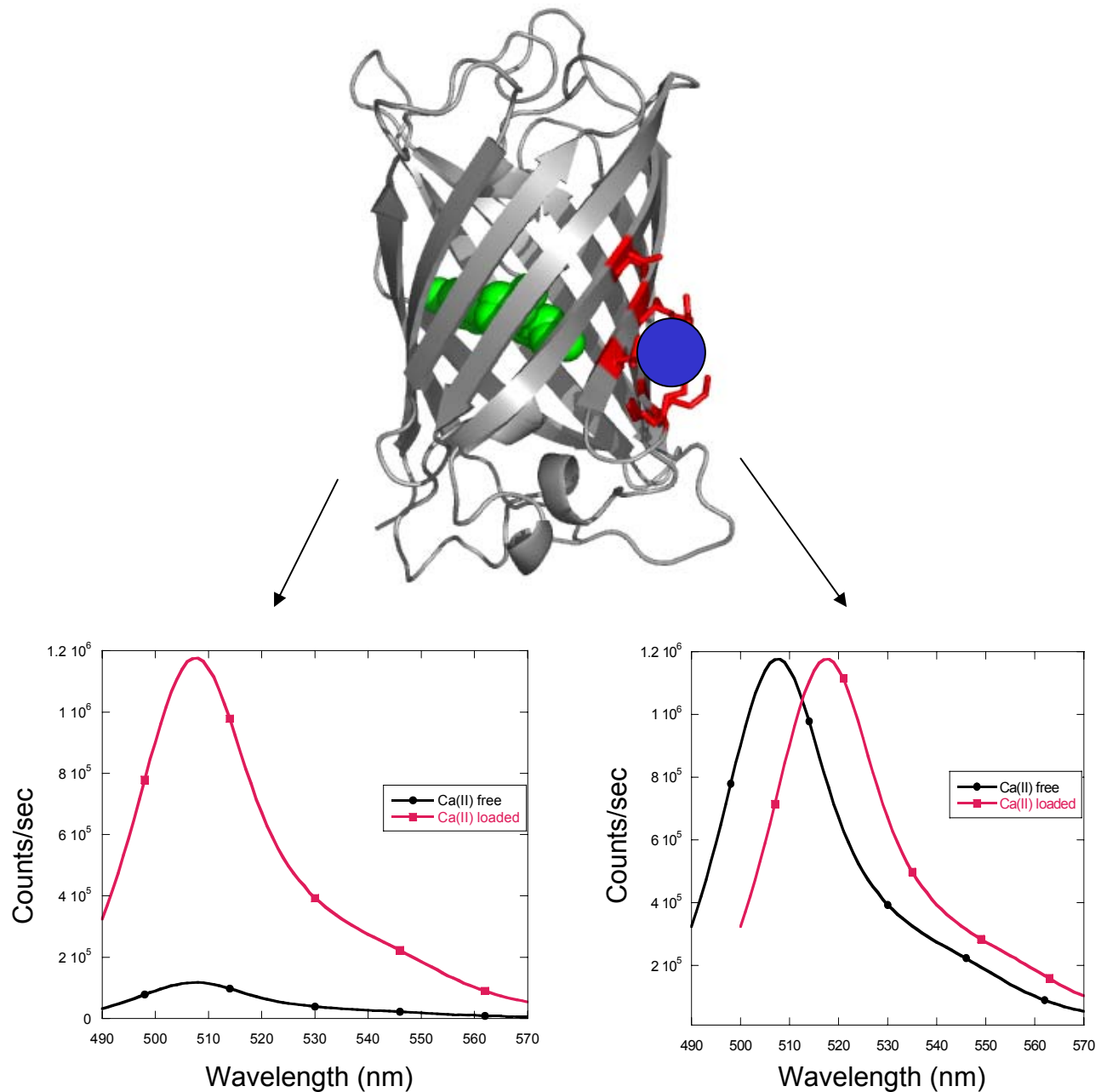


Fig 1.11 The two possibilities of fluorescence change caused by calcium binding to a designed fluorescent protein are illustrated. An increase in fluorescence is desired for experimental ease in the use of microscopes to monitor live cells. A wavelength shift would be desired for in vitro measurements, but the shift would necessarily be large to monitor with the use of microscopes that employ filters.

used as a bidentate with both oxygens binding to calcium (1.12). EF hands contain the binding ligands in a short sequence and are known as continuous sites (Fig 1.13).

Discontinuous binding sites do not contain the ligands in a short sequence, but, rather, from various parts of the protein with the site forming by the fold of the protein. Trypsin from *S. griseus* and proteinase K are examples of calcium binding proteins with discontinuous binding sites (Fig 1.14) (73, 74).

One of the most well studied calcium binding proteins is calmodulin, a ubiquitous protein that contains four calcium binding sites, two each in two domains. The calcium-binding sites are known as EF-hands with the helix-loop-helix structure first characterized by Dr. Robert Kretsinger (75-78). Upon binding calcium, calmodulin undergoes a drastic conformational change, exposing the hydrophobic helix that can then bind to target molecules, such as myosin light chain kinase. The four sites have been studied in a variety of methods, such as through cleavage of the two domains, individual peptides, and study of the intact protein.

Most natural calcium binding proteins contain more than one calcium binding site and undergo conformational changes upon binding. The binding sites are subject to cooperativity, metal-metal interactions, and environmental factors (60). The study of the key determinants for calcium binding has been an on-going endeavor for decades. There are several factors that have been shown to be important in calcium binding. The EF hands in the proteins have an intrinsic calcium binding ability based on the type, charge, and arrangement of the calcium ligands. Since the binding process is highly cooperative, the calcium affinity observed for the intact protein also contains

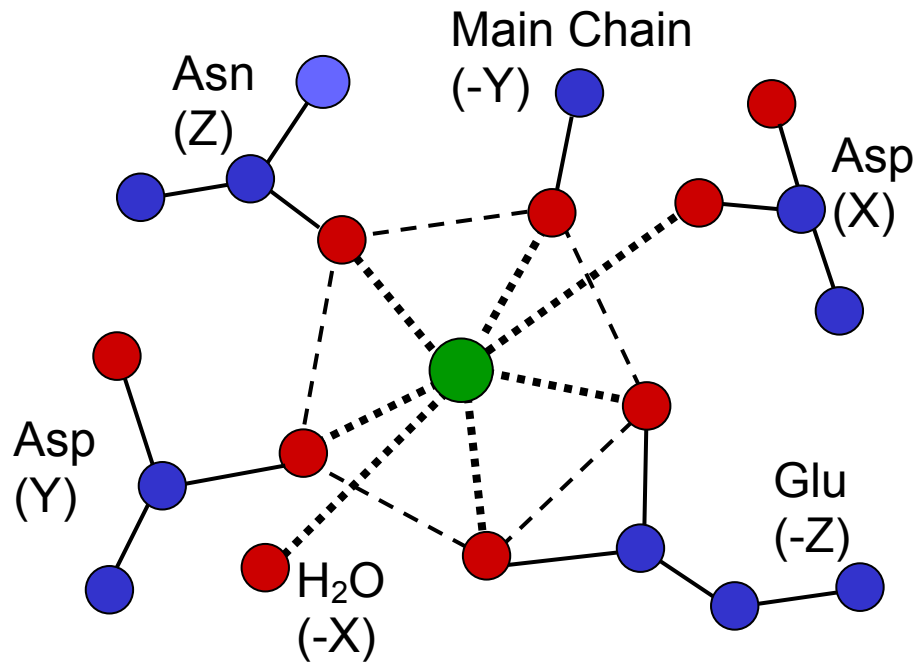


Fig 1.12 Pentagonal bipyramidal binding geometry of EF hand proteins with Glu as the bidentate. The actual residues shown are from loop III of calmodulin. The red spheres indicate oxygen. The dark blue spheres are carbon, and the light blue sphere is nitrogen. The dashed line indicates bonds to calcium.

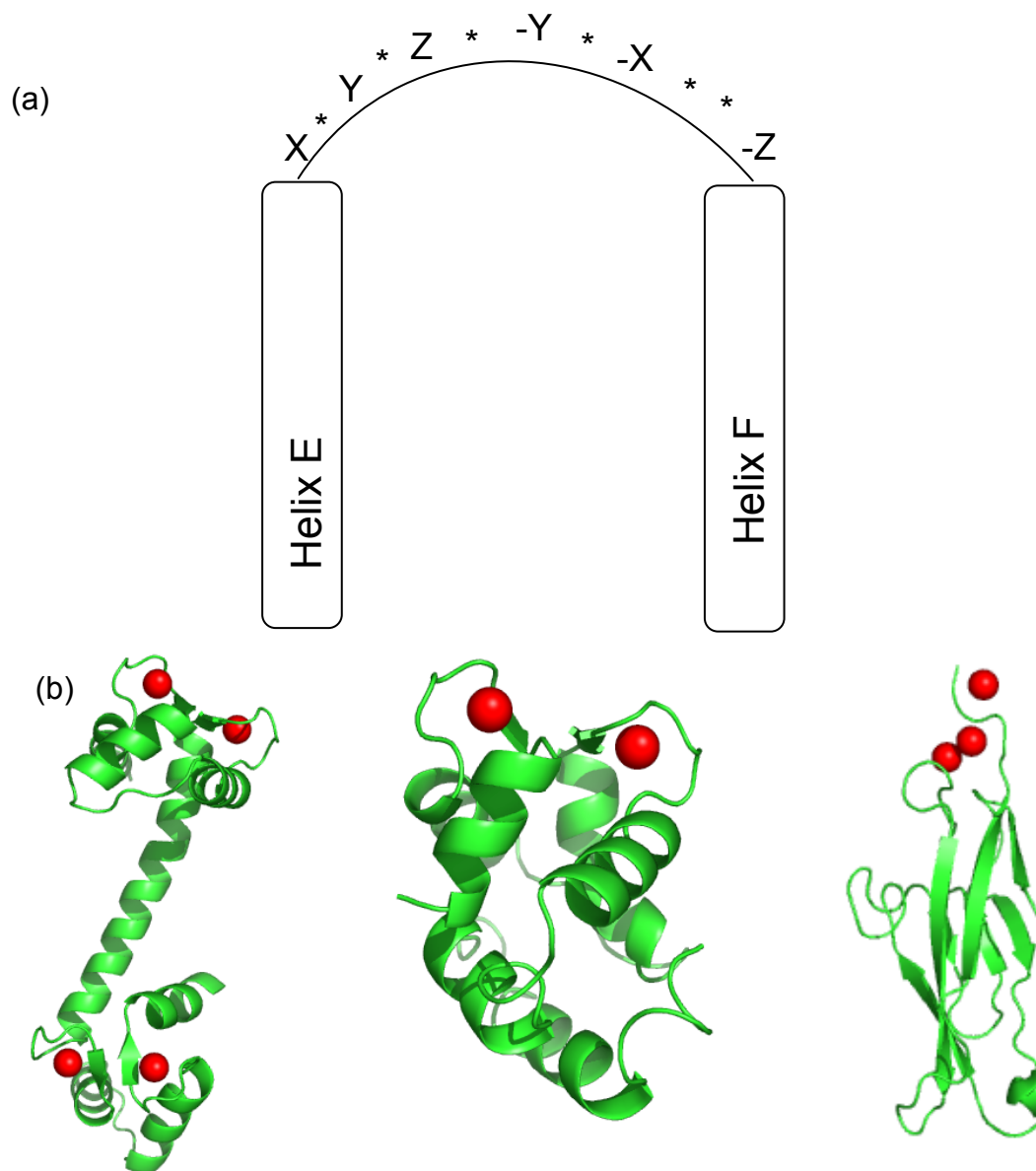


Fig 1.13 (a) Illustration of the continuous calcium binding sequence of the EF hand with the binding ligand positions given by the X, Y, Z coordinates most commonly used. The coordinates are $X = 1$, $Y = 3$, $Z = 5$, $-Y = 7$, $-X = 9$, and $-Z = 12$, which are binding residues for calcium. Differences in these amino acids identity changes the binding affinity of the loop and accounts for the different affinities of different proteins with the same motif. Position 12 ($-Z$) is usually a glutamate. (b) Pymol illustrations of calmodulin (79) and parvalbumin (80) demonstrating EF hand calcium binding sites and cadherin (81), a non-EF-hand CaBP.

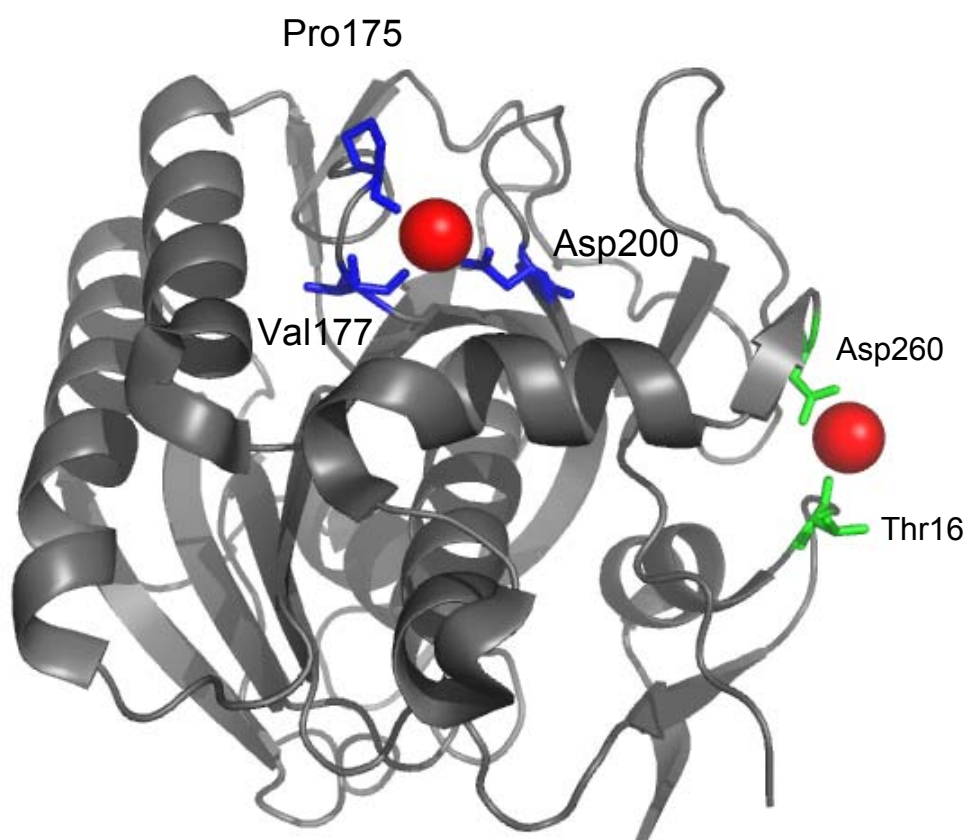


Fig 1.14 Proteinase K with the two calcium (red) ions and binding sites (ligands in blue and green) highlighted (2PRK pdb) and visualized with Pymol (49). These two discontinuous sites also contain water as calcium ligands.

contributions from the metal-metal interactions and the cooperativity of the protein. The charge balance created by the oxygens from Glu and Asp is likely the reason for those two types of residues occurring most often in calcium binding. In addition, these two residues hydrogen bond to other amino acids—sidechain or mainchain amide and often the sidechains of the other binding ligands—providing increased stability of the protein upon calcium binding. The number of charged ligands in the calcium coordination sphere also plays a role in calcium binding affinity. The environment of the calcium binding site also affects the affinity. Linse and Forsen have shown that a more electronegative environment causes a stronger binding affinity for a given calcium site and that surrounding electrostatic environment affects the cooperativity of calcium binding in multi-site systems (82, 83). With all of the understanding gleaned in the last 30 years, quantitative estimation of the key factors for calcium binding is yet to be established. Therefore, to systematically reveal the key determinants for calcium binding requires a new strategy and model system.

1.7 Our Design Approach and Previous Work in the Yang Lab

To understand site specific calcium binding affinity of each EF loop of calmodulin and to estimate the cooperativity of couple EF hand motifs, Yang and coworkers have developed a grafting approach by engineering individual EF hand motifs into a host protein (84, 85). We have also developed a design approach to understand the key factors for calcium binding by creating calcium binding sites in a host protein that does not intrinsically bind calcium. An initial survey of the literature was performed to ascertain the most common calcium binding properties observed for natural calcium

binding proteins with the assets desired for our design, such as a strong binding affinity and selectivity over other metals. The approach initially employs computer programs that search the backbone of a protein, with the desired angles and distances input from the user, to locate possible calcium binding sites. These identified sites contain the necessary geometry for calcium binding once the suggested mutations are made. The output of the computer programs are analyzed for the best possible sites based on several criteria. Once a site or several sites are chosen, mutagenesis is carried out to engineer the designed protein. Expression, purification, and biophysical studies are performed on the protein to understand the calcium binding affinity, geometry, etc.

Previously in our laboratory, numerous calcium binding proteins have been engineered based on domain 1 of the rat cell adhesion molecule CD2 (cluster of differentiation) (86-89). Fig 1.15 demonstrates one of these designed proteins, 7E15-CD2, characterized by Dr. Anna Wilkins Maniccia. The designed calcium binding proteins maintain the original structural properties and cell adhesion functions (86-88). These proteins have been shown to bind calcium with a range of affinities based on their unique positions in the protein, protein environment, and ligand type and charge. The effect of ligand type and coordination sphere charge on calcium binding as well as the effect of the electronegative environment on calcium binding affinity has been illustrated by work in our laboratory.

1.8 Our Approach to Engineer Calcium Sensors

Proteins with the intrinsic ability to report on changes in the cellular environment could provide a diagnostic tool to monitor calcium and report calcium changes.

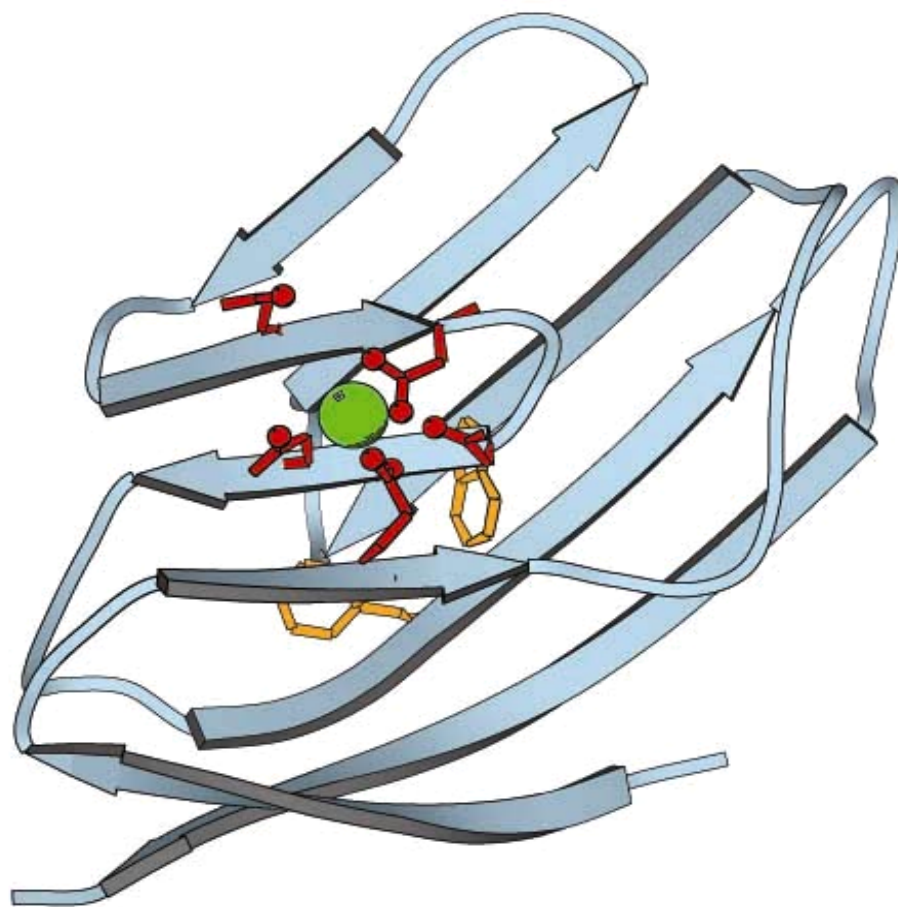


Fig 1.15 Designed protein 7E15-CD2, which exhibits a nanomolar Tb(III) binding affinity and a low micromolar Ca(II) binding affinity, is illustrated.

Fluorescent proteins, such as Green Fluorescent Protein (GFP) from *Aequorea victoria*, or jellyfish, and Discosoma Red (DsRed) from coral contain an intrinsic fluorescence with their own chromophores formed during folding and have a β -can structure that is different from CD2, which is an Ig-fold. We hypothesize that fluorescent proteins with different calcium binding affinity and strong selectivity can be successfully designed using our design approach. In addition, we hypothesize that a calcium binding site engineered into the chromophore sensitive locations could provide a change in the fluorescence of the chromophore upon binding (Fig 1.11) thereby allowing for observation of calcium inside living cells. Our approach is to design a calcium-binding site in a fluorescent protein so that a change in fluorescence will be observed upon calcium binding.

The design process to engineer a calcium-binding site into a non-calcium-binding protein incorporates current knowledge about natural calcium-binding proteins, including continuous (EF-hand type) and discontinuous calcium-binding sites as discussed in section 1.7. Computer programs were initially utilized to identify possible binding sites. The output sites were evaluated and possible sites were chosen based on our established criteria. Several sites were examined for metal binding properties, structure, expression in mammalian cells, and calcium response in mammalian cells. The most promising sites were chosen for further study.

1.9 The Objective of this Dissertation

In this dissertation, several studies on the design of calcium sensors using a small molecule dye and designed calcium binding proteins will be discussed.

Chapter 2 discusses the materials and methods utilized in the progress of this dissertation. The molecular biology to obtain the mutated DNA is detailed. Expression and purification of the designed proteins, along with differences between fluorescent and non-fluorescent designed proteins, are described. Structural and metal binding analysis protocols are given in detail. Mammalian cell expression and calcium response measurements are also illustrated.

Chapter 3 discusses the near infrared calcium binding dye synthesized by Dr. Christian Mason and studied by this researcher. The metal binding analysis of the dye is detailed.

Chapter 4 discusses the design process of the variants, including the criteria for evaluating the sites. The mutagenesis, expression, and purification are described and discussed. The biophysical analysis and metal binding studies of the designed proteins are also described and discussed.

Chapter 5 communicates the mammalian screening of the designed proteins and details the discovery of the Site 177's fluorescence in HeLa cells. The calcium response and optimization studies of Site 177 are discussed. The production of a brighter sensor containing the 177 binding site is detailed.

Chapter 6 describes the second generation of designed sensors chosen after the lessons observed from the first generation. The new criteria utilized in selecting the

new sites are discussed. The molecular biology, screening, and calcium response in the cytosol and in the ER are detailed.

Chapter 7 is a summary of all of the work detailed in this dissertation since the work is varied in its designation. The chapter endeavors to bring together the knowledge gleaned from this work.

1.10 The Significance of this Dissertation

The significance of this work is several fold. First, the process of designing calcium binding sites in GFP will provide further knowledge on the key factors of calcium binding and will demonstrate that our design process can be utilized in a multitude of proteins. The ability to understand the intricate properties of calcium binding and calcium dependent processes would provide insights into the molecular basis of diseases related to improper binding of calcium. Second, applying our design approach to the creation of a calcium sensor eliminates many of the drawbacks for the currently available sensors. The designed sensors will not be FRET based and will report calcium binding by a change in the intrinsic fluorescence of the host protein. With a single site designed into the protein, there will be no interference from endogenous proteins. In addition, the single site will allow for easier and quicker data analysis as it will directly report calcium changes in each part of the cell and not rely on binding to target molecules. Also, the designed sensors can be targeted to different locations in the cell, such as the ER, where the study of calcium handling is essential. Third, our study will contribute to the knowledge of the chromophore formation of fluorescent proteins, such as GFP and DsRed, by demonstrating the amino acids necessary for

proper formation. In addition, the comparison of optical properties of EGFP variants expressed in bacterial systems versus protein expressed in mammalian systems will generate knowledge on the protein folding pathway and the environment necessary for proper chromophore formation. Fourth, this work will further our ability to design calcium binding proteins to control their function.

Chapter 2 Materials and Methods

2.1 Near Infrared Calcium-binding Dye 15C5-774

2.1.1 Synthesis

The synthesis was performed by Dr. Christian Mason at Georgia State University. All reagents were obtained from Aldrich. A solution of IR-786 Iodide (550 mg, 0.9 mmol) and 4-aminobenzo-15-crown-5 (270 mg, 0.95 mmol) in anhydrous *N,N*-dimethylformamide (10 ml) was heated to 140 °C for 2 h under nitrogen atmosphere. After cooling, the solution was stirred and treated dropwise with aqueous tetrafluoroboric acid (24%, 2 ml), which caused crystallization of the complex 3 (15C5-774)·2HBF₄. The crystalline precipitate was filtered and washed with water. Crystallization from an acetone/methanol mixture by addition of tetrafluoroboric acid followed by filtration, washing with water and then ethyl ether, and drying at 70 °C/1.0 mmHg gave an analytically pure product: yield 500 mg (63%); mp>200 °C (decomp.); ¹H NMR (dimethyl sulfoxide-d₆/tetramethylsilane, 400 MHz, 30 °C) δ 1.68 (s, H), 1.88 (t, *J*=6 Hz, 2H), 2.73 (t, *J*=6 Hz, 2H), 2.88 (t, *J*=6 Hz, 2H), 3.37 (s, 6H), 3.65 (m, 6H), 3.85 (m, 4H), 3.90 (m, 4H), 4.20 (m, 4H), 4.28 (m, 4H), 5.69 (d, *J*=12 Hz, 2H), 7.01 (t, *J*=7 Hz, 2H), 7.07 (d, *J*=7 Hz, 2H), 7.27 (t, *J*=7 Hz, 2H), 7.40 (t, *J*=7 Hz, 2H), 7.42 (d, *J*=8 Hz, 2H), 7.78 (d, *J*=12 Hz, 2H), 8.25 (s, 1H); ¹³C NMR (dimethyl sulfoxide-d₆, 100 MHz, 30 °C) δ 20.9, 25.6, 27.3, 28.1, 28.9, 29.6, 31.4, 46.8, 68.2, 68.3, 68.7, 69.4, 70.6, 94.0, 99.9, 101.8, 107.2, 108.2, 111.3, 116.0, 121.0, 121.5, 121.7, 122.3, 125.1, 126.0, 127.9, 128.5, 130.5, 134.4, 134.5, 138.2, 139.5, 140.9, 142.7, 142.8, 143.7, 148.7, 148.9, 153.7, 165.5, 172.6; Vis-NIR (methanol:Tris [20:80 v/v] pH 7.4) λ_{max}=774 nm (ε=42 600

$\text{M}^{-1} \text{cm}^{-1}$), which varies with pH changes. Analysis, calculated for

$3(\text{C}_{46}\text{H}_{56}\text{BF}_4\text{N}_3\text{O}_5) \cdot 2\text{HBF}_4$: C, 63.05; H, 6.52; N, 4.79. Found: C, 63.31; H, 6.28; N, 4.64.

2.1.2 Absorbance analysis

All absorbance measurements were taken on a Shimadzu UV-1601 spectrophotometer interfaced to a PC operating under Windows 98. The data analysis was performed using Microsoft Excel 2000 and KaleidaGraph 3.0. All chemicals used were ACS grade reagents. All metals tested were in the chloride salt form. The titrations were performed with stock solutions of 15C5-774 containing varying concentrations of metal in 20% MeOH and buffered with 10 mM Tris. The Tris buffer was chelexed with Bio-Rad Laboratories Chelex 100 Resin and adjusted to pH 7.4 with HCl. The pH was measured with a Beckman 360 pH meter by removing 1 ml increments and measuring with a small electrode. A stock solution of 15C5-774 in 100% MeOH was made by dissolving 1.2 mg of dye in 5 ml of MeOH for a concentration of $\sim 275 \mu\text{M}$.

2.1.3. Metal titrations

First, stock solutions of metal in Tris buffer were made through serial dilutions from 1 M to 1 mM. Then 1 ml dye/metal stock solutions containing a constant $19.52 \mu\text{M}$ dye concentration (using $275 \mu\text{M}$ stock dye in MeOH) and various metal concentrations (using stock metal in Tris) were made with the Tris/MeOH buffer. A zero point was made with dye, Tris, and MeOH (no metal) at the same concentration as the 1 ml stocks, and its absorbance was recorded. A certain volume was removed from the cuvette and placed in the waste container. The same volume of one of the dye/metal

stock solutions was placed into the cuvette. After mixing well, the absorbance of the dye at that metal concentration was recorded. These steps were repeated until saturation was reached. Depending on the metal being tested, saturation was reached at about 400 μM –60 mM.

2.1.4 Data analysis

The metal concentration at each point was calculated using Eq 2.1:

$$[\text{metal}] = \frac{(V_{LC} * M_C) + (V_A * M_S)}{V_T}$$

where V_{LC} is the volume left in the cuvette after removal of the exchange volume, M_C is the molarity of the volume in the cuvette, V_A is the volume added to the cuvette, M_S is the molarity of the stock solution of the volume added, and V_T is the total volume in the cuvette after the volumes are exchanged (normally 1 ml).

The K_d values were calculated by creating a scatter plot of the fractional change versus the metal concentration. Fractional change is given in the Eq 2.2:

$$F = \frac{A_p - A_0}{A_{\max} - A_0}$$

where A_p is the absorbance of that data point, A_0 is the absorbance of the zero point, and A_{\max} is the absorbance at the most saturated point. The fractional change was then fit with a curve using the Eq 2.3, which assumes a 1:1 metal:chelate complex:

$$F = \frac{([P]_T + [M]_T + K_d) - \sqrt{([P]_T + [M]_T + K_d)^2 - 4[P]_T[M]_T}}{2[P]_T}$$

where $[D]_T$ is the total dye concentration, $[M]_T$ is the total metal concentration, and K_d is the dissociation constant of the reaction. When this equation is input into KaleidaGraph, the K_d is graphically estimated and can be adjusted as necessary to achieve the best result.

2.1.5 pH dependence

For the pH dependence studies, the pH of Tris for the lower pH work was adjusted to 6 with HCl. For the higher pH study, new Tris buffer was prepared, treated with Chelex-100 resin to remove background calcium, and left at pH 8.7. The stock metal solutions for calcium and magnesium were made with this Tris buffer in 1 ml volumes using serial dilutions. The sample solutions were made with these metal solutions. An additional zero point (without metal) was made to test the initial pH. The pH of the titrated solution was tested after the titrations were complete.

2.2 Site-directed Mutagenesis

Site-directed mutagenesis of the designed proteins was carried out utilizing polymerase chain reaction. All primers were designed in-house and purchased from Sigma-Genosys or Operon. The primers were reconstituted in EB buffer (10 mM Tris, pH 8.5) and phosphorylated according to the manufacturer's protocol for T4 PNK (phosphonucleotide kinase) (Promega). PCR was carried out with a MJ Research (without heated lid) or Techne (with heated lid) thermocycler. Reactions carried out in the MJ Research thermocycler were topped with a drop of mineral oil to prevent evaporation. The polymerase employed was either cloned *pfu* or turbo *pfu* (Invitrogen), and the PCR was completed following the manufacturer's protocols. The primers are

listed in table 2.1 for the first generation and table 2.2 for the second generation of designed sensors. Following PCR, the DNA was separated on a 0.8% agarose gel and extracted from the gel using a Qiagen gel extraction kit. The linear DNA was then ligated with T4 DNA ligase (Promega) following the manufacturer's instructions for 22 hrs at 4 °C with the addition of approximately 3 mM ATP to provide energy for the reaction. The circular DNA was transformed into *E. coli* (either DH5 α or Top10) competent cells and plated on Luria-Bertani plates with the appropriate antibiotic for the host vector, usually ampicillin. Several colonies from the plate were grown overnight at 37 °C with agitation in 10 mL LB-antibiotic, and the DNA was purified with either a Qiagen Miniprep kit or an Eppendorf Fast Plasmid Mini kit. The DNA was then sequenced at the core facility at GSU.

2.3 Competent Cell Preparation

E. coli cells are made chemically competent with calcium chloride. A fresh LB no antibiotic plate is quadrant streaked with glycerol stocks of *E. coli* cells and allowed to grow overnight at 37 °C. A single colony is inoculated into 10 mL of LB (no antibiotic) and grown overnight at 37 °C. The overnight growth is transferred into fresh LB (no antibiotic) in a 100x dilution into 200 or 400 mL of media and allowed to grow to an optical density of 0.5. Samples are taken near the flame. The cells are then centrifuged at 3K for 5 min after balancing near the flame in a previously autoclaved 500 mL Oakridge centrifuge bottle. The supernatant is discarded and the pellet is resuspended in 100 mM CaCl₂ by gently swirling (previously autoclaved). If the cells are grown in

Table 2.1 The primers utilized to engineer the first generation of designed proteins.

Designed Protein	Mutation(s)	Primer Name	Primer Sequence
120	V120N, R122D, K113D	EGFP120FOR EGFP120BACK	GACACCCTGA <u>AACAACGAC</u> ATCGAGCTG GCCCTCGAAGTCCACCTCGGCG
120b	V120N, R122D, L15N	EGFP120FOR 120_122BACK 15FORW 15BACK	GACACCCTGA <u>AACAACGAC</u> ATCGAGCTG GCCCTCGAACTTCACCTCGG GTGCCCATCAATGTCTGAGCTGGTC CACCCCGGTGAACAGCTCCTC
177	I171D, S175D, V176A, Q177N	EGFP177FOR EGFP177BACK	ACGGC <u>GACGCGAAC</u> CTCGCCGACC CCTCGT <u>CGTTGTGG</u> CGGATCTTG
194a	L194N, K79D, K85D	194FORW 194BACK 79_85FORW 79_85BACK	GGCCCCGTGAATCTGCCCCGAC GTCGCCGATGGGGGTGTTCT GACTTCTTCGATTCCGCCATGCCC GTGCTGATCCATGTGGTCGGGGT
194b	L194N, K79D, S86D	194FORW 194BACK 79_86FORW 79_85BACK	GGCCCCGTGAATCTGCCCCGAC GTCGCCGATGGGGGTGTTCT GACTTCTTCAAGGACGCCATGCC GTGCTGATCCATGTGGTCGGGGT
229	M78N, H81D H199D	78_81FORW 78_81BACK 199FORW 199BACK	GACCACAATAAGCAGGACGACTTCTTC GGGGTAGCGGCTGAAGCACTG CCCGACAACGACTACCTGAGCAC CAGCAGCACGGGGCCGTCG
	I229D	229FORW 229BACK	GCCGCCGGGGGACACTCTCGG GGTCACGAACTCCAGCAGG

Table 2.2 The primers utilized to engineer the second generation of designed proteins.

Designed Protein	Mutation(s)	Primer Name	Primer Sequence
Site 1	L194E	L194E_FORW	GGCCCCGTGG <u>GAG</u> CTGCCCCGAC
		L194E_BACK	GTCGCCGATGGGGGTGTTCTG
	S2D	S2D_FORW	CTAGAATGGTGG <u>ACA</u> AAGGGCGAGG
		S2D_BACK	AGGGCCCGGATCCGAGCTCG
	L15D,	L15D_FORW	GTGCCCATCG <u>ACG</u> TCGAGCTGGAC
		L15D_BACK	CACCCCGGTGAACAGCTCCTC
Site 2	R122E,	R122E_V120S_FORW	GACACCCTGT <u>CGA</u> AC <u>GAG</u> ATCGAGCTG
	V120S	R122E_V120S_BACK	GCCCTCGAACTTCACCTCGGC
Site 3	F83D	F83D_FORW	CAGCACGACG <u>ACT</u> TCAAGTCCGC
		F83D_BACK	CTTCATGTGGTCGGGGTCGCG
	I152E,	152_154_161_FORW	CAGAAGAACGGCG <u>ACA</u> AAGGCGAAC
	A154D,	152_154_161_BACK	<i>CTTGTC</i> <u>GTCCGT</u> <u>GTC</u> ATAGACGTTG
	I161D		

Designed Protein	Mutation(s)	Primer Name	Primer Sequence
Site 4	T59D	T59D_FORW	CCCTGGCCCC <u>GAC</u> CTCGTGACC
		T59D_BACK	CACGGGCAGCTTGCCGGTGG
	I136S, L141N	136_141_FORW	CACAAGA <u>AAC</u> GAGTACAACACTACAACAGC
		136_141_BACK	CCCCAGGG <u>AGT</u> TGCCGTCCTCC
	Q177E	Q177E_FORW	GGCAGCGTG <u>GAG</u> CTCGCCGAC
		Q177E_BACK	GTCCTCGATGTTGTGGCGGATC
	F100E	F100E_FORW	CACCATCTCC <u>GAG</u> AAGGACGACGG
		F100E_BACK	CGCTCCTGGACGTAGCCTTGG
Site 5	L7D, V12N	L7D_V12N_FORW	GGGTGA <u>AAC</u> CCCATCCTGGTCGAG
		L7D_V12N_BACK	CGGTGAAGT <u>CCT</u> CCTCGCCCTTGC
	F114D, L119E	F114D_L119E_FORW	GACACCG <u>AGG</u> TGAACCGCATCGAG
		F114D_L119E_BACK	GCCCTC <u>GTC</u> CTTCACCTCGGCG
	M88S	M88S_FORW	CAAGTCCGCCT <u>CGC</u> CCCGAAGGC
		M88S_BACK	AAGAAGTCGTGCTGCTTCATGTG
Site 6	M88T	M88T_FORW	CAAGTCCGCC <u>ACG</u> CCCGAAGG
		M88S_BACK	AAGAAGTCGTGCTGCTTCATGTG

400 mL of media, 24 mL of CaCl_2 should be used. The cells are then incubated on ice for at least 30 min. The cells are centrifuged at 5.5K for 7 min and the supernatant is discarded. The pellet is resuspended in cold 100 mM CaCl_2 (5 mL for 400 mL of growth) and 15% glycerol (previously autoclaved) by gentle swirling. The cells are then aliquotted into autoclaved 1.7 mL centrifuge tubes and stored at -80°C for later use.

2.4 Incorporating EGFP Gene in Different Vectors

For expression of the proteins in *E. coli*, the DNA was subcloned into the pet28a vector, which contains a kanamycin resistance gene and a multiple restriction site. The DNA and the vector were digested for 3-4 hrs at 37°C with *Bam*HI and *Eco*RI enzymes following the manufacturer's suggestions. After digestion, the DNA was separated on a 0.8% agarose gel and purified with a Qiagen gel extraction kit. The desired gene was then ligated to the vector with T4 DNA ligase as detailed above. The DNA was transformed into DH5 α competent cells and allowed to grow in LB medium at 37°C overnight. Individual colonies were grown in 10 mL LB-ampicillin (100 $\mu\text{g/mL}$) overnight, and the DNA was purified with the Qiagen Miniprep kit. All subclones were verified by automated sequencing at the core facility at GSU. For expression in mammalian cells, the DNA was subcloned into pcDNA3.1+ in the same manner as the pet28a subclone.

2.5 Expression and Purification of Histidine tagged GFP

2.5.1 Expression of GFP and the variants

The DNA was transformed into BL21(DE3) and plated on LB-kanamycin (30 $\mu\text{g/mL}$ kanamycin) plates. Single colonies were inoculated in 10 mL LB-kan overnight

at 37 °C with agitation. The overnight inoculum was transferred into 1 L of fresh LB-kan and allowed to grow to an OD₆₀₀ of 0.6. The growth was then induced with 0.2 mM IPTG and allowed to grow for 3-4 hr. The cells were harvested by centrifugation at 7K for 20 min. The cell pellets were stored at –20 °C and retained for purification.

After expression, the fluorescence of GFP and the variants was measured with a Fluostar Microplate Reader. This instrument allows insertion of a microplate containing samples and provides a readout of the fluorescence intensity. Samples (1 mL) of the expression were taken at 1 hr intervals up to 3 hr. For overnight growths, samples were also taken the following morning. The bacteria were pelleted at 14 K rpm, and the media was removed. The pellet was resuspended in 200-400 µL of 10 mM Tris, pH 7.4. the cells were then added to the Corning 96 well plate with 10 mM Tris, pH 7.4 as the background. The fluorescence was then monitored by the Fluostar. To begin with the Fluostar instrument, double click the “Fluo32” shortcut on the desktop. Click Run. Go to **Test Setup** on the menu and click **Layout**. Click Create Layout. Click **New**, choose 96 well plate, enter a *name*. Select cells for samples. Choose standard, blank, and samples to be tested from the drop down menu on the left, then click in the grid on the right at the appropriate place. For example, if the standard is in the top left well, select standard from the drop down menu and then click in the top left cell—the program will highlight that cell and label it accordingly. Click **OK** when finished. Go to **Test Setup** on the menu and click **Tests**. Click **New**, well mode, select microplate brand—we use Corning, 96. Click **Layout**, enter the excitation and emission filters of your choice, the

other factors do not need to be changed. Click **OK** twice. To insert the plate into the instrument, click **plate out** on the menu buttons at the top of the screen. The plate holder will eject, place the plate into the holder. Click **plate in** on the menu buttons. Click **Measure** on the menu buttons (looks like a stop light). Choose the profile you made from the tests list. Click **Plate ID**, type a *filename*. Click **Gain**. Select the entire grid or select the highest fluorescence sample, click **well adjustment**—the machine will measure for the gain and make the adjustments. Click **OK**. Click **Start**. When the measurement is finished, usually about 1 min, go to **Results** on the menu and choose **Excel**. The software will export your results to Excel. In Excel, double click on the *filename* you entered. Click **Update**. Choose the **Evaluation** spreadsheet at the bottom. Delete the last table that is filled with #DIV. The results will be displayed as raw data and as corrected with the blank, copy the spreadsheet into a new workbook to save. The spreadsheet can also be printed at this point.

2.5.2 Purification of GFP and the variants

For purification, a 5 mL nickel chelating column connected to a FPLC was utilized. The FPLC was first prepared by washing the Ni^{2+} column with water for 15-20 min to remove any storage solvent. The column was then loaded with Ni^{2+} by washing with 0.1 M Ni^{2+} for 5-10 min. The column was then washed again with water to remove any unbound nickel, and the column was equilibrated with Buffer A (50 mM PO_4 , 250 mM NaCl, pH 7.4) for 10-15 min. The cell pellet was resuspended in 10 mL of lysis buffer (20 mM Tris, 100 mM NaCl, 0.1% Triton X-100, pH 8.0) and sonicated to break the cell membrane. The sonication was separated by centrifugation at 17K for 30 min,

and the supernatant was collected. The supernatant was filtered and injected into the previously prepared FPLC. Generally, 3 or 4 mL of the supernatant was injected for each wash cycle. The protein was allowed to bind to the column and washed with Buffer A until the absorbance returned to baseline. Injections and wash cycles were repeated until all protein was loaded onto the column. The protein was eluted with a gradient of imidazole in phosphate buffer (Buffer A plus 0.5 M imidazole) with a gradient method. GFP usually eluted at ~250 mM imidazole, and fractions in this range were collected in 4 or 8 mL portions. The purity of the fractions were verified by SDS-PAGE, and the pellet after sonication was checked for remaining protein by SDS-PAGE. The programs for the FPLC are listed in table 2.3.

Fractions containing imidazole were combined and dialyzed into 10 mM Tris, 1 mM DTT, 1% glycerol. The protein's concentration was measured by UV/vis absorbance at 280 nm using Beer's Law ($A = \epsilon cl$) and an extinction coefficient calculated for EGFP ($5690 \cdot \#Trp + 1280 \cdot \#Tyr$) of $21,890 \text{ M}^{-1} \text{ cm}^{-1}$. All protein was stored with 1% glycerol at 4 °C on ice or in 20% glycerol at -20 °C.

In the case of several of the designed variants, the insoluble protein after sonication was solubilized with 8 M urea. The solution was diluted 10x into buffer and centrifuged to remove cellular debris. The supernatant was injected into an FPLC joined to a size exclusion column to remove undesirable proteins (10 mM Tris, pH 7.3), and the fractions were analyzed by SDS-PAGE for purity and presence of the desired protein.

Table 2.3 FPLC programs for his-tagged protein purification. B is buffer B.

Program 6		Program 7	
Break	Conditions	Break	Conditions
Point		Point	
0.0	0% B	0.0	0% B
	Flow Rate = 5 mL/min		Flow Rate = 5 mL/min
	Fraction Size = 0 mL		Fraction Size = 8 mL
	Buffer Valve Position = Pos1		Buffer Valve Position =
			Pos1
	Inject Valve Position = Load		Inject Valve Position = Load
	Set Peak Collect = no		Set Peak Collect = no
	Autozero = no		Autozero = no
	Event Mark = no		Event Mark = no
10.0	Autozero = yes	1.0	10% B
11.0	Inject Valve Position = Inject	3.0	10% B
	Autozero = yes	40.0	100% B
13.0	Inject Valve Position = Load		Fraction Size = 0 mL
73.0	End Method	42.0	100% B
		45.0	0% B
			End Method

2.6 Hitrap Q Purification

To further purify the protein, a Hitrap Q anion exchange column was employed. Before use, the column was equilibrated with 5 column volumes (25 mL) of start buffer (20 mM Tris, pH 8.0), 5 column volumes of elution buffer (20 mM Tris, 1 M NaCl, pH 8.0), and then 5 column volumes of start buffer. The initial injection sample was diluted with start buffer. Protein was continually injected into the column and the column was washed with start buffer to remove contaminating proteins until all protein was bound to the column or the column was completely colored with protein. The protein was then eluted with a gradient of elution buffer. EGFP usually eluted at ~400 mM NaCl. The column was then washed with 100% elution buffer to remove any remaining contaminants. The column was washed with start buffer and ddH₂O before storage. The further purified protein was concentrated down in 20% glycerol with the Amicon pressure concentrator and dialyzed against 10 mM Tris, 1 mM DTT to exchange buffer and remove salt. The protein was then stored in 20% glycerol at -20 °C in aliquots of 1 mL. The protein's concentration was measured by UV/vis absorbance (after dialyzing and adding 20% glycerol) at 280 nm using Beer's Law ($A = \epsilon cl$) and an extinction coefficient of 21,890 M⁻¹ cm⁻¹.

2.7 Protein Refolding with Urea

The cell pellet was thawed and 8 M urea was added in small increments (one mL or less) to the cell pellet until the pellet dissolved. Once the pellet was dissolved, the mixture was 10x diluted into the appropriate buffer (Tris usually) with dropwise additions

of the mixture into the buffer while stirring. Once all of the urea/cell pellet was added to the buffer, the mixture was centrifuged for 15-20 mins at 17 K to separate the solubilized protein from the cell parts and insoluble proteins. The supernatant and pellet were collected and analyzed on SDS-PAGE. The supernatant was dialyzed in a 3 KDa dialysis membrane in a large volume of buffer overnight at 4 °C to remove the urea.

2.8 Circular Dichroism of Variant Proteins

Far UV circular dichroism (CD) of wild type and variant proteins was performed on a Jasco 810 spectropolarimeter equipped with a Peltier temperature control unit and connected to a PC. All measurements were performed with a cell pathlength of 1 mm, either 50 or 100 nm/min scan speed, and four accumulations. The protein concentration was 10 or 15 μ M, and the buffer for metal binding studies was 10 mM Tris, 1 mM DTT, 1% glycerol, pH 7.4. The buffer for pH dependence without calcium was 20 mM phosphate, 1 mM DTT, 1% glycerol. The buffers for pH dependence with calcium were acetate or citrate, MES, PIPES, and Tris and all contained 1 mM DTT and 1% glycerol.

2.9 Thermal Denaturation of Designed Proteins by Circular Dichroism

The thermal stability of the designed proteins was measured by Far-UV CD from 260 nm to 200 nm in the temperature range of 10-100 °C with 5 °C increments. The samples were made with 10 μ M of protein and with either 1 mM EGTA or 1 mM calcium in 10 mM Tris, 1 mM DTT, 1% glycerol, pH 7.4. The 1 mm pathlength rectangular cell was used, which holds 300 μ L of sample, and was closed with parafilm during the

operation. The signal was monitored at 216 nm with 600 sec (10 min) between each temperature to equilibrate at that temperature. The scan speed was 50 nm/min. A scan of the entire spectrum was recorded at each temperature.

2.10 GFP Fluorescence Spectroscopy

Fluorescence studies were performed on a Photon Technologies, Inc. Lifetime Fluorimeter. All terbium fluorescence experiments utilized an excitation of 280 nm, excitation slit widths of 8 nm, and emission slit widths of 12 nm. The emission was scanned from 500 nm to 600 nm with the monitored peak at 545 nm. A glass plate filtered the second order scattering at 560 nm.

GFP fluorescence was monitored from 500 nm to 600 nm with the excitation at 488 nm, 482 nm, or 398 nm, depending on the variant protein. Trp fluorescence of the GFP variants was monitored with excitation at 280 nm and emission between 300 and 400 nm. The slit widths were adjusted as necessary for the proper intensity range.

2.11 Measuring Metal Effects on Histidine Tagged Proteins

The fluorescence of the protein (1 μ M) was monitored with and without metal on a PTI Lifetime fluorimeter. The excitation was 482 nm, and the emission from 490 to 570 nm was recorded. Titrations were performed by keeping the protein concentration constant and increasing the metal concentration until the signal no longer changed. The metal binding affinities were calculated assuming a 1:1 protein:metal ratio using equation 2.3 shown in section 2.4.1.

2.12 Metal Binding Analysis

To analyze the data by Specfit/32, the data must first be prepared in a text spreadsheet in the proper setup for Specfit/32 to read. The spreadsheets were prepared in Microsoft Excel and saved as *.txt files for import into Specfit/32. For terbium binding to a single site protein, the components included in the spreadsheet are total metal concentration and total protein concentration at each titration point. For competition between a protein and another chelator for metal, the components are the total metal concentration, the total protein concentration, and the total chelate concentration (such as a dye). An example of a multicomponent titration spreadsheet is shown in table 2.4. Nm stands for number of measurements (13 in this case and must be included in the left column next to each component concentration), Nw for number of wavelengths (for example 500 nm to 600 nm is Nw = 100), and Nc for number of components. The model 1 is for ligand binding. The three rows below that information are the metal concentration, protein concentration, and the dye concentration. The $[H^+]$ row is the hydronium ion concentration, which is the inverse log of the pH. The titration spectra are then copied below the $[H^+]$ row with the wavelengths in the leftmost column and each spectra beneath the appropriate titration point. A note of caution should be made here that any errors in the spreadsheet (typographical or otherwise) will result in errors in the binding affinity calculation. Be very careful to examine the spreadsheet before proceeding to Specfit/32.

Table 2.4 An example of the spreadsheet imported into Specfit/32 to obtain the protein K_d from the dye competition assay. The rows continue to the end of the wavelengths measured, and the columns continue to the right for the number of data points (i.e. metal concentrations). Nm stands for number of measurements, Nw for number of wavelengths, and Nc for number of components. The model 1 is for ligand binding. The three rows below that information are the metal concentration, protein concentration, and the dye concentration. The $[H^+]$ row is the hydronium ion concentration, which is the inverse log of the pH.

NAME							
X/Z Mode	Nm	Nw	Nc	Model	X-axis	Y-axis	Z-axis
1	13	91	3	1	0	2	0
13	0.00E+0	4.88E-06	1.45E-05	2.86E-05	4.67E-05	7.27E-05	1.05E-04
13	3.96E-05	3.96E-05	3.96E-05	3.96E-05	3.96E-05	3.96E-05	3.96E-05
13	2.59E-05	2.59E-05	2.59E-05	2.59E-05	2.59E-05	2.59E-05	2.59E-05
$[H^+]$ =	6.31E-08	6.31E-08	6.31E-08	6.31E-08	6.31E-08	6.31E-08	6.31E-08
560	3312.9	7045.1	13345	24315	32706	49273	5.90E+04
561	3601.4	7808.1	15213	26894	36771	5.41E+04	6.49E+04
562	4196.7	8655.8	17036	29890	41427	6.04E+04	7.33E+04
563	4389.1	9351.1	18195	32547	4.48E+04	6.69E+04	8.00E+04
564	5090.9	10507	20147	36730	5.00E+04	7.40E+04	8.83E+04
565	5347.6	11320	21904	3.90E+04	5.40E+04	7.96E+04	9.63E+04
566	5833	12537	23750	4.25E+04	5.79E+04	8.68E+04	1.04E+05
567	6134	13242	25638	4.61E+04	6.32E+04	9.35E+04	1.11E+05
568	6543.3	14153	27334	4.89E+04	6.74E+04	9.88E+04	1.20E+05
569	7085.3	14775	2.89E+04	5.10E+04	7.13E+04	1.03E+05	1.26E+05
570	7474.8	15586	3.00E+04	5.41E+04	7.45E+04	1.09E+05	1.33E+05
571	7527	16344	3.16E+04	5.66E+04	7.84E+04	1.16E+05	1.40E+05

To calculate the binding affinity of the titrated species, open Spefit/32 and click the menu choice "Import". Choose "Multiscan Data Files". A window will open to import the files. Select the appropriate file and click "Import Files" or simply double click on the desired file. Click "Exit". A graph of the data should appear. Select "Model" on the top menu and choose "M/L/H⁺ Complex". A new window will open to allow the user to input the appropriate information for the titration. An example of the window is shown in figure 2.1. The Species column includes all components present in the titration, free and bound, such as the free metal, free protein, and the metal:protein complex. For the inputs, 0 is no component, and 1 and higher is the number of components in that particular species. For example, a terbium:protein titration would include 100 for the metal free, 010 for the protein free, and 110 for the metal:protein complex. A dye competition assay with protein would include 1000 for metal free, 0100 for dye free, 0010 for protein free, 1100 for metal:dye complex, and 1010 for metal:protein complex. To add the necessary number of species by clicking "Add" on the bottom. To change the 0,1 for each species, click in the box for that species, click in the "M" or "L" box as appropriate and click the up and down arrows to change the number. The "Colored" column applies to the components that contribute to the measured spectra. The boxes should be checked for protein:terbium complexes, dye, or dye:metal complexes since these species contribute to the spectra. Leave "Known Spectra" blank. The "Fixed" column refers to the binding affinities in the Log(β) column. Single components or species are 0 in the Log(β) and are fixed. The box should be unchecked for the binding affinity being calculated. For competition assays, the known binding affinities should be

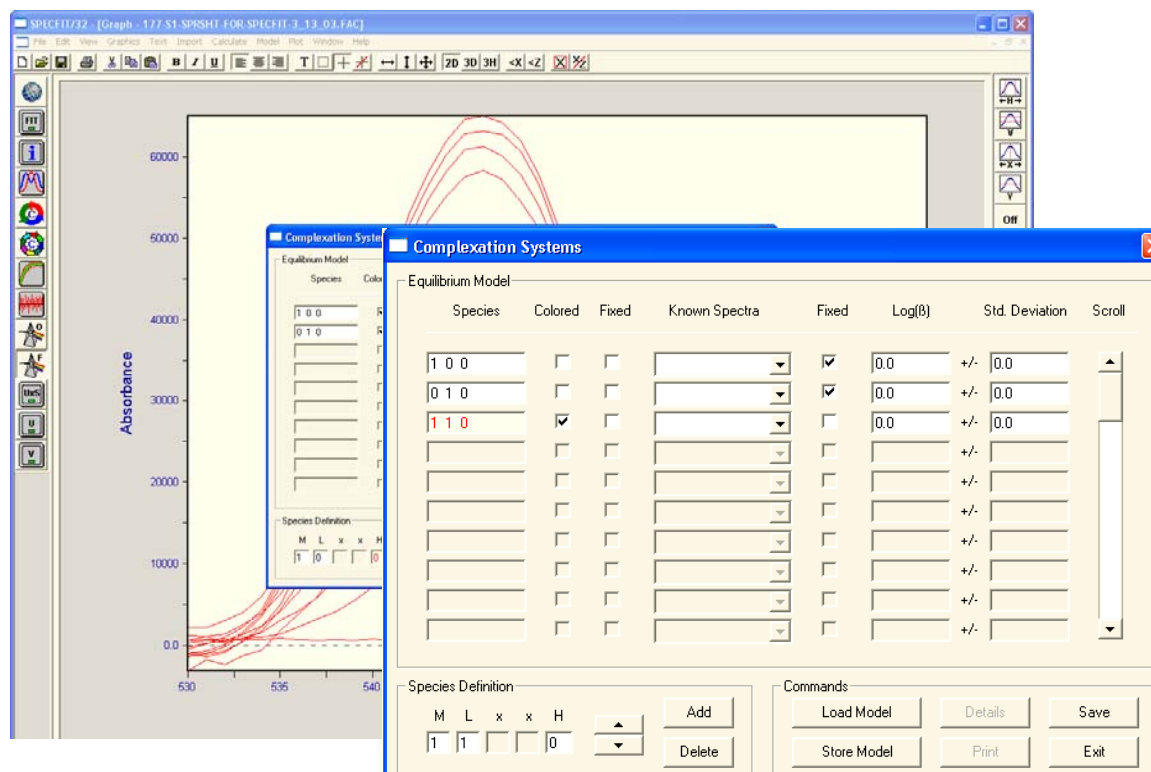


Fig 2.1 A screen capture of Specfit/32 is shown to illustrate the program's use in calculating binding affinities. The complexation systems model is utilized to calculate metal:ligand interactions, whether the ligand is protein or another molecule. The user inputs the appropriate components in the Species column. The case of terbium binding to a single binding site on a protein is illustrated in the blown up image of the Complexation Systems window. The panel of buttons on the left are for fitting the data (Fit) and viewing the fit after the fitting routine (Extract).

included with the fixed box checked. The affinity must be provided as the log K_a . To

convert from K_d , use the equation 2.4:

$$\log(\beta) = \log\left(\frac{1}{K_d}\right)$$

Click “Save”. The window will disappear. Click the “Fit” button on the left side. The number in the Log(β) box for the complex species in the binding affinity. However, the Log(β) actually equals log K_a . To convert to K_d , use the following equation 2.5:

$$K_d = \frac{1}{\text{inverse log of } K_a} = \frac{1}{10^{\log \beta}}$$

The results can be printed by clicking the “Print” button. Click “Exit”. Click the “Extract” button on the left to view the data fit. The fit can be saved as an ascii file for graphing in another program by choosing “File” and “Save As”, select the folder and type the filename. The file will be saved with a *.csv extension.

2.13 Terbium Binding Affinities for the Variant Proteins

An experiment was performed with Site 120 and Site 177 with constant terbium concentration (12 μ M) and increasing protein concentration. The buffer was 10 mM Tris, 1 mM DTT, 1% glycerol, pH 7.4, and the protein concentration was increased in increments of 2 up to 10 μ M. Terbium fluorescence was monitored with a spectra recorded at each protein concentration.

For terbium FRET titrations of 120, 177, and 194a, the beginning protein concentration was 3 μ M, and the buffer was 20 mM PIPES, 10 mM KCl, 1 mM DTT, 1% glycerol, pH 6.8. A 1.0 mM or 5.0 mM stock terbium containing the same concentration of protein was directly added into the protein samples during titration. Blank samples

were measured with buffer and increasing terbium at the same concentrations as the protein samples. The raw data was baseline corrected, and the integrated area was calculated for the peak of interest. The integrated area was utilized to calculate the dissociation constants. Also, the data was fit with Specfit/32, a global fitting program developed by Dr. Robert Binstead.

For site 194b, the above conditions were initially employed, but protein precipitation was observed. Other buffer conditions were attempted to retain solubility: 10 mM Tris, 1 mM DTT, 1% glycerol, pH 7.4 and 50 mM Tris, 1 mM DTT, 1% glycerol, pH 7.0. Also, lower protein concentrations of 1 and 1.5 μ M were tested. Also, a Hamilton automatic titrator was installed on the PTI fluorimeter during this time so it was utilized during the titrations. The cuvette volume was 2.5 mL of protein with stock terbium at 400 μ M or 1 mM (no protein) added in during the titration.

2.14 Protein-dye Calcium Competition

The samples for the protein-dye calcium competition were made by first making a stock solution of protein (30 or 40 μ M) and Rhodamine-5N (~20 μ M) in 10 mM Tris, 1 mM DTT, 1% glycerol, pH 7.4. An aliquot of 1 mL was taken from the stock and 10 μ L of 100 mM CaCl_2 was added. The solutions were allowed to equilibrate at 4 $^{\circ}\text{C}$ for 30 mins. To the fluorescence cells was added 1 mL of the protein-dye stock, and 10 μ L of buffer was added to dilute the samples by the same amount as the calcium solution. The fluorescence was then performed with a pathlength of 1 cm, excitation slit widths of 1 nm, and emission slit widths of 4 nm. The excitation was 552 nm, and the emission

was scanned from 560 to 650 nm. Volumes of the calcium-dye-protein stock were added and allowed to equilibrate for 10 mins. The spectrum was then taken for each calcium concentration. After the titration, the dye concentration was verified by visible absorbance at 552 nm with an extinction coefficient of $63,000 \text{ M}^{-1}\text{cm}^{-1}$ for calcium loaded Rhodamine-5N. The data was fit with the program Specfit/32.

2.15 Protein-Terbium Metal Competition

Sites 120 and 177 were investigated for metal binding by loading the protein (3 μM) with 50 μM of terbium and then adding 10 mM calcium, 10 mM magnesium, or 100 μM lanthanum. Site 177 was also monitored with additions of 100 μM , calcium 1 mM calcium, and 10 mM potassium. The samples were made in 10 mM Tris, 1 mM DTT, 1% glycerol, pH 7.4. The fluorescence was measured with excitation at 280 nm at slit widths of 8 and 12 nm for the excitation and emission, respectively, when measured on the PTI fluorimeter noted previously. Site 120 was measured on a newly obtained PTI fluorimeter (noted as PTI2) with slit widths of 6 nm for all.

The wild type EGFP was tested for calcium induced changes in the chromophore fluorescence by measuring the fluorescence in the presence and absence of 1 mM calcium. The protein concentration was 3 μM , and the buffer was 10 mM Tris, 1 mM DTT, 1% glycerol, pH 7.4. The excitation was 482 nm with excitation and emission slit widths of 2 nm.

2.16 pK_a Measurements of EGFP and EGFP Variants

To measure the chromophore pK_a of EGFP and the variant proteins, separate samples were made at each pH to be measured and the absorbance and fluorescence of the samples were examined. Various buffers were utilized to maintain the pH at each desired value, which are listed in table 2.5. DTT (1 mM) and 1% glycerol were added to each buffer prior to use. The stock buffers were made by Dr. Jin Zou in this laboratory for everyone's use with aliquots taken by each lab member. The protein concentration was ~10 μM for each mutant. The samples were allowed to equilibrate at 4 °C overnight. A baseline was run for each pH with the appropriate buffer before the sample at that pH was measured. The absorbance was measured from 600 nm to 200 nm so all protein peaks would be included. The cuvettes were cleaned between pH samples with 1% Liqui-nox to remove any protein. The pH was measured for each sample after the spectra were acquired.

For fluorescence, the samples for absorbance were diluted 10x (in duplicate) with the appropriate buffer for a final concentration of ~1 μM. One set of samples was maintained without calcium while 1 mM calcium was added to the other set. The samples were allowed to equilibrate overnight at 4 °C. The fluorescence was measured with the excitation at 482 nm, the excitation slit width at 1.5 nm, and the emission slit width at 2 nm. The emission was scanned from 490 to 570 nm. The sample at pH 9 was measured first so the slit widths could be set for optimal intensity, and the samples were measured with decreasing pH. The cuvettes were cleaned with 1% Liqui-nox

Table 2.5 A list of the buffers utilized for the pH dependence measurements.

Buffer	pH
0.5 M Acetate (CH_3COOH)	4.0
10 mM Acetate	4.5
10 mM MES (2-Morpholinoethanesulfonic acid)	5.0, 5.2, 5.7, 6.0
10 mM PIPES (1,4-Piperazinediethanesulfonic acid)	6.5, 7.0
10 mM Tris [Tris (hydroxymethyl) aminomethane]	7.4, 8.0, 8.5, 9.0

between samples. Separate cuvettes were used for the samples with and without calcium. The pH of each sample was measured after the spectra were obtained.

2.17 Quantum Yield Measurements of EGFP, L194N, and L15N

All protein was freshly purified before use. The protein samples were made in low concentrations (0, 0.4, 0.8, 1.2, 1.6, 2 μ M) as to avoid inner filter effects, and were made in duplicate in 10 mM Tris, 1 mM DTT, 1% glycerol, pH 7.4. Quartz fluorescence cells were utilized for both absorbance and fluorescence measurements. The UV/vis spectrometer was baselined with the buffer from 600 to 300 nm for EGFP and from 600 to 240 nm for the mutants. The fluorescence was measured with slit widths of 2 nm for the excitation and 1.5 nm for the emission with an excitation wavelength of 488 nm. The sample was then removed from the fluorimeter and the absorbance was immediately measured. This was repeated for all concentrations. The cells were washed with ddH_2O between samples.

The integrated area for the fluorescence spectra was calculated for each concentration and was then plot vs. the absorbance at 488 nm. The equation:

$$Q_x = Q_{ST} \left(\frac{\text{slope}_x}{\text{slope}_{ST}} \right) \left(\frac{\eta_x^2}{\eta_{ST}^2} \right)$$

with Q_x as the quantum yield of the sample, Q_{ST} as the quantum yield of the standard, the slope of the linear fit for the fluorescence integrated area vs. absorbance for the sample and the standard, and η as the solvent viscosity was utilized. Initially, the literature value for EGFP was treated as the standard and the EGFP samples were

cross-referenced with each other. The average value obtained in-house for EGFP was used in the calculations for the mutants.

The extinction coefficients for EGFP at 488 nm and for the mutants at 280 and 488 nm were calculated with the same data from the quantum yield measurements. The absorbance at the desired wavelength was plotted vs. the sample concentration (M) and a linear fit was obtained. The slope of the fit is equivalent to the extinction coefficient times the pathlength, which was 1 cm in this case.

2.18 Chromophore Reduction

The protein L194N/S86D was tested for chromophore reduction by adding β -mercaptoethanol or dithiothreitol (DTT) and monitoring the fluorescence changes. The protein (1 μ M) was incubated with 5%, 10%, 20%, 30%, and 50% β -mercaptoethanol for 30 mins at 4 °C with and without 1 and 10 mM calcium in 10 mM Tris, 1% glycerol, pH 7.4. DTT was also tested at 10 mM with and without 1 mM calcium. The fluorescence emission was monitored with excitation at 398 nm and at 488 nm with slit widths of 1 nm for all.

2.19 Mammalian Cell Culture

HeLa cells were obtained from Dr. Monica Lurtz in Dr. Charles Louis's laboratory. HEK293 cells were obtained from Dr. Zhi-ren Lui's laboratory. CHO cells were obtained from Dr. Ludmilla Pereglyna's laboratory. Vero cells were obtained from Dr. Teryl Frey's laboratory. All of these cells are adherent, and stocks are grown on 100 mm cell culture dishes. When confluence is reached (~95%), the cells are passaged and

allowed to continue to grow. The cells are passaged by removal of medium, wash with HBSS⁻ buffer, and addition of 1 mL of 1x trypsin. After the cells detach, the trypsin and cells are diluted with 9 mL of HBSS⁻. The cells are triturated ~10 times to fully suspend the cells. One to two mL is plated back, and the rest of the cells are discarded. Nine mL of fresh media is added to the plate and triturated ~5 times. The cells are placed back into the 37 °C incubator and allowed to grow with 5% CO₂ until they reach confluence again. The media for the HeLa cells is Dubelco's Modified Eagle's Medium (DMEM, Sigma) with 1 g/L glucose and L-glutamine, sodium bicarbonate, 10% fetal calf serum (FCS), and 1% Penicillin-streptomycin (Pen-strep or PS). The media for the HEK293 cells is the same as for the HeLa cells except the glucose is 4.5 g/L. The media for the CHO cells is Ham's F-12 with sodium bicarbonate, 10% FCS, and 1% Pen-strep. The media for the Vero cells is the same DMEM as for the HeLa cells. In general, the cells were passaged every 2-3 days.

To prepare the media for the HeLa cells, dissolve one bottle of DMEM (Sigma) with 1 g/L glucose and Glutamax in 800 mL of ddH₂O. Add 3.7 g of NaH(CO₃) (44 mM) and dissolve. Adjust the pH to 7.2 to 7.3 with 6 M HCl. Add the media to a graduated cylinder and bring to 1 L. Filter the media in the laminar flow hood with a Sterivex 0.22 µm filter into autoclaved glass bottles. Store at 4 °C. Before using the media for cell culture, add 50 mL Fetal Calf Serum (FCS) and 5 mL Penicillin-Streptomycin (Pen-Strep) to 500 mL of media.

To prepare the HBSS⁻ buffer, dissolve one bottle of Hank's Balanced Salt Solution without divalent cations in 800 mL of ddH₂O. Add 0.0238 g of HEPES (10 mM), 0.42 g of NaHCO₃ (5 mM), and 0.38 g (1 mM) EGTA. Dissolve all reagents and adjust the pH to 7.2 to 7.3 with 5 M NaOH. Add the solution to a graduated cylinder and bring to 1 L with ddH₂O. Filter the buffer with 0.22 µm Sterivex into autoclaved glass bottles and store at 4 °C.

To prepare HBSS⁺⁺ buffer, dissolve one bottle of Hank's Balanced Salt Solution with divalent cations in 800 mL of ddH₂O. Add 0.0238 g of HEPES (10 mM), 0.42 g of NaHCO₃ (5 mM), and 0.38 g (1 mM) EGTA. Dissolve all reagents and adjust the pH to 7.2 to 7.3 with 5 M NaOH. Add the solution to a graduated cylinder and bring to 1 L with ddH₂O. Filter the buffer with 0.22 µm Sterivex into autoclaved glass bottles and store at 4 °C.

2.20 Cryogenic Stock Preparation

Cryogenic stocks of the four cells lines were made by first trypsinizing the cells as usual to remove them from the plate. The cells were diluted to 10 mL with HBSS⁻ buffer and fully resuspended. The cells were collected in a 15 mL sterile centrifuge tube, and a 10 µL sample was taken to count the cells. The cells were centrifuged at 700 rpm for 5 min. The cells were counted on a hemacytometer under a microscope with a 10x objective. Once pelleted, the supernatant was removed from the cells and discarded. The cells were resuspended in enough cell-freezing medium (regular medium with 5% DMSO) for $2-5 \times 10^6$ cells/mL. Aliquots of 1 mL were made in

cryogenic vials. The vials were placed in an alcohol freezing box (1°C/min) and placed at –80 °C overnight. The vials were then transferred to a cryobox and let at –80 °C or were placed in a liquid nitrogen cryo tank for long-term storage. The liquid nitrogen is replenished approximately every 6 weeks since it evaporates over time.

2.21 Plate Preparation and Transfection of Sensor DNA

For transfections, the plates were prepared one or two days ahead of time. For confocal or inverted microscope imaging, 35 mm plates with glass coverslips were utilized and plated with $\sim 0.5 \times 10^6$ cells. For the transfection, the liposome (Lipofectamine2000, Invitrogen) was mixed with Opti-MEMI media and allowed to equilibrate for 5 mins at room temperature. The DNA (2 µg per plate) was mixed with Opti-MEMI. The DNA and liposome solutions were then mixed together (DNA:liposome 1:3) and allowed to equilibrate for 20 mins in the dark at room temperature. During this time, the plates were washed 2 times with 1-2 mL Opti-MEMI to remove serum. The DNA-liposome mixture was then added to the plates along with additional Opti-MEMI. The cells were incubated for 4-5 hr at 37 °C and 5% CO₂. The media was changed to fresh media and left at 30 °C for 48-72 hrs.

2.22 Fluorescence Imaging of Variant Proteins by Inverted Epifluorescence

A Zeiss Axiovert 200 inverted fluorescence microscope was employed to screen the mutants for fluorescence. For screening, plastic dishes were utilized and the 40x dry objective or the 20x dry objective was used for imaging. The cells were inspected with transmitted light and all three available filter sets, DAPI, FITC, and Texas Red. The

camera's exposure time was adjusted based on the brightness of the fluorophore.

Images were taken with the Zeiss Axiovision software, saved in the *.zvi format, and exported into *.jpg.

2.23 Calcium Response by Inverted Epifluorescence Microscopy

An inverted epifluorescence microscope (Zeiss Axiovert 200) was utilized for calcium response measurements *in vivo*. The microscope is equipped with a Xenon Arc Lamp, filters for DAPI, FITC, and Texas Red, and transmitted light. An Axiocam 5 CCD camera is connected to the microscope at a right angle to the stage. The microscope is connected to a computer with Zeiss Axiovision 4.0 software for data collection and analysis. The microscope is also equipped with 10x, 20x, and 40x dry objectives that contain correction collars for use with plastic. A Fluar Ph3 40x oil objective or a 100x Neofluar oil objective was utilized for calcium response measurements. Fields containing healthy, confluent, fluorescent cells were located by use of the binoculars. The software was then set to show live images through the camera, the shutter was turned to send 80% of the light to the camera, and the binoculars were turned off (to remove magnified room light). Images were obtained at appropriate exposure times for the sensor being imaged. The images were saved in both the Zeiss *.zvi format and in *.jpg for ease of use in other programs. For calcium imaging, a time series in black and white (smaller file sizes) was performed with 30 s intervals between images and 17-20 images were obtained. The fluorescence light was shuttered off between images so that the cells were only exposed to light during the image acquisition to decrease photobleaching. Three images were taken before any additions to establish a baseline.

Ionomycin (2 μ M, premixed in 100-200 μ L of HBSS⁺⁺) was added to the dish, and two images were taken. Calcium was then added in 10 mM or 20 mM increments (premixed in 100-200 μ L of buffer) to a total concentration of 60 mM, and images were taken after each addition. The data analysis was performed with the Axiovision software on the microscope computer or with the free version available from the Zeiss website in our laboratory. Regions of interest were drawn around each cell, and the intensity table was exported into Microsoft Excel for graphing. In Excel, the data was plotted with the intensity on the y axis and the time on the x axis. Comparable experiments were normalized, averaged, and error bars were plotted.

All calcium response experiments with the Nikon inverted epifluorescence microscope were performed by Dr. Monica Lurtz in Dr. Charles Louis's laboratory (University of California, Riverside). The coverslips containing the transfected cells were placed into a holder with 2 mL of HBSS⁺⁺ and onto the microscope stage. Transmitted and fluorescent light with a 40x or 100x oil immersion objective were utilized to locate a field with healthy, fluorescent cells, preferably with some confluency to maintain the cells' health during the experiment. Exposure times were adjusted for each fluorophore to obtain the maximum range of intensities for each image. In general, control experiments with EGFP utilized two neutral density filters and 40 ms exposure. Images for the calcium response experiments with the designed sensors underwent 40 ms exposure without the neutral density filters. The standard FITC filter with excitation at 490 nm and emission centered at 520 nm was utilized. Experiments

were performed with additions of 2 μ M ionomycin and three additions of 20 mM calcium by removing 0.5 mL to 1 mL of the bathing medium from the dish, mixing the reagent to be added with the bathing medium, and applying the mix to the dish. Stable baselines were obtained before and after the ionomycin addition to ensure no artifacts were detected. After calcium addition, the calcium was removed by washing with a semi-perfusion system back (a pump removed bathing medium while a pipet was utilized to add buffer to the dish) to 1.8 mM calcium (normal for HBSS⁺⁺) and the fluorescence decrease was recorded. After the calcium was reduced to buffer conditions, the calcium was again increased to monitor the fluorescence change. These experiments were performed multiple times (more than 8 plates) to ensure statistically relevant changes.

Other experiments were performed with addition of calmidazolium to block the calcium pumps and thapsigargin to empty the ER calcium stores. The ionomycin and calcium additions were then repeated under these conditions.

2.24 Calcium Response by Confocal Microscopy

To measure the fluorescence change *in vivo* when agonists were introduced for variant 177 when expressed in HeLa and HEK293 cells, a Zeiss inverted confocal microscope was employed (Core Facility, GSU). The microscope is equipped with UV, Argon, and He/Ne lasers. The Argon laser at high power (nearly maxed) was utilized to excite in the 488 nm region with the proper band pass filters to measure fluorescence at approximately 510 nm (FITC bandpass 505-530 nm) with a 100x oil immersion objective. The coverslip was placed into a holder with 2 mL of HBSS⁺⁺ and onto the

microscope stage. Transmitted and fluorescent light was utilized to locate fields that contained transfected, fluorescent, healthy cells. The laser power and Z-planes were adjusted to obtain the best image. Single images were taken of the field before the timecourse was performed. The timecourse was executed with 30 s intervals between scans to allow enough time for additions. Ionomycin (1-2 μM) was added after the first 2-4 scans and allowed to stabilize for 3-4 scans. Calcium in 10-20 mM concentrations was added 1-3 times and images were continually taken. The outside calcium was washed away by exchanging the buffer with HBSS⁺⁺. All experiments were performed several times to ensure reproducibility.

Once the images were obtained, the LSM510 software was utilized to quantitate the fluorescence change after addition of calcium by drawing regions of interest outlining the cells. The intensity at each time point was obtained and graphed vs. time. Microsoft Excel was utilized to graph and analyze the data.

2.25 Transfection of 177c3 for Suspension Growth in HeLa Cells

To transfect the HeLa cells to grow in suspension, 6 100 mm plates were grown to confluency. They were then transfected with the DNA to encode the 177c3 variant protein. The DNA (12 μg per plate) was mixed with Opti-MEM1, and the Liposome (Lipofectamine 2000, Invitrogen) was mixed with Opti-MEM1 in a 1:3 ratio with the DNA (36 μL per plate). The DNA-Opti and Lipofectamine-Opti was then mixed together and allowed to incubate at room temperature in the dark for 20 mins. The plates were washed with Opti-MEM1 two times to remove all traces of serum. The DNA-

Lipofectamine was then added to the plates along with 9 mL of fresh Opti-MEMI. The plates were incubated for 4 hrs at 37 °C with 5% CO₂. The transfection media was then removed, and the cells were harvested by trypsin treatment and centrifugation for 5 mins at 1000 rpm. The cells were resuspended in the MantaRay sterile, disposable bottle in 400 mL of fresh DMEM with 10% FCS and 1% PS. The cells were allowed to grow for 6 days at 30 °C in a non-CO₂ incubator with the MantaRay bottle placed on a stir plate. Fresh media was added each day to a total of 1 L.

2.26 Fluorescence of 177c3 after Expression in Suspension HeLa Cells

After 6 days, the 177c3 transfected HeLa cells were harvested by trypsin treatment and centrifugation. The cells were washed once with HBSS⁺⁺ and recentrifuged. The cells were then resuspended in 5 mL of 10 mM Tris, pH 7.4 by trituration. The cells were sonicated with 20 sec intervals six times. The solution was centrifuged at 17 K for 20 mins to separate the cell membrane from the supernatant. The supernatant was then examined by fluorescence spectroscopy.

One mL of the supernatant was placed into a 1 cm pathlength quartz fluorescence cuvette. The excitation was scanned from 300 to 500 nm with excitation slit widths of 4 nm and emission slit widths of 4 nm with the emission set to 510 nm. The emission was then scanned from 500 to 600 nm with the excitation at 450 nm, 469 nm, and 483 nm. Emission scans were performed with the excitation at 483 nm with several additions of 100 µM calcium until precipitation was observed.

Chapter 3 Study of a Near Infrared Calcium-binding Dye

3.1 Rationale for Development of Near Infrared Calcium Sensitive Dye

The measurement of intracellular calcium and other metal concentrations has benefited greatly by the development of dyes whose binding affinities correlate to the cellular environments (90-93). Currently, most of the commercially available dyes are either absorbance or fluorescence based indicators with optical activities in the ultraviolet or visible regions of the spectrum (32). For example, the commercially used dyes Fura-2 and Indo-1 are excited between 300 and 600 nm (92), and Calcium Crimson has the longest excitation wavelength of 593 nm (32). One of the challenges to be solved is the existence of background interference from cell parts and contaminants in the ultraviolet and visible regions. The accurate measurement of intracellular calcium concentration, especially with penetration to multiple layers of cell tissue and high sensitivity, remains to be developed as an analytical method (43). The use of a metal binding dye with chromophore activity in the near infrared region has the advantage of greatly reduced background interference since most biomolecules do not have absorbance in this wavelength region (94). Akkaya et al. has reported several squaraine-based metal-binding near infrared dyes, including chemosensors with EDTA and BAPTA chelating moieties, which could sense calcium concentration (94, 95). With these dyes, the addition of calcium results in a decrease of the NIR signal. However, the detailed metal binding properties have not been reported. In this chapter, the synthesis and detailed analysis of a novel metal binding dye 15C5-774 that binds metals with micromolar affinity is described. This abbreviation denotes a metal binding

benzo-15-crown-5 moiety (15C5) linked at the meso position to a heptamethine cyanine as shown in figure 3.1. The crown ether-substituted cyanine absorbs at 774 nm in methanol and Tris buffer (20:80 v/v).

3.2 Design of 15C5-774

The compound, 15C5-774, was synthesized by Dr. Christian Mason formerly of Georgia State University. 15C5-774 is a NIR chromophore-modified crown ether. The properties of crown ethers as metal binding compounds have been reported extensively (96-109). The size of the crown ether ring may be varied to provide a proper cavity for metal binding based on the size of the metal. In particular, the cavity of benzo-15-crown-5 has a diameter of 1.7–2.2 Å, depending on conformation (98). This cyclic ether can easily accommodate calcium, which has a radius of 0.99 Å.

The second functional unit of 15C5-774 is an indolium heptamethine cyanine that absorbs in the NIR region. The crown ether is linked to the central *meso* position of the cyanine. The wavelength and intensity of absorption of heptamethine cyanine chromophores are greatly affected by a substituent at the meso position as shown by our collaborator (110). More importantly, the equilibrium conformation of an electron donating *meso*-substituent, such as an amino group, greatly influences the absorption by affecting conjugation of the substituent with the electron deficient cationic chromophore. Accordingly, this finding was explored in the design of 15C5-774. It was reasoned that a conformational change of the crown ether moiety upon binding calcium ion would induce absorption changes at the NIR chromophore, thereby providing a basis for the metal determination (111).

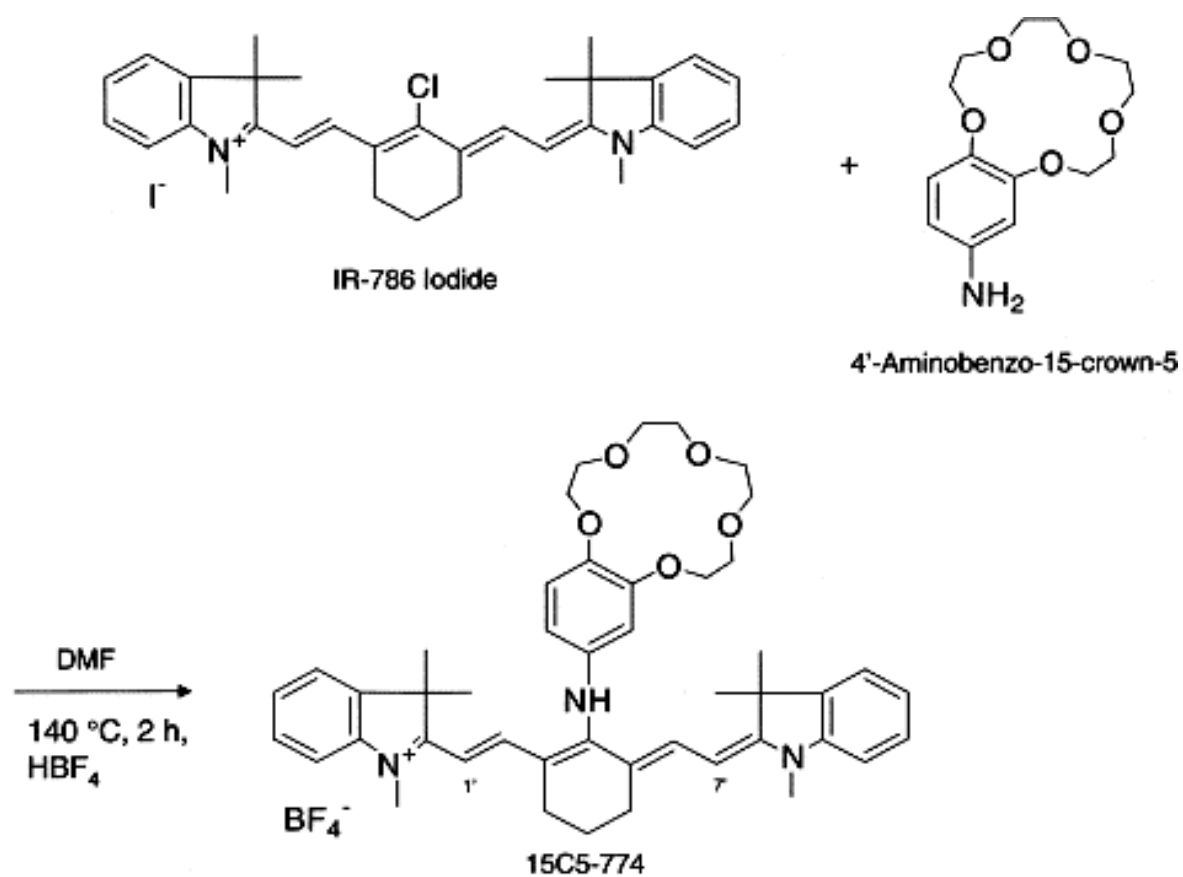


Fig 3.1 Synthesis of 15C5-774

3.3 Solution properties of 15C5-774

When stored in a solid form at $-20\text{ }^{\circ}\text{C}$, in the dark, and under a dry atmosphere, 15C5-774 is stable indefinitely. Stock solutions in methanol or other organic solvents are stable for at least a month when protected from light and oxygen and stored at $4\text{ }^{\circ}\text{C}$, as monitored by Vis-NIR spectroscopy. In aqueous methanol at $23\text{ }^{\circ}\text{C}$ in the presence of oxygen and in the dark, the compound is stable for at least 7 days, as shown by ^1H NMR spectroscopy. On the other hand, at $23\text{ }^{\circ}\text{C}$ in the presence of light and oxygen, the solutions are less stable. A slight decrease in the NIR absorption was observed under these conditions after several hours. Accordingly, freshly made solutions in a methanol:aqueous solvent mixture (20:80 v/v) were used in this work to minimize environmental factors that influence dye degradation.

3.4 Metal binding affinities and selectivity of 15C5-774

The Vis-NIR absorption spectra of 15C5-774 in a Tris/MeOH buffer at physiological pH 7.4 in the absence of calcium and as a function of calcium concentration are shown in figure 3.2. The metal-free compound has a NIR absorption band centered at 774 nm with a Sorens shoulder at about 710 nm and two visible bands at 566 and 445 nm. The visible absorption at 566 nm is unusual in that it is normally not observed for heptamethine cyanines. This phenomenon is discussed in more detail in Section 3.5.

The addition of calcium ion results in the decrease of absorbance at all wavelengths (Fig 3.2). The fractional changes of the absorptions at both 774 and 566 nm of the dye can be fitted very well using equation 3, suggesting the formation of a 1:1

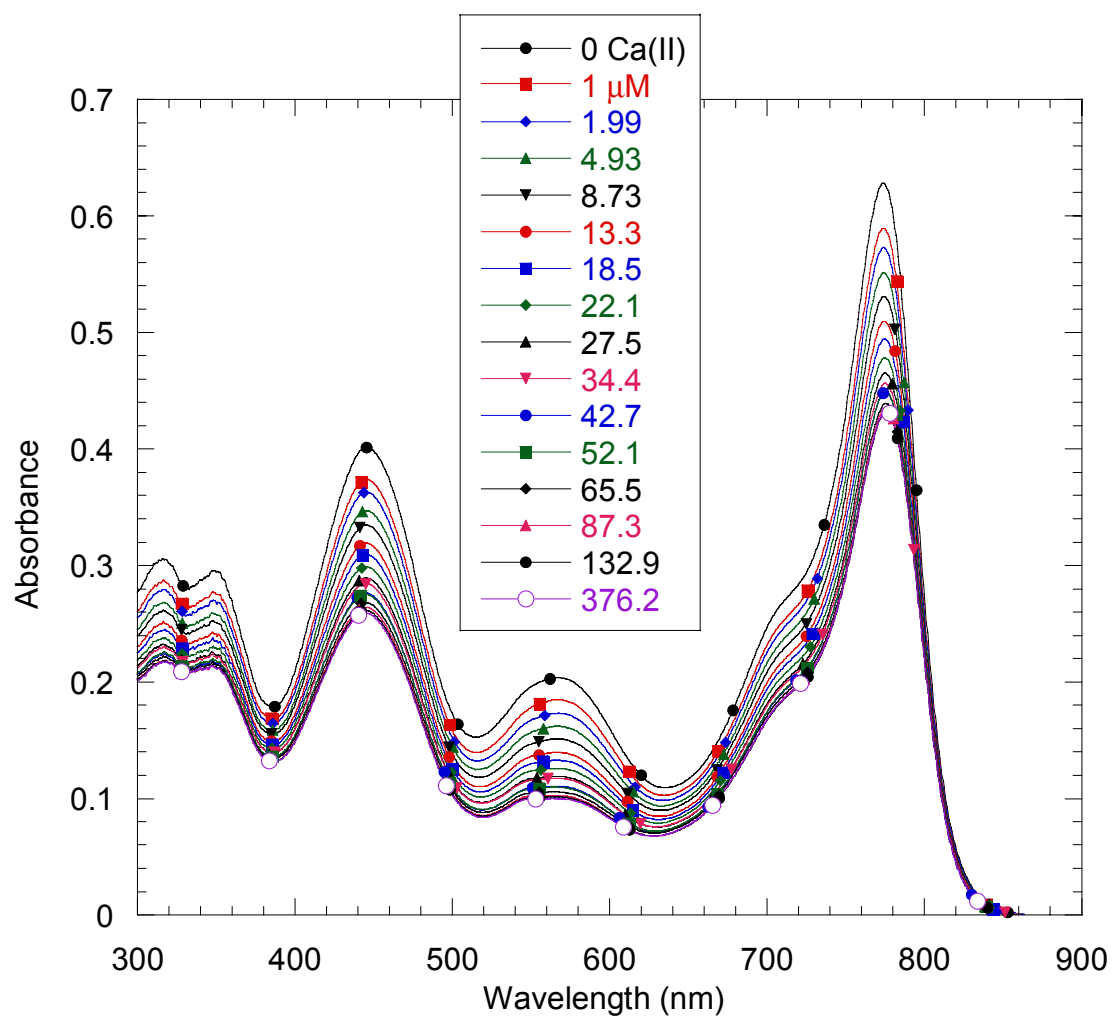


Fig 3.2 Absorbance spectra of 19.52 μM 15C5-774 with increasing concentrations of CaCl_2 in 10 mM Tris buffer and 20% MeOH (v/v) pH 7.4.

dye:metal complex (Fig 3.3) (112, 113). Since the calculated K_d values based on the fractional intensity change at all absorption bands are identical, a summary of the affinities based on the NIR absorption is reported in Table 3.1.

Calcium is the strongest binding metal of the ions examined. With a K_d average of 3.2 μM , the strong affinity of 15C5-774 for Ca^{2+} indicates that this dye could be used for monitoring intracellular calcium concentrations between the physiological resting and stimulated cell states since intracellular calcium concentrations vary from 0.1 to 10 μM . The strong affinity is consistent with a good molecular fit of calcium ion within a cavity of 15-crown-5. With metal ions of other sizes the binding affinity is not as strong. With a decrease in the ionic radii of metal ions from 0.99 Å for calcium to 0.68 and 0.63 Å, this dye shows a slightly weaker binding affinity to zinc and magnesium with K_d values of 11.4 and 7.2 μM , respectively. These smaller ions may not be able to form bonds efficiently with all of the oxygens in the crown. Strontium has an ionic radius of 1.12 Å, which is larger than that for calcium, and the affinity of this dye for strontium decreases about 4-fold. Its larger size prevents the ion from fitting efficiently into the cavity in the crown. Therefore, 15C5-774 shows metal selectivity for metal ions with ionic size close to the size of a crown cavity (Table 3.1). In comparison to these divalent metal ions, the size selectivity of 15C5-774 is smaller for monovalent ions.

In summary, the results for both divalent and monovalent metal ions suggest that both the size and charge are the two key determinants contributing to the metal affinity of 15C5-774. For similarly sized ions such as calcium and sodium, the dye binds 2.5 fold stronger to divalent calcium than monovalent sodium. The binding affinity of

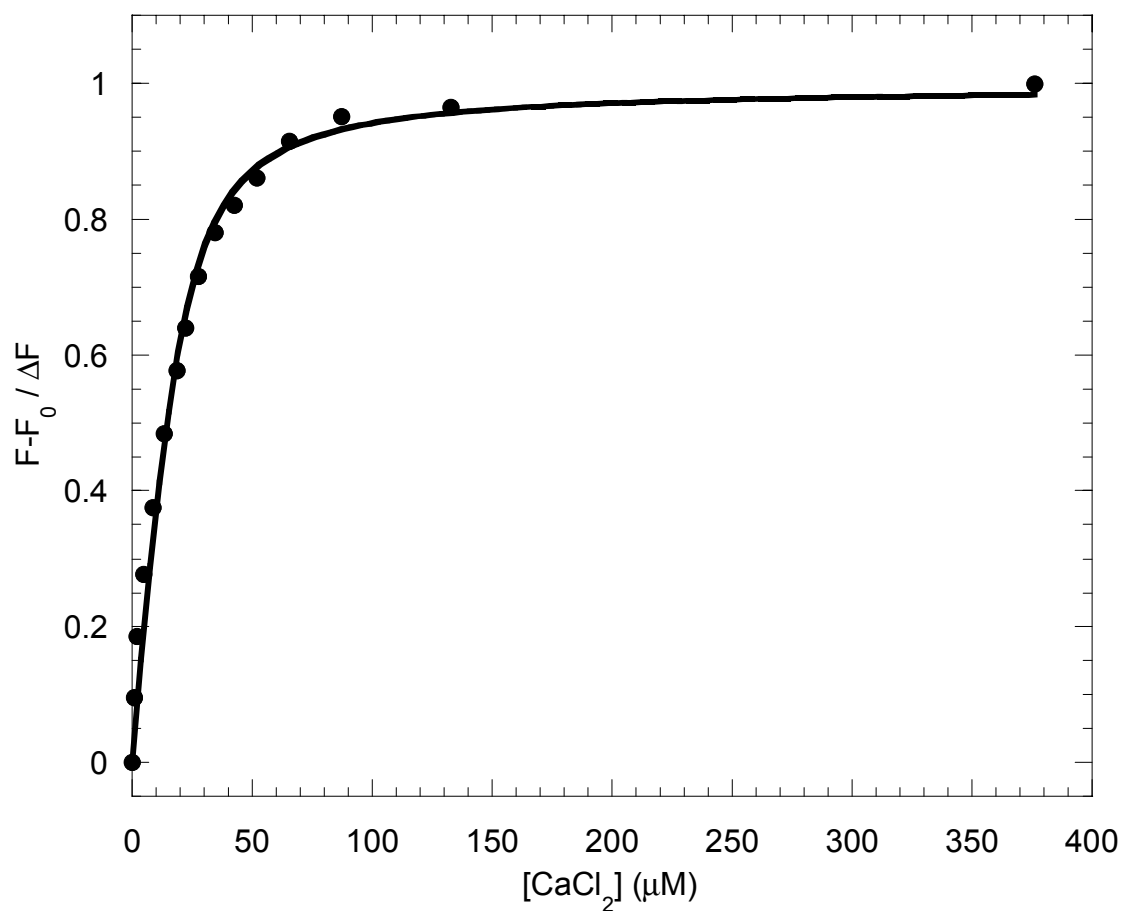


Fig 3.3 Fractional change of the absorbance at 774 nm as a function of Ca^{2+} concentration in 10 mM Tris and 20% MeOH (v/v) pH 7.4. The solid line was generated by using the fractional change equation 3 assuming the formation of a 1:1 metal:dye complex. A virtually identical function was obtained by using the wavelength of 566 nm under otherwise identical conditions.

Table 3.1 Binding affinities of 15C5-774 and the ionic radii of the metals studied with the affinity measured at 774 nm.

Metal	K_d (μM)	Ionic radius (Å)
Zn ²⁺	11.4 ± 4.6	0.63
Mg ²⁺	7.2 ± 2.3	0.66
Li ⁺	21.8 ± 3.1	0.68
Na ⁺	10.7 ± 0.9	0.97
Ca ²⁺	3.2 ± 2.3	0.99
Sr ²⁺	10.1 ± 0.2	1.12
K ⁺	10.6 ± 1.1	1.33

monovalent lithium is about 3-fold weaker than that of magnesium, despite the similar ionic size.

3.5 pH dependence

To test the pH dependence of 15C5-774, the Vis-NIR spectra of the metal-free compound and in the presence of calcium or magnesium were taken in the appropriate Tris buffer at a lower and higher pH than the physiological pH of 7.4. The spectra of the dye change with pH (Fig 3.4). The spectra at pH 8.7 lack absorption at 566 nm and are typical for a heptamethine cyanine chromophore. The unusual absorption at 566 nm appears with decreasing pH, gradually increases in intensity, and becomes dominant at pH 6. These spectral changes are fully reversible with subsequent increases in pH of the acidified solution. On the other hand, the binding affinities of magnesium remain unchanged from pH 6–9 while the calcium affinity at pH 6 is identical to that at pH 7, and the affinity at pH 8.7 is decreased only 1.5-fold. These results are highly encouraging for our planned development studies of 15C5-774 as a practical reagent for metal determination *in vivo*. More specifically, variations in physiological pH will have a negligible effect on the calcium determination under different pH conditions *in vivo* that, at present time, are difficult to monitor. Interestingly, in addition to calcium determination, the strong pH dependence of the 566 nm absorption of 15C5-774 may be simultaneously used as the basis for the pH estimate *in vivo*.

Additional studies are needed to understand the presence of the 566 nm absorption in the spectrum of 15C5-774 under low pH conditions. It appears that, in addition to the normal $s^0 \rightarrow s^1$ transition at 774 nm, a new electronic excitation becomes

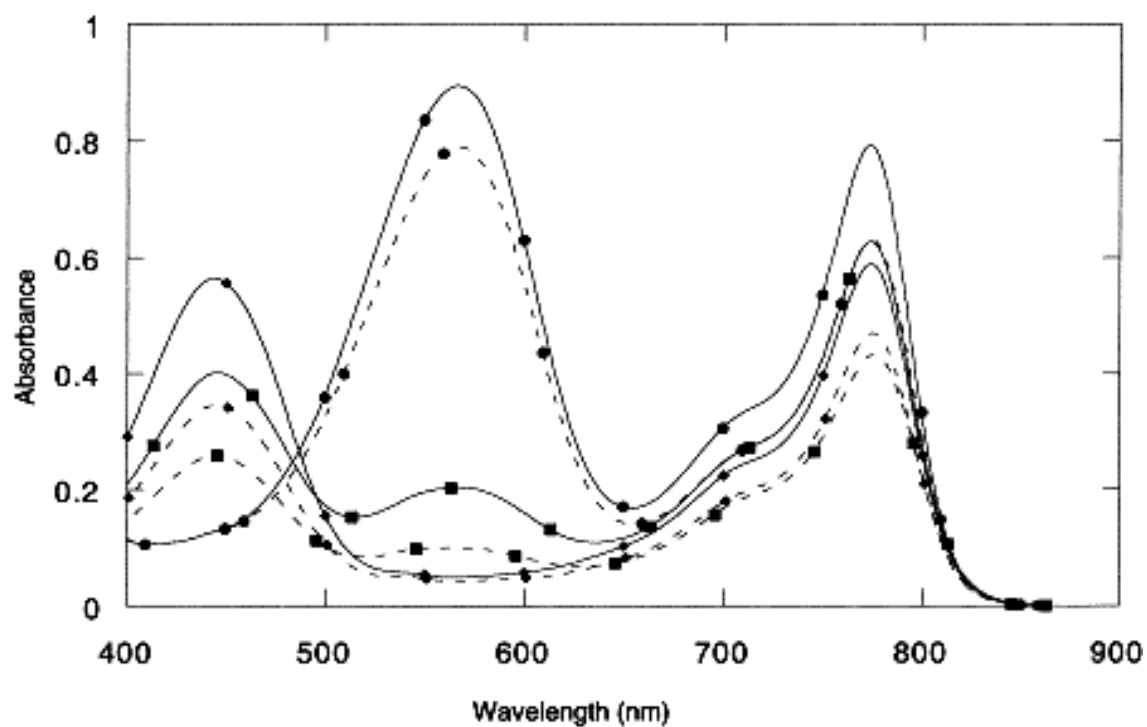


Fig 3.4. A comparison of the Ca^{2+} free (—) and Ca^{2+} loaded (---) spectra of 15C5-774 at pH 6 (●), pH 7.4 (■), and pH 8.7 (▲) in Tris:MeOH (80:20 v/v).

important for the protonated compound. Most likely, the 566 nm absorption results from excitation of the intramolecular complex between the protonated crown ether and the cyanine chromophore. Consistent with this suggestion are the results of our previous experimental and computational studies that showed the presence of net negative charges on carbons 1' and 7' of the heptamethine chain of cyanines (114).

3.6 Comparison of 15C5-774 and commercially available dyes

The binding affinity of 15C5-774 for calcium is in the same range as commercially available indicators that are frequently used for intracellular study. Dyes such as FURA-2, INDO-1, and Mag-FURA-2 have nanomolar to micromolar dissociation constants for calcium (92, 115, 116). Our dye is well within this range. However, these dyes have maximum absorbance in the ultraviolet to visible regions of the spectrum where background interference is high. Our dye has maximum absorbance in the near infrared region where background interference is nearly nonexistent. Also, illuminating in the near infrared avoids the tissue damage that is seen with ultraviolet irradiation.

Much like FURA-2 and INDO-1, 15C5-774 should be protected from light whenever possible since it will undergo photodegradation. In normal working conditions, however, photodegradation does not severely affect the results since it takes 90 min of constant illumination for a loss of absorbance to be observed whereas INDO has been shown to lose absorbance within 10 min of constant exposure (117). If the dye is protected from light, it is stable over several days, longer in organic solvents. Like FURA-2 and INDO-1, 15C5-774 should be stored at -20°C , but, when protected from light, storage in solution at room temperature over several days does not affect the

dye's stability. Unlike FURA-2 and INDO-1, the binding affinity of 15C5-774 is not greatly affected by pH.

As a means of transporting the dye into the cell for metal analysis, the dye can be made into ester derivatives in a similar manner as with commercially available dyes. The synthesis of ester-substituted near-infrared cyanine dyes has been previously reported by our collaborators (111, 118). Also, microinjection, a technique often used, can be used as a means to transport the dye into the cell (43). Once inside the cell, concentration can be monitored by near UV absorbance (~290 nm), which does not change upon calcium binding. The absorbance at this wavelength is only concentration dependent from the indolium portion of the dye. The development of a dye with a wavelength shift upon calcium binding, by closer coupling of the cyanine chromophore and the metal binding moiety, is currently underway.

3.7 Conclusions

A novel metal binding near-infrared dye with the advantage of avoiding background interference and possible damage from illumination in the UV-Vis region, 15C5-774, was designed, synthesized, and analyzed for its metal binding properties. The solution properties were examined, and the spectral properties of 15C5-774 were investigated by absorbance and NMR spectroscopy. The solubility of 15C5-774 is comparable to commercially available dyes, and 15C5-774 has been shown to be somewhat more stable. The metal binding affinities of 15C5-774 are in micromolar range for all metals tested and follow the order $\text{Ca}^{2+} > \text{Mg}^{2+} > \text{Sr}^{2+} \approx \text{K}^+ \approx \text{Na}^+ > \text{Zn}^{2+} > \text{Li}^+$. The calcium affinity of 15C5-774 is in the same range as FURA and INDO derivatives,

indicating that 15C5-774 can be used to monitor intracellular calcium concentrations. The dye could also be used for in vitro work, such as for protein competition assays, since its metal binding affinities are in the region needed to compare to many calcium binding proteins (119, 120). An additional advantage of 15C5-774 is that, while the binding affinities change only slightly with a pH change, the spectral properties do alter with pH allowing the dye to be used to monitor pH fluxes.

Chapter 4 Design of Calcium-binding Sensors: the first generation

4.1 Rationale for Engineering Calcium Biosensors by Design

As discussed in Chapter 1, although the literature has detailed several researchers' attempts at this task, there is still a strong need to develop calcium sensors with a large range of calcium binding affinities to sense calcium signal changes in different cellular compartments. One of the first steps to design calcium sensors is to engineer calcium binding sites in fluorescent proteins with different calcium binding affinities. The goal of the project discussed in this chapter is to create calcium binding sites in green fluorescent protein using our established design approach. There are numerous reasons to engineer a calcium biosensor by design. The use of small molecule dyes has been prevalent in the past, but the desire to understand the temporal and spatial changes in calcium concentration in relation to events in the cell compartments necessitates the creation of a new type of sensor. The creation of a calcium-binding fluorescent protein that can be directly expressed by cells, targeted to specific cell compartments, directly measured for fluorescence changes caused by calcium binding, and designed in a multitude of emission wavelengths will greatly enhance the study of calcium in living systems. In this chapter, the design strategy employed in devising calcium-binding green fluorescent proteins will be discussed. The chosen sites will be detailed, and the biophysical properties of bacterially expressed and purified GFP variants will be discussed.

4.2 Design of Potential Calcium Binding Sites

4.2.1 Computational Design

There are 80 structures of green fluorescent protein available in the protein data bank to date. Most of these files contain mutations for various purposes. Three of those pdb files, 1B9C, 1GFL, and 1EMM, were utilized as the base structures for the design to ascertain if any difference would be found in the computation. The 1B9C structure is known as the cycle 3 mutant (or GFPuv) and contains F99S, M153T, and V163A (121). This structure is reported to be a tetramer, and the fluorescence of this mutant is 30,000 times brighter than the wild type protein. This structure was chosen for the basis of design due to its apparent better folding. The 1EMM file contains the F64L mutation and is reported to be a dimer (122). The 1GFL file contains the Q80R random mutation. This structure was the first structure solved by Yang and Phillips shortly after the discovery of green fluorescent protein (123). The first chain in the dimers or tetramers in the pdb file was utilized for the computation since the structures of the oligomers. Initially, the possible calcium binding sites were identified by computer algorithms with the desired parameters, including the oxygen-calcium-oxygen angle, the oxygen-calcium distance, the ligand type, and the number of ligands (86-89). The ligands for the binding site were one bidentate Asp and four unidentate ligands from Asp, Asn, Glu, and Gln. The calcium-oxygen length was allowed to be in the range of 2.0 to 3.0 Å. The oxygen-calcium-oxygen angles are theoretically 72°, 144°, and 90° so the ranges of 30°-120°, 90°-180°, 45°-135° were allowed for the calculations. We chose the most popular geometry for a calcium binding site of pentagonal bipyramid as the

calcium coordination site. As shown in figure 4.1, one of the coordinating ligands was unfilled to allow water to serve as a ligand. These parameters were input into the computer program, Dezymer, to search along the backbone of the protein to find possible locations for a design site. However, the program does not take electrostatic interactions into account. Also, to distinguish between Asp and Asn and between Glu and Gln, bench experiments would have to be performed. After Site-search, refinement was performed where the sites were minimized based on the ideal geometry of pentagonal bipyramid.

4.2.2 Selection of putative calcium binding sites

After the computer algorithms were complete, several criteria were utilized to rank and finally choose sites. Initially, the computer algorithms provided a data set of ~10,000 sites for the pdb 1B9C. These sites were examined and inappropriate sites were removed. First, any sites that involved the central helix (i.e. amino acids 56 to 71), especially the chromophore, were removed from the data set. Second, sites that contained mutation of hydrophobic residues, especially those that were involved in the hydrophobic core, were removed to avoid folding disruptions caused by replacing hydrophobic residues with charged residues. Third, solvent inaccessible residues, such as Phe8 with a solvent accessibility of 2.6, were removed since a solvent accessibility is necessary for calcium binding. The solvent accessibility was evaluated with GetArea and is shown in Table 4.1 (124). Residues with low solubility or those pointing inside the barrel were not considered. However, it must be noted that GetArea does not always correctly identify residues pointing in or out of the barrel as observed by close

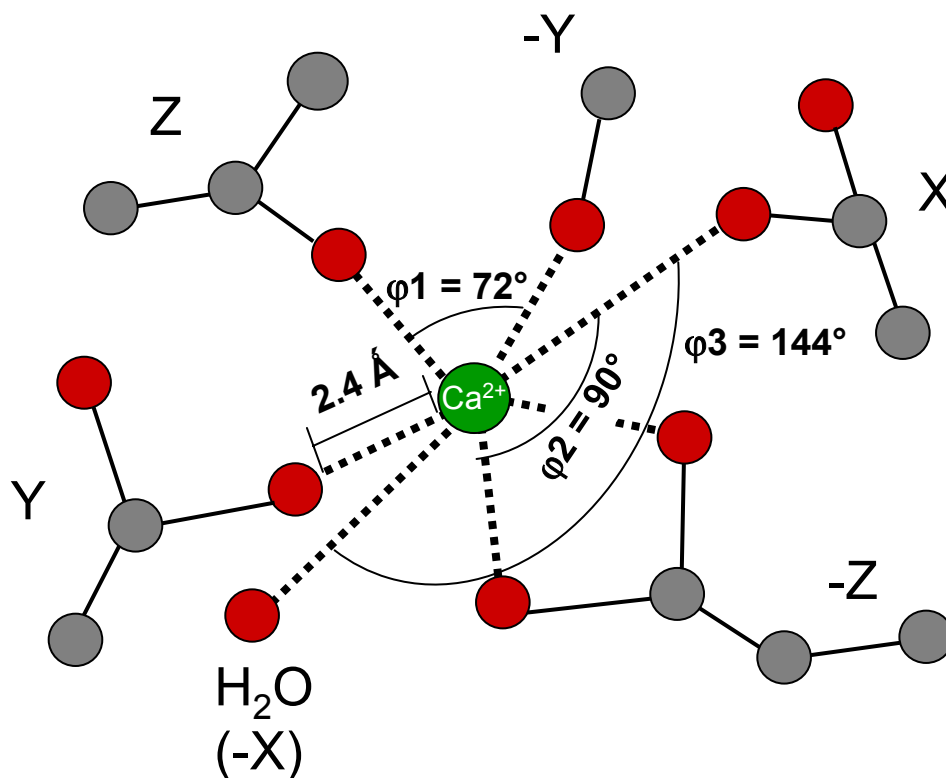


Fig 4.1 The ideal pentagonal bipyramidal geometry of a calcium binding site with the oxygen-calcium-oxygen angles of 72° for the ligands located in the pentagon (ϕ_1), 90° for the X position in relation to the pentagon (ϕ_2), and 144° for the X-Ca(II)-X angle (ϕ_3) illustrated. The ideal distance between calcium and oxygen is 2.4 Å. During the design process, ϕ_1 was allowed to range from 30° to 120°, ϕ_2 ranged from 45° to 135°, and ϕ_3 ranged from 90° to 180°.

Table 4.1 Solvent accessibility of GFP using the 1B9C pdb file and calculated with the GetArea program (124). “Total” is the total solvent accessibility of the residue, “apolar” is the solvent accessibility of the backbone for each amino acid, “sidechain” is the solvent accessibility of the amino acid sidechain, “ratio” is the ratio of the sidechain surface area to the random coil value, “In/Out” is the cutoff for solvent exposure with “out” being a ratio of >50% and “in” being a ratio of <20%.

Residue	Residue Number	Total	Apolar	Sidechain	Ratio (%)	In/Out
GLY	4	30.41	3.86	0	34.9	
GLU	5	65.85	26.57	63.85	45.2	
GLU	6	123.5	65.7	107.24	75.9	o
LEU	7	58.29	48.94	45.43	31.1	
PHE	8	2.6	0.23	0.23	0.1	i
THR	9	93	64.54	82.03	77.2	o
GLY	10	42.71	41.51	0	49	
VAL	11	81.24	58.88	58.88	48.1	
VAL	12	7.07	7.07	6.46	5.3	i
PRO	13	59.58	59.58	59.51	56.6	o
ILE	14	1.36	0	0	0	i
LEU	15	66.15	66.15	66.15	45.2	
VAL	16	0	0	0	0	i
GLU	17	52.99	15.46	52.19	37	
LEU	18	3.61	0.86	0	0	i
ASP	19	89.23	25.64	86.65	76.7	o
GLY	20	6.32	1.62	0	7.2	i
ASP	21	36.34	12.24	36.34	32.2	
VAL	22	0	0	0	0	i
ASN	23	56.69	21.4	26.82	23.5	
GLY	24	51.8	35.31	0	59.4	o
HIS	25	91.22	73.68	86.35	55.9	o

LYS	26	154.6	103.08	146.02	88.8	o
PHE	27	3.29	2.22	1.28	0.7	i
SER	28	27.09	15.28	27.09	35	
VAL	29	1.46	0	0	0	i
SER	30	36.17	21.08	34.54	44.6	
GLY	31	0.15	0.01	0	0.2	i
GLU	32	92.57	43.33	91.13	64.5	o
GLY	33	16.12	6.45	0	18.5	i
GLU	34	81.52	16.03	80.94	57.3	o
GLY	35	0.97	0.97	0	1.1	i
ASP	36	19.8	4.16	19.8	17.5	i
ALA	37	4.79	2.89	2.89	4.4	i
THR	38	68.17	55.73	49.11	46.2	
TYR	39	144.86	96.68	133.93	69.4	o
GLY	40	0.17	0.17	0	0.2	i
LYS	41	65.15	30.27	64.33	39.1	
LEU	42	3.56	3.56	3.56	2.4	i
THR	43	46.84	43.9	46.84	44.1	
LEU	44	1.23	1.23	0.72	0.5	i
LYS	45	41.49	26.83	41.16	25	
PHE	46	0	0	0	0	i
ILE	47	14.97	14.97	14.97	10.2	i
CYS	48	2.8	0	0	0	i
THR	49	83.02	51.15	47.59	44.8	
THR	50	72.74	46.75	35.4	33.3	
GLY	51	44.32	41.42	0	50.8	o
LYS	52	154.29	122.04	140.99	85.7	o
LEU	53	5.77	1.82	1.82	1.2	i
PRO	54	25.46	25.3	14.18	13.5	i

VAL	55	0.53	0	0	0	i
PRO	56	9.23	9.23	4.33	4.1	i
TRP	57	10.71	10.48	10.48	4.7	i
PRO	58	3.39	2.49	2.49	2.4	i
THR	59	3.04	1.3	0	0	i
LEU	60	0	0	0	0	i
VAL	61	3.88	1.87	1.87	1.5	i
THR	62	29.19	21.71	12.26	11.5	i
THR	63	4.89	2.1	0	0	i
PHE	64	5.06	5.06	0	0	i
VAL	68	13.07	1.15	1.14	0.9	i
GLN	69	16.48	14.88	16.44	11.4	i
CYS	70	0	0	0	0	i
PHE	71	0	0	0	0	i
SER	72	0	0	0	0	i
ARG	73	88.41	30.57	86.57	44.3	
TYR	74	3.42	0.13	0.29	0.2	i
PRO	75	28.42	28.42	25.97	24.7	
ASP	76	124.72	40.62	107.85	95.4	o
HIS	77	101.26	81.68	74.97	48.5	
MET	78	0.9	0.9	0.71	0.4	i
LYS	79	64.59	48.63	62.7	38.1	
GLN	80	109.46	45.54	103.84	72.3	o
HIS	81	8.31	8.29	8.29	5.4	i
ASP	82	1.53	0.96	1	0.9	i
PHE	83	0.23	0.23	0.23	0.1	i
PHE	84	0.05	0.05	0.05	0	i
LYS	85	6.02	6.02	6.02	3.7	i
SER	86	22	11.65	4.89	6.3	i

ALA	87	3.58	3.03	0	0	i
MET	88	6.22	0	0	0	i
PRO	89	71.2	68.08	68.08	64.7	o
GLU	90	67.74	35.12	59.54	42.2	
GLY	91	0	0	0	0	i
TYR	92	0	0	0	0	i
VAL	93	17.88	17.55	17.55	14.3	i
GLN	94	9.03	2.36	8.96	6.2	i
GLU	95	61.6	18.39	60.96	43.2	
ARG	96	7.84	2.28	3.61	1.8	i
THR	97	52.95	32.51	52.95	49.9	
ILE	98	0.71	0.71	0.71	0.5	i
SER	99	38.69	6.87	36.76	47.5	
PHE	100	1.76	0.01	0.01	0	i
LYS	101	116.25	82.41	105.31	64	o
ASP	102	100.3	42.1	75.62	66.9	o
ASP	103	27.28	5.72	1.74	1.5	i
GLY	104	2.55	2.01	0	2.9	i
ASN	105	25.32	3.02	25.32	22.2	
TYR	106	0	0	0	0	i
LYS	107	79.04	73.65	73.88	44.9	
THR	108	8.29	1.73	2.4	2.3	i
ARG	109	90.48	54.53	88.97	45.5	
ALA	110	3.38	3.38	3.11	4.8	i
GLU	111	44.17	8.86	44.17	31.3	
VAL	112	1.13	1.13	1.13	0.9	i
LYS	113	52.3	36.47	52.3	31.8	
PHE	114	22.63	6.57	6.57	3.6	i
GLU	115	66.97	47.8	55.24	39.1	

GLY	116	70.69	52.96	0	81.1	o
ASP	117	108.76	47.75	97.94	86.7	o
THR	118	34.19	33.65	34.19	32.2	
LEU	119	0	0	0	0	i
VAL	120	4.79	4.79	4.79	3.9	i
ASN	121	2.68	0	2.68	2.3	i
ARG	122	103.13	51.62	99.83	51.1	o
ILE	123	5.28	0.34	0.17	0.1	i
GLU	124	108.78	40.15	107.43	76.1	o
LEU	125	5.26	1.34	0	0	i
LYS	126	94.79	88.91	94.79	57.6	o
GLY	127	0	0	0	0	i
ILE	128	67.17	67.17	65.47	44.4	
ASP	129	107.94	30.31	71.35	63.1	o
PHE	130	11.87	0.01	0	0	i
LYS	131	95.64	60.16	84.41	51.3	o
GLU	132	146.23	52.83	137.25	97.2	o
ASP	133	105.46	52.85	88.95	78.7	o
GLY	134	8.87	8.87	0	10.2	i
ASN	135	31.08	0.31	30.77	26.9	
ILE	136	0	0	0	0	i
LEU	137	23.45	11.79	11.79	8.1	i
GLY	138	31.61	14.74	0	36.3	
HIS	139	87.74	70.13	74.13	47.9	
LYS	140	65.26	55.81	65.16	39.6	
LEU	141	14.89	0.35	0.29	0.2	i
GLU	142	67.25	28.09	57.3	40.6	
TYR	143	65.8	47.49	47.07	24.4	
ASN	144	44.86	30.46	41.32	36.1	

TYR	145	21.17	5.39	6.09	3.2	i
ASN	146	42.23	18.09	32.56	28.5	
SER	147	56.78	35.43	50.43	65.2	o
HIS	148	8.98	8.06	2.84	1.8	i
ASN	149	48.48	4.28	44.4	38.8	
VAL	150	4.82	4.82	4.82	3.9	i
TYR	151	119.33	94.44	118.67	61.5	o
ILE	152	1.68	0.17	0.15	0.1	i
THR	153	47.7	34.17	47.7	44.9	
ALA	154	25.57	8.08	8.07	12.4	i
ASP	155	1.39	0.78	0.62	0.5	i
LYS	156	139.66	110.5	124.92	75.9	o
GLN	157	155.26	66.58	111.97	77.9	o
LYS	158	107.36	62.38	87.03	52.9	o
ASN	159	62.44	31.08	62.42	54.6	o
GLY	160	0	0	0	0	i
ILE	161	0	0	0	0	i
LYS	162	71.36	53.53	71.36	43.4	
ALA	163	0.15	0	0	0	i
ASN	164	67.34	28.57	67.12	58.7	o
PHE	165	13.3	13.02	3.08	1.7	i
LYS	166	107.05	85.49	97.48	59.3	o
ILE	167	3.18	3.18	3.18	2.2	i
ARG	168	92.51	55.79	92.51	47.3	
HIS	169	2.69	2.69	1.9	1.2	i
ASN	170	35.81	4.19	35.44	31	
ILE	171	1.63	1.61	1.61	1.1	i
GLU	172	120.14	37.8	90.44	64	o
ASP	173	115.7	54.16	71.38	63.2	o

GLY	174	61.56	40.05	0	70.6	o
SER	175	65.38	55.68	53.7	69.4	o
VAL	176	60.18	42.82	42.82	35	
GLN	177	6.73	4.03	2.82	2	i
LEU	178	36.28	36.28	36.28	24.8	
ALA	179	0	0	0	0	i
ASP	180	27.65	1.1	27.65	24.5	
HIS	181	2.08	1.89	1.93	1.2	i
TYR	182	110.21	80.51	104.29	54	o
GLN	183	4.54	0.06	0	0	i
GLN	184	40.15	4.35	40.03	27.9	
ASN	185	0.24	0.24	0	0	i
THR	186	31.29	21.78	31.29	29.5	
PRO	187	24.32	7.8	7.8	7.4	i
ILE	188	68.5	48.14	40.83	27.7	
GLY	189	18.41	3.04	0	21.1	
ASP	190	143.85	48.65	97.31	86.1	o
GLY	191	33.12	30.24	0	38	
PRO	192	135.61	129.39	118.7	100	o
VAL	193	20.09	3.28	1.6	1.3	i
LEU	194	82.96	82.96	79.91	54.7	o
LEU	195	58.72	40.71	40.71	27.8	
PRO	196	5.29	0.38	0.03	0	i
ASP	197	90.93	33.7	84.58	74.8	o
ASN	198	104.17	37.21	91.63	80.2	o
HIS	199	5.54	4.44	0.06	0	i
TYR	200	58.73	22.45	58.73	30.4	
LEU	201	0	0	0	0	i
SER	202	31.8	11.75	31.01	40.1	

THR	203	16.51	13.03	15.94	15	i
GLN	204	86.2	20.03	85.61	59.6	o
SER	205	14.36	2.64	2.46	3.2	i
ALA	206	63.62	63.15	57.26	88.2	o
LEU	207	17.83	0	0	0	i
SER	208	54.5	46.12	49.78	64.3	o
LYS	209	88.39	71.16	76.88	46.7	
ASP	210	49.18	11.91	43.01	38.1	
PRO	211	135.61	108.12	97.94	93.1	o
ASN	212	130.16	31.83	104.91	91.8	o
GLU	213	29.68	3.49	15.14	10.7	i
LYS	214	196.05	131.43	165.09	100	o
ARG	215	125.76	68.56	115.23	58.9	o
ASP	216	31	8.5	23.09	20.4	
HIS	217	6.52	6.15	6.48	4.2	i
MET	218	0	0	0	0	i
VAL	219	24.72	24.71	24.71	20.2	
LEU	220	2.17	2.17	2.17	1.5	i
LEU	221	52.1	51.84	51.84	35.5	
GLU	222	21.6	0.7	21.6	15.3	i
PHE	223	86.22	86.15	86.15	47.8	
VAL	224	0.99	0.9	0.67	0.6	i
THR	225	43.81	34.09	43.81	41.3	
ALA	226	0.25	0	0	0	i
ALA	227	31.18	31.18	27.55	42.5	
GLY	228	50.96	26.21	0	58.4	o
ILE	229	42.73	36.58	31.83	21.6	
THR	230	175.21	111.51	122.69	100	o

examination of the crystal structure. For example, Val120 points out of the barrel in the crystal structure, but it is noted as inside by GetArea. Therefore, examination of the crystal structure was also utilized during this process to examine the potential calcium binding residues. Fourth, the remaining sites were then ranked based on their location in the protein. Sites in the loop regions with higher flexibility were considered “safe” to mutate without disrupting the protein folding while sites involving the β -strands were considered more aggressive. Fifth, since fewer mutations will more likely allow proteins to retain their native conformation, sites with natural pockets but inappropriate residues were examined as possible mutation positions. The sites were ranked for the number of required mutations in these natural pockets. Sixth, the distance from the chromophore was also evaluated since the requirement for a sensor is that calcium binding must cause a change in the fluorescence of the protein. Lastly, the clash with close residues was considered to decide if further mutations would be necessary.

Once all of these steps were achieved, six sites were chosen for study. They are Site 120, Site 120b, Site 177, Site 194a, Site 194b, and Site 229 (Table 4.2 and Fig 4.2). Sites 120 and 120b are located in the middle of the barrel very near the chromophore. They differ by two residues, 120 includes K113D and E17 whereas 120b includes L15N and E111. These two sites were chosen due to their proximity to the chromophore and to the natural pocket that the residues form. Since they are located on the β -strands, they could feasibly cause a large change in chromophore fluorescence upon calcium binding. Site 177 is located on the end of the barrel in the

Table 4.2 A table of the design sites engineered into Green Fluorescent Protein.

Design Site	Calcium-binding Ligands	Average Distance to the Chromophore (Å)
120	E115, V120N, R122D, K113D, E17	14
120b	E115, V120N, R122D, E111, L15N	14
177	Q177N, I171D, D173, S175D, N135	22
194a	E5, D82, K79D, L194N, K85D	15
194b	E5, D82, K79D, L194N, S86D	15
229	D197, H199D, M78N, H81D, I229D	13

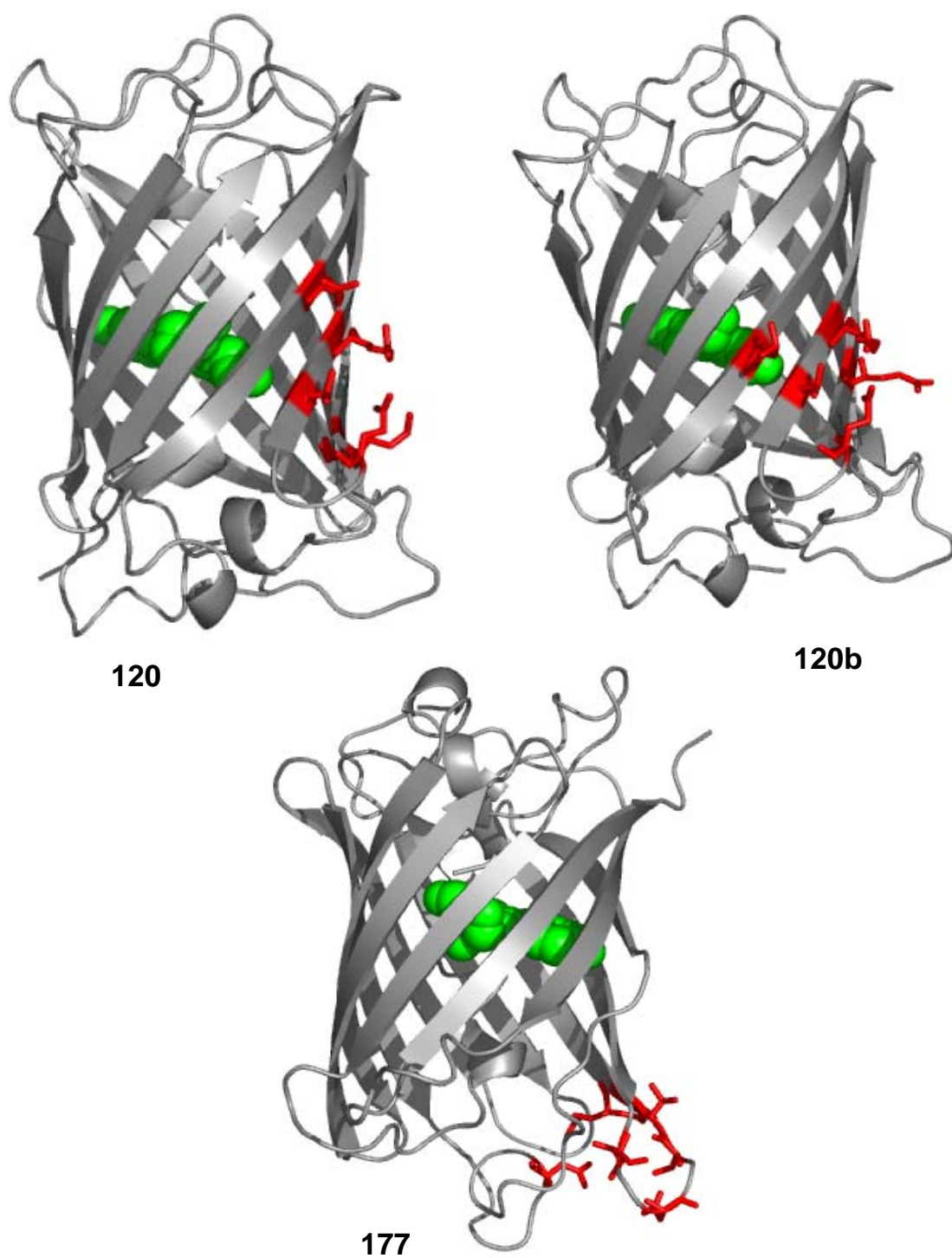
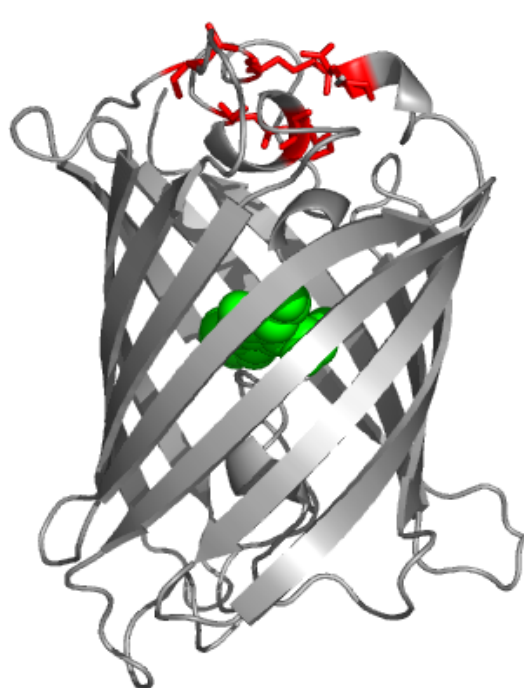


Fig 4.2 Illustrations of the models highlighting the locations of the designed proteins with the ligands illustrated in red and the chromophore in green. The pdb 1b9c and the program Pymol were utilized for these depictions.



194a



194b



229

loop regions. This site was chosen to reduce possible misfolding of the protein since the loops are more flexible, and mutations in the loop regions are less likely to interrupt the fold. In addition, the flexible loops should more easily form the proper calcium binding geometry. Sites 194a and 194b are also located in the loop region on the opposite side of the barrel from 177. These sites differ by one residue; 194a contains K85D whereas 194b contains S86D. These two sites with one amino acid difference were chosen to provide a way to test the variation in the properties of the pocket without drastically changing the location since K85 interacts with different residues than S86. Also, the change of this single residue shifts the calcium binding pocket, which allows us to further test and understand the outcome of our design process and may provide different chromophore effects upon calcium binding. Including sites that are in nearly the same location with only one residue difference allowed us to test the ability of the designed site to form the proper calcium pocket, to modulate the binding affinities by the location of the binding residue, and, in the event that one or more of the residues caused misfolding, to narrow down which residues were the cause. For example, the lysine to aspartate mutation in sites 120 and 194a could cause misfolding due to charge repulsion. This would be immediately recognized if the site without this mutation were fluorescent, but the site with it was not or if it failed to express well. Site 229 is located in the loop region on the same side lengthwise of the barrel as the 194 sites but is shifted widthwise. This site was chosen due to its natural pocket and its location. The sites in differing locations in the protein were chosen also to elucidate the chromophore sensitive locations for further modifications to the designed sensors.

4.3 Engineering a Calcium-binding Protein

To engineer the designed calcium-binding sites into the host protein, site-directed mutagenesis was employed. The host protein, EGFP, was a kind gift from Dr. Teryl Frey of GSU. EGFP contains the mutations F64L/S65T, which enhance the fluorescence, and V22L/M218I/H231L, which seem to be silent mutations. The sequence is illustrated in figure 4.3. The numbering of the sequence is in accordance with the pdb numbering to keep in agreement with the computer algorithm output. The oligonucleotide primers were devised to incorporate the desired mutations and to match the rest of the DNA so that the polymerase would only include the desired mutations. Standard polymerase chain reaction (PCR) was utilized, as detailed in Chapter 2, section 2.2, to change the nucleotides to the ones that would code for the designed ligands. The primers are listed in Table 2.1. Sites 120 and 120b required two rounds of PCR each. Site 177 was created with only one round of PCR. Sites 194a and 194b were engineered with two rounds of PCR. Site 229 required three rounds of PCR. These mutations were performed in the cloning vector pGEM11 due to the length limitations of the *pfu* polymerase available at that time.

For expression, the designed sites were subcloned into the pet28a vector, which includes an N-terminal 6 histidine tag for purification (Fig 4.4). The vector can also code for a 6 histidine tag on the C-terminal with the insertion of a single nucleotide for the proper frame. The DNA utilized for this project contains a stop codon (TAA) so that no tag is included at the C-terminal. There are ~30 amino acids between the N-terminal tag and the start of EGFP since the vector contains a thrombin cleavage site to remove

1/1	31/11
atg gtg agc aag ggc gag gag ctg ttc acc ggg gtg gtg ccc atc ctg gtc gag ctg gac	
M V S K G E E L F T G V V P I L V E L D	
61/21	91/31
ggc gac gta aac ggc cac aag ttc agc gtg tcc ggc gag ggc gag ggc gat gcc acc tac	
G D L N G H K F S V S G E G E G D A T Y	
121/41	151/51
ggc aag ctg acc ctg aag ttc atc tgc acc acc ggc aag ctg ccc gtg ccc tgg ccc acc	
G K L T L K F I C T T G K L P V P W P T	
181/61	211/71
ctc gtg acc acc ctg acc tac ggc gtg cag tgc ttc agc cgc tac ccc gac cac atg aag	
L V T T L T Y G V Q C F S R Y P D H M K	
241/81	271/91
cag cac gac ttc ttc aag tcc gcc atg ccc gaa ggc tac gtc cag gag cgc acc atc ttc	
Q H D F F K S A M P E G Y V Q E R T I F	
301/101	331/111
ttc aag gac gac ggc aac tac aag acc cgc gcc gag gtg aag ttc gag ggc gac acc ctg	
F K D D G N Y K T R A E V K F E G D T L	
361/121	391/131
gtg aac cgc atc gag ctg aag ggc atc gac ttc aag gag gac ggc aac atc ctg ggg cac	
V N R I E L K G I D F K E D G N I L G H	
421/141	451/151
aag ctg gag tac aac tac aac agc cac aac gtc tat atc atg gcc gac aag cag aag aac	
K L E Y N Y N S H N V Y I M A D K Q K N	
481/161	511/171
ggc atc aag gtg aac ttc aag atc cgc cac aac atc gag gac ggc agc gtg cag ctc gcc	
G I K V N F K I R H N I E D G S V Q L A	
541/181	571/191
gac cac tac cag cag aac acc ccc atc ggc gac ggc ccc gtg ctg ctg ccc gac aac cac	
D H Y Q Q N T P I G D G P V L L P D N H	
601/201	631/211
tac ctg agc acc cag tcc gcc ctg agc aaa gac ccc aac gag aag cgc gat cac atg gtc	
Y L S T Q S A L S K D P N E K R D H I V	
661/221	691/231
ctg ctg gag ttc gtg acc gcc gcc ggg atc act ctc ggc atg gac gag ctg tac aag taa	
L L E F V T A A G I T L G M D E L Y K *	

Fig 4.3 DNA and protein sequence of the host EGFP with the numbers referring to the nucleotide and amino acid, respectively.

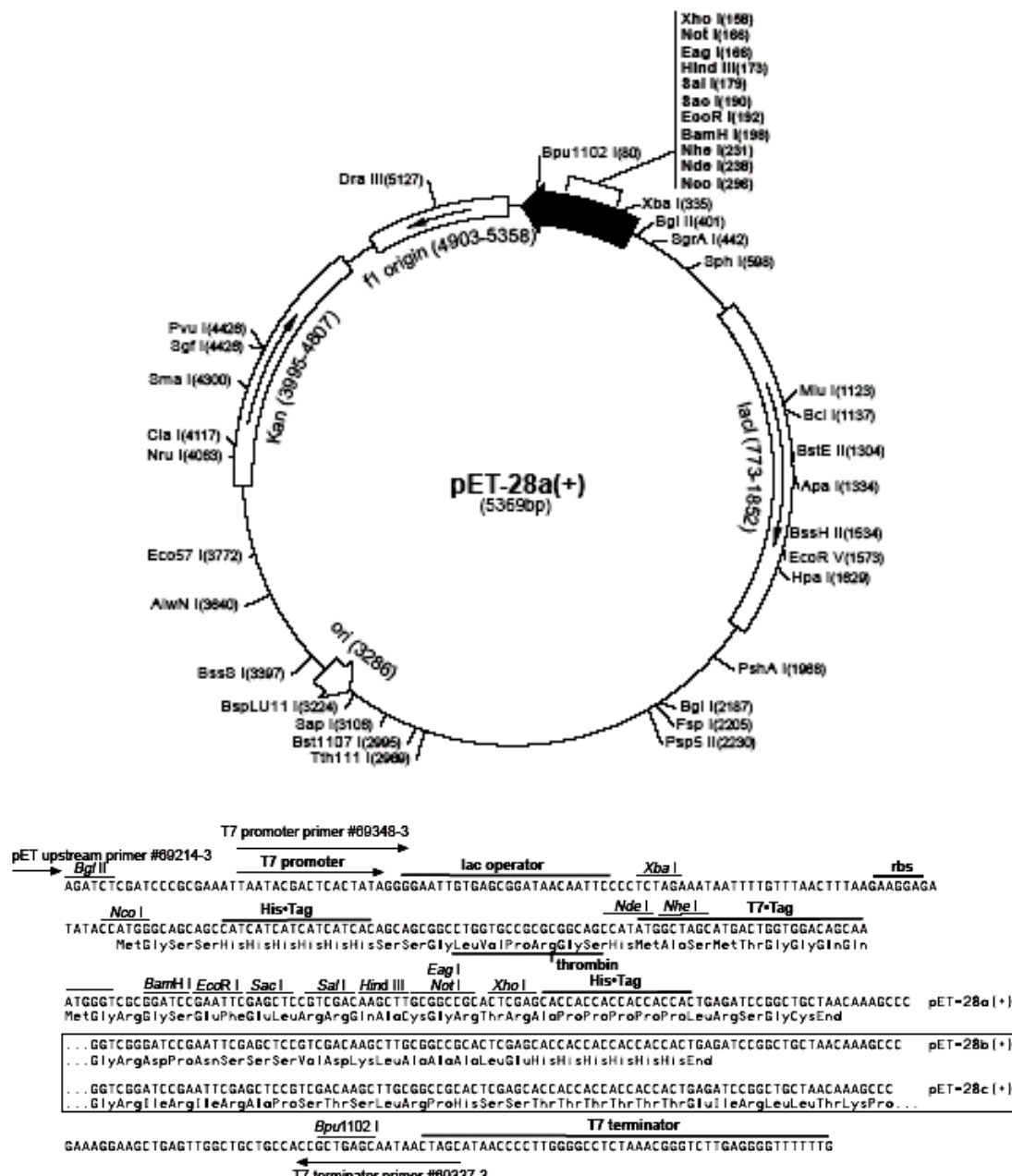


Fig 4.4 The vector map of pet28a with the details of the multiple cloning site is shown as taken from Novagen at www.novagen.com.

the histidine tag if necessary, a T7 tag coding region to facilitate protein detection through western blot or immunoprecipitation and/or to improve protein expression yield, and a multiple cloning site as shown in figure 4.4. The subclone was completed by double digestion with restriction enzymes that form sticky ends for ligation, *Bam*HI and *Eco*RI. After the subclone was verified through automated sequencing, the DNA was transformed into DH5 α *E. coli* for DNA amplification and into BL21(DE3) *E. coli* cells for expression.

4.4 Expression and Purification of EGFP and Calcium-binding Variants

4.4.1 Expression of EGFP and the designed proteins

EGFP expresses very well in BL21(DE3) *E. coli* grown in Luria-Bertani medium and is strongly fluorescent when the temperature is reduced to 30 °C after induction with 0.2 mM IPTG at an optical density (OD) of 0.6. The protein expresses at 37 °C, but it is not fluorescent, which has been well documented in the literature (63). However, with expression at 30 °C after induction, it is common to obtain 20-30 mg of pure protein per 1 L of medium (Chapter 2.5). As shown in figure 4.5, the EGFP band just above the 28 kDa marker band increases with time after induction. The cell pellet is colored yellow under room lights and glows green under a handheld UV light at 354 nm due to EGFP expression, as illustrated in figure 4.5.

When the full designed sites—120, 177, and 194a—were expressed under the same expression conditions as EGFP in BL21(DE3) and LB medium with the temperature reduced to 30 °C after induction, they were not colored. As shown in figure 4.6, the cell growth and SDS-PAGE results indicate that the cells grew well and that the

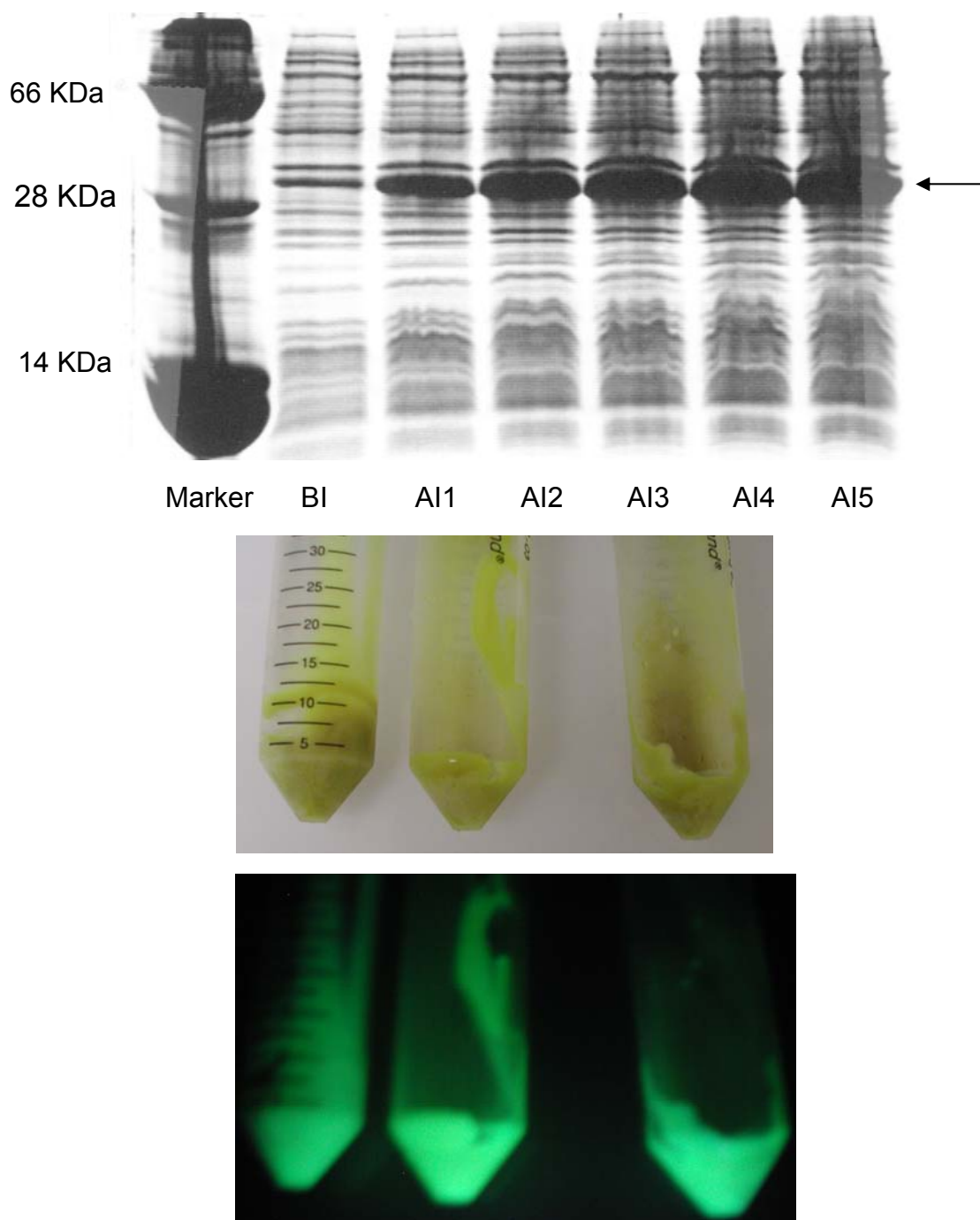


Fig 4.5 SDS-PAGE gel of the expression (top) of EGFP when expressed with the pet28a vector in LB media. The lanes in the gel are before induction and 1-5 hr after induction. Pictures of EGFP under standard room lights (middle) and under UV excitation handheld light at 366 nm (bottom) indicating the strong fluorescence of EGFP even when still in the cell pellet.

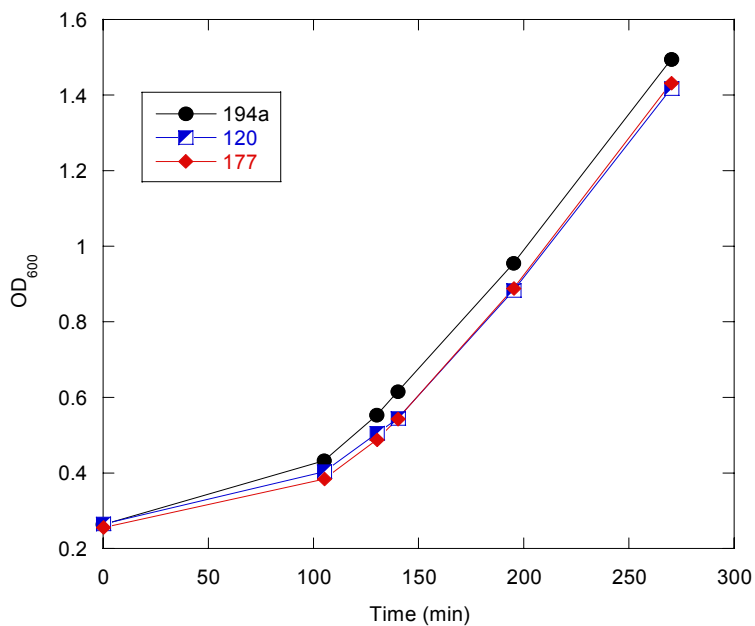
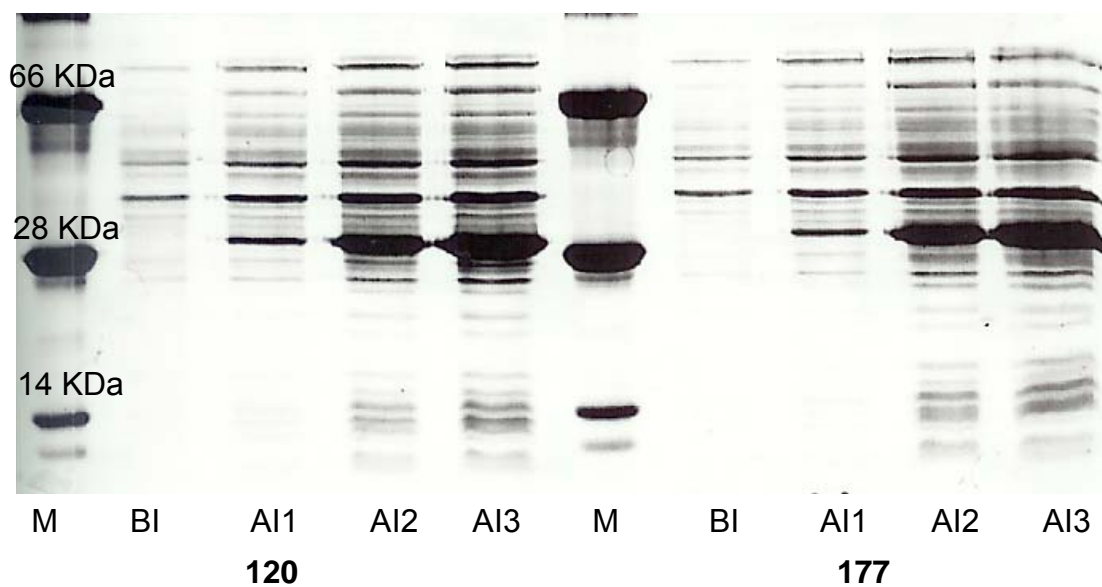


Fig 4.6 SDS-PAGE gel of the expression of 120 (left) and 177 (right) in LB-kanamycin and BL21(DE3) *E. coli*. The lanes are labeled for marker (M), before induction (BI), and after induction for 1-3 hrs (AI1, AI2, AI3). The band just above 28 kDa is the EGFP variant. The cell growth curve (bottom) illustrates that the cells grew well during the expression with induction (0.2 mM IPTG) at approximately 0.6 OD.

protein expressed at high levels as indicated by the large band above 28 kDa. However, the pellet after expression did not emit fluorescence. Fluostar, a microarray fluorescence instrument, was utilized with the appropriate filters for GFP fluorescence to ascertain if the variants were fluorescent as shown in figure 4.7. The intensities from these trials were the same as the baseline. As demonstrated in Table 4.3, expression trials were completed to determine the optimal conditions so that the proteins would gain color—including different *E. coli* strains, various media, different IPTG concentrations at induction, expression time, and leading protein—but none of these trials demonstrated colored designed protein. Different *E. coli* strains were tested because each strain has its own unique properties that could allow the proteins to fold better, such as a reducing or oxidizing cytosolic environment. JM109 *E. coli* did not express the protein well nor did Rosetta-GAMI cells. Different media were also tested due to their different environmental properties. It has been found that adding salt to the media allows for better protein production (125)(unpublished observations), but the increased salt concentration in the SV media did not produce fluorescent protein although the proteins were well expressed. IPTG (isopropyl β -D-thiogalactoside) is a commonly used chemical to induce expression of vectors containing the lac operon. The concentration of IPTG is protein, vector, and cell strain dependent so the amount for the variants was tested. Concentrations from 0.1 mM to 0.8 mM did not yield fluorescent protein although a large amount of protein was produced. In addition, the proteins were expressed without induction with IPTG and grown for 24-48 hrs to ascertain if less protein in the cells would allow the proteins to fold properly and become

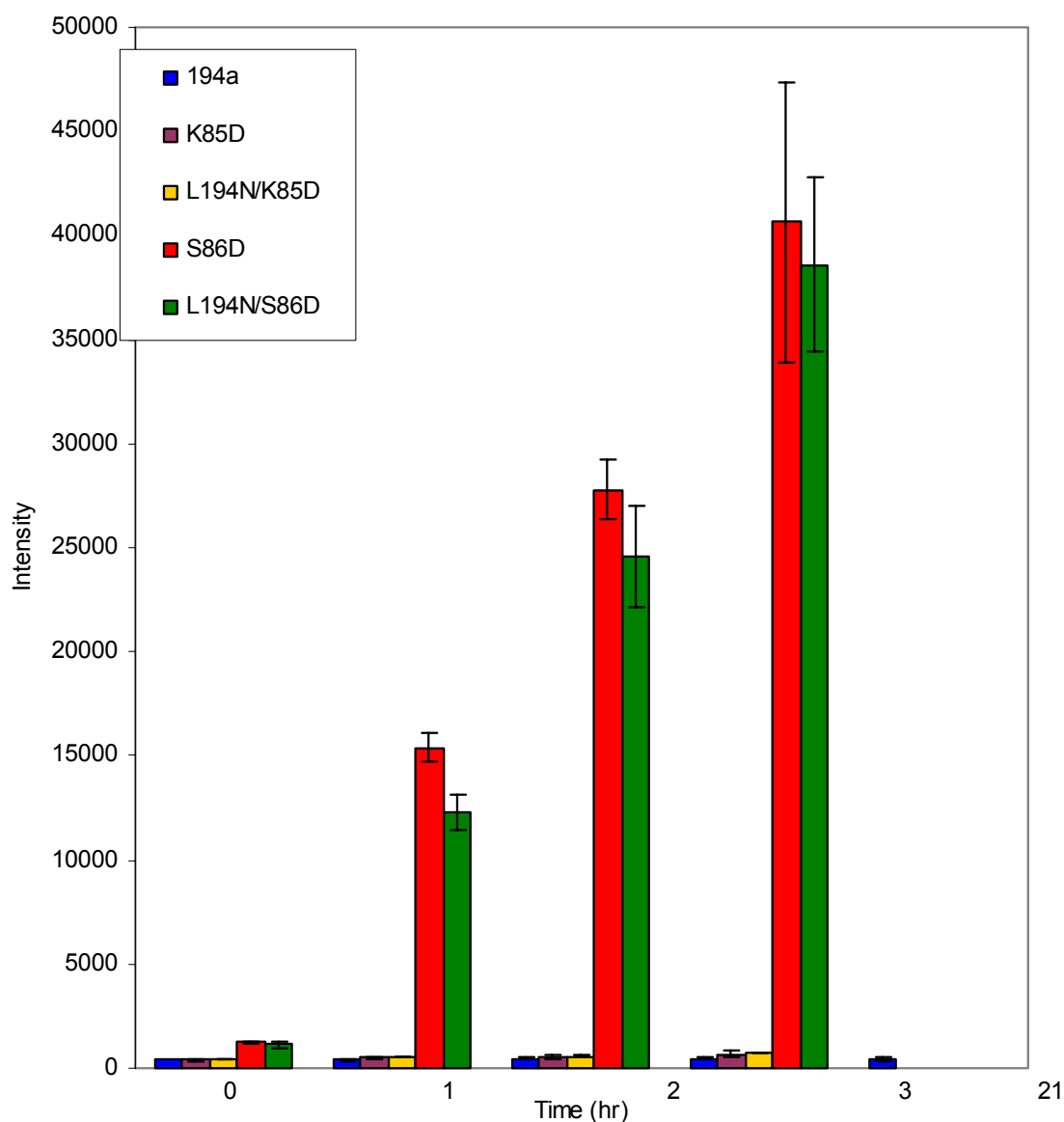


Fig 4.7 A graph of the Fluostar microplate assay results for the expression of designed protein 194a and four of its variants, K85D, S86D, L194N/K85D, and L194N/S86D, is shown to illustrate the use of the microplate reader in determining if protein fluorescence is indicated. Site 194a does not become fluorescent even after 21 hr of expression. These results are similar for sites 120 and 177. The variants containing K85D also do not indicate fluorescence, implying that this mutation is detrimental to chromophore formation. The variants containing the S86D mutation are fluorescent, indicating that this mutation does not disrupt chromophore formation.

Table 4.3 Summary of the conditions tested to provide EGFP variant fluorescence.

Condition
BL21(DE3) in LB media
BL21(DE3) in SV media
JM109 in LB media
Temperature at 25 °C after induction
0.1-0.8 mM IPTG
Expression up to 48 hrs
Expression with GST at the N-term

fluorescent. The amount of IPTG could influence protein folding because it affects the rate of protein expression. If the protein is expressed too quickly in large amounts, it may not have time to fold properly and be sent to inclusion bodies too quickly. Varying the amount of IPTG could help the protein fold since GFP is known to need time to mature, up to several days for the wild type protein from jellyfish. This is also the reason why the protein was expressed over several days with induction, to ascertain if extra maturation time was necessary. In addition, expression trials were performed by Dorinda Nelson, a summer McNair student. The expressed site 229 indicated no fluorescence with each of the above conditions tested.

Although several growth conditions were varied, the designed proteins 120, 177, 194a, and 229 remained colorless when expressed in bacteria. Waldo and Terwilliger indicated the use of a leading protein that is known to fold well under a variety of conditions to improve the folding of the desired protein (126). In that study, they employed glutathione-S-transferase (GST) fused to a GFP variant and monitored the expression and folding rates of the variant. They found that an N-terminal fusion of GST to GFP remained soluble and increased in brightness, indicating better tertiary packing, while the GFP variant without the leading protein aggregated as inclusion bodies. The variant proteins were expressed with GST at the N-terminus. EGFP indicated color and fluorescence when expressed with GST with the temperature reduced to 30 °C after induction, but the designed proteins did not. However, the variant proteins express in high yield with large bands indicated on the SDS-PAGE except for expression in the JM109 cells.

4.4.2 Purification of EGFP and the designed proteins

As illustrated in figure 4.8, to purify EGFP for biophysical studies, the protein was released from the cell pellet by sonication after the pellet was suspended in lysis buffer (section 2.5) and centrifuged to separate the soluble protein from the insoluble cell elements. The protein was then loaded onto a previously prepared nickel chelating column (Amersham Biosciences). Histidine tagged proteins will bind to chelated nickel allowing for contaminant proteins to be washed away. EGFP was then removed from the column by competition with imidazole, which binds to the nickel by virtue of its similarity to histidine. The eluted protein was then dialyzed against 10 mM Tris, 1 mM DTT, 1% glycerol, pH 7.4 to remove the imidazole. The host protein, EGFP, purifies very well with high yield, 20-30 mg/L, with this method as indicated in figure 4.9. Storage of the protein in 20% glycerol at -20 °C allowed the protein to remain in good condition for up to 1 year.

EGFP has a known tendency to oligomerize in solution. This process was observed after purification of the protein by SDS-PAGE, as shown in figure 4.10. The monomer is observed just above 28 KDa and a dimer band is observed next to the 66 KDa marker band. Addition of 5% β -mercaptoethanol removes the dimer band, as shown in the bottom gel in figure 4.10. Before staining the gel, a yellow color was also observed in both bands, indicating the presence of the chromophore in both bands. Previous reports have suggested that the two surface cysteines (48 and 70) contribute to the dimerization by forming disulfide bonds (127). The use of β -mercaptoethanol reduces the disulfide bonds so that the protein does not dimerize.

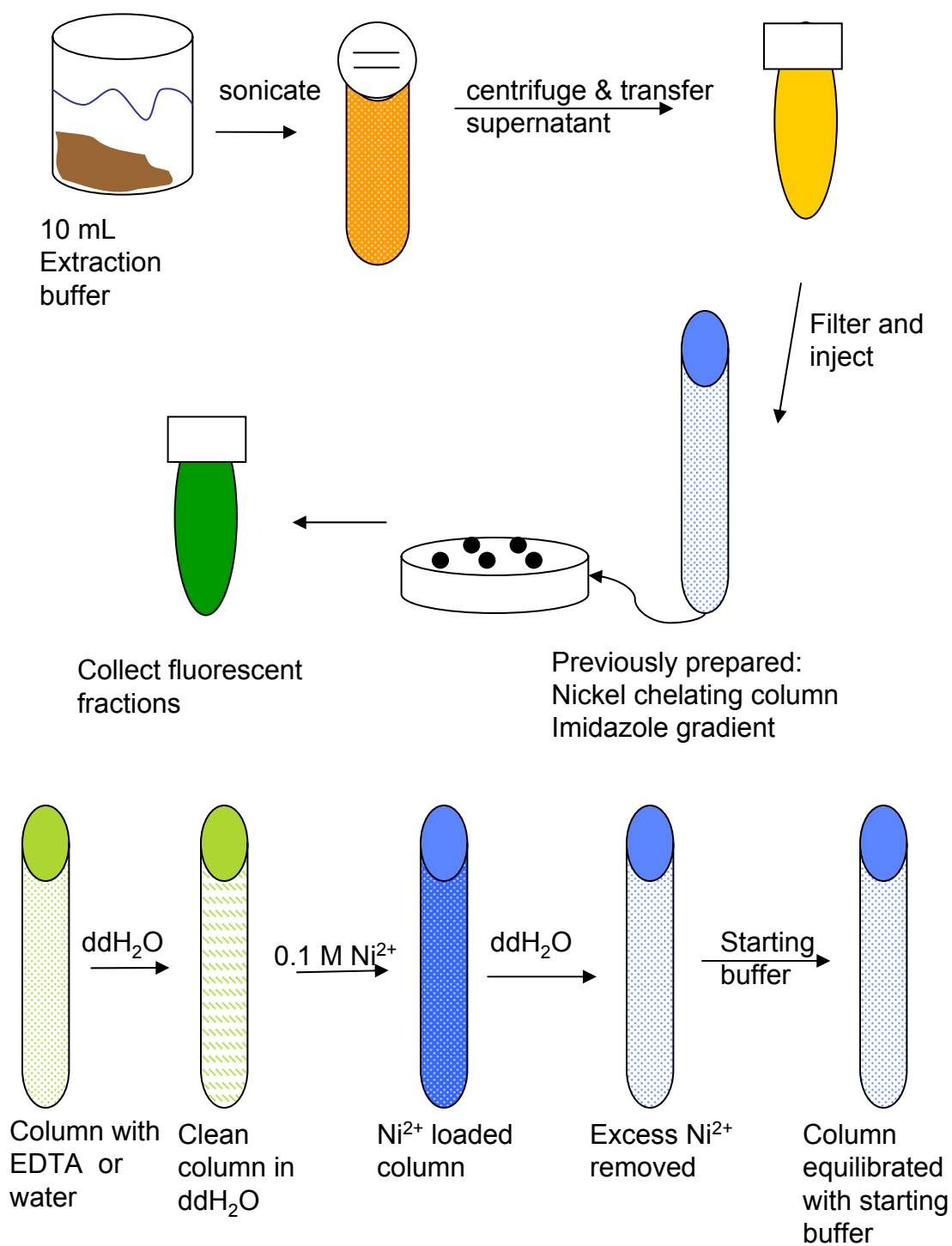


Fig 4.8 Purification scheme for EGFP utilizing the Hitrap nickel chelating column. The top indicates the overall method and the bottom indicates the preparation of the column.

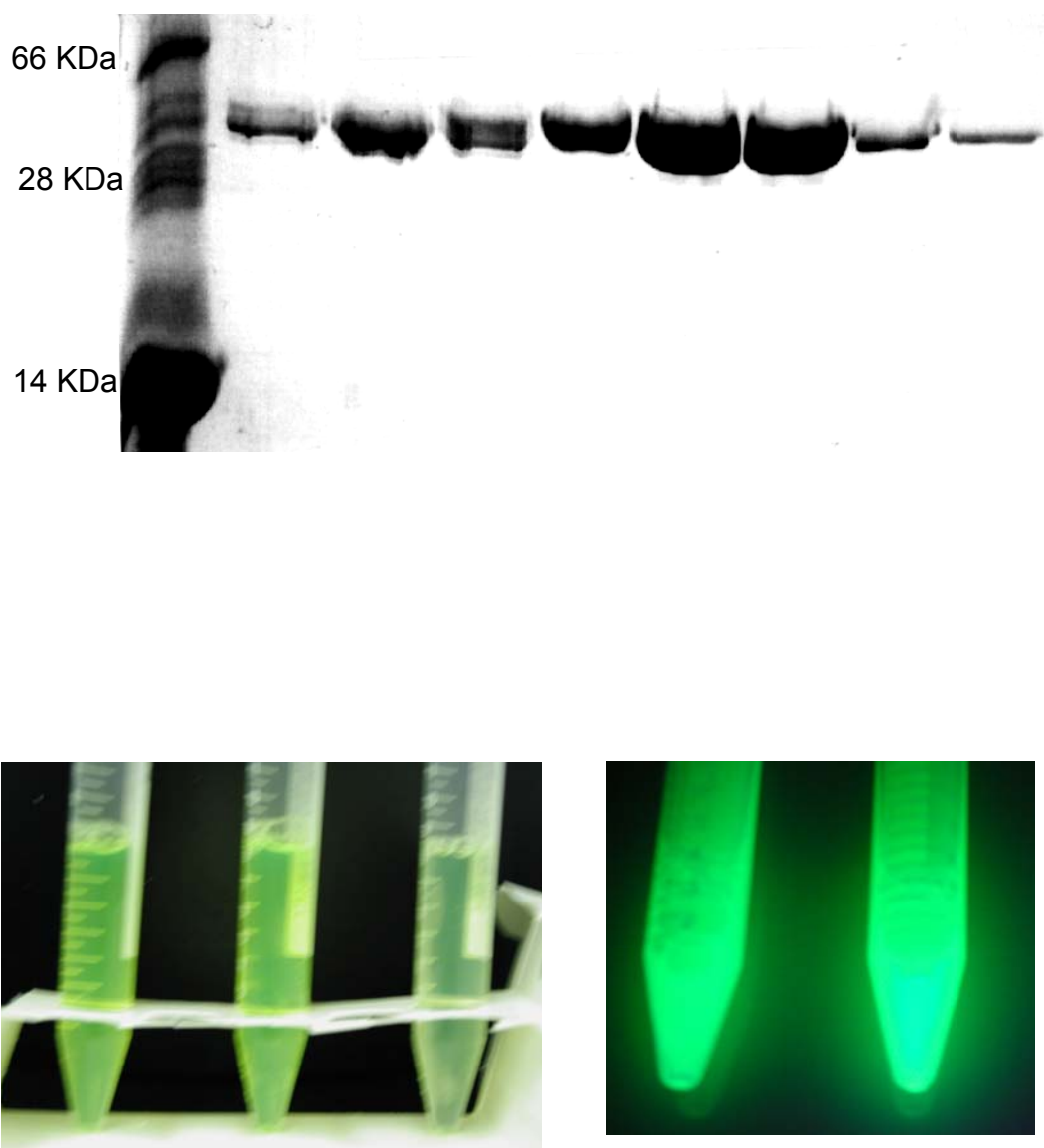


Fig 4.9 SDS-PAGE gel of the purification of EGFP after expression in *E. coli*. The lanes in the gel are the FPLC fractions after elution from the His tag chelating column. The pictures are under room lights and under a handheld UV light illustrating the fluorescence of GFP after purification.

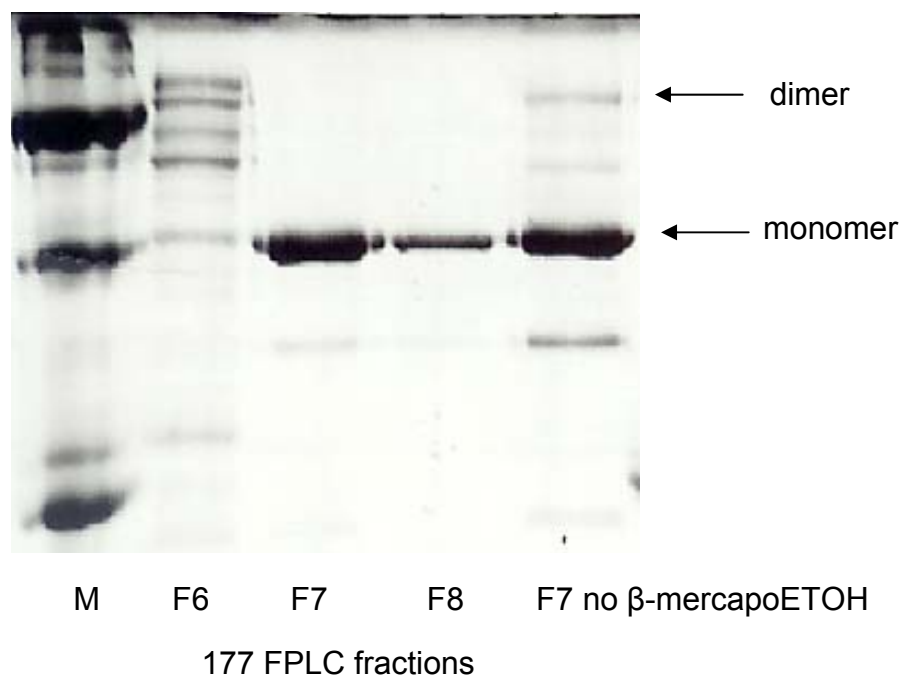
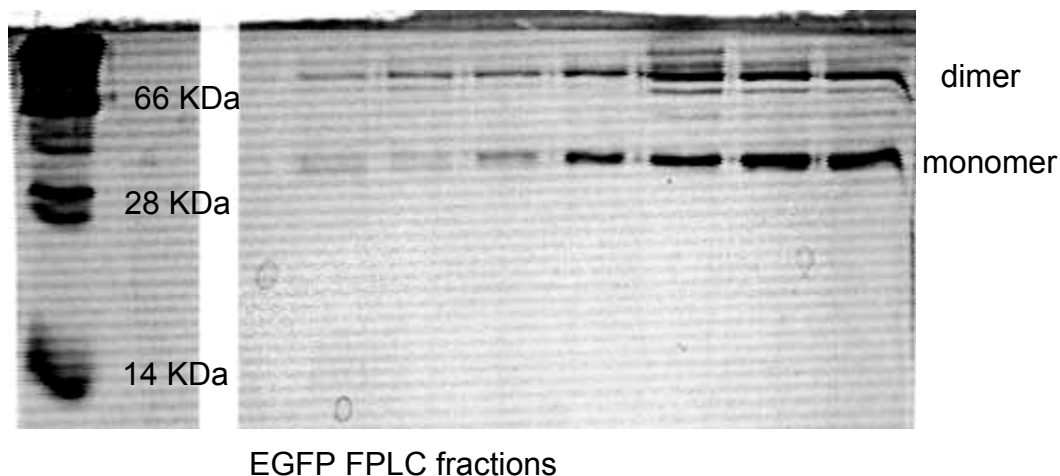


Fig 4.10 SDS-PAGE gel of purification fractions after FPLC of EGFP expressed with thepet28a vector in LB-kanamycin media and BL21(DE3) *E. coli* cells. The band above 66 KDa is the dimer formation of EGFP while the band just above 28 KDa is the monomer band. Addition of 5% β -mercaptoethanol reduced the dimer formation so that the bands became one as shown in the bottom gel of the purification of 177.

Although the variant proteins were not fluorescent, the binding of calcium to the designed pocket was still of interest to validate our design process. In addition, it was possible that the proteins could be refolded into fluorescent protein after they were purified; therefore, the designed proteins were purified. After the cell pellet was sonicated, the variant protein remained in the cell pellet, presumably as inclusion bodies, as shown in figure 4.11. The pellet was dissolved with 8 M urea to solubilize the protein. After the protein was refolded by 10x dilution into buffer (10 mM Tris, 1 mM DTT, pH 7.4), the variant protein remained in solution. It should be noted that the dilution into buffer had to progress slowly, drop by drop, to keep the protein from precipitating. To remove contaminant proteins, size exclusion FPLC with a Superdex-75 column and 10 mM Tris buffer, pH 7.4 was employed since the purification of the variant proteins was problematic utilizing the nickel chelating column. First, the variant protein eluted in many fractions at different imidazole concentrations, unlike EGFP, which would elute in 3 or 4 fractions in a narrow range of imidazole concentration. Hence, the concentration of the purified variants was quite low due to such a large volume (~20 μ M). This was likely a result of interference from denaturants allowing non-specific binding of contaminants. Unfortunately, the proteins would precipitate during the concentration process even with the addition of glycerol from 1% to 20%. When the variant proteins were purified with the size exclusion column, they generally eluted in 3 fractions so that the concentration was much higher (~100 μ M), and there was no need to concentrate the protein. Second, dialysis of the variant proteins tended

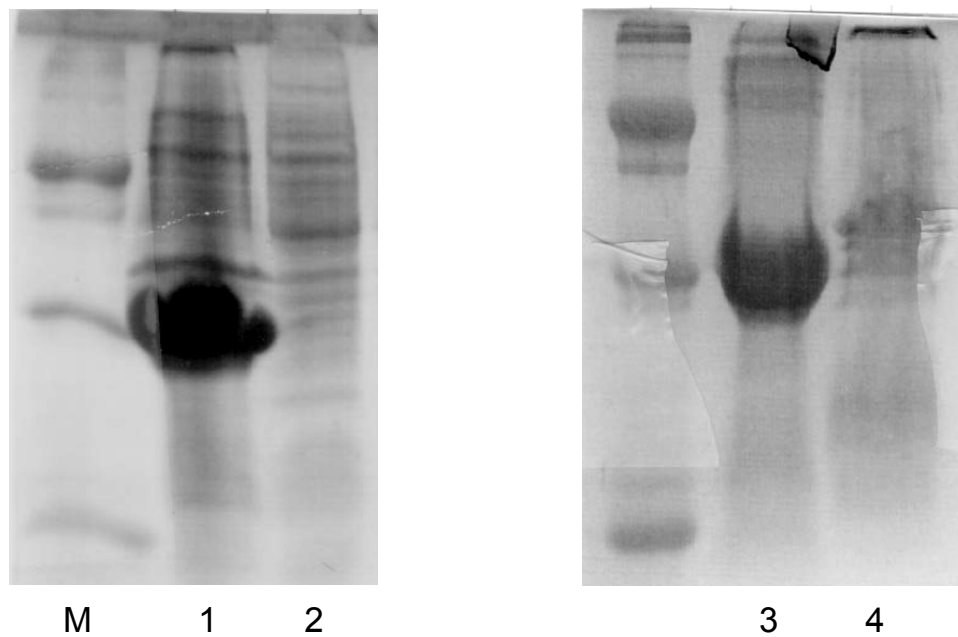


Fig 4.11 SDS-PAGE gels of site 120 purification. Lane 1 is the cell pellet after sonication. Lane 2 is the supernatant after sonication. Lane 3 is the supernatant after refolding with 8 M urea. Lane 4 is the pellet after refolding with 8 M urea. These results indicate that the protein is insoluble until refolded with urea, after which the protein remains in solution.

to result in precipitation. Purification with the size exclusion column did not require dialysis. The variant proteins were purified to >95% purity, as shown in Figure 4.10, before they were utilized for biophysical characterization and stored in 1% glycerol on ice at 4 °C or in 20% glycerol at -20 °C.

4.4.3 Purification optimization and degradation reduction with Hitrap Q FPLC

The fluorescent proteins, EGFP and the partial sites discussed in section 4.6, were observed to degrade over time, especially when stored at 4 °C on ice, and to lose fluorescence gradually. The molecular weight was observed by SDS-PAGE and mass spectrometry to be reduced to two fractions at 20 KDa and 10 KDa. In addition, the histidine tag was cleaved during storage. Two approaches were taken to resolve this problem. First, glycerol concentrations were tested to avoid induced spectral changes and precipitation upon thawing of the protein were tested (by a coworker Ning Chen). It was found that 20% glycerol could be added to the stock protein for storage at -20 °C. Second, the protein was further purified (after the Ni²⁺ chelating column) with a Hitrap Q column and a NaCl gradient to remove any contaminants that may be contributing to the degradation. The Hitrap Q column is an anion exchanger with positively charged functional groups. These functional groups will bind to negatively charged proteins while other proteins are washed away. Once bound, the protein can be eluted with a salt gradient. Contaminants will not elute at the same salt concentration as the desired protein. We hypothesized that a protease was copurifying with our proteins and causing the degradation, which is not unlikely due to the number of proteases in bacteria.

The degradation of protein samples before and after purification with the Hitrap Q column was tested weekly by SDS-PAGE. The samples were stored both on ice at 4 °C and on the bench. After 9 days, the Hitrap Q purified protein stored on the bench had degraded much like the protein that did not undergo the Hitrap Q column (but was stored on ice at 4 °C) while the protein stored at 4 °C was still intact. After 20 days, the protein that had undergone the Hitrap Q column and was left on the bench at room temperature had not degraded further while the protein that had not undergone the Hitrap Q column was degraded further. The protein kept cold was still largely intact. At 4 weeks, the protein stored on the bench was completely degraded to ~27 kDa while the protein kept cold had not degraded. This trend continued until 6 weeks later when all of the proteins had degraded to ~27 kDa. Further degradation was not observed. During this time, another protein sample that had not undergone the Hitrap Q column but had been stored in 20% glycerol at -20 °C was also tested for degradation. No degradation was observed after one month. Due to these observations, proteins were further purified with the Hitrap Q column and then stored with 20% glycerol at -20 °C to prevent degradation. No further degradation was observed except for loss of the His tag after more than one year of storage with a molecular mass reduction from 34 kDa to 28 kDa, which is the molecular weight for GFP without the histidine tag. The protein was still intact and exhibited its normal spectral behavior but would not bind to the Ni²⁺ chelating column. This loss of the His tag has been reported in the literature and does not effect the function of the protein.

4.5 Investigation of Histidine Tag Interference by Interactions with Metal Ions

Since a 6x histidine tag was utilized to purify the proteins and we are conducting metal binding analyses, the histidine tagged GFP was tested for fluorescence changes in the presence of metal ions. For protein purification, 6x histidine tags have been shown to be quite useful for obtaining large quantities of protein through binding to metal chelating columns. Amersham Biosciences, the manufacturers of the Hitrap Chelating column for His tag purification, list 232 references about protein purification utilizing their product. A Science Direct (www.sciencedirect.com) search for histidine tag yields 249 articles that largely deal with the use of histidine tags, but none of these articles address the metal interference of histidine tagged metal-binding proteins. Mohanty and Wiener studied the affects of the length and placement of the histidine tag on the expression and oligomeric state of a membrane protein, but do not discuss the effects of various metals on the protein (128). Niccolai and coworkers studied the structural effects of histidine tags on a peptide and found that the tag helps to stabilize the peptide's structure when bound to nickel (129). They also calculated the peptide structure with the histidine tags, in which it is apparent that the nickel ion is bound by the histidines. They do not, however, discuss effects of other metals or the binding affinity of nickel. With the widespread use of histidine tags for protein research, it is useful to investigate the effects of metal ions on the tagged proteins. It is important to carry out a detailed evaluation on whether the histidines could interfere with the study of designed metal binding proteins since the tags bind to metals. The binding affinities have been calculated, and metals that do not produce a fluorescence change are noted

to cause no interference in the study. A note of caution should be taken, however, that metal binding proteins have been observed to aggregate more readily upon introduction of certain metals. In this laboratory, cluster of differentiation 2 (CD2) variants were observed to precipitate upon introduction of the His tag (data not shown), but no precipitation was observed for GFP-S65T. Eleven metals were tested for interference with the histidine tag.

The effect of metal on N-terminal 6x histidine tagged GFP-S65T was tested by monitoring the fluorescence change of the protein upon addition of various metals. As shown in figure 4.12, the addition of 10 mM calcium, magnesium, potassium, and sodium (only calcium is shown) did not cause a fluorescence change of the emission spectrum with excitation at 482 nm, suggesting that these metal ions do not interfere with the histidine tag on GFP. On the other hand, as shown in figures 4.13 and 4.14, the fluorescence of 10 μ M GFP-S65T at 509 nm was observed to decrease with increasing nickel concentration. A similar effect has also been observed for zinc, cobalt, cadmium, and copper. Since these metal ions share similar coordination chemistry with similar ionic radii, they prefer to bind nitrogen from the histidine sidechain as chelating atoms. In the purification of histidine tagged proteins, metals are bound to the chelating column that will interact with the 6 histidines to immobilize the protein on the column. This interaction is known to occur with zinc, nickel, cobalt, and cadmium. Figure 4.14 shows the effect on fluorescence intensity of GFP-S65T at 509 nm (excitation at 482 nm) without metal and at saturating concentrations of the metals studied. It is clear that calcium does not have any effect on GFP-S65T fluorescence, suggesting that this metal

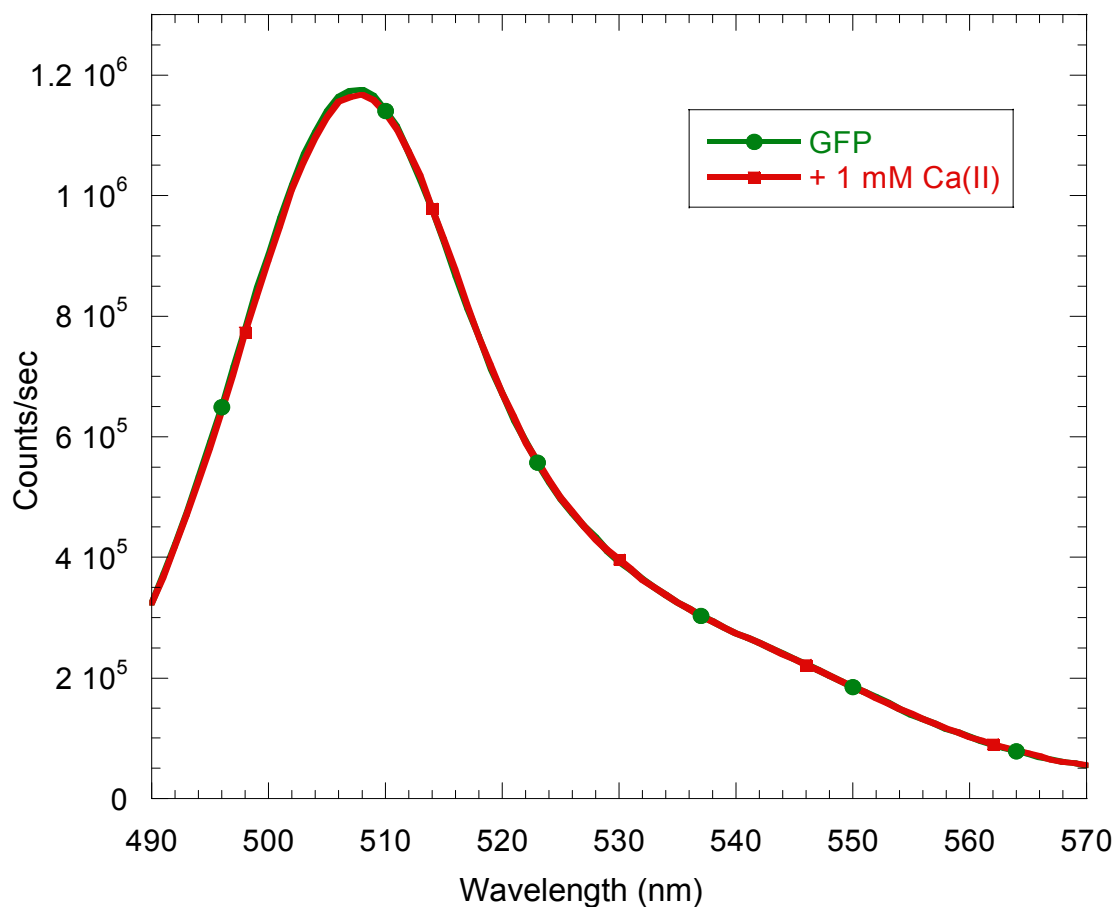


Fig 4.12 Emission spectra (excitation at 482 nm) of 10 μ M GFP in 10 mM Tris, 1 mM DTT, pH 7.4 without and with 1 mM calcium. The complete overlap in the spectra illustrates that calcium has no effect on the histidine tagged protein. The same profile is observed for magnesium, sodium, and potassium.

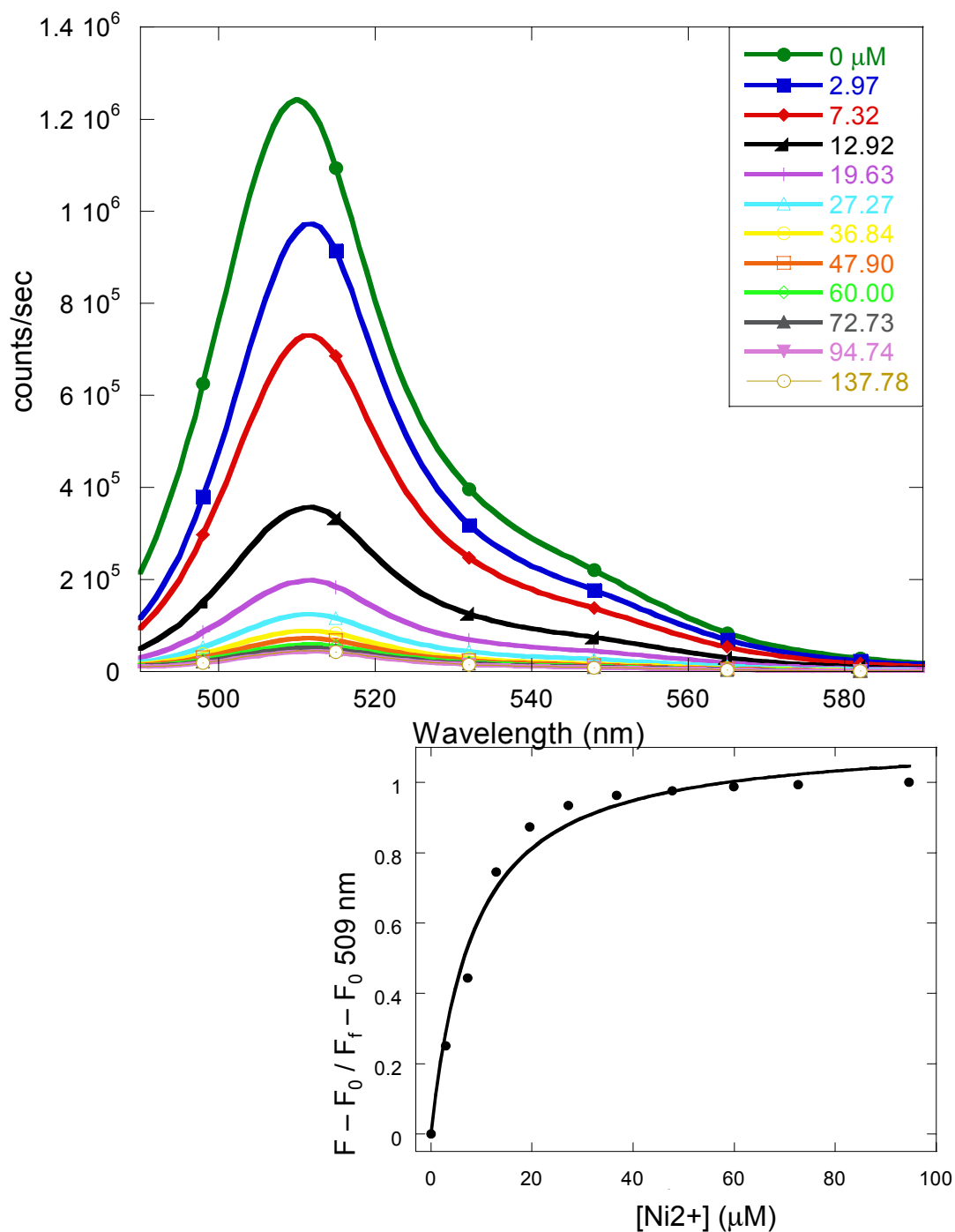


Figure 4.13 Fluorescence spectra and metal binding fit of the nickel titration of histidine tagged GFP-S65T (10 μM) indicating binding of the nickel to the histidine tag. The buffer conditions were 10 mM Tris, 1 mM DTT, pH 7.4, and the excitation was 482 nm. The fractional change data was fit with a 1:1 metal:protein binding equation given in Chapter 2.

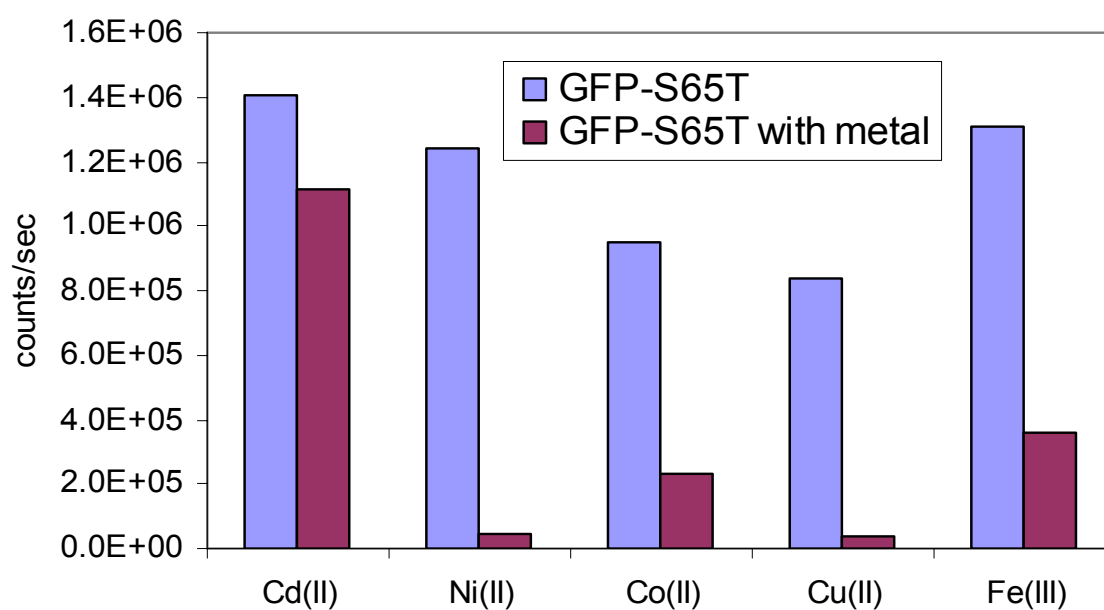


Fig 4.14 The graph indicates the overall fluorescence emission decrease at 510 nm when excited at 482 nm of 10 μ M GFP-S65T (in 10 mM Tris, 1 mM DTT, pH 7.4) caused by interference of the histidine tag with the metals presented. The bar on the left (blue) for each metal is protein without metal and the bar on the right (purple) is the protein fluorescence in the presence of saturating metal.

ion does not bind to the protein. On the other hand, zinc, cobalt, cadmium, nickel, and copper significantly quench the fluorescence. Although the chromophore is buried inside the protein and there is a distance of approximately 80 Å from the chromophore to the histidine tag (provided the His tag is not interacting with the protein), the binding of the metal to the tag results in a decrease of fluorescence. In the study of metal binding proteins, any interference from the histidine tag must be taken into account to ensure that binding affinities are measured correctly. Also, the histidine tag can cause aggregation of the protein, especially at higher metal concentrations.

By monitoring the fluorescence change at 510 nm as a function of metal ion concentration, we have obtained the metal binding affinities of histidine tagged GFP-S65T for zinc, nickel, cobalt, cadmium, and copper. Figure 4.13 illustrates the fluorescence and fractional change at 509 nm (excitation at 482 nm) as a function of nickel concentration. The K_d , calculated with the 1:1 metal binding equation (Eq. 2.3) in section 2.11, for nickel is 6.2 +/- 1.6 μ M. Table 4.4 summarizes the metal binding affinities. Cadmium, cobalt, and zinc exhibit similar affinities to nickel while copper is about 8 times weaker than nickel. This result correlates with the suggested metals utilized in purification of histidine tagged proteins and a chelating column. Copper is not generally suggested, likely because it binds weaker than the other metal ions, which is also observed in practical applications of the purification method.

Another metal, iron, was tested for its effect, but precipitation was quite evident each time it was examined even in different buffering conditions normally considered to reduce protein aggregation. However, precipitation did not occur until the metal

Table 4.4. A list of the metals studied for interference with histidine tagged proteins with the ionic radius and coordination numbers.

Metal	K_d (μM)	Ionic radius (Å)	Coordination Number
Nickel	6.2 ± 1.6	1.62	4, 5, 6
Cadmium	7.5 ± 2.4	1.71	4, 5, 6, 7, 8
Cobalt	14.5 ± 2.1	1.67	4, 5, 6, 8
Zinc	17.4 ± 2.8	1.53	4, 5, 6
Copper	50.5 ± 3.5	1.57	2, 4, 5, 6
Calcium	No effect	2.23	6, 8
Terbium	No effect	2.51	6, 8
Lanthanum	No effect	2.74	6, 8
Magnesium	No effect	1.72	4, 5, 6, 8
Sodium	No effect	2.23	4, 5, 6, 7, 8
Potassium	No effect	2.77	4, 6, 7, 8

concentration was greater than 100 μM , and fluorescence changes were observed below 100 μM , indicating that iron does have an effect on the histidine tagged protein. The exact binding affinity simply could not be calculated due to the precipitation.

4.6 Metal-binding of Designed Proteins

4.6.1 Terbium binding analysis of designed proteins

Since calcium is a silent metal ion and most of the first generation of designed calcium binding GFP variants are not fluorescent, terbium sensitized fluorescence resonance energy transfer is utilized to monitor the metal binding capability of our designed proteins. Terbium is a calcium analog with similar ionic size and binding geometry. From studies in the Yang lab, terbium has a stronger binding affinity than calcium, but the binding depends on the geometry of the binding pocket and on the value and placement of the negative charges of the ligands (86). Terbium is intrinsically fluorescent at 545 nm and can undergo energy transfer with the aromatics in a protein when it is bound to that protein and within Förster's distance of the aromatics.

4.6.2 Metal binding analysis procedure

To obtain the metal binding affinities of the designed proteins, two routines were utilized. Initially, all data were baseline corrected following Dr. Wei Yang's protocol. The data were then examined by Specfit/32, a global fitting program, and by fitting the fractional change of the integrated area with Eq 2.3. Specfit/32 utilizes a user chosen metal:ligand binding model. This model allows the user to input the number of components in the system, how the components interact with one another, which components are colored and contribute to the obtained spectra, and any known binding

affinities in the case of multiple binding components. The detailed protocol is presented in Chapter 2, section 2.12.

This method has been widely applied to obtain the terbium binding affinity for the designed proteins by titration of the protein with increasing concentrations of terbium at a constant protein concentration. As shown in figure 4.15, EGFP contains 10 tyrosines and one tryptophan. The Trp is located approximately 15 Å from the designed pocket 177, 17 Å from the 120 pocket, and 30 Å from the 194 pocket. The tyrosines are located throughout the protein with 5 of them within 20 Å of the 194 pocket. Figure 4.16 shows the enhancement of terbium fluorescence when bound to site 177 with excitation at 280 nm. The terbium binding was carried out in 20 mM PIPES, 10 mM KCL, 1 mM DTT, 1% glycerol, pH 6.8 to increase the solubility of the proteins and terbium. The terbium fluorescence enhancement was monitored at 545 nm when excited at 280 nm. Terbium has inherent weak fluorescence under this condition. It was corrected by using a terbium blank to ensure that enhancement of the fluorescence was only observed with protein binding. Once the data were obtained, it was baseline corrected following a protocol from Dr. Wei Yang in our laboratory and fit with the program Specfit/32. This program is a global fitting program that takes the entire spectrum into account. The binding affinity attained with this program and the traditional method of fitting the fractional change of the integrated area to a 1:1 binding equation (Eq 2.2) are in good agreement, indicating that the program can be used for this type of binding.

Figures 4.16, 4.17, and 4.18 illustrate the metal binding titration and fit curves of site 177, 120, and 194a. The designed proteins exhibit strong terbium binding affinities

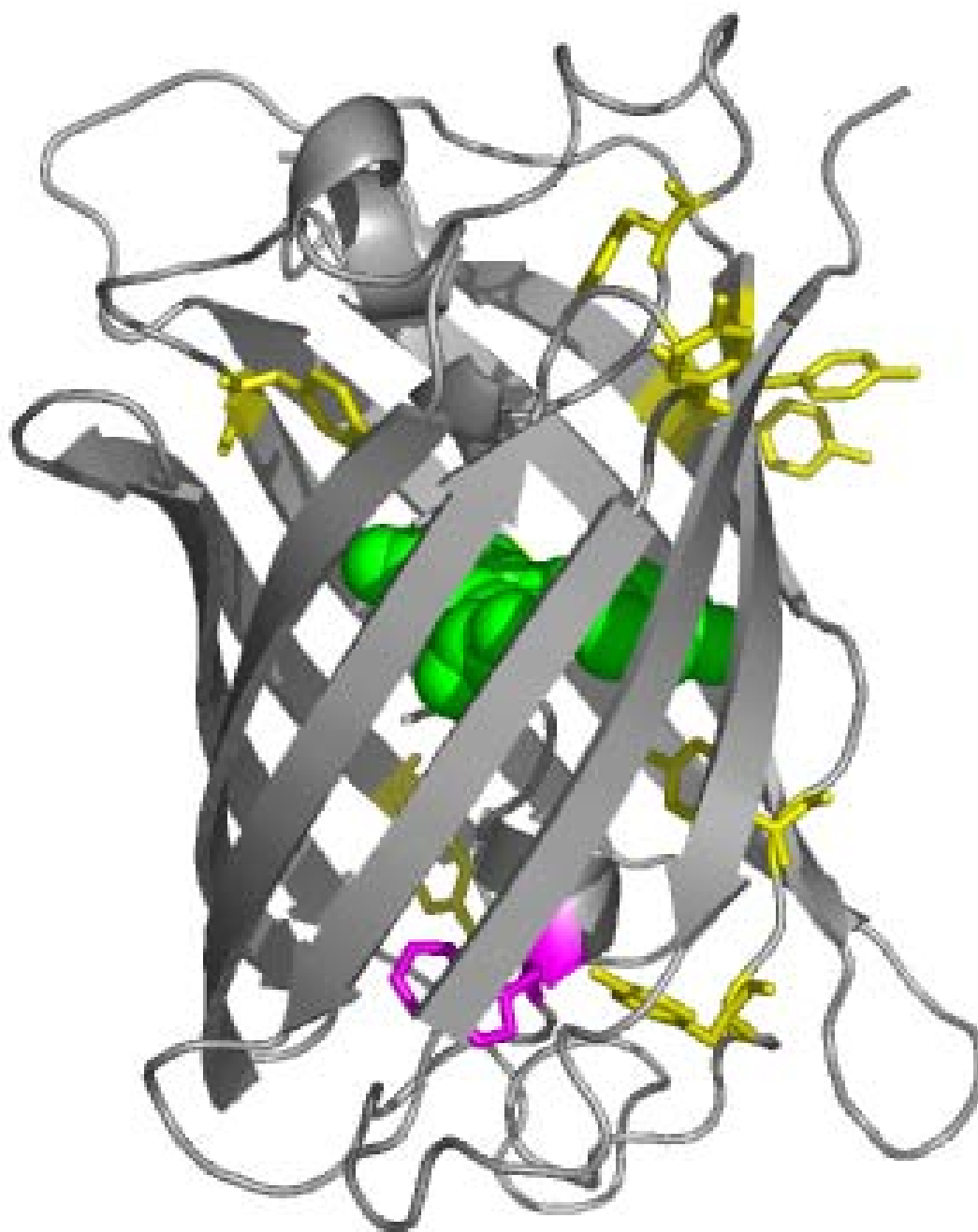


Fig 4.15 Structure of EGFP with the chromophore in green, the tyrosines in yellow, and the tryptophan in magenta.

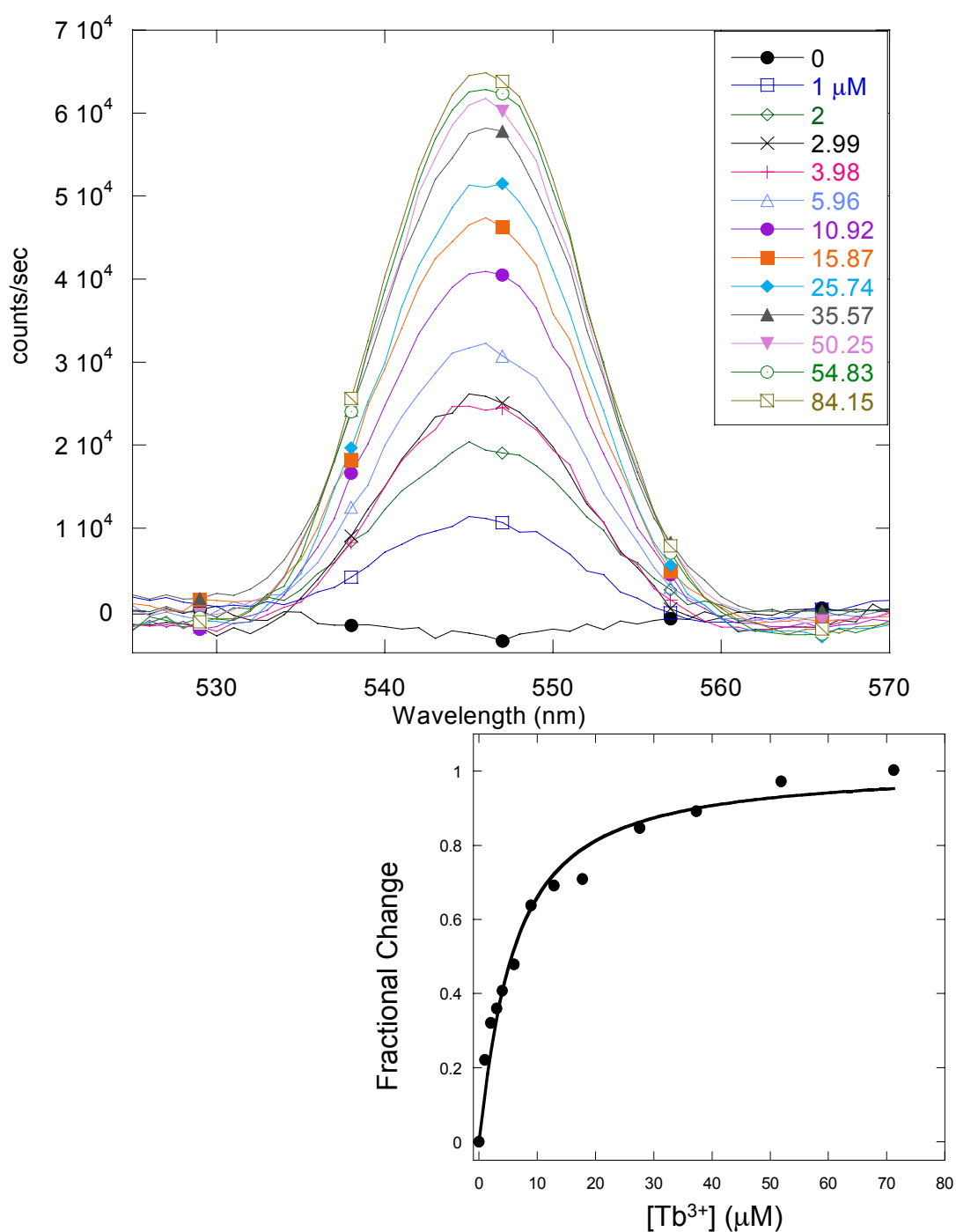


Fig 4.16 Fluorescence spectra with excitation at 280 nm and binding curve of terbium bound to a designed variant, 177 in 20 mM PIPES, 10 mM KCl, 1 mM DTT, 1% glycerol, pH 6.8. The increase in fluorescence at 545 nm indicates binding of the protein to the metal.

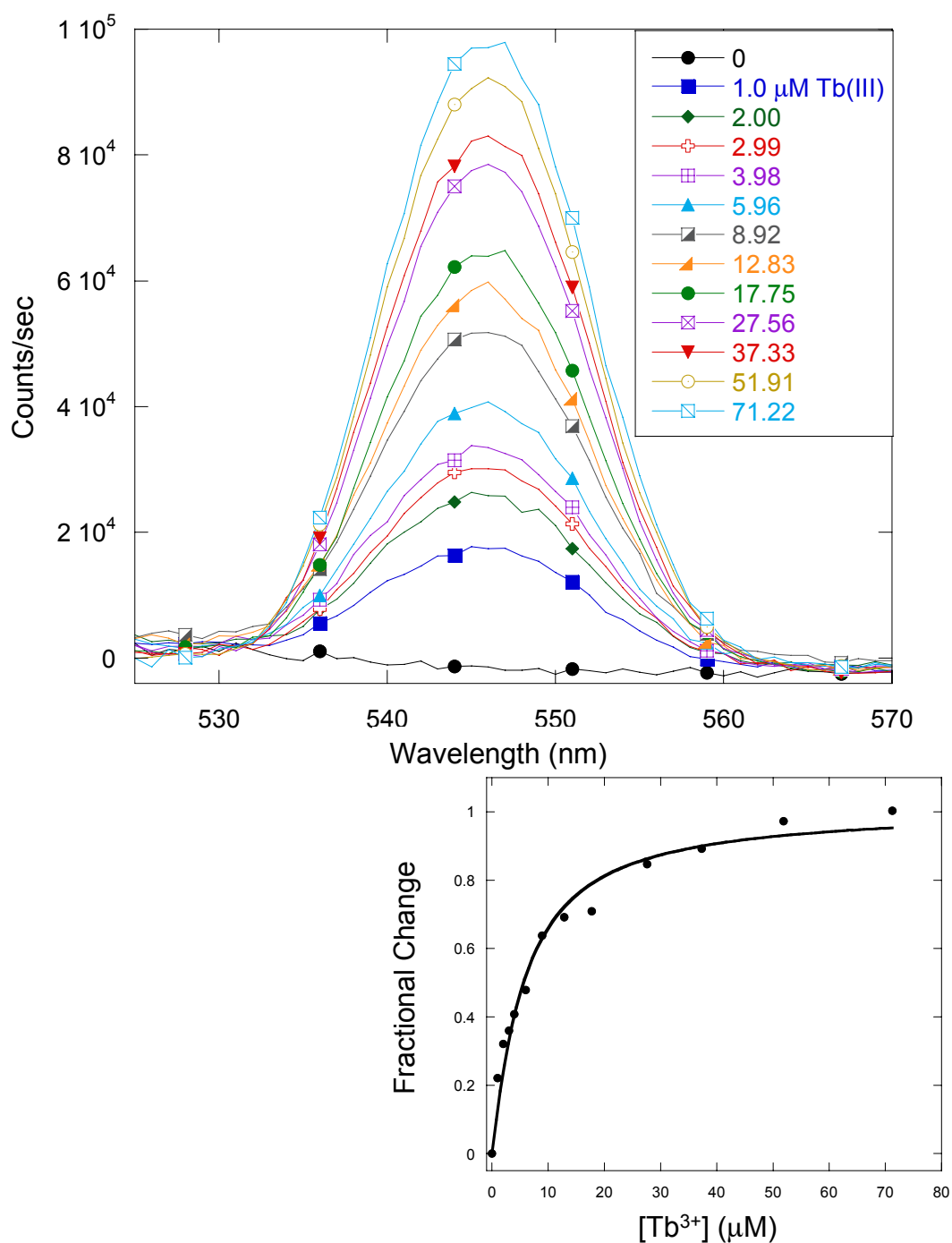


Fig 4.17 Fluorescence spectra with excitation at 280 nm and binding curve of terbium bound to a designed variant, 120 in 20 mM PIPES, 10 mM KCl, 1 mM DTT, 1% glycerol, pH 6.8. The increase in fluorescence at 545 nm indicates binding of the protein to the metal.

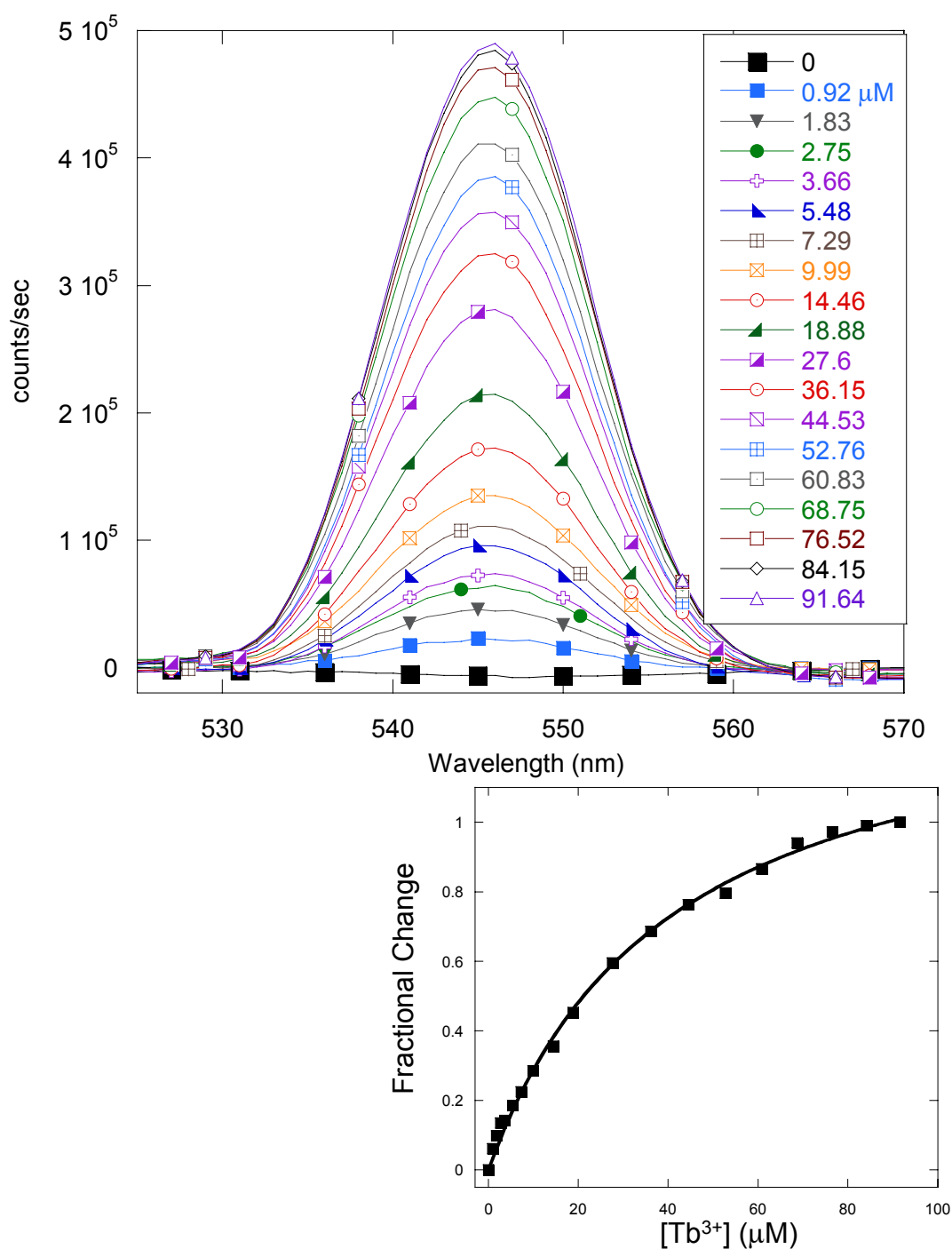


Fig 4.18 Fluorescence spectra with excitation at 280 nm and binding curve of terbium bound to a designed variant, 194a in 20 mM PIPES, 10 mM KCl, 1 mM DTT, 1% glycerol, pH 6.8. The increase in fluorescence at 545 nm indicates binding of the protein to the metal.

listed in table 4.5. Each binding affinity was obtained by averaging of 4 to 6 titrations. Site 177, with a binding affinity of 1.9 μM , has the strongest affinity of the three proteins tested. Site 120 is only slightly weaker with a binding affinity of 4.9 μM . However, Site 194a exhibits a relatively weaker affinity of 31.6 μM .

A binding affinity for 194b and terbium was attempted but conclusive results were not obtained. Initially, 3.5 μM of protein was titrated in duplicate with terbium in 10 mM Tris, 1 mM DTT, 1% glycerol, pH 7.4 as shown in figure 4.19. The K_d 's for these two titrations were 3.2 μM and 2.6 μM for an average of $2.9 \mu\text{M} \pm 0.3$. This binding affinity is on par with 177 and 120 and not similar to 194a, as would be expected since there is only one ligand difference between 194a and 194b. The terbium titrations were repeated in 20 mM PIPES, 10 mM KCl, 1 mM DTT, 1% glycerol, pH 6.8 so the binding affinities would be in the same buffering system as 177, 120, and 194a. Four trials in this system resulted in precipitation when greater than 10 μM Tb(III) was reached, with or without DTT. The titrations were then repeated in 50 mM Tris, 1 mM DTT, 1% glycerol, pH 7.0 so that the environment would be closer to that of the other three proteins with a pH of 7.0. This experiment resulted in a K_d of 26 μM but the fit of the data points were not very good with the fitting curve not following the data points. Repetition in these conditions with 1.5 μM and 3 μM of protein resulted in precipitation above 20 μM terbium. In summary, 194b exhibits a binding affinity for terbium of 2.9 μM in 10 mM Tris, 1 mM DTT, 1% glycerol, pH 7.4 but reliable binding affinities could not be obtained in the same conditions as 120, 177, and 194a. This binding affinity can not be compared with the other sites as the conditions are not the same.

Table 4.5 The binding affinities, ligands, and charge of the amino acids in the binding pocket are shown. The terbium titrations were performed in 20 mM PIPES, 10 mM KCl, 1 mM DTT, 1% glycerol, pH 6.8 except for 194b, which was in 10 mM Tris, 1 mM DTT, 1% glycerol, pH 7.4. The calcium titrations were performed in 10 mM Tris, 1 mM DTT, 1% glycerol, pH 7.4 for all of the designed proteins.

Design Site	Ligands	Charge of a.a.	Tb(III) K_d (μM)	Ca(II) K_d (μM)
120	E,N,D,D,E	-4	4.9 ± 0.2	57.2 ± 1.6
177	N,D,D,D,N	-3	1.9 ± 0.4	59.7 ± 4.8
194a	E,D,D,N,D	-4	31.6 ± 12.9	95.5 ± 6.6
194b	E,D,D,N,D	-4	2.9 ± 0.3	37.7 ± 4.5

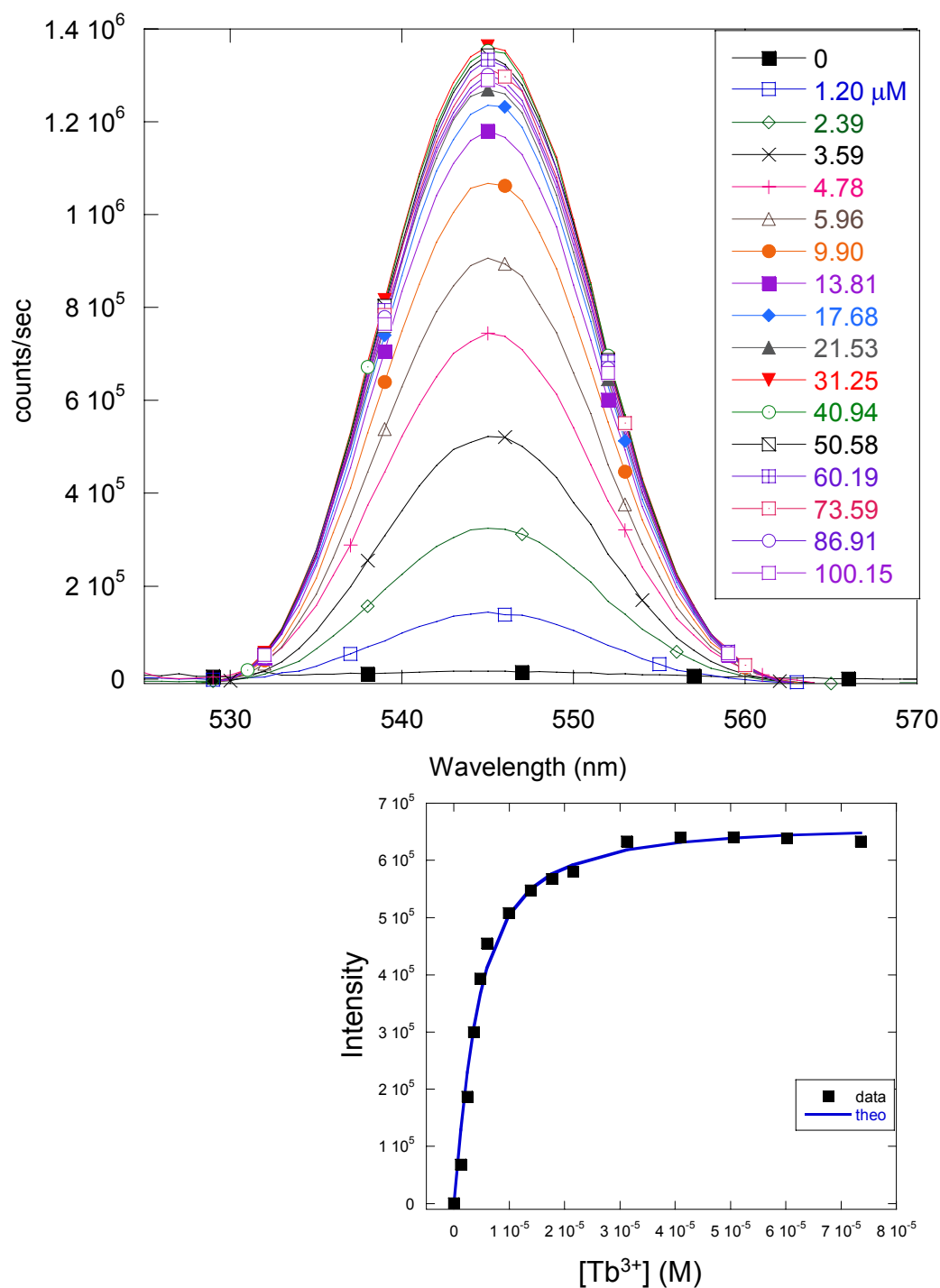


Fig 4.19 Fluorescence spectra with excitation at 280 nm and binding curve of terbium bound to a designed variant, 194b in 10 mM Tris, 1 mM DTT, 1% glycerol, pH 7.4. The increase in fluorescence at 545 nm indicates binding of the protein to the metal.

4.6.2 Metal selectivity of designed proteins

The designed proteins were investigated for metal selectivity through competition with terbium by calcium, magnesium, and lanthanum. If these other metals bind to the same pocket, the terbium fluorescence will be decreased upon addition of the metals, indicating a competition between the two metals for the same binding pocket. Calcium indicated the largest decrease in fluorescence, suggesting that calcium binds to the designed proteins and can compete for terbium binding. Magnesium at 10 mM also exhibited a decrease, but it was not as large as the calcium with 100 times more magnesium. As shown in figure 4.20, 1 mM calcium nearly abolished the terbium fluorescence enhancement for site 177, but the fluorescence is only decreased by half at 10 mM magnesium. Therefore, although magnesium can bind to the protein, it does not compete as well as calcium, indicating a relatively weaker binding affinity for magnesium. Addition of 100 μ M lanthanum indicated a decrease that was not as large as the calcium and comparable with the magnesium decrease. Of the designed proteins, site 177 indicated the largest decrease in terbium fluorescence upon introduction of calcium with nearly all fluorescence eliminated. Site 120 exhibits a half maximal decrease in fluorescence with 1 mM calcium as shown in figure 4.21. Addition of 10 mM magnesium to 120 with terbium indicated the same decrease in fluorescence as calcium, suggesting that 120 is not as selective for calcium over magnesium as 177.

4.6.3 Calcium-binding affinity through dye competition

Calcium binding dye competition was further utilized to obtain calcium binding affinities. Calcium does not exhibit a spectroscopic signal that can be monitored

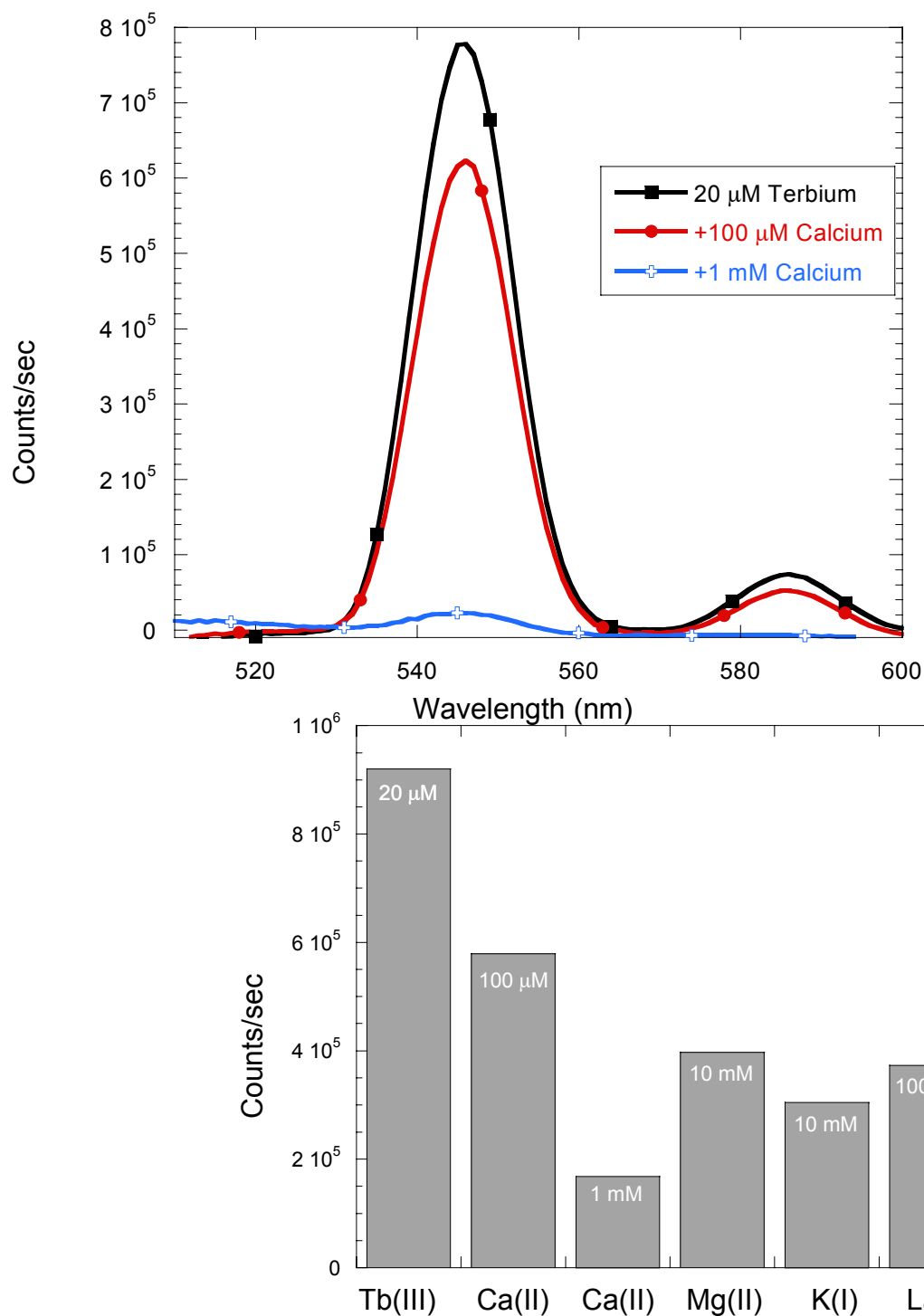


Fig 4.20 Fluorescence spectra of the binding competition of 177 with terbium for other metals in 10 mM Tris, 1 mM DTT, 1% glycerol, pH 7.4. The spectra details the calcium competition. Excitation was at 280 nm for energy transfer.

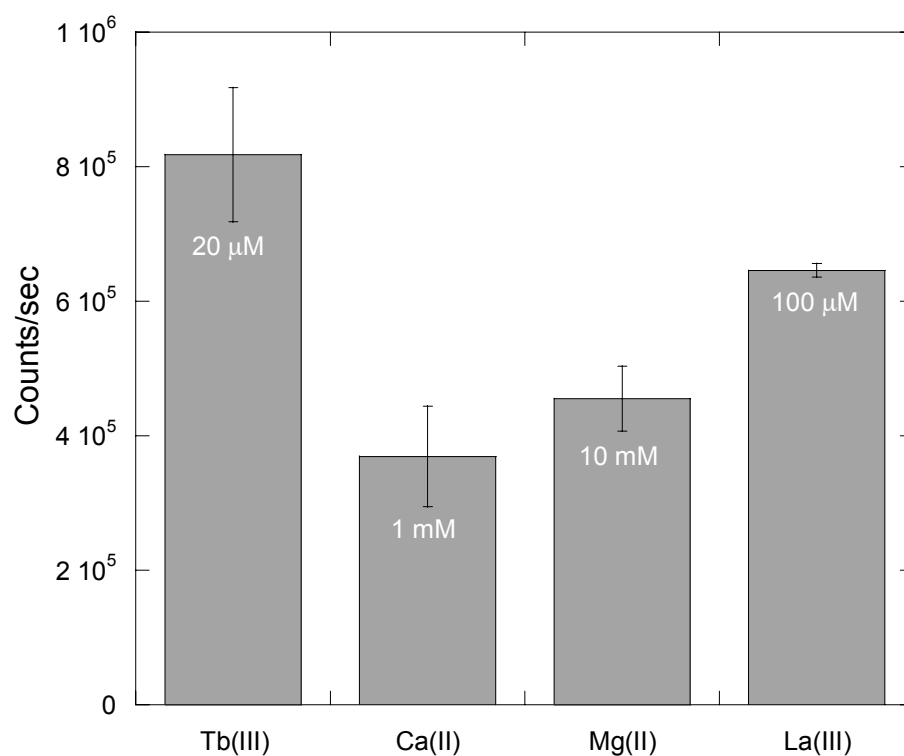


Fig 4.21 The decrease in terbium FRET enhancement observed when other metals compete for binding to site 120 is shown (10 mM Tris, 1 mM DTT, 1% glycerol, pH 7.4). Site 120 is not as selective for calcium over magnesium as site 177.

directly. Calcium isotopes, such as calcium-45, can be used in NMR experiments but the large quantities of protein that are needed exceed the concentration limits of these designed proteins in addition to the high cost. Concentrating these proteins causes precipitation that is not relieved by additives allowed in NMR experiments. Since the full designed sites do not exhibit fluorescence and the aromatics do not change signal upon calcium addition, dye competition is a valuable method to ascertain the calcium binding affinity. Rhodamine-5N (Molecular Probes, Inc.) is a commercially available calcium binding dye that indicates a large fluorescence signal increase when calcium is bound (section 1.3). Rhodamine-5N is perfectly suited for use with green fluorescent proteins since it is a red fluorophore and the excitation and emission are far from the GFP derivatives' excitation and emission wavelengths. The protein and dye excite at different wavelengths since Rhodamine-5N is a red fluorophore so no interference was observed between the two fluorophores. This method can be employed to obtain the true binding affinity in addition to monitoring the calcium-dependent chromophore fluorescence change.

The calcium titration was performed in buffer chelexed with Chelex-100 resin (BioRad) to remove background calcium. The protein was pretreated with the CalciumSponge (Invitrogen) to remove background calcium. Addition of calcium gradually enhances the fluorescence signal at 578 nm when excited at 552 nm as shown in figure 4.22. When the calcium concentration is greater than 400 μM , no further fluorescence increase is observed, indicating saturation. Rhodamine-5N indicates a 500 fold increase in fluorescence signal upon calcium binding. The

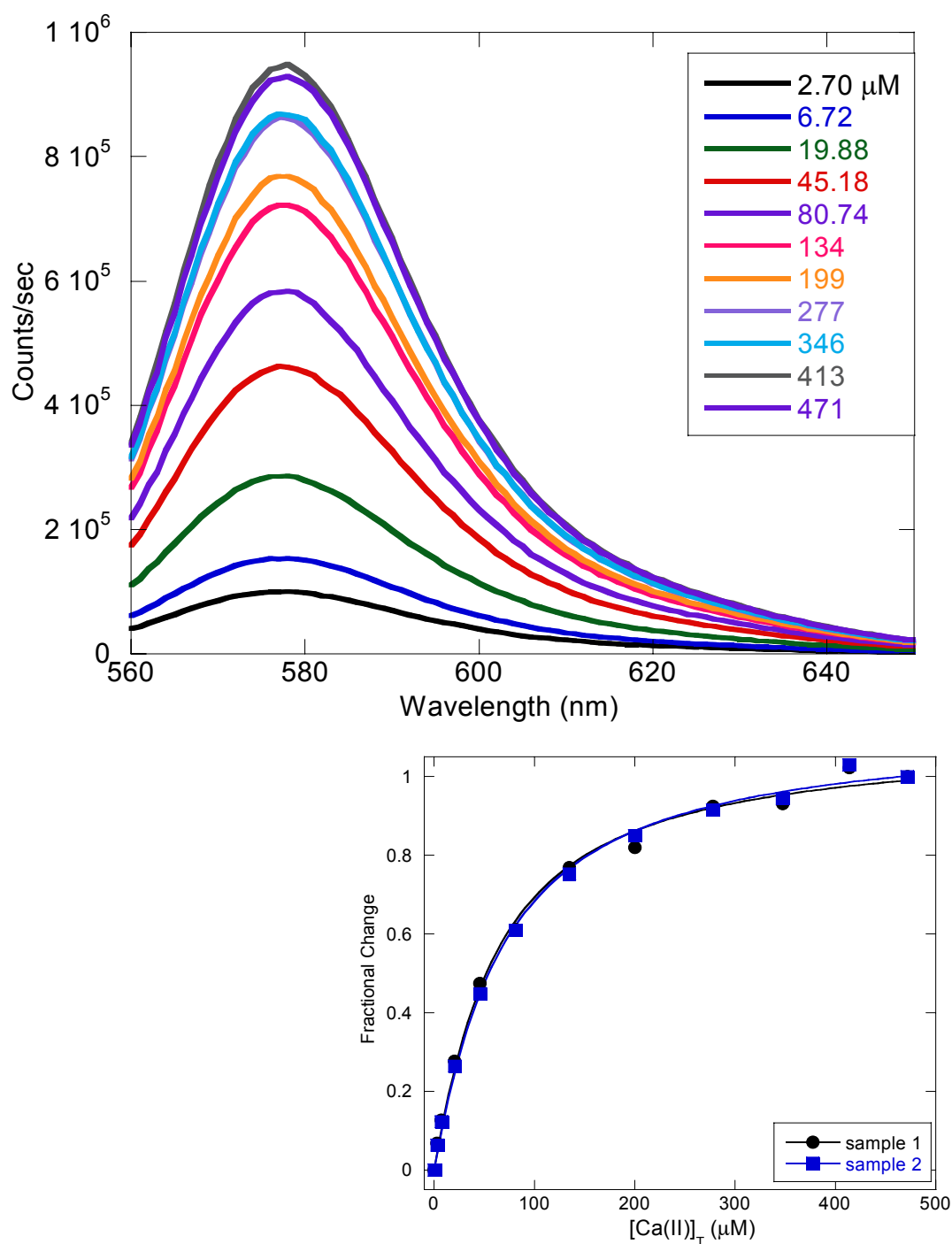


Fig 4.22 The spectra (top) of the titration of Rhodamine-5N with calcium with excitation at 552 nm in 10 mM Tris, 1 mM DTT, pH 7.4. The fit of the fractional change with the 1:1 metal binding equation is shown (bottom).

fractional change of the integrated area of the fluorescence is well fitted by a 1:1 binding equation, demonstrating a binding affinity of $54.13 \pm 3.7 \mu\text{M}$ in our conditions (10 mM Tris, 1 mM DTT, 1% glycerol, pH 7.4) using equation 2.3. This affinity is in a good range for our designed proteins since their Tb(III) binding affinities are low micromolar as detailed in table 4.5. The obtained K_d of $54 \mu\text{M}$ is different from the reported value by the manufacturer, Molecular Probes, Inc. They report a binding affinity for calcium of $320 \mu\text{M}$, but their buffer conditions contain a large amount of salt, weakening the measured binding affinity (10 mM MOPS, 100 mM KCl, pH 7.2). A note of caution should be made here that the measured binding affinity of Rhodamine-5N varies with small changes in buffer conditions. Rhod-5N alone should be titrated with calcium each time a competition assay is performed so that the conditions are the same as for the protein-dye solution. Failure to do so could yield not only incorrect binding affinities but fits that appear incorrect due to improper calculation when the data points are actually satisfactory.

The dye competition assay was carried out for designed proteins 194a, 194b, 120, and 177 in 10 mM Tris, 1 mM DTT, 1% glycerol, pH 7.4 utilizing twice as much protein as dye. The titration was performed with constant dye ($\sim 20 \mu\text{M}$) and protein concentration ($\sim 40 \mu\text{M}$) and increasing calcium concentration until saturation of the signal was observed, as demonstrated in figure 4.23. The binding affinities for the designed proteins were calculated utilizing a global fit of the spectra from 560 nm to 650 nm in Specfit/32 with the metal and two ligand model as detailed in section 2.12. An

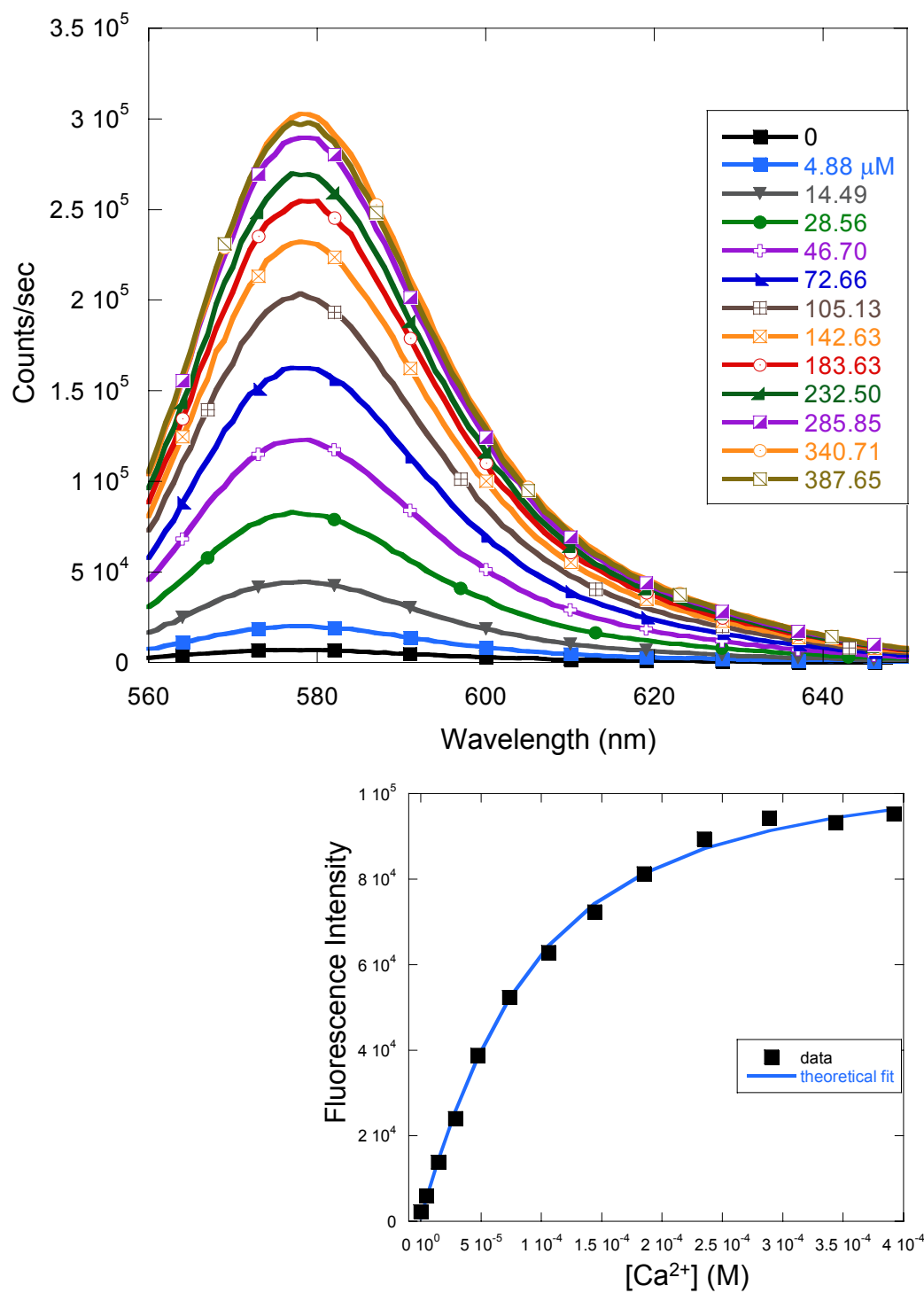


Fig 4.23 Fluorescence spectra and Specfit/32 fit of Rhod-5N in competition with Site 177 for calcium binding with the excitation wavelength of 552 nm and in 10 mM Tris, 1 mM DTT, 1% glycerol, pH 7.4.

example of the spreadsheet created for input into Specfit/32 is shown in table 2.4. After reading the data into Specfit, a model is chosen based on the type of experiment. The model utilized for the dye competition assay include free metal, protein, and dye along with dye bound to metal and protein bound to metal. The calculated binding affinity of Rhodamine-5N was included as well (as obtained in our laboratory). An example of the data fit obtained for sites 177 and 194a are shown in Figures 4.23 and 4.24. The reported affinities are the average of two titrations for site 120, three titrations for site 194b, and four titrations for sites 177 and 194a. As shown in table 4.5, all four full design sites exhibit reproducible binding affinities of $95.5 \pm 6.6 \mu\text{M}$ for 194a, $37.7 \pm 4.5 \mu\text{M}$ for 194b, $57.2 \pm 1.6 \mu\text{M}$ for 120, and $59.7 \pm 4.8 \mu\text{M}$ for 177.

The designed site 194b contains three mutations, L194N/S86D/K79D (Table 4.2), with the binding pocket proposed to be formed by those three mutations and the native residues E5 and D82. The difference between 194b and 194a is the mutation S86D in 194b and K85D in 194a. The binding affinity of 194b at $37.7 \mu\text{M}$ is stronger than the similar design site 194a with a binding affinity of $95.5 \mu\text{M}$. Part of the reason for this strengthening could be that the S86D mutation in 194b is not as drastic as the K85D mutation in 194a. Mutation of a hydroxyl to a carboxylic acid introduces one additional polar oxygen with a partial charge shared between the two oxygens. The size of the Asp and Ser sidechains are highly similar with both containing only one methylene group. Hydrogen bonds with the surrounding residues would not be disrupted. Mutation of the positively charged lysine to aspartate both reduces the size

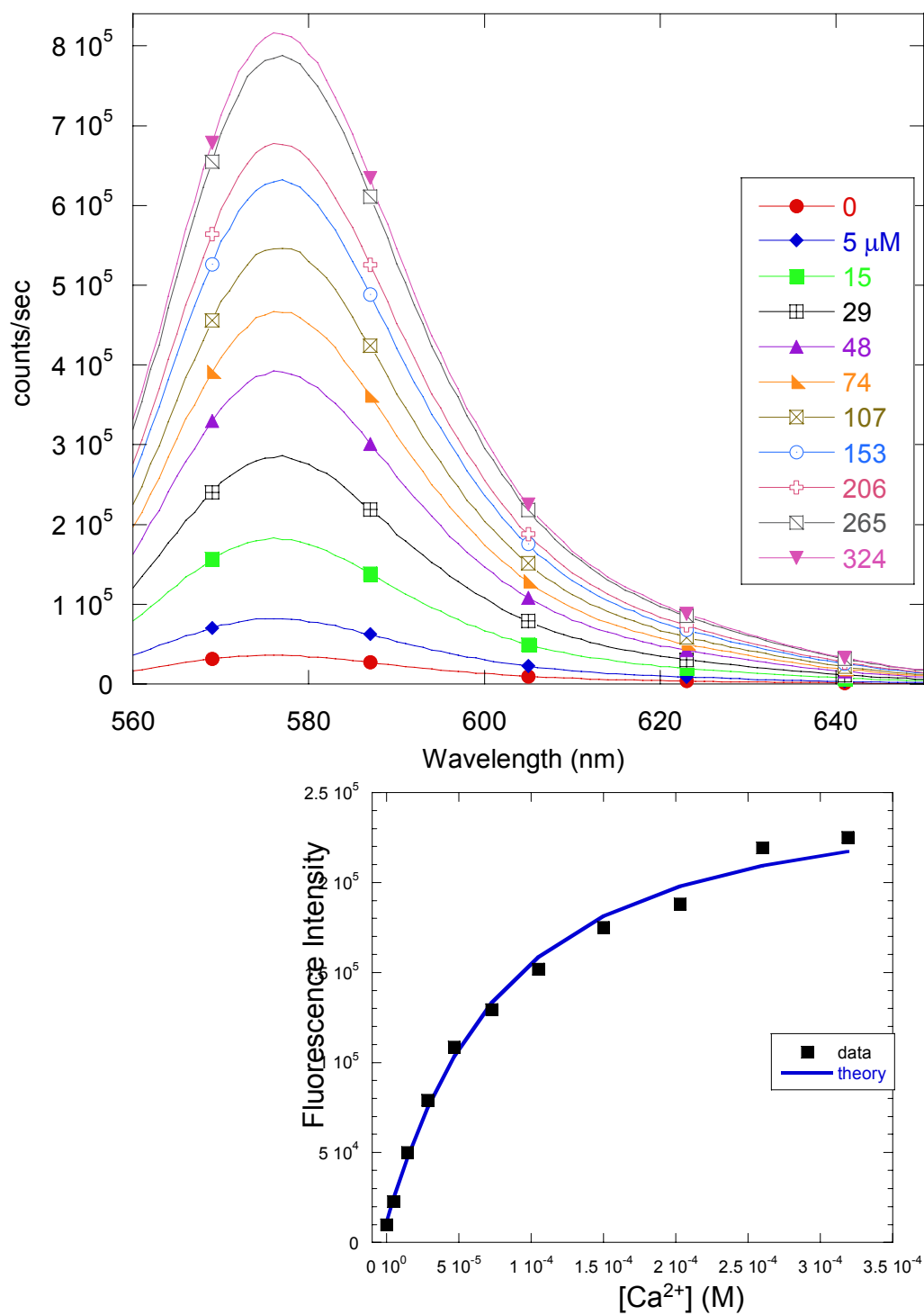


Fig 4.24 Fluorescence spectra and Specfit/32 fit of Rhod-5N in competition with Site 194a for calcium binding with the excitation wavelength of 552 nm and in 10 mM Tris, 1 mM DTT, 1% glycerol, pH 7.4.

of the sidechain and introduces an opposite charge. Lysine contains 4 methylene groups in addition to the NH_3^+ group versus the small methylene and carboxylate of Asp. The hydrogen bonds or ionic contacts that Lys would make would not necessarily still be intact with the mutation to Asp due to both the size and the charge. K85D may cause repulsion in the binding pocket so that the binding affinity is not as strong as 194b with S86D.

The partial site of 194b missing the K79D mutation, L194N/S86D is fluorescent when expressed in bacteria. The inherent binding affinity was tested with Rhodamine-5N competition to compare the intrinsic affinity of the binding site with the effects on the chromophore fluorescence upon calcium binding. L194N/S86D exhibits an average binding affinity of $5.9 \pm 0.2 \mu\text{M}$ for duplicate samples when fit with the global fitting program, Specfit/32. However, the program attempts to fit to a double exponential model, as indicated by figure 4.25, which is not suitable for the data. Fitting the data with a competition binding equation and obtaining the K_d produces $2.2 \mu\text{M}$, but the data do not fit this equation well either as shown in figure 4.26. Examination of the data indicated that saturation was not reached. The binding affinity of this protein is actually weaker than 120, 177, and 194a so that saturation of the dye's signal will be reached at much higher calcium concentration ($> 400 \mu\text{M}$). This result indicates that Rhodamine-5N is not a suitable competition dye for L194N/S86D. Since L194N/S86D exhibits green fluorescence, the direct chromophore emission change was monitored upon addition of calcium to obtain a calcium binding affinity, as shown in figure 4.27. The

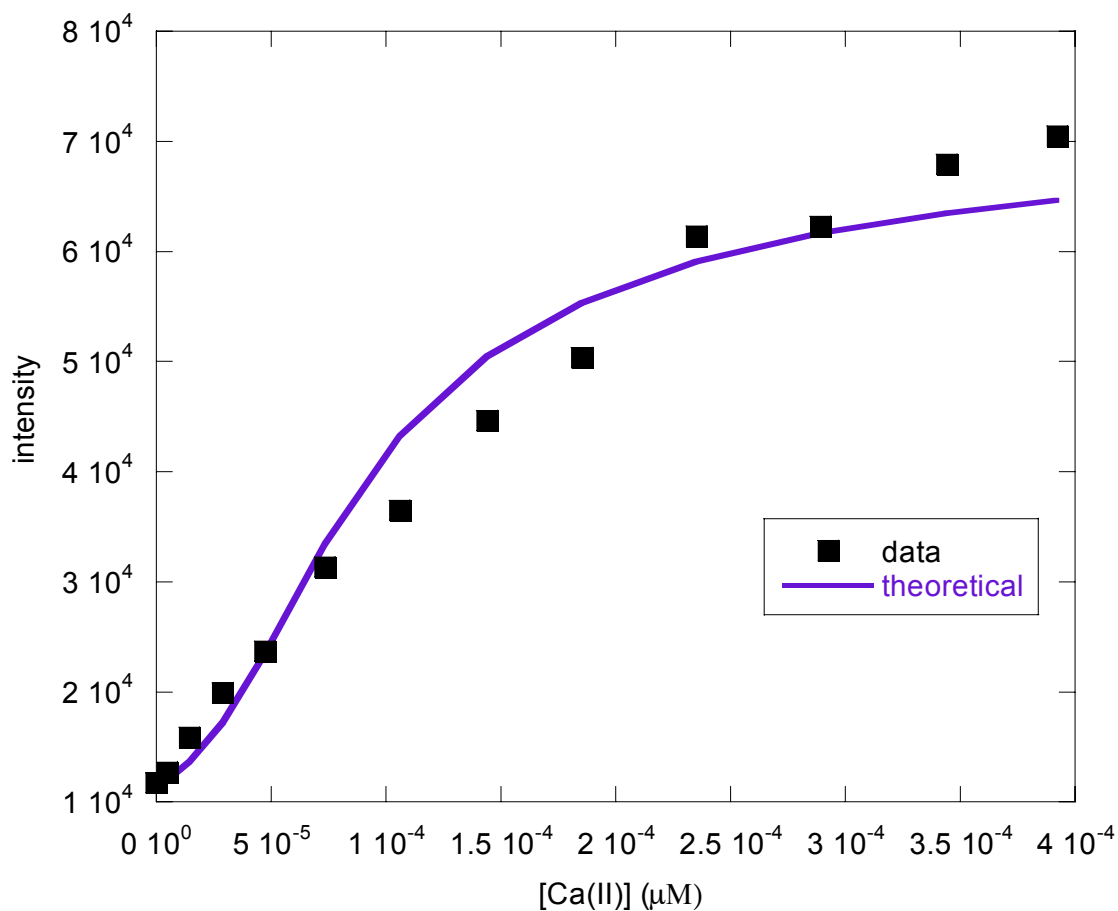


Fig 4.25 Specfit/32 global fit of the competition of 45 μM L194N/S86D and 20 μM Rhod-5N for calcium binding with the excitation wavelength of 552 nm and in 10 mM Tris, 1 mM DTT, 1% glycerol, pH 7.4. The program globally fits the entire spectrum to a double exponential model, which is not the best fit for the data.

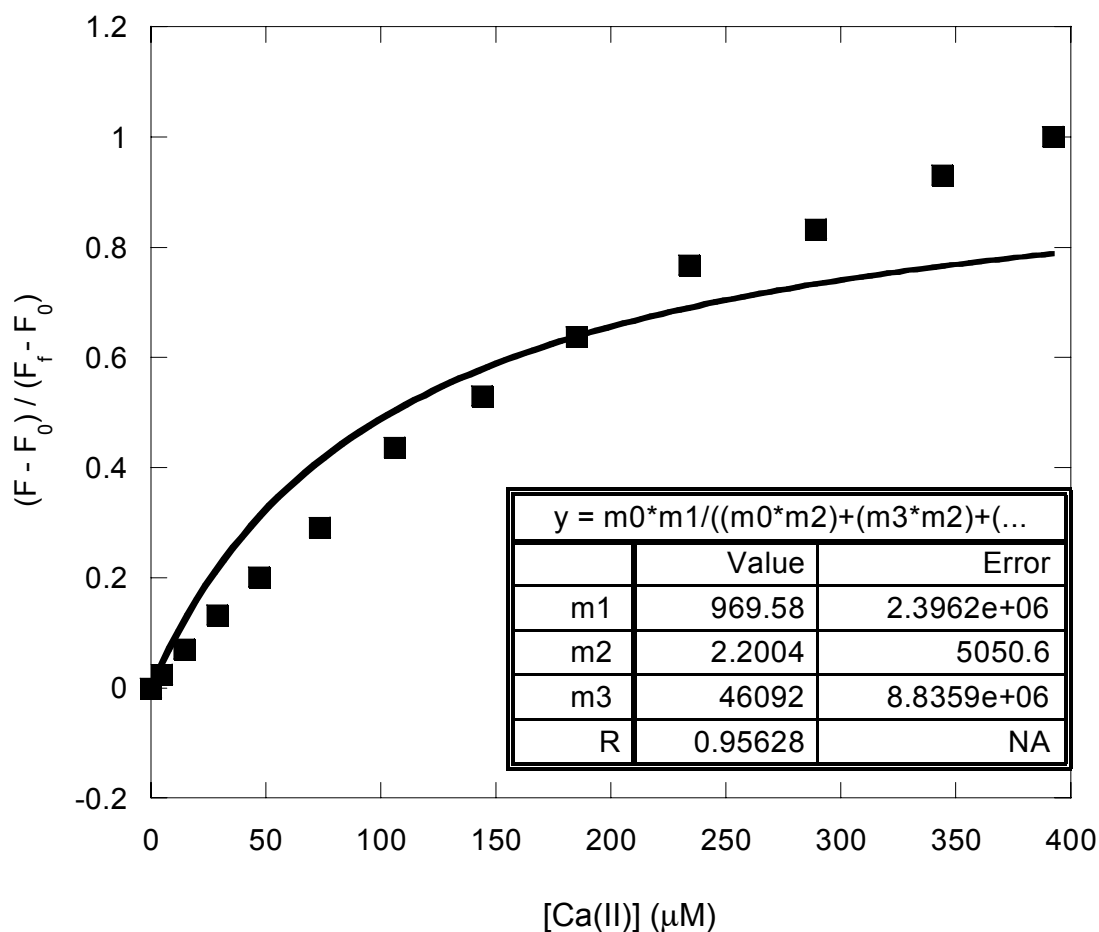


Fig 4.26 Fit of the competition of 45 μM L194N/S86D and 20 μM Rhod-5N for calcium in 10 mM Tris, 1 mM DTT, 1% glycerol, pH 7.4 with the equation

$$F = Kd1 * [M2]T / ((Kd1 * Kd2) + ([M1]T * Kd2) + ([M2]T * Kd1))$$

where $Kd1$ is the Rhod-5N binding affinity, $Kd2$ is the protein affinity, and M is metal. This equation does not fit the data well, and examination of the data indicates that saturation was not reached.

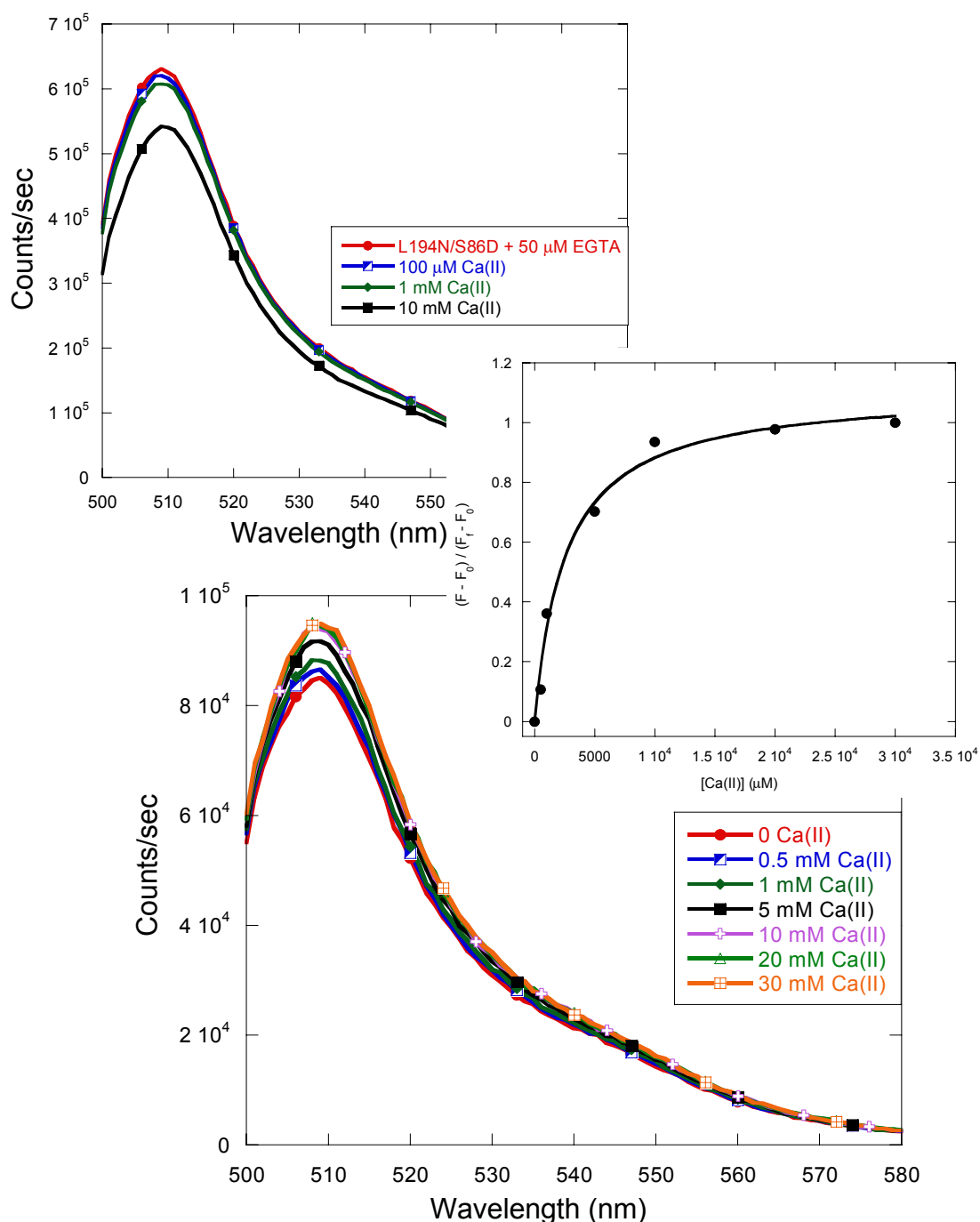


Fig 4.27 Chromophore emission change of L194N/S86D upon addition of calcium with the excitation at 482 nm on top and 398 nm on bottom (in 10 mM Tris, 1 mM DTT, 1% glycerol, pH 7.4). The fractional change vs. the calcium concentration was fit with a 1:1 metal binding equation and produced a K_d of 2.6 mM.

increase in fluorescence with excitation at 398 nm is concurrent with a decrease in fluorescence with excitation at 482 nm. This ratiometric change indicates a change in the chromophore's ionic state due to calcium binding with a shift to the neutral state evident. Fitting the fractional change vs. calcium with a 1:1 metal binding equation indicates a K_d of 2.6 mM, which is in the same range as calcium buffer proteins and extracellular calcium binding proteins. This protein possesses very bright fluorescence, similar to wild type, and may be useful for the study of extracellular calcium changes due to signaling events.

In summary, using different metal binding assays, such as Tb(III)-FRET and dye competition, we have shown that the designed GFP calcium binding proteins, sites 120, 177, and 194a, exhibit calcium and terbium binding with a selectivity for calcium over magnesium. These results were promising and exciting because they demonstrate the feasibility of our design approach and illustrate that the approach can be used in different proteins. Our laboratory initially established the design approach utilizing CD2 domain 1 from rat (cluster of differentiation 2). The net charge and ligand type, the electrostatic environment, and the location of the binding pocket have been tested in CD2. The terbium and calcium binding affinities for the same calcium binding pocket with different ligands followed the trend of strongest affinity for the most negatively charged pocket (-5) and weakest for the least charged (-2). In addition, differences were observed for the ligand types of Asn, Asp, Gln, and Glu for 7E15 variants. The change of Asn to Gln weakened the terbium binding but strengthened the calcium affinity due to the increased size of the sidechain, which allows the coordination

geometry to change. The use of this approach in multiple proteins signifies that the approach is working as hypothesized, and that it can be employed to study the intrinsic properties of calcium binding in differing protein environments as well as to engineer calcium binding proteins for multiple purposes. Table 4.5 summarizes the metal binding affinities for sites 177, 120, 194a, and 194b. Overall sites 177 and 120 exhibit similar binding affinities for terbium and calcium with the terbium affinity approximately 10 times greater than calcium. Site 194a exhibits the weakest affinity for both terbium and calcium. Sites 120 and 194a have a -4 charge while site 177 has a -3 charge. This seems counter to the expected result of a more negatively charged pocket exhibiting a stronger binding affinity, but the location and surrounding environment of the binding site also plays a role in binding affinity. Site 194a has fewer surrounding negative charges (4) than 177 (8) as shown in figure 4.28 and summarized in table 4.6, which likely plays a role in its reduced affinity. Also, site 194a has only two surrounding positive charges, which are likely not enough to stabilize the surrounding negative charges once the mutations were present to form the calcium binding pocket. The presence of the negative charges without stabilizing positive charges likely results in repulsion of the negative charges so that the pocket can not correctly form to bind calcium with as strong an affinity as 177 and 120. Site 177 has 8 surrounding negative charges and 7 surrounding positive charges. The presence of so many charged ligands likely allows for a greater extent of hydrogen bonding and salt bridges so that the binding pocket is more stable, hence the stronger binding affinity than 194a. Site 120 does not have many surrounding charges, 2 negative and 1 positive. With so few

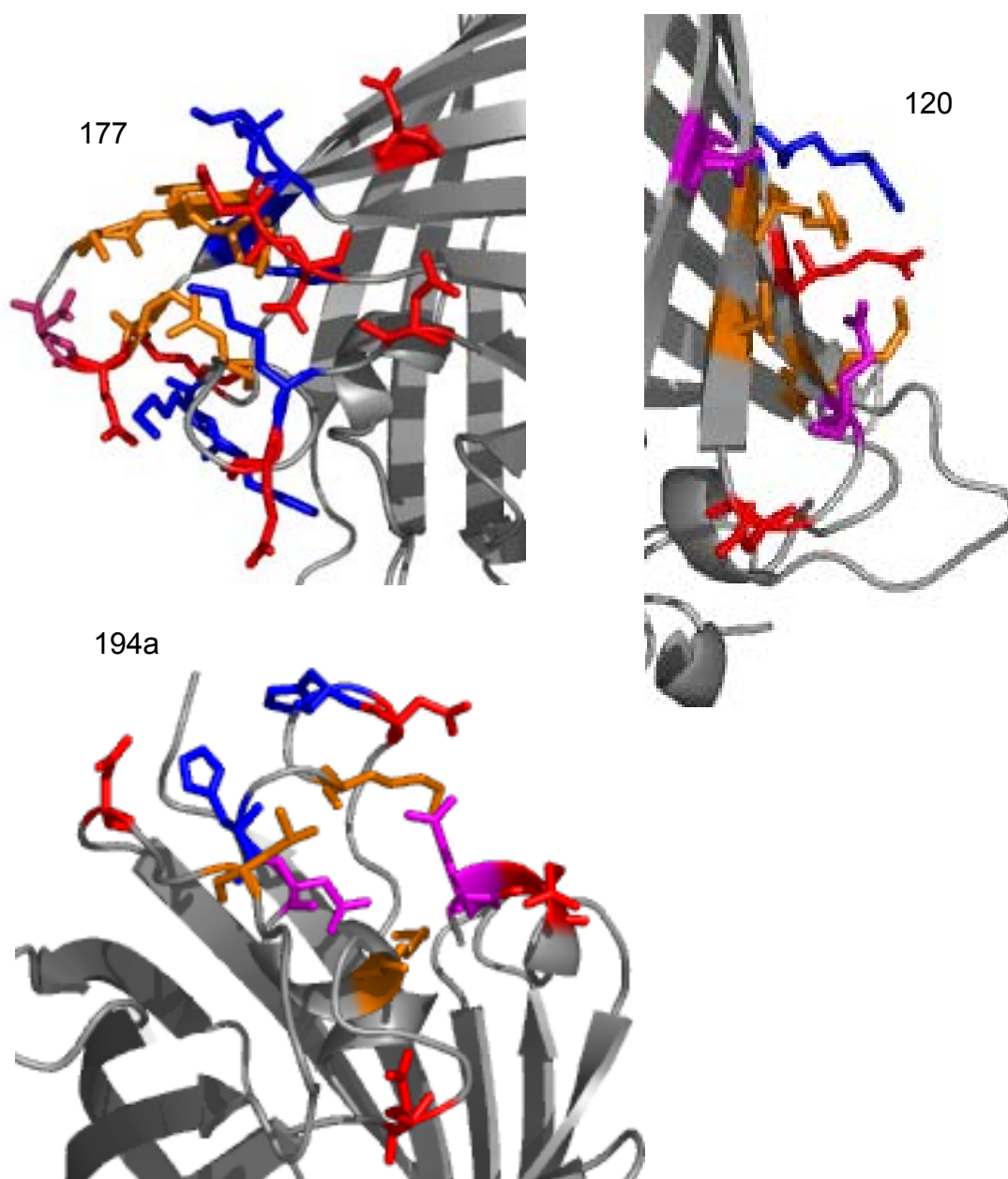


Fig 4.28 Illustrations of the three studied binding sites with the binding ligands shown in orange except for the natively negative ligands, which are shown in magenta. The surrounding negative charges are shown in red, and the surrounding positively charged amino acids are shown in blue. Site 177 has many negative (8) and positive (7) charges surrounding the pocket while sites 120 (2 negative, 1 positive) and 194a (4 negative, 2 positive) have fewer of both.

Table 4.6 A summary of the surrounding positive and negative charges for each studied binding pocket.

Site 177 Surrounding negatively charged a.a.	Distance to the binding pocket (Å)	Surrounding positively charged a.a.	Distance to the binding pocket (Å)
D133	13	K101	5
E132	19	K52	21
D102	8	K140	8
D103	8	H139	10
E172	12	H169	5
E142	20	R168	7
D180	10	K131	10
D129	17		
Site 120 surrounding negatively charged a.a.	Distance to the binding pocket (Å)	Surrounding positively charge a.a.	Distance to the binding pocket (Å)
E111	9	R109	13
D117	10		
Site 194a surrounding negatively charged a.a.	Distance to the binding pocket (Å)	Surrounding positively charge a.a.	Distance to the binding pocket (Å)
D76	14	H81	5
E6	13	H77	12
D197	10		
E90	14		

charges, the repulsion is likely less than for site 194a so that the binding affinity is stronger. In addition, the ability of the residues to form the correct binding geometry through the flexibility of the ligands and/or through the flexibility of the backbone affects the binding affinity. Site 120 is the least flexible of the design sites because the ligand residues are all located in β -sheets. Site 177 is in the middle range of flexibility with two ligands in the β -sheets and the rest in the loops. Site 194a is the most flexible with all of its residues located in the loop regions. Site 120's reduced flexibility likely allows the geometry to correctly form whereas the high flexibility, combined with the repulsion of the negative charges, of 194a may not allow for the correct pentagonal bipyramid for calcium to bind with strong affinity. Although site 177 contains largely backbone flexible residues, the combination of the surrounding positive and negative charges likely reduce the flexibility with formation of salt bridges and hydrogen bonds so the geometry is formed. The ligand type plays a role in calcium binding. If the sidechains are too long to form the correct geometry and distort the pocket, calcium can not bind as strongly as if the pocket forms the ideal pentagonal bipyramid. Although the variants were designed to form this geometry, the computer algorithms utilized do not take into account the effect of the surrounding residues or the ability for the residues to reposition in response to repulsion or attraction by surrounding residues. For example, L194N of site 194a is located on a separate, quite long loop that is away from the other ligands. Perhaps this residue is not long enough to make full contact with calcium, reducing the affinity, or the residue is pushed further away from the other ligands due to repulsion. Sites 120 and 177 likely have such similar binding affinities because the difference in

the net negative charge in the binding pocket is overcome by the flexibility aspects of the pocket and the surrounding charge environment. The combination of the local surrounding charge, the flexibility of the backbone, and the ability of the residues to form the preferred geometry contribute to the range of binding affinities measured for the designed sites. The different terbium and calcium binding affinities for the three sites is likely due to several factors since calcium binding affinity is dependent on local environment, ligand type, overall binding pocket charge, and formation of the correct geometry.

4.7 Optical Properties of EGFP and the Designed Proteins

4.7.1 Absorbance of EGFP and its variants

The absorbance and fluorescence of bacterially expressed and purified EGFP and the variant proteins was examined. EGFP exhibits a maximum absorbance peak at 482 nm with a shoulder centered at 398 nm in 10 mM Tris, 1 mM DTT, 1% glycerol, pH 7.4 as illustrated in figure 4.29. These two peaks represent the anionic and neutral state of the chromophore, respectively (63). EGFP has two mutations, S65T and F64L, with S65T thought to cause the shift of the chromophore's state from neutral, as observed in the wild protein, to anionic. The Ser65Thr has been hypothesized to stabilize the ionized form of Glu222, which hydrogen bonds to Tyr66 in the wild protein, so that the phenolate absorbs light around 470 nm. In addition, Thr203 is thought to stabilize the hydroxyl form of the chromophore, causing light to be absorbed at 400 nm. Since Thr203 is not mutated in EGFP, the small shoulder at 398 nm is observed. When the fluorescence excitation profile of EGFP was examined, it was noticed that there are

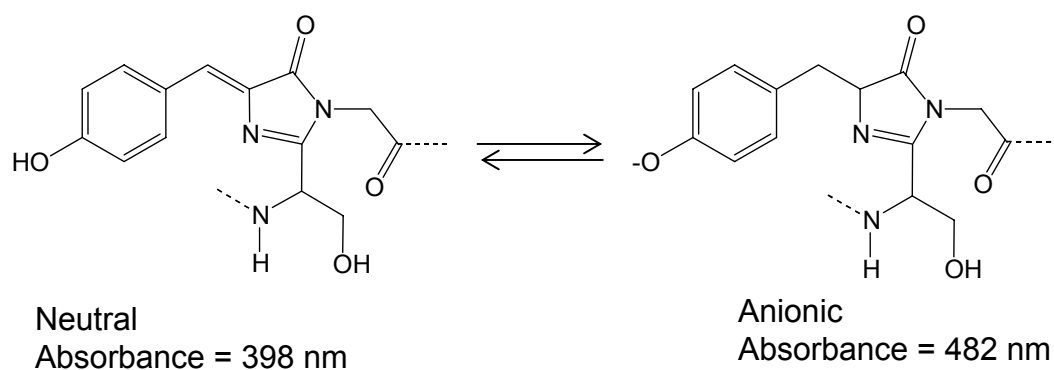
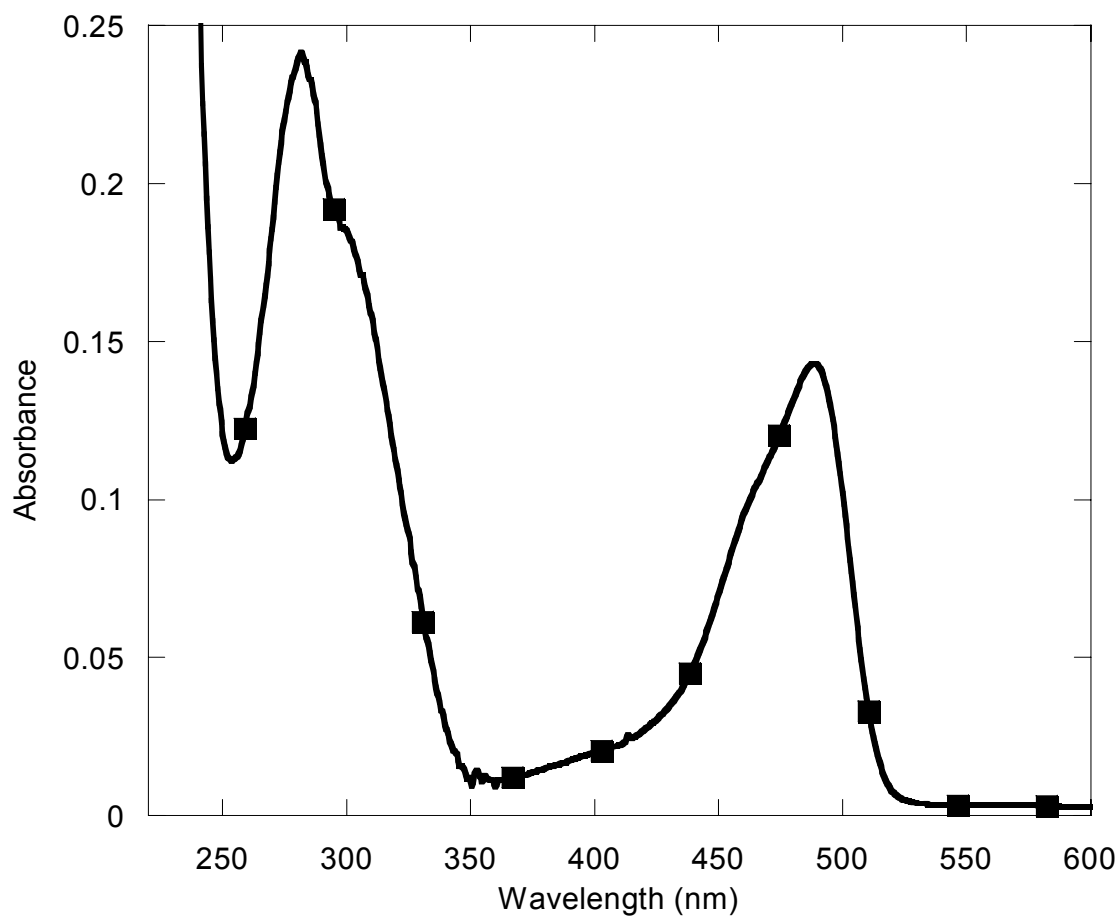


Fig 4.29 Absorbance spectra of EGFP (top) in 10 mM Tris, 1 mM DTT, 1% glycerol, pH 7.4 with the chromophore absorbance observed at 482 nm and the aromatics' absorbance at 280 nm. The neutral (left) and anionic (right) states of the chromophore of GFP are illustrated (bottom).

several peaks in close proximity that all cause emission at 510 nm. These excitation peaks, 470 nm, 482 nm, and 490 nm are likely excitations of different intermediate states of the chromophore. These states can not be observed in absorbance. The overall peak centered at 482 nm is observed.

The three bacterially expressed variants, 120, 194a, and 177 were examined for absorbance from 220 nm to 600 nm. As detailed above, the chromophore should exhibit a peak at 398 nm and/or 482 nm if the protein is folded and the chromophore is shielded. If the protein is unfolded, a peak at 387 nm should be observed as it is for EGFP at low pH (Fig 4.30). Sites 120, 194a, and 177 did not exhibit a chromophore absorbance peak but do demonstrate an aromatic absorbance peak at 280 nm, as shown in figure 4.31. Since even the unshielded chromophore peak at 387 nm was not present, it is likely that the chromophore did not form during folding of the protein in bacterial cells. This can be attributed to slight repulsion of the negatively charged calcium pocket, which likely causes some rearrangement of the sidechains so that Ser65 and Gly67 are not in close enough proximity to undergo the initial nucleophilic attack that cyclizes the backbone amide of Gly67 with the sidechain of Ser65 to form the imidazolidine ring.

4.7.3 Chromophore fluorescence of EGFP and its variants

EGFP contains one Trp and 10 Tyr residues as shown in figure 4.15. These residues would normally intrinsically fluoresce. With excitation at 280 nm, emission could be observed between 300 (tyrosine emission) and 350 nm (free tryptophan emission) for the aromatics. When the aromatic fluorescence was first measured, it was

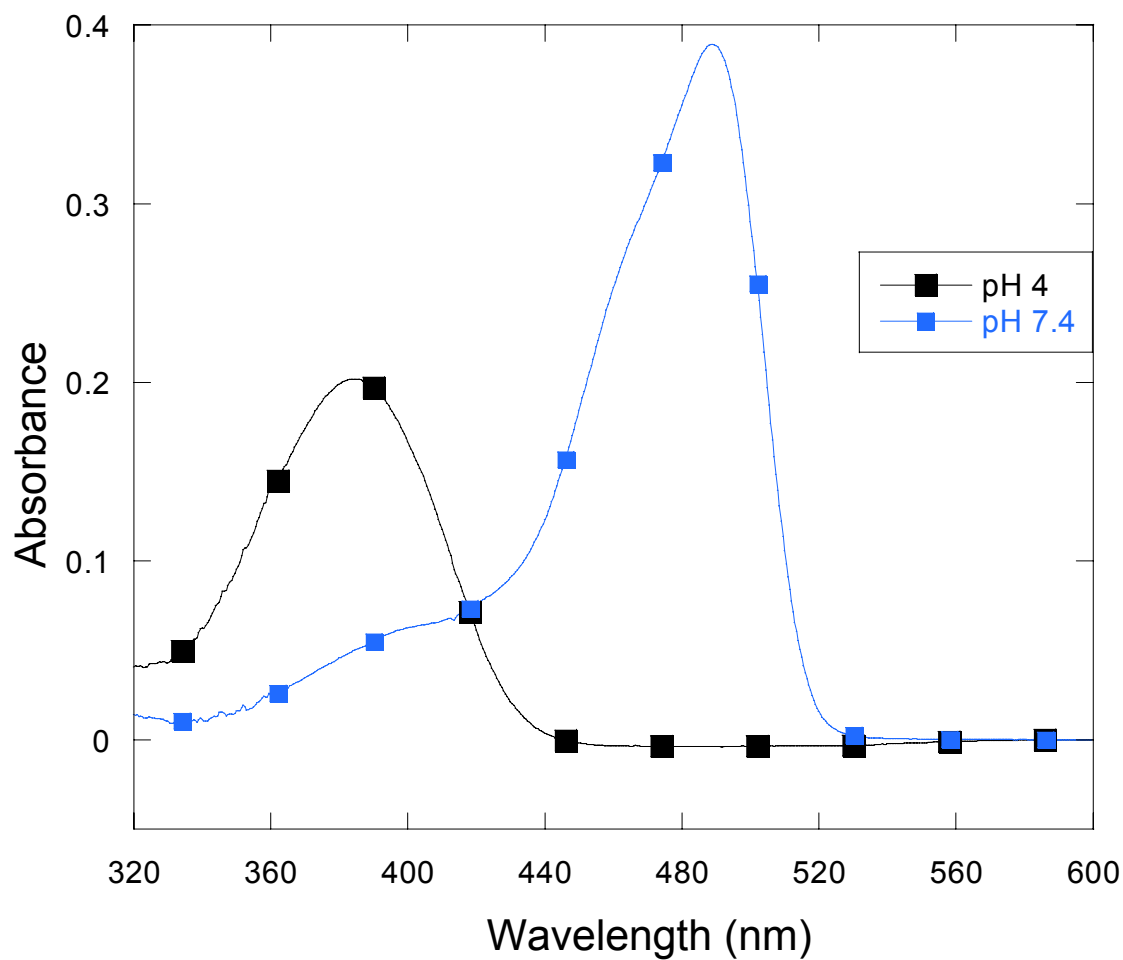


Fig 4.30 Absorbance spectra of EGFP at pH 4 (0.5 M acetate, 1 mM DTT, 1% glycerol) and pH 7.4 (10 mM Tris, 1 mM DTT, 1% glycerol) illustrating the absorbance of the chromophore at 387 nm when the protein is unfolded as opposed to the peaks at 398 nm and 482 nm at pH 7.4.

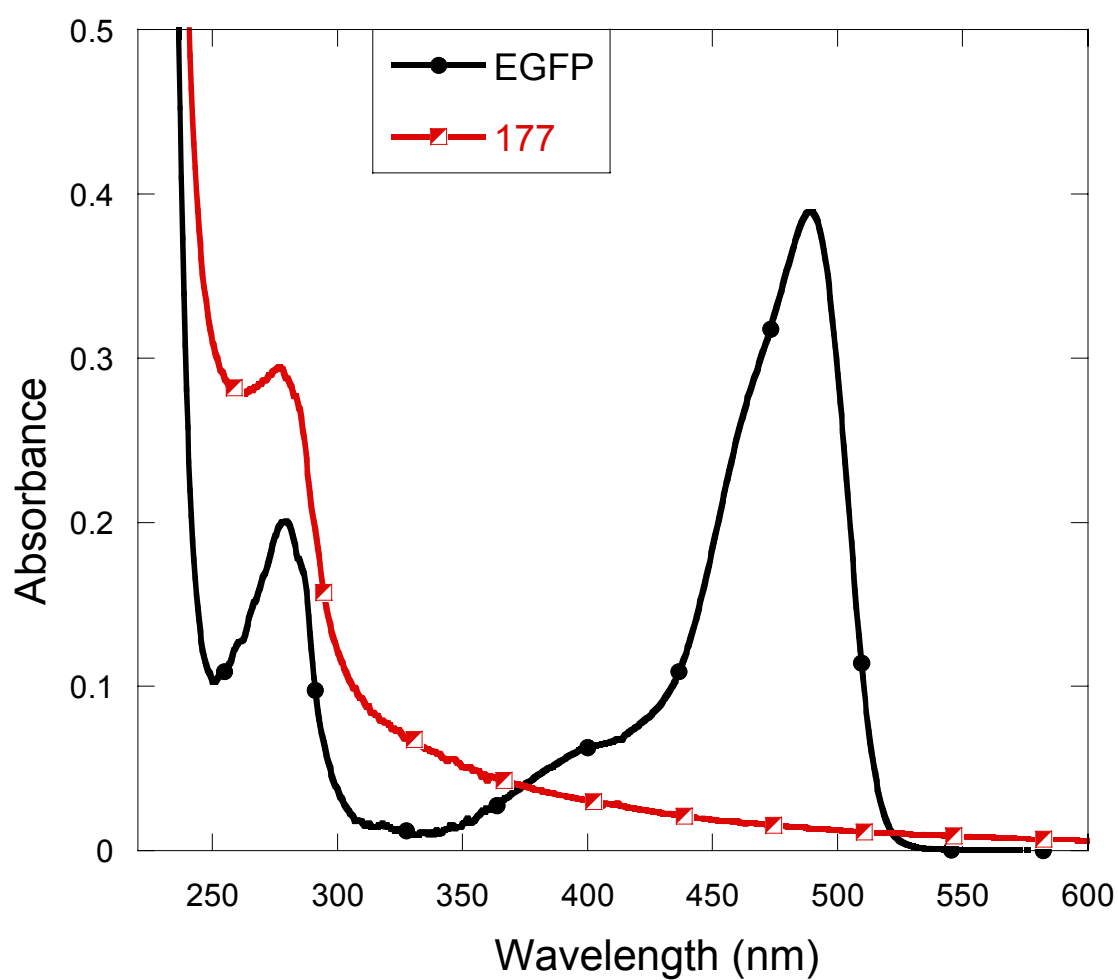


Fig 4.31 Absorbance spectra of EGFP and the designed protein 177, in 10 mM Tris, 1 mM DTT, 1% glycerol, pH 7.4, illustrating the lack of chromophore absorbance. Designed proteins 120, 194a, and 194b exhibit similar absorbance spectra.

observed that the water scattering peak was stronger than the aromatic emission with a peak observed at 313 nm for water when excited at 280 nm (Fig 4.32). Raman scattering of water occurs 3382 cm^{-1} red shifted from the excitation, which is calculated to be 313 nm for excitation at 280 nm with the equation $c = \lambda\nu$. As the excitation wavelength was changed, the water emission shifted accordingly. To overcome this problem, it was observed that placing a glass plate with a long pass of 300 nm in front of the emission lens removed the water scattering peak. Emission of the aromatics in EGFP was observed at 320 nm, indicating that the tryptophan is largely buried since free tryptophan emits at 350 nm. Tyrosine fluorescence is much weaker than tryptophan so it is likely overcome by tryptophan's emission. Interestingly, L194N/S86D indicates a Trp peak at 340 nm, suggesting that this mutant has a slightly opened tertiary structure so that Trp is more exposed to solvent than in EGFP (Fig 4.33). Intriguingly, the aromatics also undergo energy transfer with the chromophore with emission of the chromophore observed at 510 nm when the aromatics are excited at 280 nm. The fluorescence of the energy transfer is about 10% larger than when the protein is excited at 398 nm (Fig 4.34). The energy transfer was observed by exciting the chromophore from 260 nm to 488 nm while measuring the emission at 510 nm. A profile of the energy transfer is shown in figure 4.35. It is clear that emission of EGFP at 510 nm contains contributions from the aromatics with excitation at 280 nm and from the neutral state of the chromophore with excitation at 398 nm with each of these exhibiting fluorescence an order of magnitude less than excitation at 482 nm.

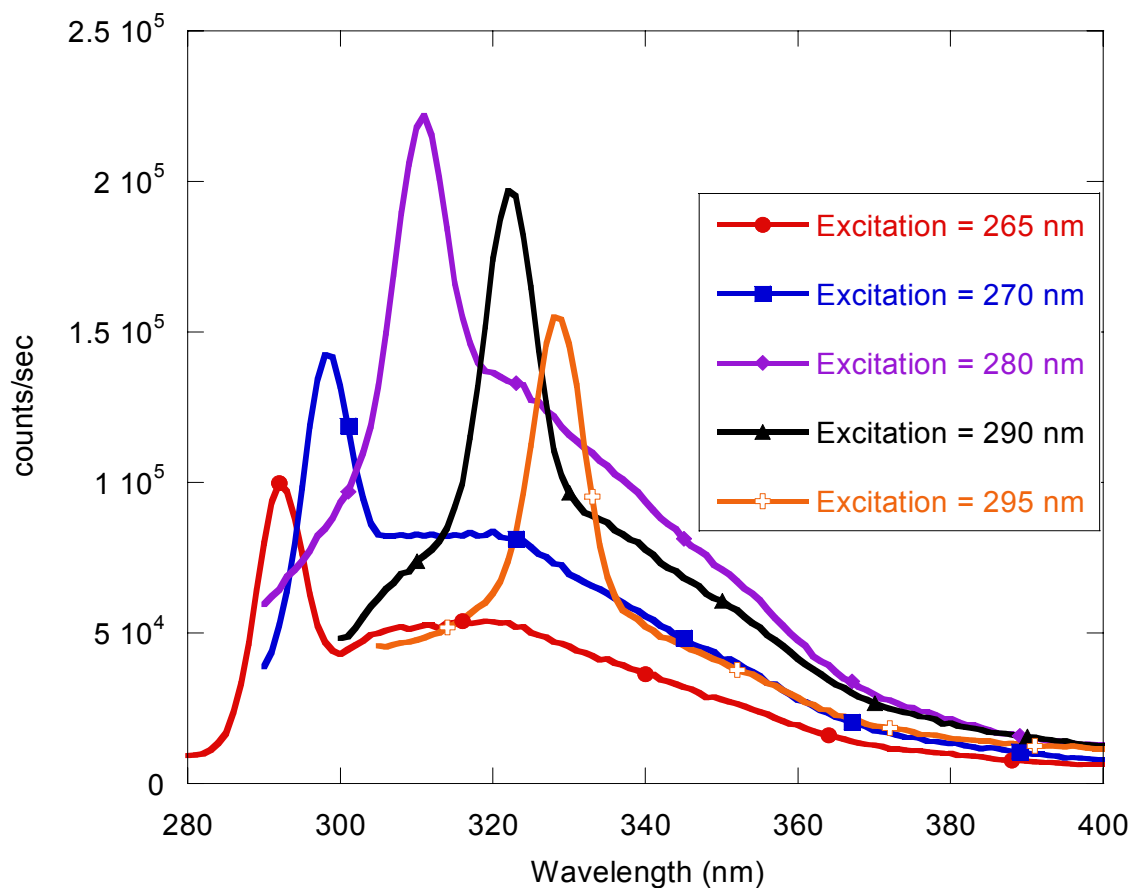


Fig 4.32 Emission spectra of GFP with the water scattering peak evident as it changes emission wavelength along with a change in the excitation wavelength. The peak at 320 nm that is apparent with excitation at 265 nm is the emission of the aromatics of GFP. The water scattering peak is more intense than the aromatics. Addition of a glass plate filter, LP300, removes the water scattering peak.

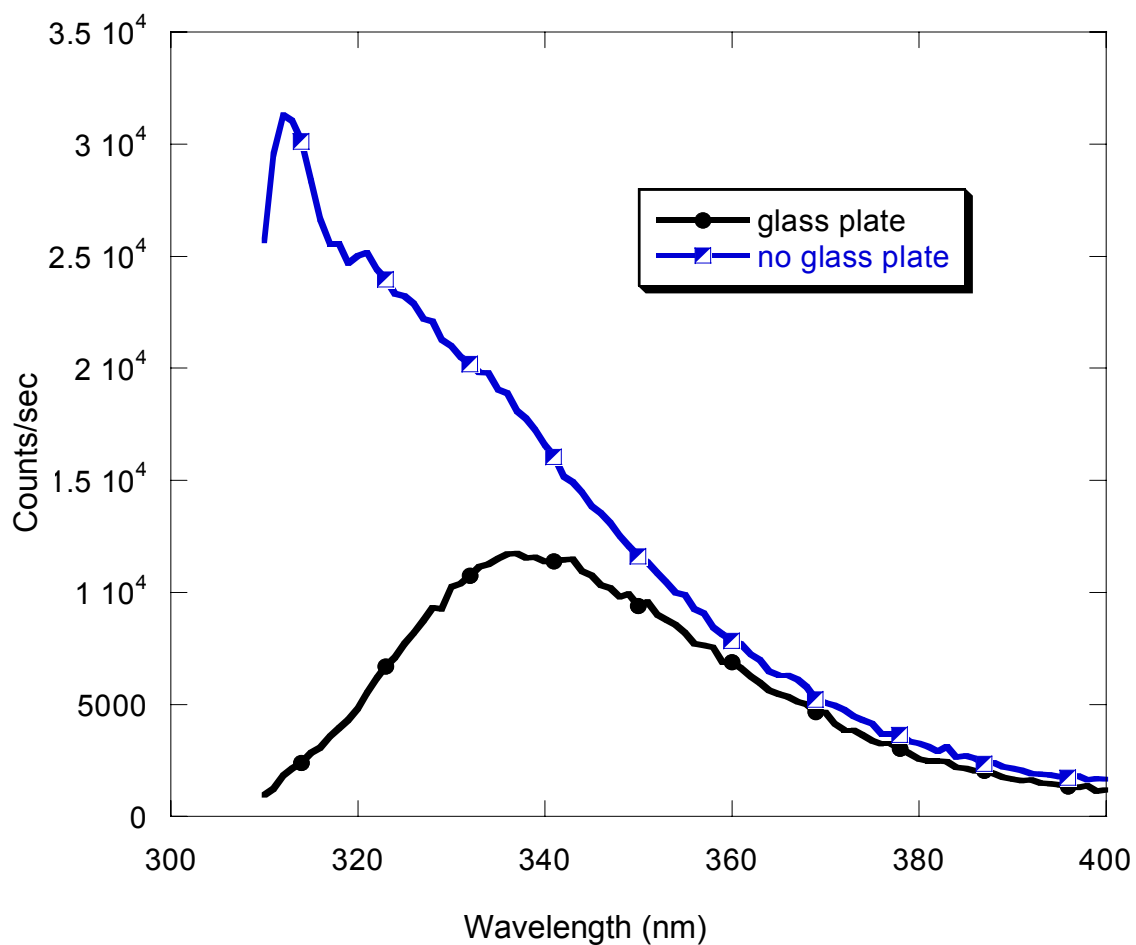


Fig 4.33 Aromatic fluorescence emission with excitation at 280 nm of L194N/S86D (10 mM Tris, 1 mM DTT, 1% glycerol, pH 7.4) illustrating the ability of the glass plate filter to remove the water scattering peak from the spectrum. The emission of the aromatics at 337 nm indicates that the aromatics are partially exposed to solvent.

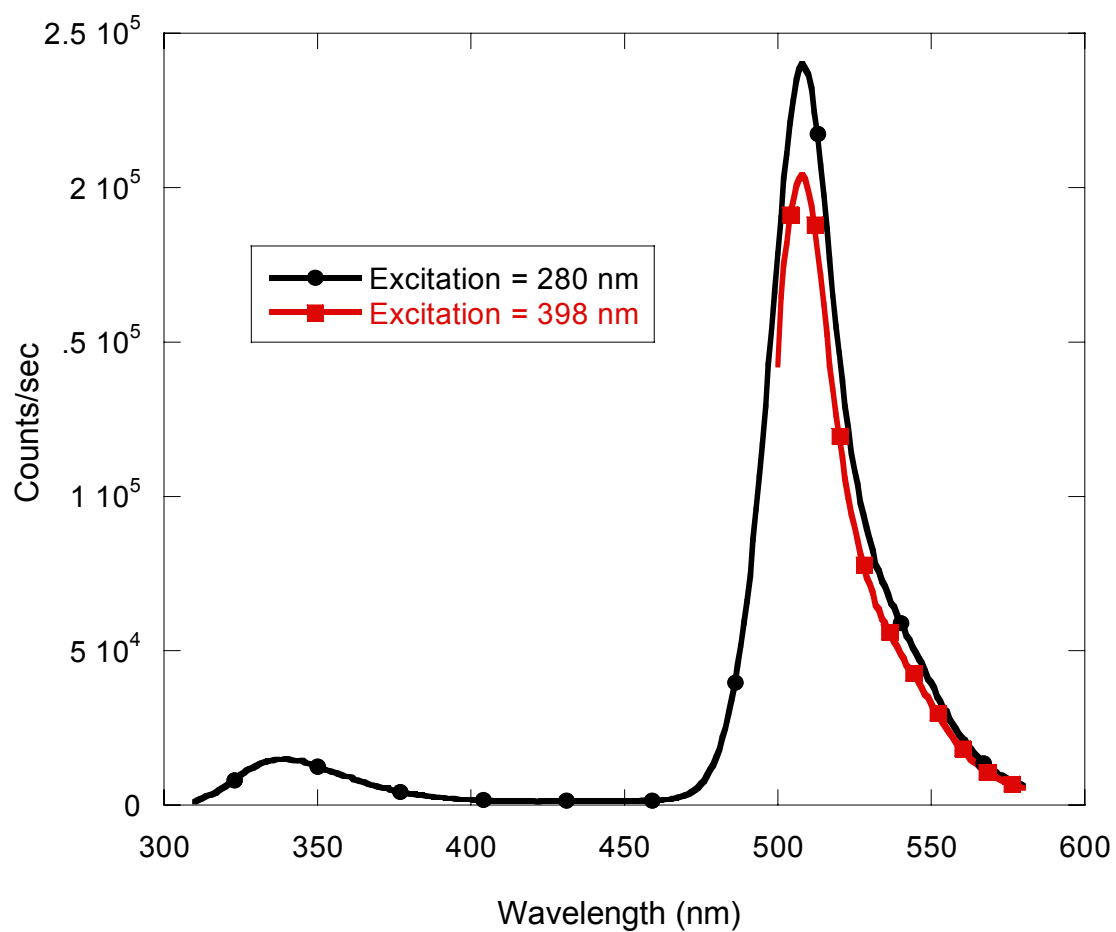


Fig 4.34 Emission of EGFP L194N/S86D with varying excitations to illustrate the energy transfer from the aromatics to the chromophore.

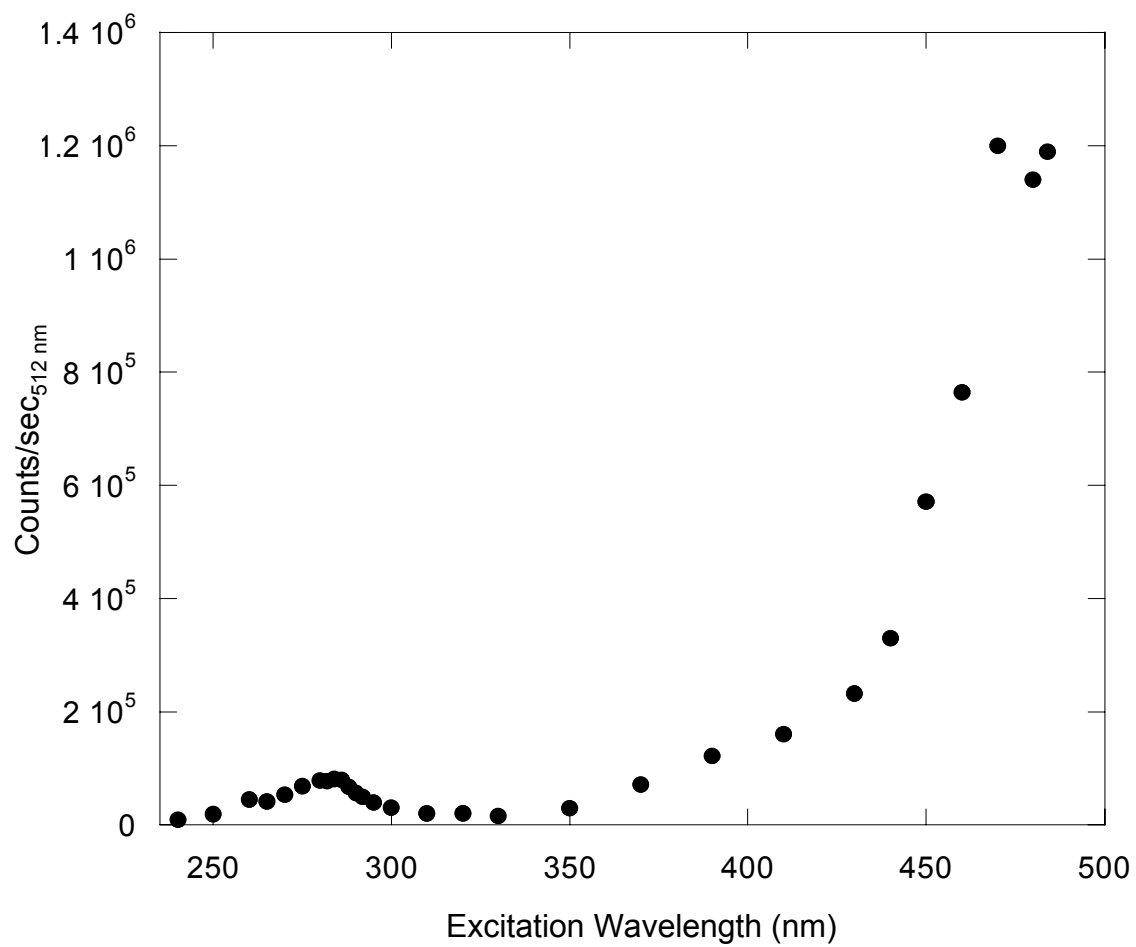


Fig 4.35 Energy transfer of EGFP observed between the aromatics and the chromophore with emission at 510 nm and varying excitation.

When the designed proteins were examined by fluorescence, no peak was observed at 510 nm with excitation at 488 nm. An excitation profile from 300 nm to 490 nm with the emission monitored at 510 nm did not reveal a chromophore excitation peak. There are two possibilities in the loss of the chromophore fluorescence of the designed proteins: 1) the chromophore fails to form or 2) the chromophore forms but is non-fluorescent. In case 1, if the sidechains of the chromophore-forming amino acids are not in close enough proximity, the reaction will not occur to allow for the cyclization and chromophore formation. In this case, the tertiary packing must decrease, which may be due to repulsion from the negative sidechains introduced into the protein to form the binding site. In case 2, the protein is packed enough to allow the chromophore to form but the tertiary packing is loose enough to permit solvent interaction with the chromophore. The chromophore when free in solution only exhibits very weak fluorescence due to energy loss by interaction with the solvent. Work in our laboratory by Ning Chen has shown that the chromophore is still intact even when the protein with a preformed chromophore has been cleaved into two pieces, but only very weak fluorescence is observed if the chromophore-containing portion is isolated from the other half. Since no chromophore absorbance or fluorescence was observed for sites 120, 194a, and 177, it is most plausible that the chromophore did not form during folding of the protein in bacteria. This explanation is further supported by the results that these designed proteins are located in the cell pellet forming insoluble inclusion bodies. As shown in figure 4.11, refolding of the proteins is required for purification.

4.8 Conformation Analysis of Secondary Structure by CD

After the variant proteins were purified, several biophysical methods were employed to ascertain the proteins' secondary and tertiary structure in comparison to the wild type protein, EGFP. Figure 4.36 illustrates the far UV CD spectra of EGFP, which exhibits a β -sheet secondary structure with a negative maximum at 216 nm, consistent with its secondary structure elucidated by X-ray crystallography. The variant proteins all exhibit the same CD profile as EGFP with negative maxima at 216 nm (Fig 4.37). Under the same conditions, the secondary structure of the modified proteins is intact although the modified proteins are not fluorescent. EGFP and the variant proteins were examined for CD changes upon the addition of metal ions as shown in figure 4.38 for 194a, but no overall changes were observed with the addition of calcium, lanthanum, or terbium.

4.8.1 pH effects on GFP variants

The pH profile of the variant proteins was also studied by Far UV CD from pH 4 to 9. It has been accepted in the literature that GFP unfolds below pH 5 because the green color and fluorescence is no longer observed below this pH. However, this conclusion in literature does not make use of CD and is solely based on absorbance and fluorescence properties. To test the pH effects on the secondary structure of the proteins, 15 μ M protein was incubated with a series of buffers from pH 4 to 9 as given in table 2.5. Their CD spectra were acquired and the spectra of the background contribution from buffer was subtracted. Utilizing CD, EGFP and the variant proteins do

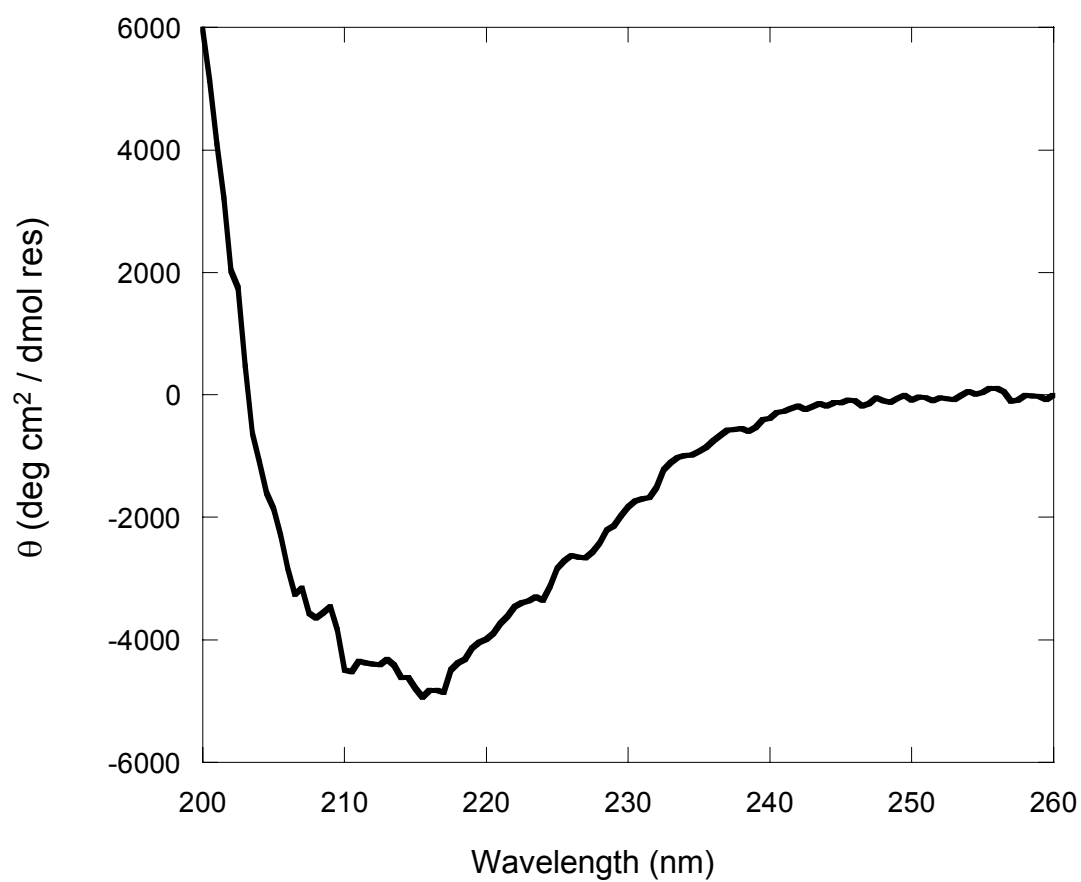


Fig 4.36 Circular dichroism of EGFP in 10 mM Tris, 1 mM DTT, 1% glycerol, pH 7.4 and 25 °C. The negative maxima at 216 nm indicates β -sheet secondary structure.

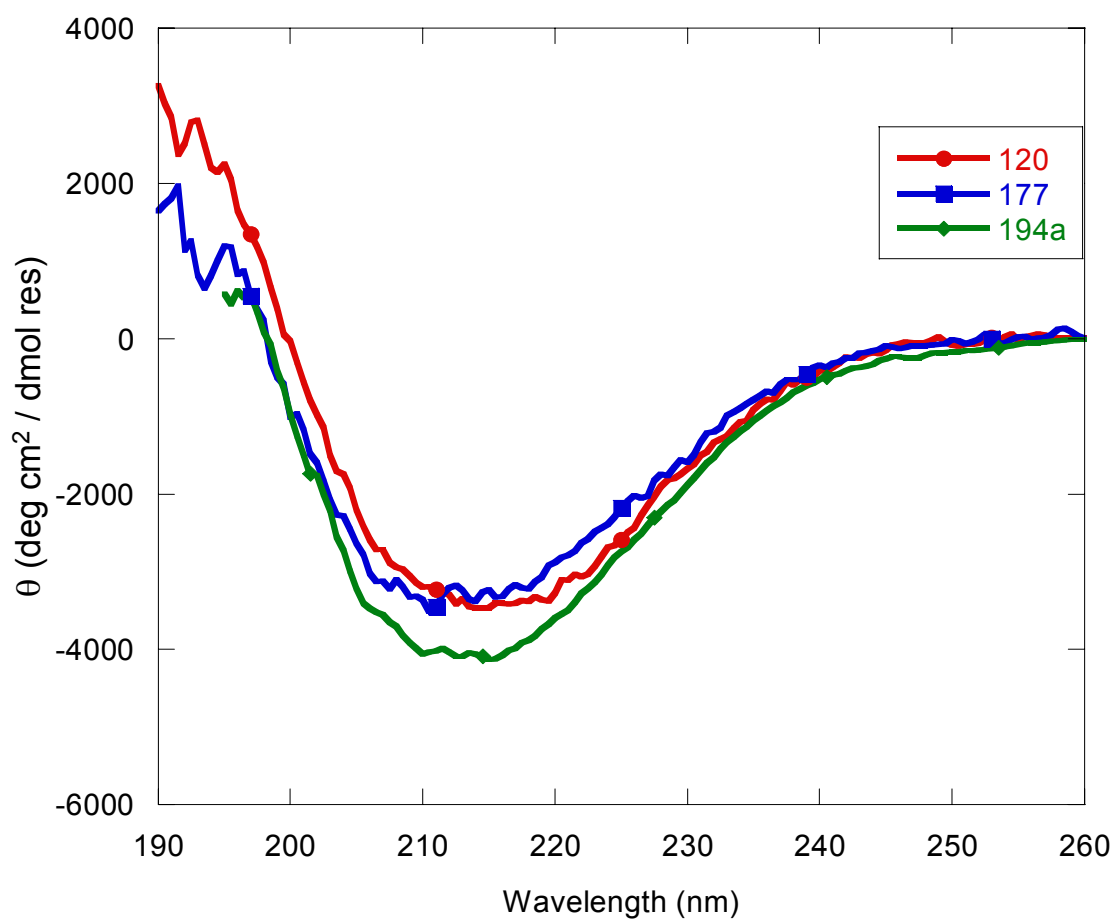


Fig 4.37 Circular dichroism of 120, 177, and 194a in 10 mM Tris, 1 mM DTT, 1% glycerol, pH 7.4 illustrating the β -sheet secondary structure of the designed proteins.

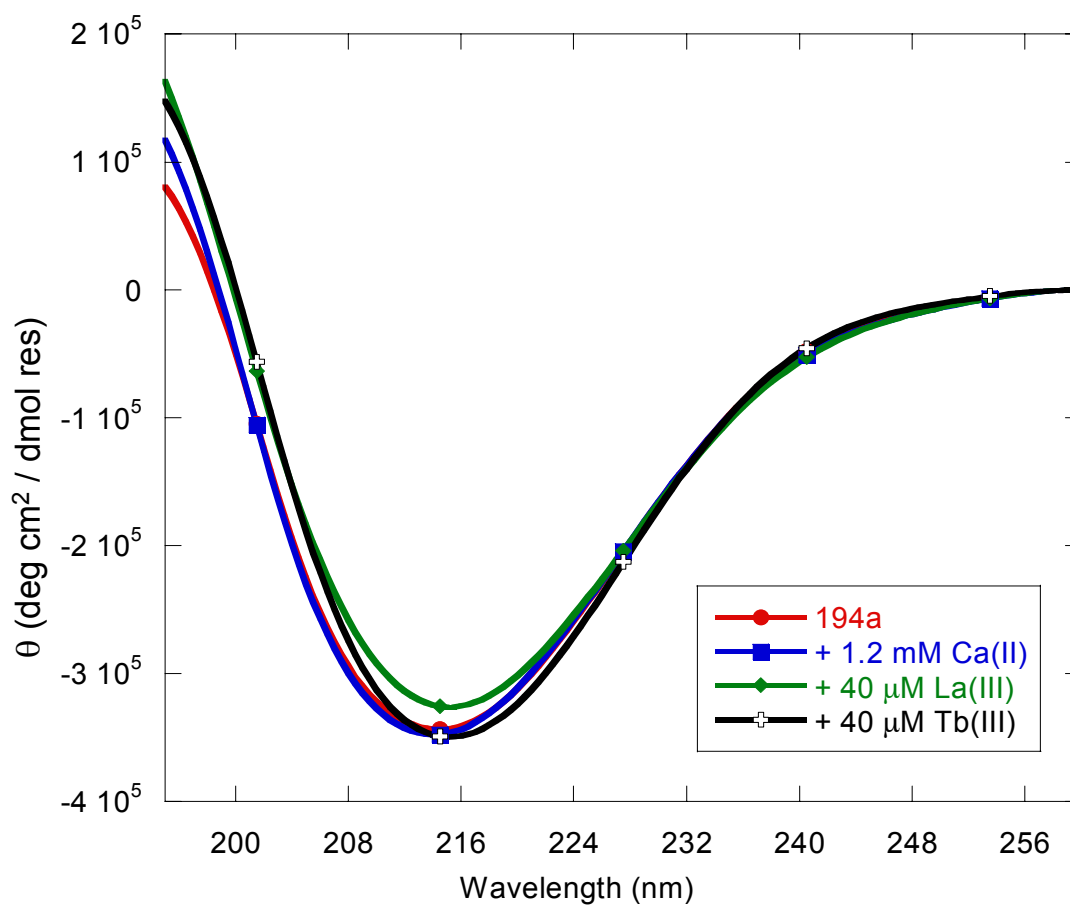


Fig 4.38 CD spectra of designed protein 194a with calcium, lanthanum, and terbium in 10 mM Tris, 1 mM DTT, 1% glycerol, pH 7.4. Designed sites 120 and 177 and the host protein EGFP exhibit similar results. The negative maxima at 216 nm indicates β -sheet secondary structure, which does not change upon introduction of metals.

not completely unfold below pH 5. In fact, the β -sheet secondary structure is still observed at pH 4 although no color is detected (Fig 4.39). The signal is slightly more negative at pH 9 than pH 4, but no other differences are observed. At higher pH's, there is a slight 2 nm blue shift, but this does not seem to indicate a significant change in the secondary structure. When the spectrum was observed in the presence of 1 mM calcium, there were no evident changes at the various pH values. This finding indicates that the protein is not completely unfolded and still maintains its secondary structure. It is likely that the protein loses its tertiary packing, therefore causing the loss of the chromophore fluorescence, but maintains the β -sheet formation. Since the chromophore requires the shielding of the barrel to exhibit fluorescence, this could likely be a reason that the full site variant proteins do not exhibit fluorescence although their secondary structure is intact. This could also contribute to the reversible folding of GFP reported in the literature. It has been reported that GFP reversibly unfolds in 8 M urea. Perhaps this state aids in the refolding if the tertiary packing is not stringent so the protein able to reform the tertiary packing when the urea is removed.

Since the full site variants indicated secondary structure that did not change upon addition of metal or with varying pH but no fluorescence was indicated, several endeavors were undertaken to reform the tertiary packing so the chromophore would fluoresce. The proteins were refolded with 8 M urea after purification and with 6 M GuHCl, but no fluorescence was observed.

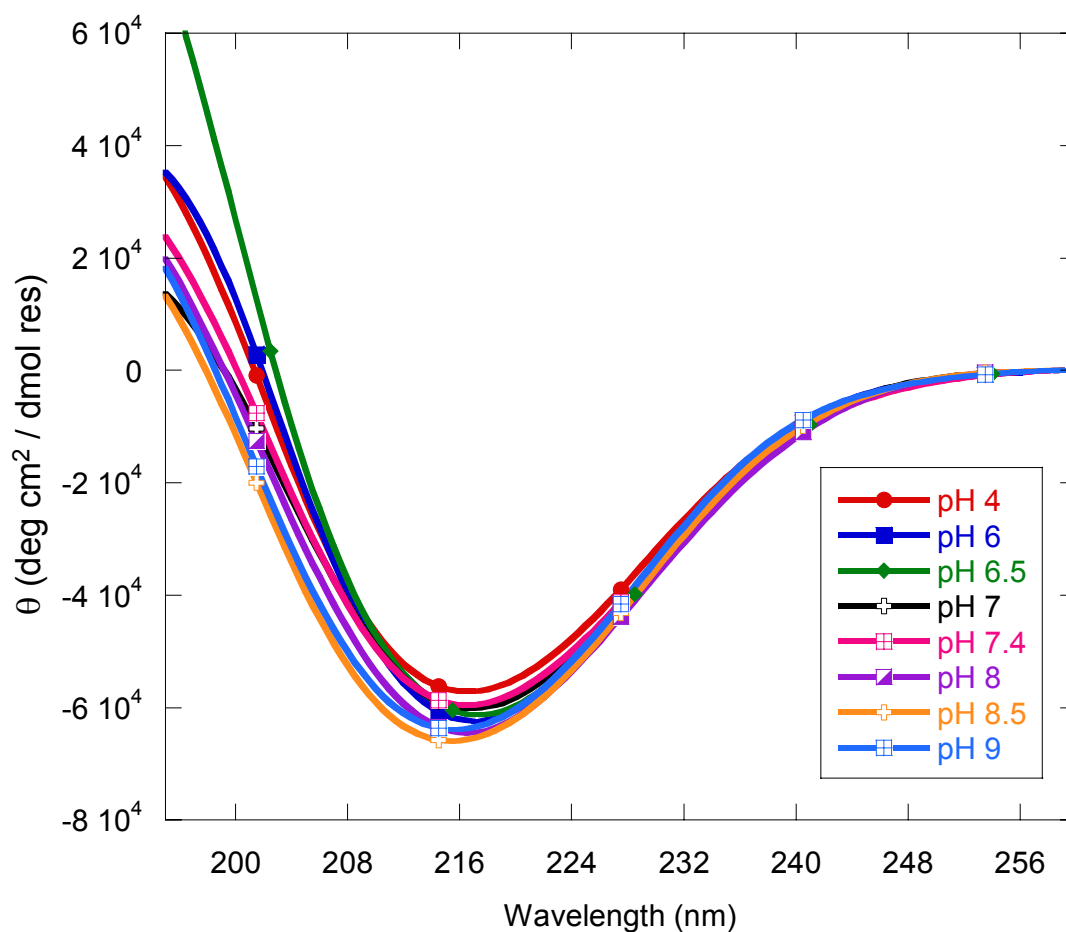


Fig 4.39 CD spectra of designed protein 120 at various pH values to study the effect of pH on the protein's secondary structure. There appears to be very little effect of pH from 4 to 9 on the structure. The complete loss in structure proposed by the literature certainly does not occur for these mutants at low pH. The pH dependence with 1 mM calcium is the same.

4.9 Endeavoring to Understand Fluorescence Loss of the Designed Proteins

4.9.1 *Partial design sites*

In an effort to understand which residues caused the fluorescence loss of the designed proteins so a) the residues could be removed from the design site and replaced with other residues and b) the residues would not mutated in the future, partial sites were engineered and their spectral properties were examined. The partial sites were largely taken from initial products from PCR. Since 177 was mutated all in one step, there are no partial products for it. These partial sites are listed in table 4.7.

The single mutations L15N, L194N, V120N, R122D, K85D, and S86D have all been expressed as well as the double mutations L15N/R122D, L194N/S86D, L194N/K85D, and L15N/V120N. The Fluostar microplate reader was utilized to quantitate the formation of the chromophore as shown in figure 4.7. One mL samples were taken from the 1 L flask of *E. coli* growth expressing each protein. The solution was centrifuged at 14 K rpm for 1-2 min until pelleted. The supernatant was removed and the pellet was dissolved in 200 μ L of 10 mM Tris, 1 mM DTT, 1% glycerol, pH 7.4. This solution was placed into a Corning 96 well plate. The plate was placed into the microplate reader, and the protocol detailed in section 2.5.1 was followed with excitation at 460 nm and emission at 520 nm, which are the available filters for the instrument. L15N, L194N, S86D, L15N/R122D, and L194N/S86D indicate a strong green color upon expression. L15N, L194N, and L194N/S86D have been purified and studied. Their

Table 4.7. A table of the partial sites studied with the final fluorescent mutations shown in green.

Design Site	Calcium-binding Ligands	Partial Site 1	Partial Site 2
120	E115, V120N, R122D, K113D, E17		
120b	E115, V120N, R122D, E111, L15N	L15N V120N R122D	L15N/ V120N L15N/ R122D
177	Q177N, I171D, D173, S175D, N135, V176A		
194a	E5, D82, K79D, L194N, K85D	L194N K85D	L194N/ K85D
194b	E5, D82, K79D, L194N, S86D	L194N S86D	L194N/ S86D
229	D197, H199D, M78N, H81D, I229D	M78N, H81D	M78N, H81D, I229D

chromophores are comparable to wild type in absorbance and fluorescence profile and exhibit similar quantum efficiency, although the efficiency is slightly smaller than EGFP.

V120N exhibits a weak green fluorescence upon expression, and L15N/V120N exhibits no color upon expression. K85D indicates no color upon expression. Mutating the lysines causes some disruption in the fold of the protein, especially when the lysine mutation is coupled with other mutations. Also, the V120N mutation is too drastic for the protein. When the protein structure was examined, it was noted that V120 is buried under the other ligands in the design site, likely to shield the hydrophobic residue from water as shown in figure 4.40. When the residue is mutated to an Asn, there is likely repulsion between the Asn sidechain and the other close residues R122D and L15N. Since this site is in the middle of the barrel and close to the chromophore, the repulsion causes a more drastic fluorescence loss. Summer work by Dorinda Nelson indicated that none of the partial sites of 229 were fluorescent. It is likely that mutating His81 severely disrupts the fold of the protein.

The 194 family of designed proteins, as illustrated in figure 4.41, contains two mutations that lead to fluorescence loss. Mutation of K79D should be avoided since it alone causes fluorescence loss. This is likely a result of mutating a long, positively charged sidechain to a shorter, negatively charged sidechain. The hydrogen bond and charge contacts that K79 makes with other amino acids in the protein can not necessarily be made by 79D, which could disrupt the tertiary packing and/or chromophore formation. Mutation of K85D also exhibits the same result, likely for the

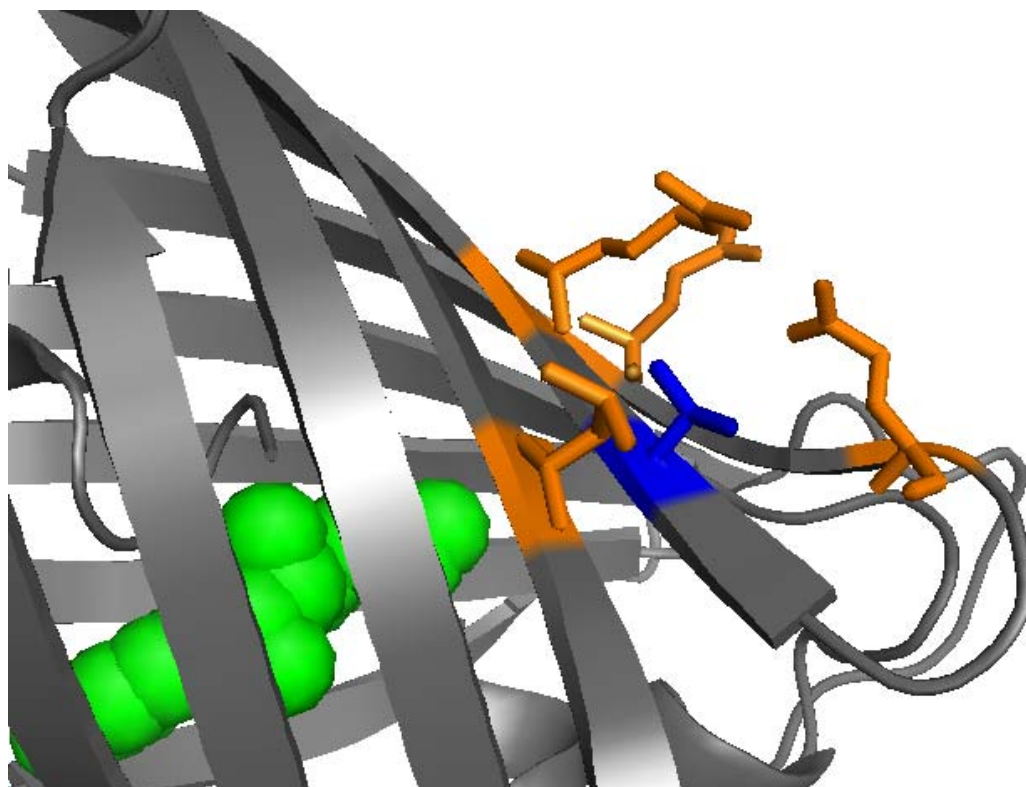


Fig 4.40 Pymol picture of EGFP site 120 to illustrate the position of V120 in the design site. The residue is buried beneath the other residues in the design site, which likely shields it from water since it is a hydrophobic residue. The fluorescence loss of this protein is likely due to repulsion of this residue and the others in the site.

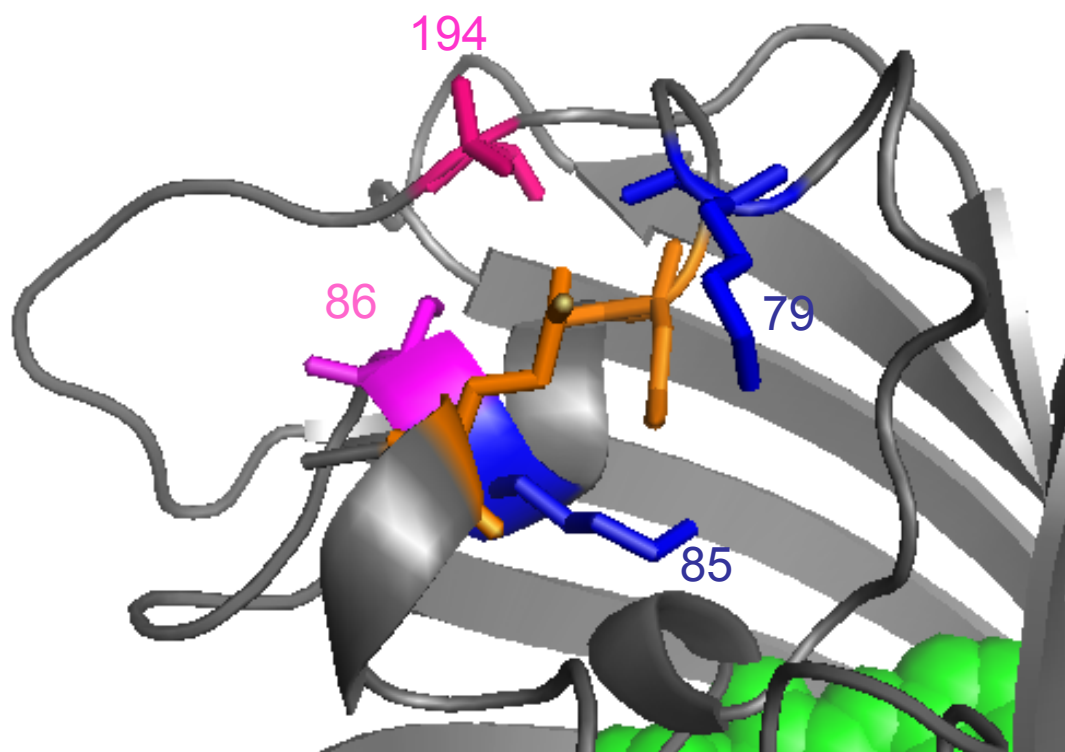


Fig 4.41 An illustration of the 194 family of designed proteins with 194 shown in pink, 86 in magenta, and 85 and 79 in blue. The two native amino acids, E5 and D82 are shown in orange. Repulsion of K85D with the surrounding residues likely causes the fluorescence loss. S86D is more solvent exposed and less likely to disrupt charge and hydrogen bond contacts that help to keep the fold of the protein intact. Also, K85D is in closer proximity to the chromophore than S86D, which may affect the hydrogen bond network observed of the chromophore.

same reason. When S86D is mutated, the change is not as severe as the K to D mutations so the tertiary packing is disrupted as significantly.

4.9.2 pK_a measurements of EGFP and partial site mutants

The pK_a values of EGFP and the variants L15N and L194N, summarized in table 4.8, were measured by absorbance and fluorescence spectra from pH 4 to 9 in various buffers to maintain the pH. The absorbance was monitored from 600 nm to 220 nm. As shown for EGFP in figure 4.42, the neutral peak at 398 nm increases upon acidification while the anionic peak at 482 nm decreases upon acidification. The chromophore peak blue shifts at pH 4, indicating that the protein is unfolded so that the chromophore is no longer shielded from the solvent. A global fit of absorbance spectra from 325 nm to 600 nm for pH 4 to 9 revealed a pK_a of 5.83 ± 0.02 , but the global fit excluding pH 4, since the absorbance peak is blue shifted and does not share the same isosbestic point, yields a pK_a of 5.95 ± 0.02 . The absorbance at 398 nm and 488 nm was also fit with an equation for two asymptotes at the low and high pH values with a slope of -1 (Eq. 4.1) or +1 (Eq. 4.2) (130):

$$Y = \frac{A * 10^{-pH} + B * 10^{-pK_a}}{10^{-pH} + 10^{-pK_a}} \quad \text{Eq 4.1}$$

$$Y = \frac{A * 10^{-pK_a} + B * 10^{-pH}}{10^{-pK_a} + 10^{-pH}} \quad \text{Eq 4.2}$$

Table 4.8 The pK_a values of EGFP, L15N, and L194N as measured by absorbance and fluorescence in various buffers to maintain the pH at each desired value.

Protein	Average of Absorbance at 398 nm	Average of Absorbance at 488 nm	Average of emission at 510 nm, excitation 398 nm	Average of emission at 510 nm, excitation 482 nm	Average of emission at 450 nm, excitation 398 nm
EGFP	6.04 ± 0.01	5.93 ± 0.01	5.65 ± 0.01	5.72 ± 0.00	6.11 ± 0.06
L15N	5.95 ± 0.02	5.79 ± 0.01	5.63 ± 0.10	5.67 ± 0.02	6.10 ± 0.08
L194N				5.83 ± 0.02	

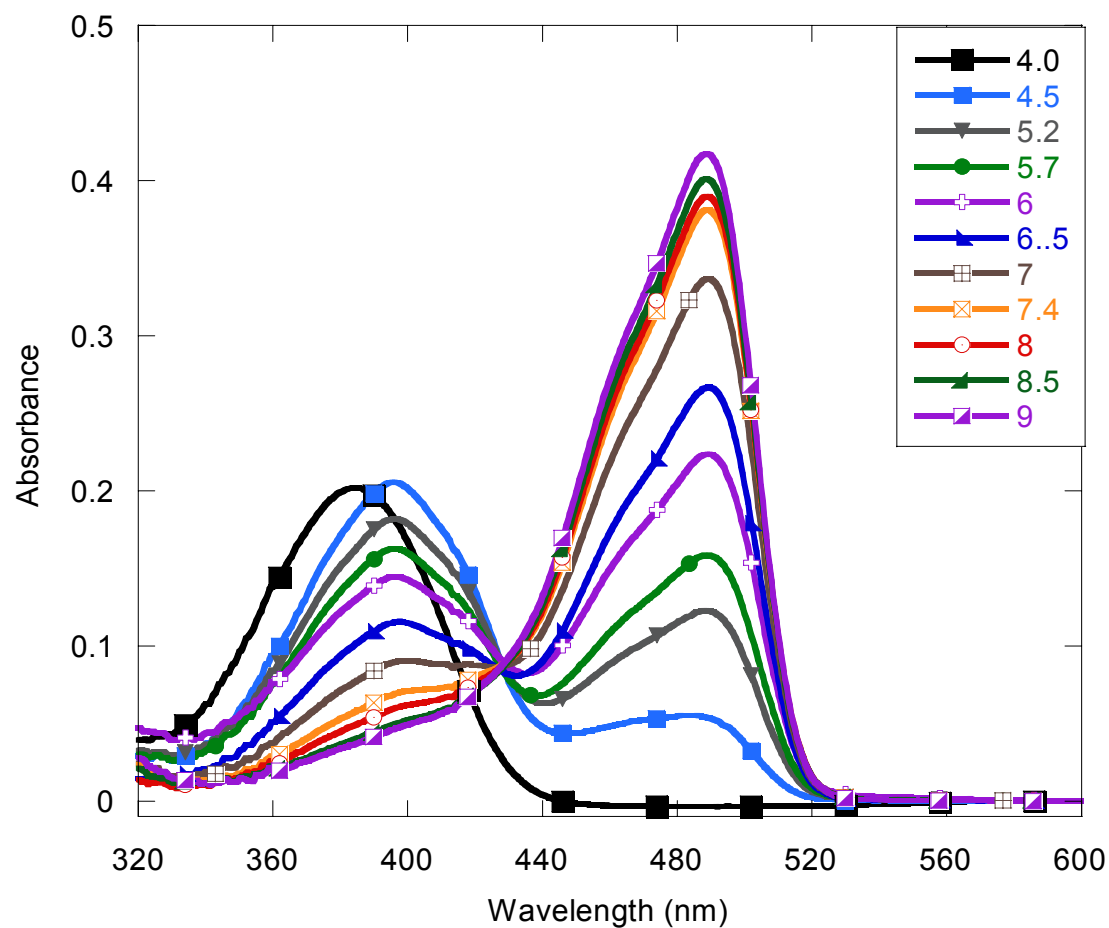


Fig 4.42 Absorbance spectra of EGFP at various pH demonstrating the pH dependence of the chromophore. The various buffers utilized to control the pH are listed in table 2.5.

The equations for input into Kaleidagraph are:

$$(m1+m2*10^{(-m3)}/10^{(-m0)})/(1+10^{(-m3)}/10^{(-m0)}); m1=\text{max}; m2=\text{min}; m3=\text{pK}_a \text{ estimate}$$

$$(m2*10^{(-m0)}+m1*10^{(-m3)})/(10^{(-m0)}+10^{(-m3)}); m1=\text{max}; m2=\text{min}; m3=\text{pK}_a \text{ estimate}$$

with the minimum and maximum values taken from the data. The pK_a obtained from the fit of the absorbance at 398 nm was an average 6.04 ± 0.01 for duplicate samples as shown in figure 4.43. Fitting the 488 nm absorbance yielded an average of 5.93 ± 0.01 for duplicate samples (Fig 4.43). These two pK_a values are in good agreement, as they should be for two titrating species as indicated by the isosbestic point.

The fluorescence was also monitored from pH 4 to 9 between 420 nm and 580 - nm with excitation at 398 nm and between 500 and 580 nm for excitation at 482 nm as shown in figure 4.44. Fitting of the single wavelength data does not agree with the global fit of the data with Specfit/32 for the fluorescence data. For the 510 emission with excitation at 398 nm or 482 nm yields nearly identical pK_a values of 5.65 ± 0.01 and 5.72 ± 0.00 , respectively, when fit with the two asymptote equations 4.1 and 4.2 as shown in figures 4.45 and 4.46. However, the emission at 450 nm with excitation at 398 nm does not agree with the pK_a value obtained for the 510 nm emission with an average pK_a of 6.11 ± 0.06 at 450 nm as shown in figure 4.45. The emission has been proposed to be due to the neutral state of the chromophore, which is able to fluoresce at lower pH but not at higher pH due to fast internal proton transfer that leads to the anionic state and emission in the green rather than blue spectrum (131-133). The pK_a

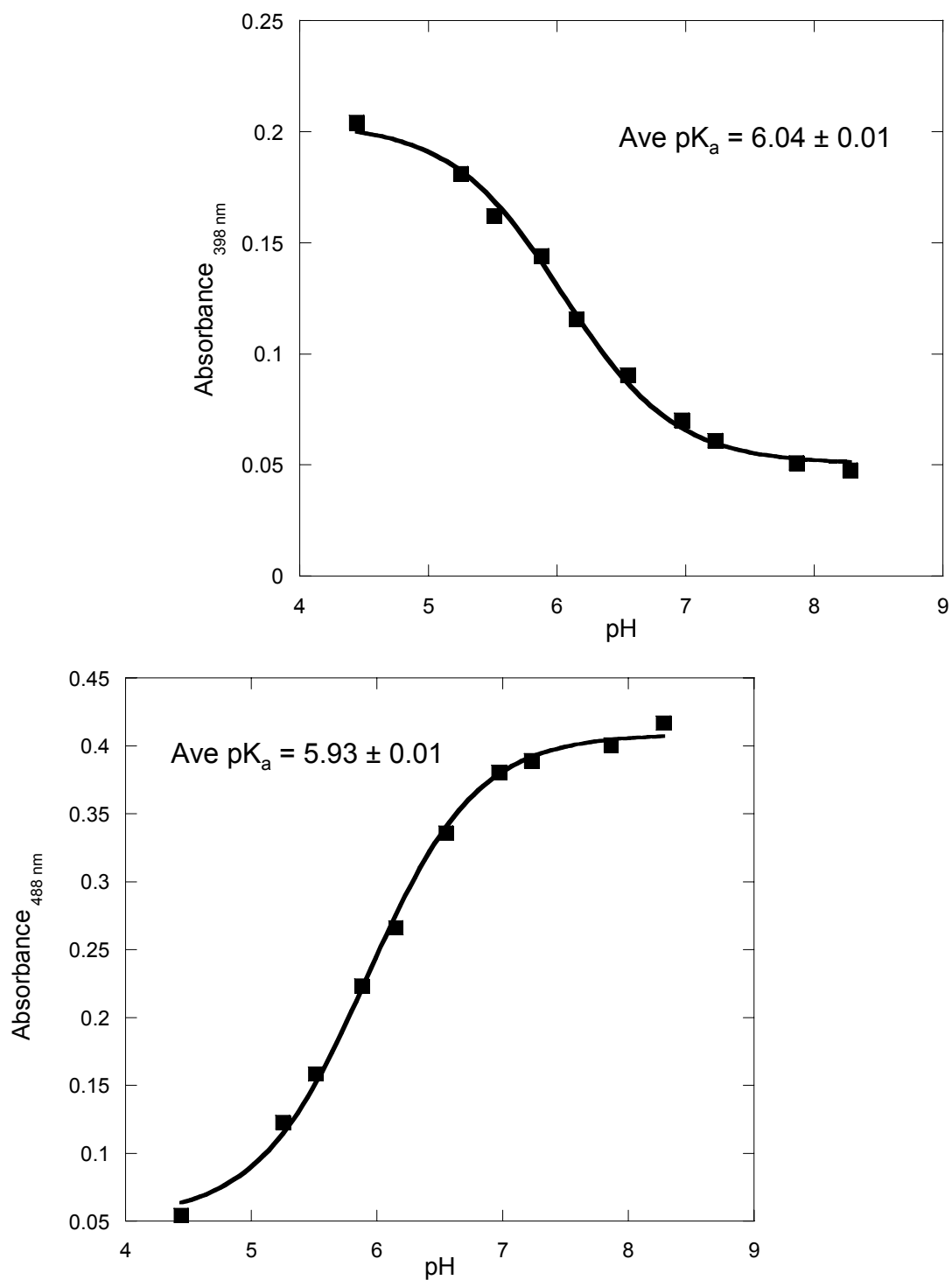


Fig 4.43 Plots of the absorbance at 398 nm (top) and 488 nm (bottom) of 10 μ M EGFP at various pH to calculate the pK_a of the protein's chromophore.

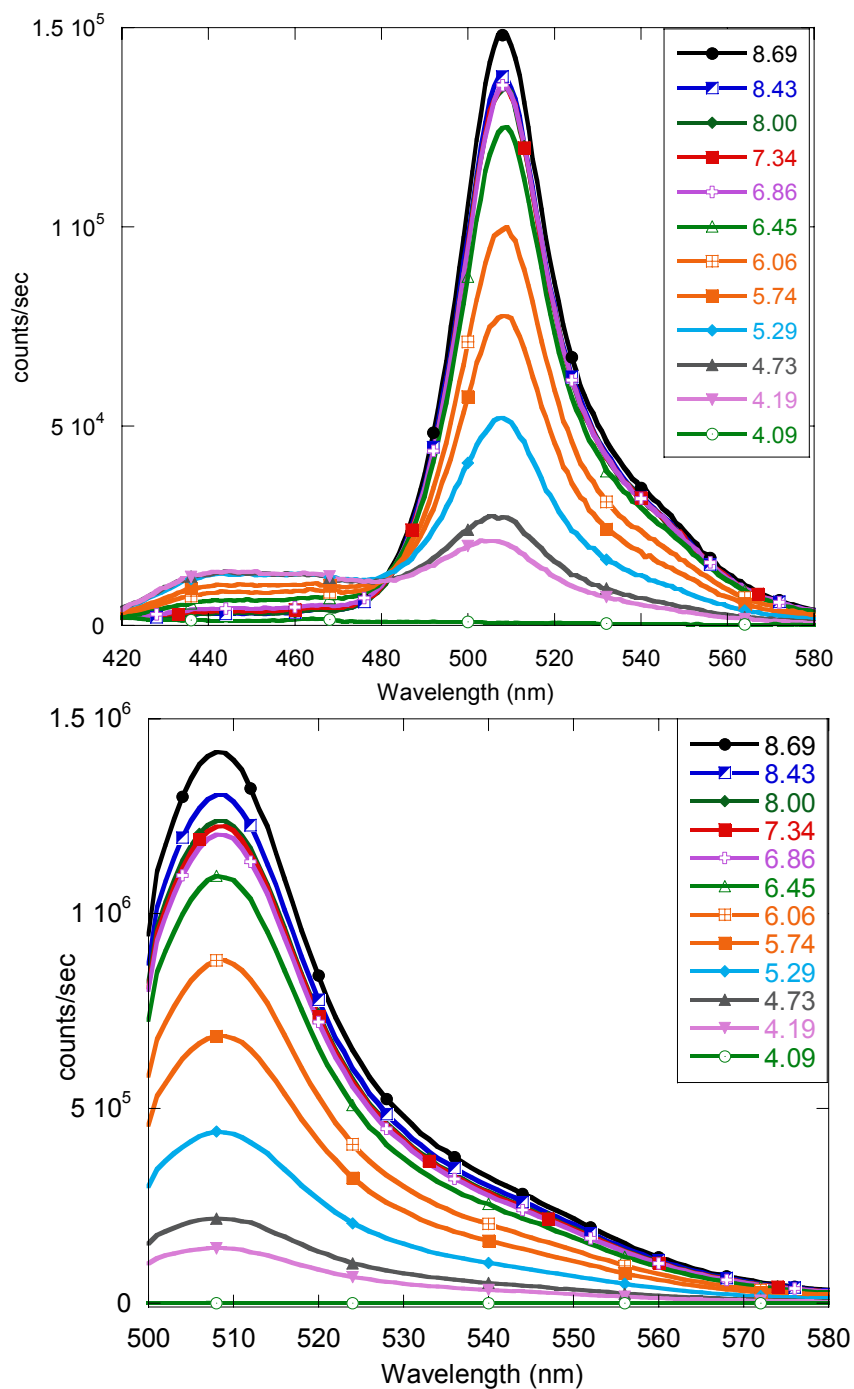


Fig 4.44 EGFP pH dependence by fluorescence with excitation at 398 nm (top) and 482 nm (bottoms) and all slit widths set to 2 nm bandwidth. The pH was maintained by various buffers with the correct pK_a to hold the pH near the desired value. The emission at 510 nm decreases as the emission at 450 nm increases upon acidification with excitation at 398 nm.

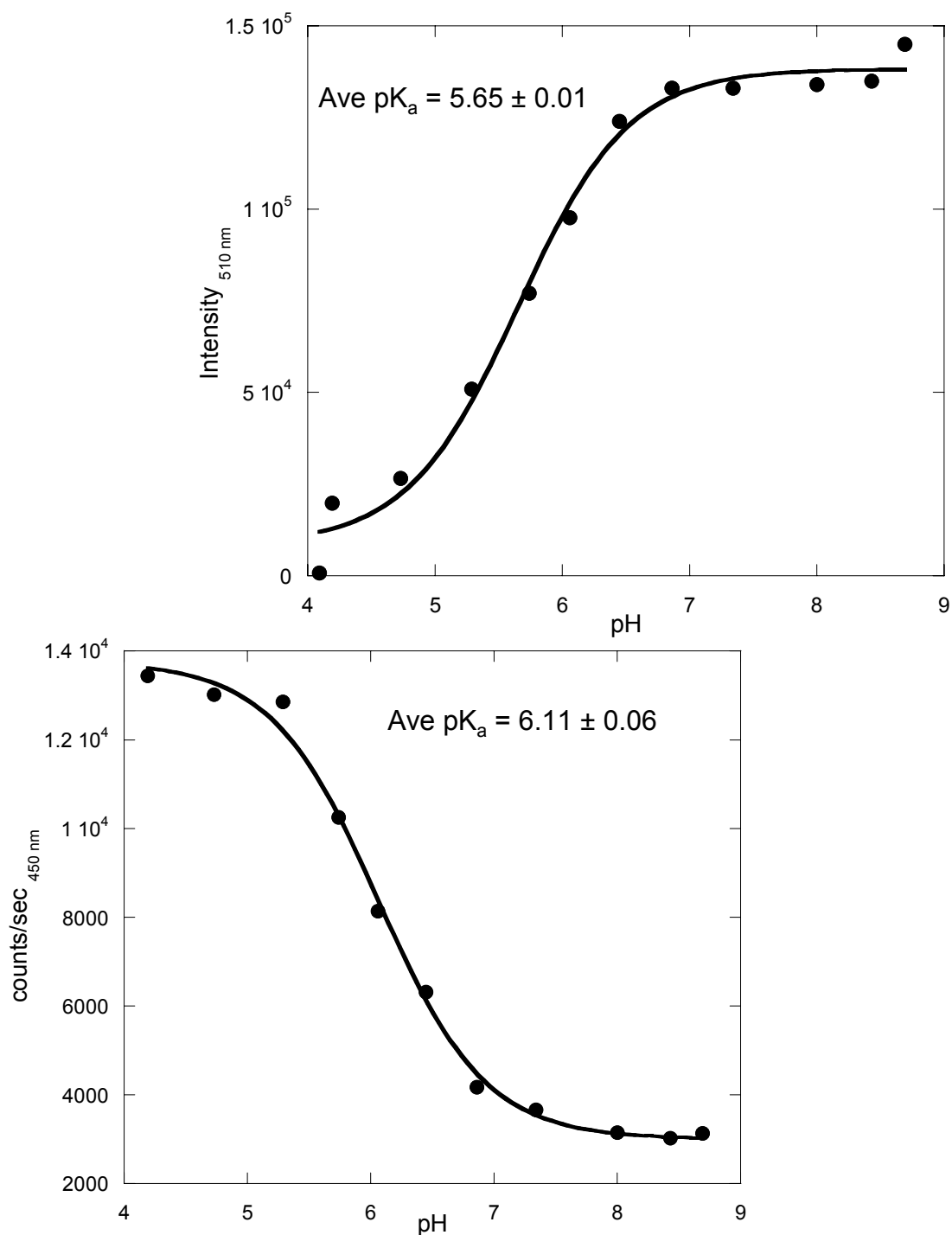


Fig 4.45 Plots of the fluorescence at 510 nm (top) and 450 nm (bottom) with excitation at 398 nm of 1 μ M EGFP at various pH to calculate the pK_a of the protein's chromophore. The pK_a values differ for emission at 510 nm and 450 nm, which is explained in the literature as excited state proton transfer.

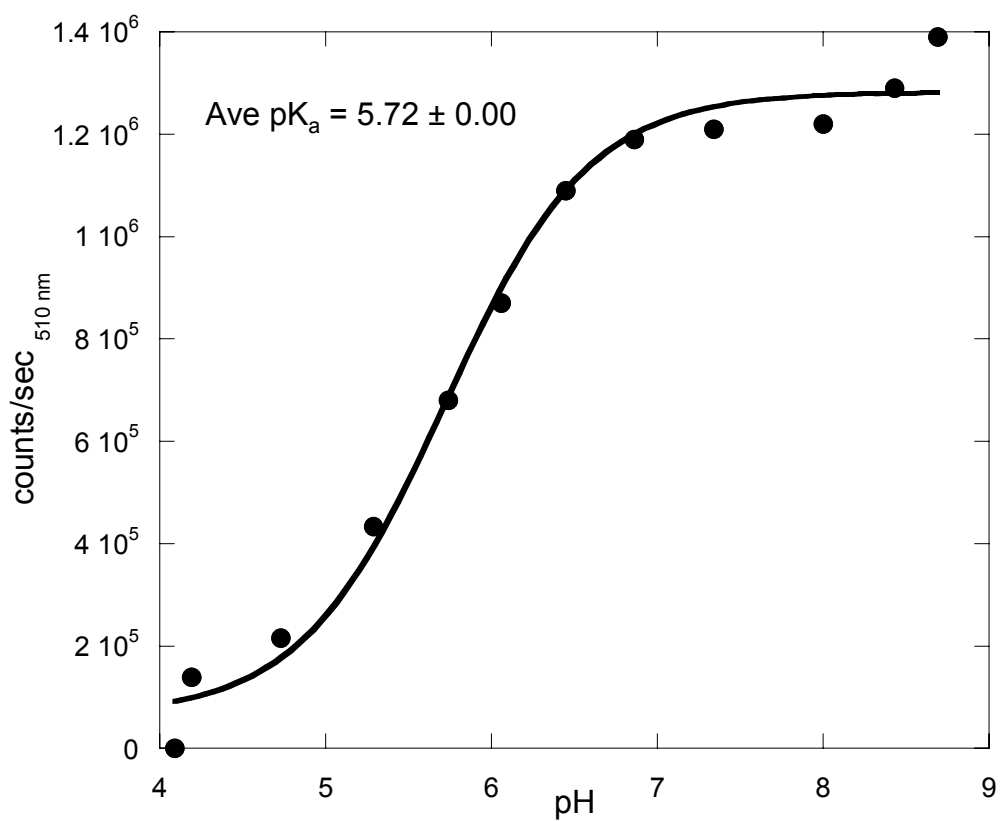


Fig 4.46 Plot of the fluorescence at 510 nm with excitation at 482 nm of 1 μ M EGFP at various pH to calculate the pK_a of the protein's chromophore. The pK_a values differ for emission at 510 nm for the two different excitations are within error of one another.

calculations for fluorescence data are convoluted by this proton transfer so that the 450 nm emission does not match the 510 nm emission exactly, although the difference is only ~ 0.3 . A global fit of the spectra produces a pK_a of 6.9, but this difference between the global fit and the single wavelength fit is likely due to the contribution of the intermediate state confounding the data and the discrepancies due to the excited state proton transfer.

Measurement of L15N and L194N mutants of EGFP indicated similar results. The absorbance of L15N at 398 nm produced an average pK_a of 5.95 ± 0.02 for duplicate samples, and the absorbance at 488 nm generated a pK_a of 5.80 ± 0.01 . The fluorescence at 510 nm when excited at 482 nm indicated an average pK_a of 5.67 ± 0.02 for duplicate samples. The pK_a measured with 398 nm excitation and emission at 510 nm was 5.63 ± 0.10 . The emission at 450 nm does not match the pK_a for emission at 510 nm similar to wild type EGFP with an average pK_a of 6.10 ± 0.08 . L194N was not tested as in depth as L15N, but the pK_a with fluorescence at 510 nm and excitation at 482 nm was measured to be an average of 5.83 ± 0.02 for duplicate samples. This value is in good agreement with L15N and EGFP.

4.9.3 Quantum yield measurements of partial sites and EGFP

The literature reports the quantum yield of EGFP as 0.60. EGFP was initially measured in duplicate to ensure that the experimental conditions were appropriately designed. Quantum yields were obtained by measuring the emission at 510 nm with excitation at 488 nm and absorbance at 488 nm of EGFP and the variants with protein

concentrations from 0 to 2 μM . The quantum yields, summarized in table 4.9, calculated from in-house experiments were 0.606 and 0.59996 (~ 0.6) (Fig 4.47). The measured quantum yield of L15N indicated an average of 0.44 ± 0.0007 (Fig 4.48). The quantum yield for L194N was an average of 0.43 ± 0.0014 . The extinction coefficients at 488 nm were also calculated from this data with EGFP at $49,311 \text{ M}^{-1}\text{cm}^{-1}$ (similar to literature values) (63), L194N at $44,804 \text{ M}^{-1}\text{cm}^{-1}$, and L15N at $51,015 \text{ M}^{-1}\text{cm}^{-1}$, all with R values of 0.99 or better (Fig 4.49). The calculated extinction coefficient of EGFP, $21,890 \text{ M}^{-1}\text{cm}^{-1}$, is generally utilized to calculate the protein concentration and to ensure that all of the protein has a formed chromophore. The extinction coefficients of the variants were calculated at 280 nm to be 20,792 and $21,412 \text{ M}^{-1}\text{cm}^{-1}$ for L15N (Fig 4.50) and L194N, respectively. These proteins still maintain large quantum yields to allow for bright imaging. In preliminary in vivo studies in HeLa cells, these proteins still indicate bright fluorescence on par with EGFP with very short exposure times necessary for imaging.

4.10 Disulfide Bonds and Chromophore Reduction

Dimerization of GFP has been reported to be due to the two surface cysteines in GFP at positions 48 and 70 (134). Also, recently developed redox sensors indicate that disulfide bond formation could affect chromophore fluorescence (135). The fluorescence emission of L194N/S86D was tested in the presence of a disulfide bond reducer, β -mercaptoethanol, to ascertain the effects of disulfide bond formation on our designed protein. As expected, increasing concentrations of β -mercaptoethanol

Table 4.9 A summary of the quantum yield and extinction coefficient measurements for EGFP, L15N, and 194N.

Protein	Quantum Yield	Extinction Coefficient at 488 nm ($M^{-1} \text{ cm}^{-1}$)	Extinction Coefficient at 280 nm ($M^{-1} \text{ cm}^{-1}$)
EGFP	0.603 ± 0.004	49,311	21,890
L15N	0.44 ± 0.001	51,015	20,792
L194N	0.43 ± 0.001	44,804	21,412

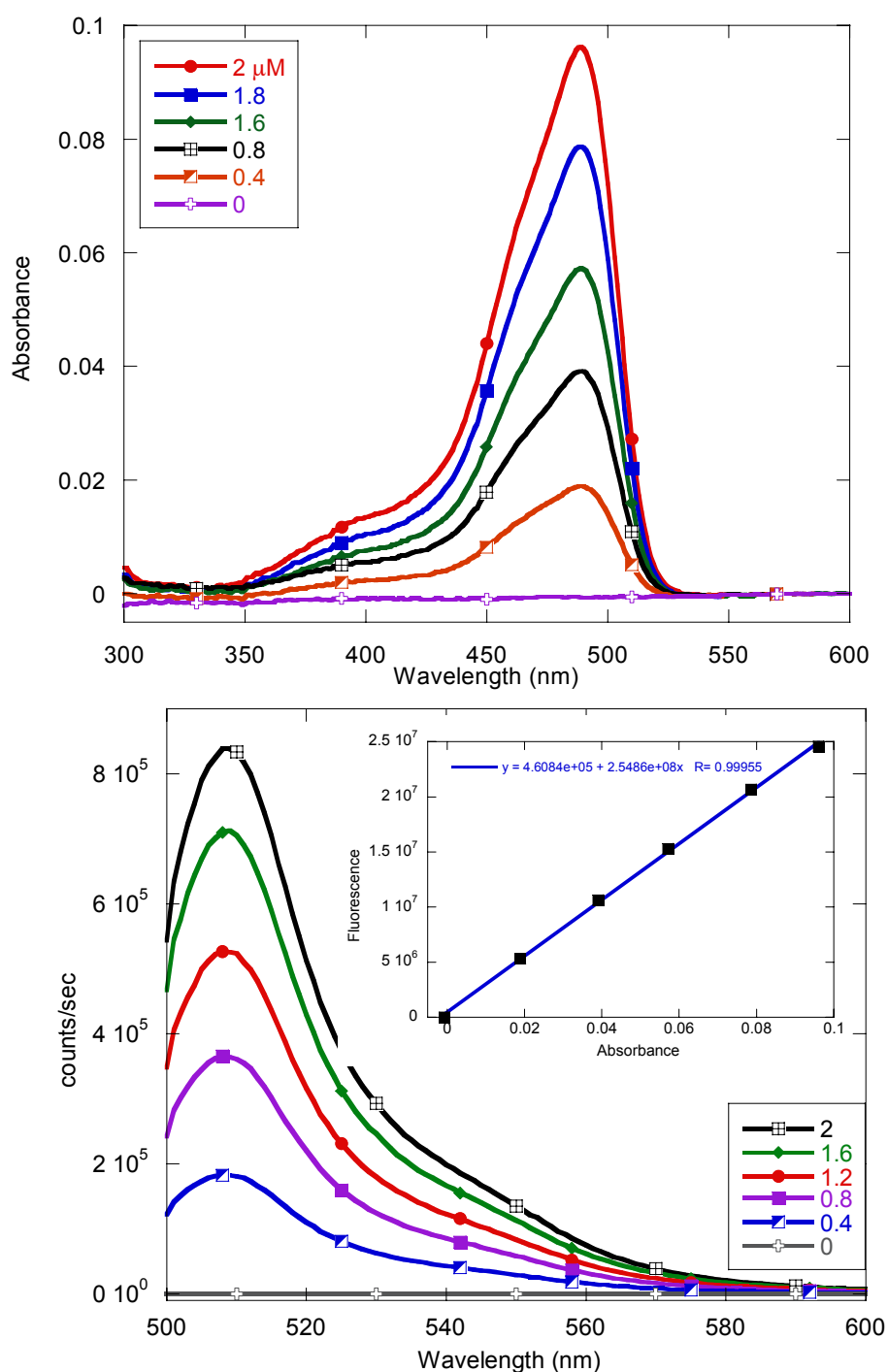


Fig 4.47 Absorbance and fluorescence spectra of EGFP in 10 mM Tris, 1 mM DTT, 1% glycerol, pH 7.4 at various concentrations to calculate the quantum yield of the protein. The fluorescence vs. absorbance fit is also shown in the inset.

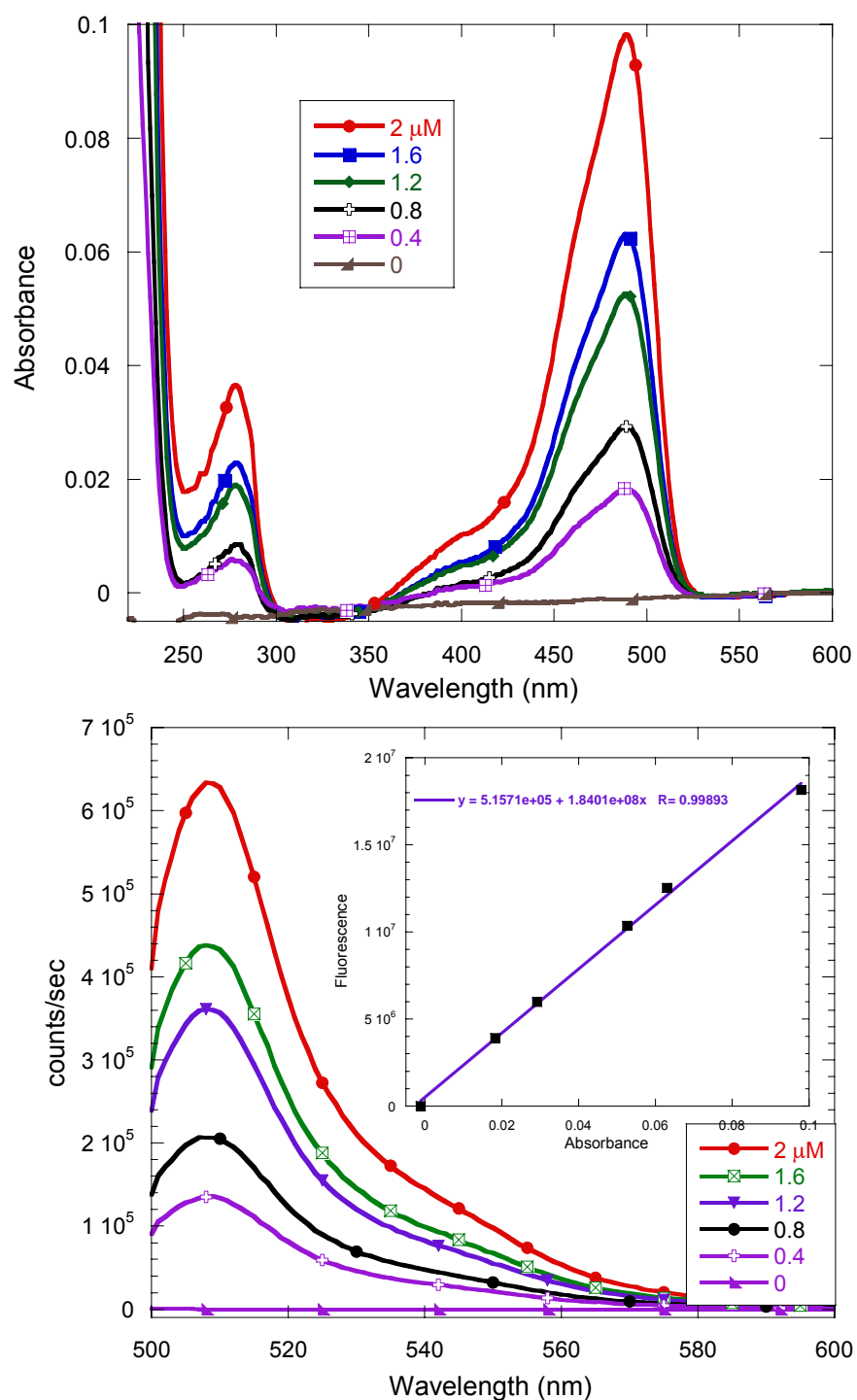


Fig 4.48 Absorbance and fluorescence spectra of L15N in 10 mM Tris, 1 mM DTT, 1% glycerol, pH 7.4 at various concentrations to calculate the quantum yield of the protein. The fluorescence vs. absorbance fit is also shown in the inset.

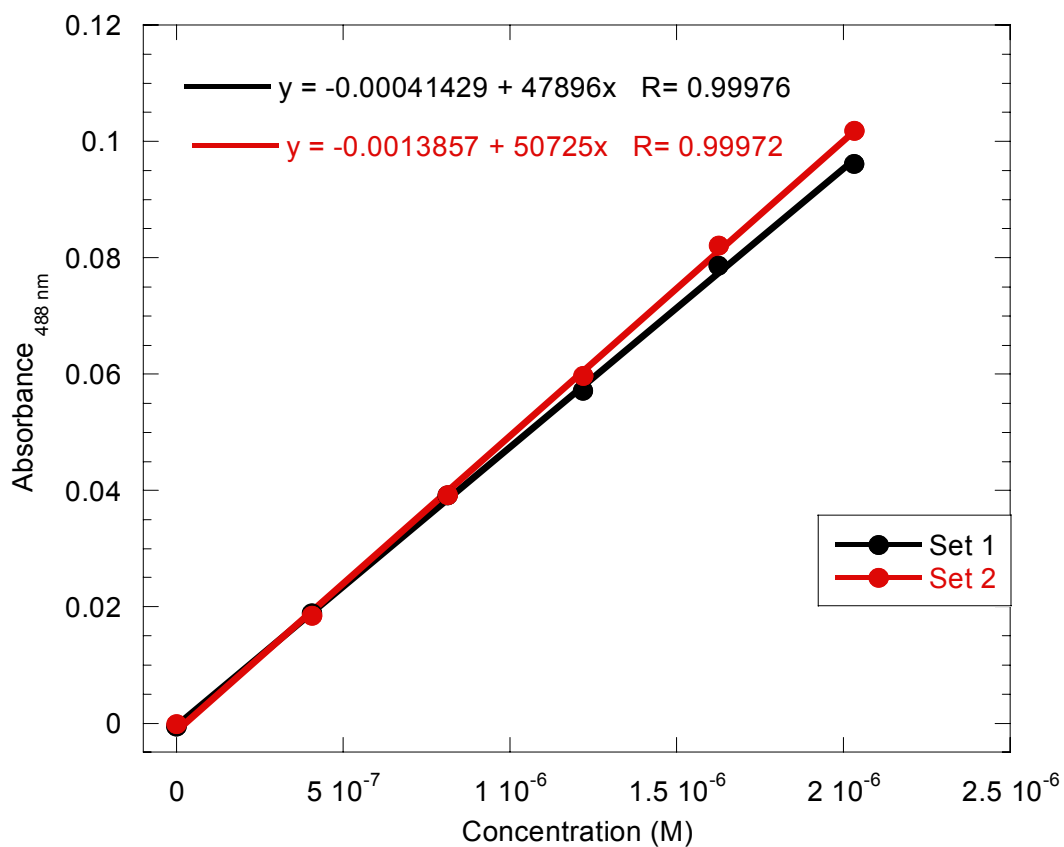


Fig 4.49 Extinction coefficient calculation for EGFP at 488 nm for two sets of data. The slope of the linear regression fit is equivalent to the extinction coefficient. The extinction coefficients for L194N and L15N were calculated in the same manner.

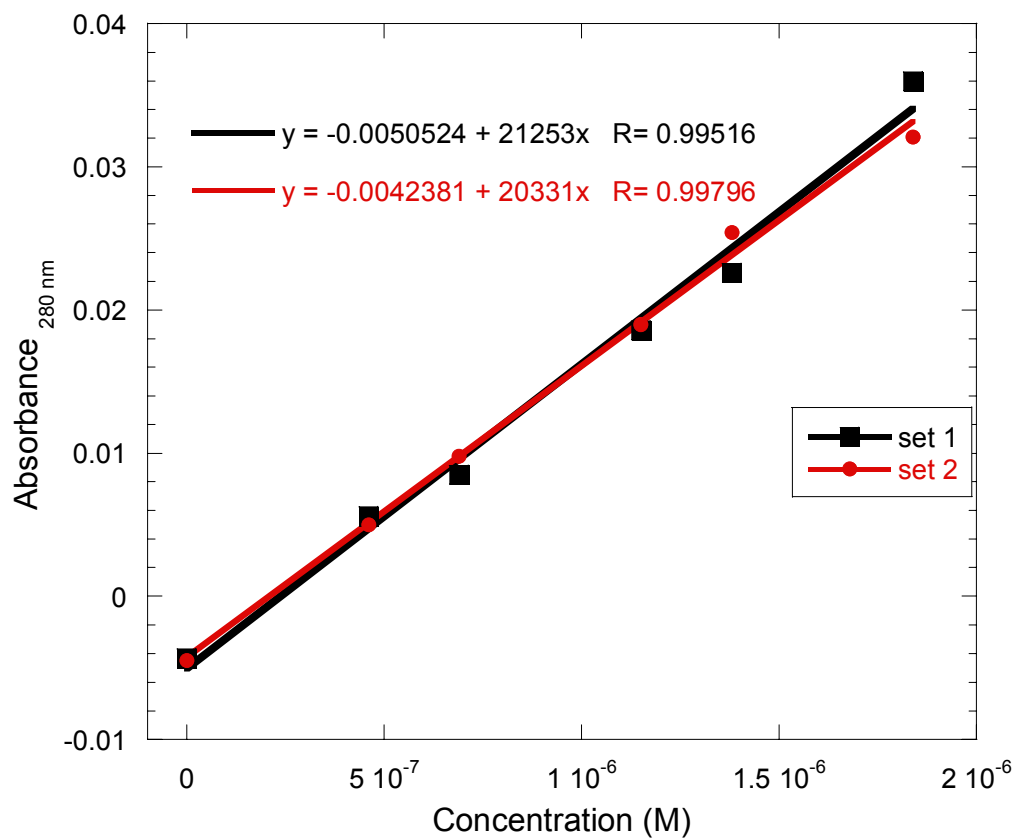


Fig 4.50 Extinction coefficient calculation for L15N at 280 nm for two sets of data. The slope of the linear regression fit is equivalent to the extinction coefficient. The extinction coefficient for L194N was calculated in the same manner.

decreased the fluorescence of the protein with complete loss observed at 50% v/v (Fig 4.51). Above ~10% v/v, the fluorescence decrease is likely due to reduction of the chromophore. However, at low percentages (<10% v/v) of β -mercaptoethanol, addition of calcium (1 and 10 mM) indicated an increase in the fluorescence over the emission with just the reducer (Fig 4.51). This could possibly be due to calcium binding which allows the chromophore to be shielded from the β -mercaptoethanol so it is not reduced to as large an extent. This chromophore reduction is not yet completely understood, but it is likely that low concentrations will reduce disulfide bond formation while larger concentrations will reduce the chromophore.

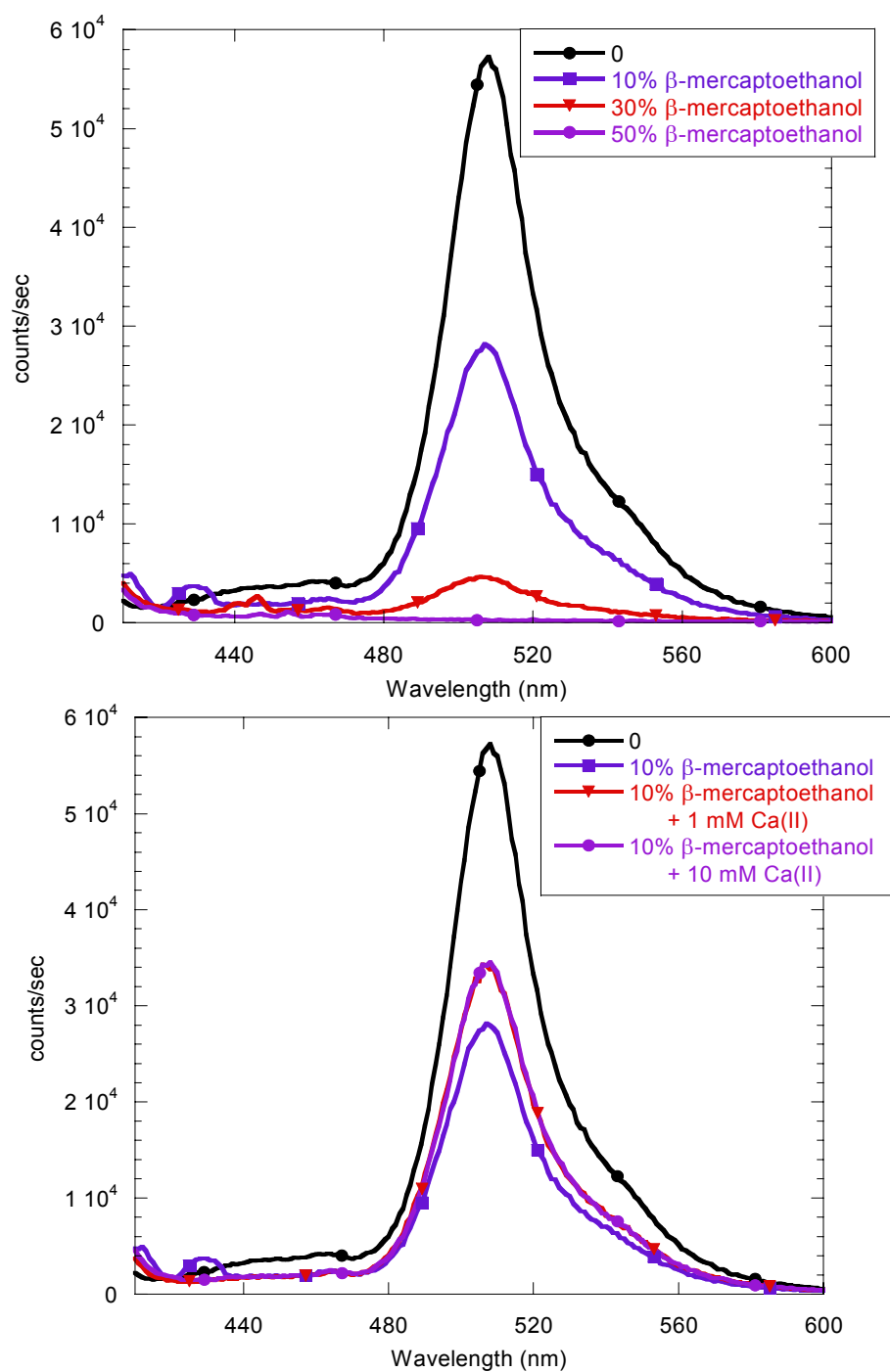


Fig 4.51 L194N/S86D in 10% β -mercaptoethanol with and without calcium excited at 398 nm. The decrease in chromophore fluorescence due to reduction of the chromophore is less with calcium than without. This may be due to some protection of the chromophore caused by the binding.

Chapter 5 The Evolution of Sensor 177

5.1 Mammalian Screening of Designed Proteins

We have constructed and studied green fluorescent proteins with designed calcium binding sites and have shown that they bind calcium with a range of affinities. One of the possible reasons for the lack of fluorescence of our designed proteins is that proteins fold differently in bacteria than in mammalian cells. GFP is a protein native to cold water jellyfish, which is a eukaryotic organism. Alberti and coworkers demonstrated that various GFP mutants exhibit differing folding efficiencies in bacteria and mammalian cells (136), indicating a difference in prokaryotic and eukaryotic protein folding mechanisms. These variants also demonstrated differing folding efficiencies from each other, and additional tags attached to the variants induced differing folding efficiencies. Sakikawa et. al. demonstrated that GFP and its variant BFP binds to the cis-cavity of the GroEL chaperone and undergoes folding inside the cis-cavity (137). Mammalian cells with subcellular compartments contain much better machinery for protein folding than bacteria, including many more folding chaperones. Since the designed proteins exhibit β -sheet secondary structure, indicating some folding, and it appears that the tertiary structure of the barrel is not well packed, the proteins were expressed in mammalian cells to ascertain if the tertiary structure would pack better allowing for formation and/or fluorescence of the chromophore. In this chapter, we will demonstrate the better folding of designed calcium binding green fluorescent proteins in mammalian cells through expression in four cell lines, HeLa, HEK293, Vero, and CHO

as shown in table 5.1. Mutations to create a brighter sensor will be detailed. The calcium response *in vivo* of these mutants will also be discussed.

5.1.1 Choice of cell lines

For mammalian cells, there are numerous cell lines available. The accessible cell lines for our laboratory are listed in table 5.1. HeLa cells are cervical carcinoma first discovered in the 1960's. Hek293 are human embryonic kidney cells that have been extensively reported in the literature as the cell line for many different applications. CHO are Chinese hamster ovary cells, which have also been considerably reported. Vero cells are kidney cells from an African monkey, which are widely used in viral research. They are much larger cells than the other 3 types, and it was thought that their subcompartments may be easier to monitor due to the larger size. Each of these cell lines has their own uniqueness that lead us to incorporate them into our study. If cancerous cells handle calcium differently than normal cells, comparison of the calcium response in HeLa and CHO cells could provide clues to that difference. Hek293 cells have been shown to produce muscarinic receptors, much like muscle and neural cells, which cause calcium spikes when stimulated with acetylcholine or carbachol. This provides another way to measure the calcium response of our designed sensors and also provides information on calcium handling in the cell. The expression of the designed sensor had to be optimized for each of the cell lines as the transfection efficiency and expression yield could vary for each.

Table 5.1 A summary of the four mammalian cell lines utilized in the characterization of the designed GFP calcium-binding proteins.

Cell line	Origin	Reasons for use
HeLa	Cervical carcinoma	Easy growth and transfection, calcium response previously monitored with calcium-binding dyes and proteins
HEK293	Human embryonic kidney	Normal cells, grow well, transfection conditions known, previously used for calcium measurements
Vero	African monkey kidney cells	Normal cells, grow well, larger cells for ease of imaging
CHO	Chinese hamster ovary	Normal cells but different type than others for comparison of calcium spatial and temporal changes

5.2 Expression of Designed Proteins in Mammalian Cells

5.2.1 Engineering mammalian cell expression constructs for expression of the designed proteins

Sites 177, 120, 194a, 229 and L194N/S86D along with EGFP were subcloned into pcDNA3.1+ vector for expression in mammalian cells (Fig 5.1). This vector contains a CMV (cytomegalovirus) promoter site that allows for expression in the mammalian system. The CMV promoter has activity in a large variety of cells so it is often utilized in initial testing of new proteins and has been shown to produce more protein than other commonly used promoters, such as SV40 (138). The vector also contains an ampicillin resistance site for preparation of the DNA in bacteria and a neomycin/geneticin resistance to allow for stable transfectants to be made. A multiple cloning site for insertion of the desired gene is also located in pcDNA3.1+. The subclone of these sites into pcDNA3.1+ proceeded as detailed in section 2.4 with no difficulties.

5.2.2 Transient transfection and expression of designed proteins

Sites 177, 120, 120b, 194a, 229, L15N/R122D and L194N/S86D were all transfected into HeLa or CHO cells with EGFP as the control as detailed in the materials and methods section 2.19. Sites 120 and 194a only exhibited an extremely weak fluorescence after 72 hrs of expression at 30 °C that quickly bleached before images could be obtained (Figs 5.2 and 5.3). The fluorescence could be seen through the binoculars on the scope and could be watched while it bleached. Expression of Site 120 for up to 10 days at 30 °C in CHO cells did not yield fluorescence. Site 120b

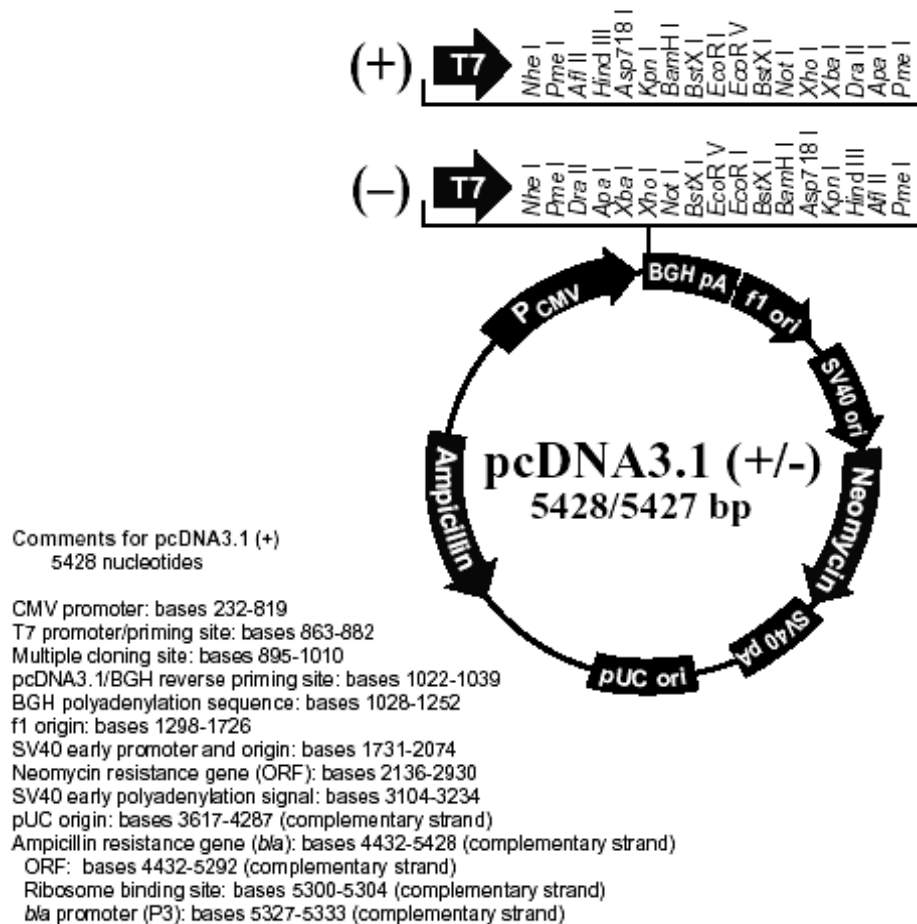


Fig 5.1 Vector map and details of the pcDNA3.1+ vector from Invitrogen. The vector allows for expression of proteins in mammalian cells with the utilization of the CMV promoter.

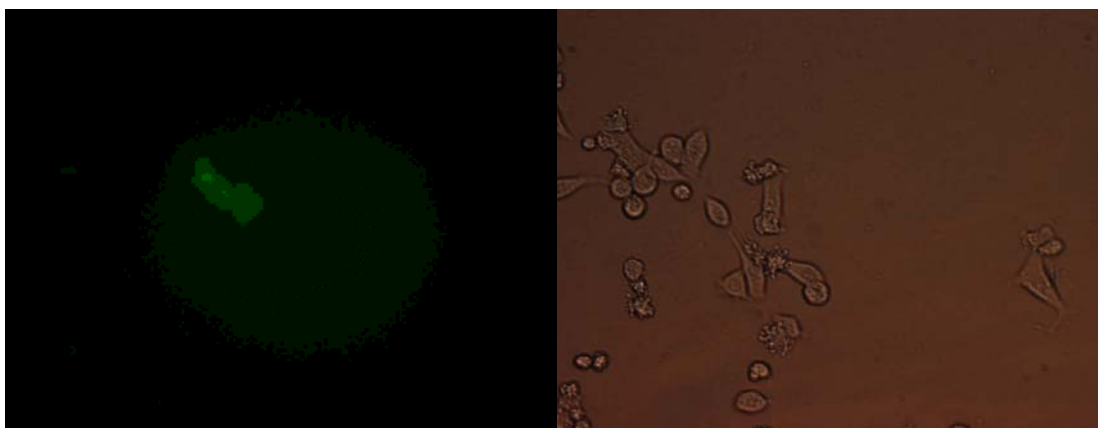


Fig 5.2 Images of site 120 in HeLa cells 72 hrs after transfection with expression at 30 °C at 40x magnification with 1500 ms exposure indicating the very weak fluorescence observed with this site. The left image was obtained with the FITC filter (490/510), and the left image is the transmitted light.

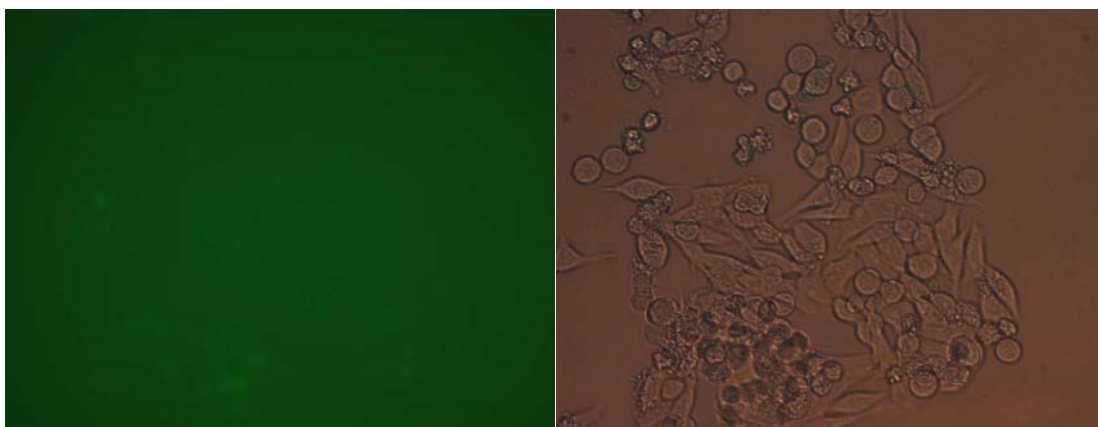


Fig 5.3 Images of 194a in HeLa cells 72 hrs after transfection with expression at 30 °C at 40x magnification with 1500 ms exposure indicating the only very weak fluorescence observed with this designed site. The left image was obtained with the FITC filter (490/510), and the left image is the transmitted light.

exhibited weak fluorescence in CHO cells after 72 hrs of expression (Fig 5.4). Site 229 exhibited no fluorescence after expression for 72 hrs at 30 °C (Fig 5.5). On the other hand, the partial sites L15N/R122D (full site is 120b) and L194N/S86D (full site 194b) were as bright as EGFP and did not exhibit bleaching with exposure up to 1 s (Figs 5.6 and 5.7). More importantly, the fluorescence of Site 177 that was bright enough to obtain images and did not bleach instantly as the full sites 120 and 194a did (Fig 5.8). Site 177, along with 120, 194, and 194b did not exhibit fluorescence when expressed in bacteria (chapter 4). The observation of green fluorescence for site 177 was very significant since it clearly demonstrates that mammalian cells have a much stronger capacity to express GFP variants with mature chromophores. Expression trials were performed on Site 177 to ascertain the expression time needed to obtain fluorescent cells, if the protein could be expressed at 37 °C, and if the protein were brighter in different cells lines.

5.2.3 Optimization of transfection conditions

Initially, the transfection and expression of EGFP was learned and optimized before the designed proteins were assessed. Further, EGFP was utilized as a control when new conditions were tested for each cell line. Sensor 177 was transfected into HeLa, Hek293, CHO, and Vero cells and the conditions were optimized for each. During the optimization of expression of any protein, several factors must be considered. The type of transfection (liposomes or calcium phosphate), brand of transfection reagent, amount of DNA, DNA:liposome ratio, expression time, and the cell line. In addition, for our designed sensors, the temperature had to be considered since

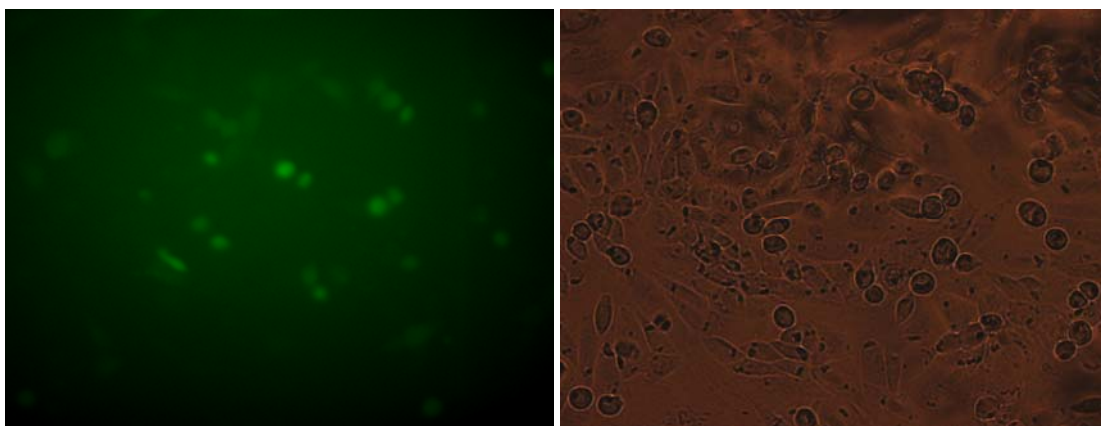


Fig 5.4 Images of Site 120b in CHO cells 72 hrs after transfection with expression at 30 °C with the FITC filter (left) and transmitted light (right) at 20x magnification with 2 s exposure. Very little fluorescence is observed and the exposure time required to capture the fluorescence is very long.

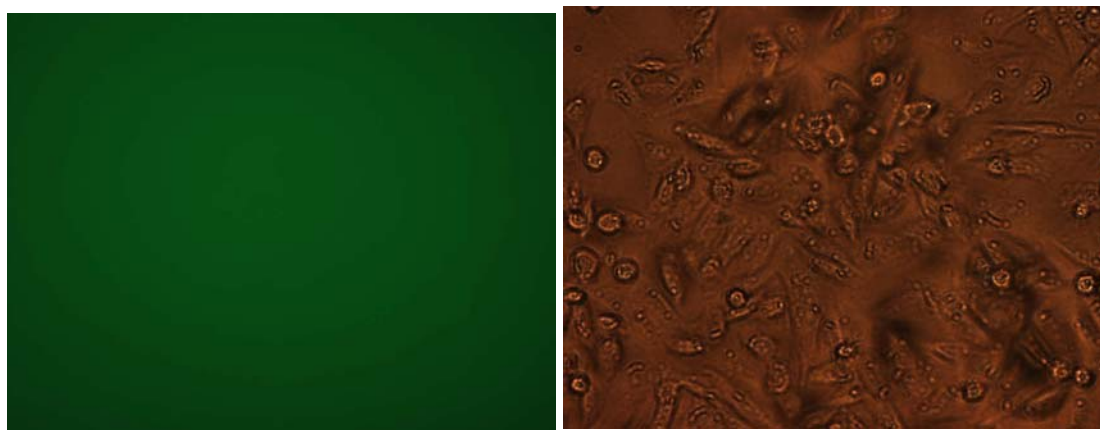


Fig 5.5 Images of Site 229 in HeLa cells 72 hrs after transfection with transmitted light and 488 nm excitation/510 nm emission at 20x magnification with 2 s exposure. No fluorescence is observed.

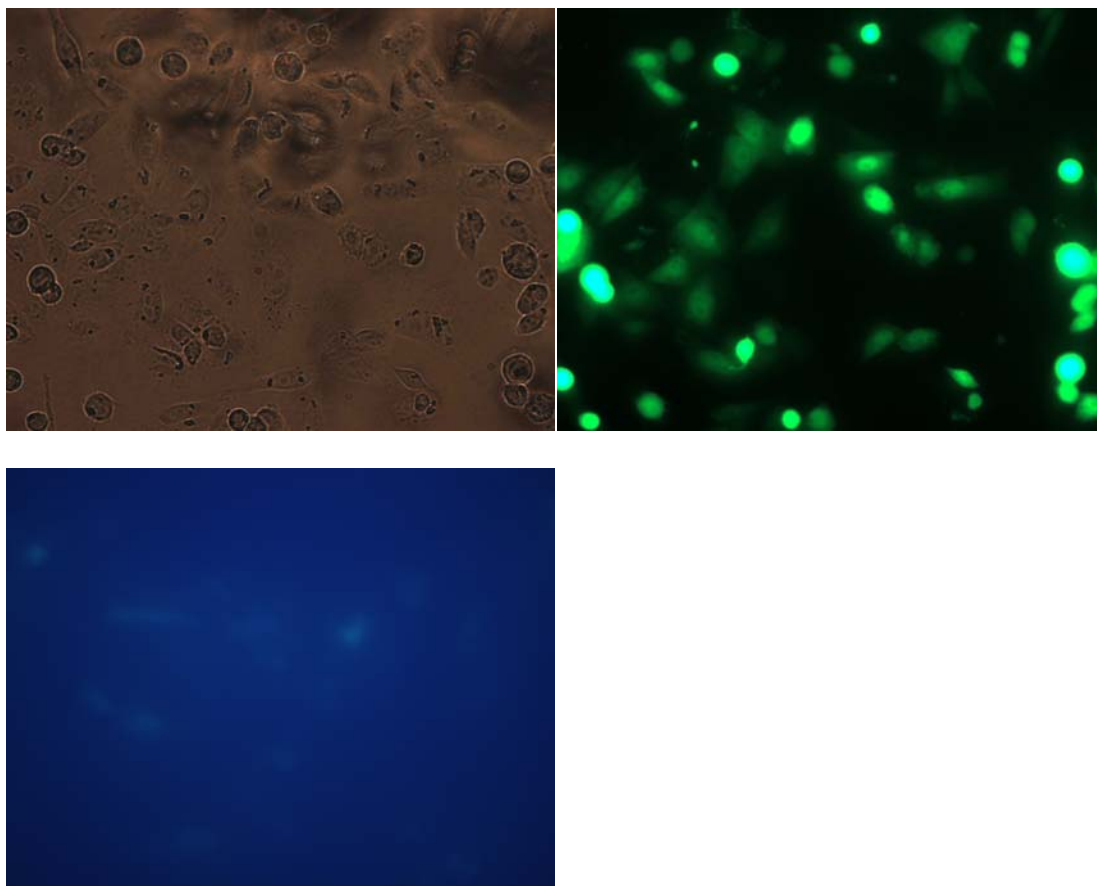


Fig 5.6 Images of L15N/R122D in CHO cells 72 hrs after transfection at 20x magnification with 100 ms exposure indicating strong fluorescence of the partial design site with short exposure time necessary to capture strong fluorescence. The top left image is transmitted light. The bottom image is UV excitation at 340 nm with emission at 450 nm, and the top right image is excitation at 488 nm with emission at 510 nm. These images also indicate that this protein exhibits some UV fluorescence, which is not seen with all of the mutants.

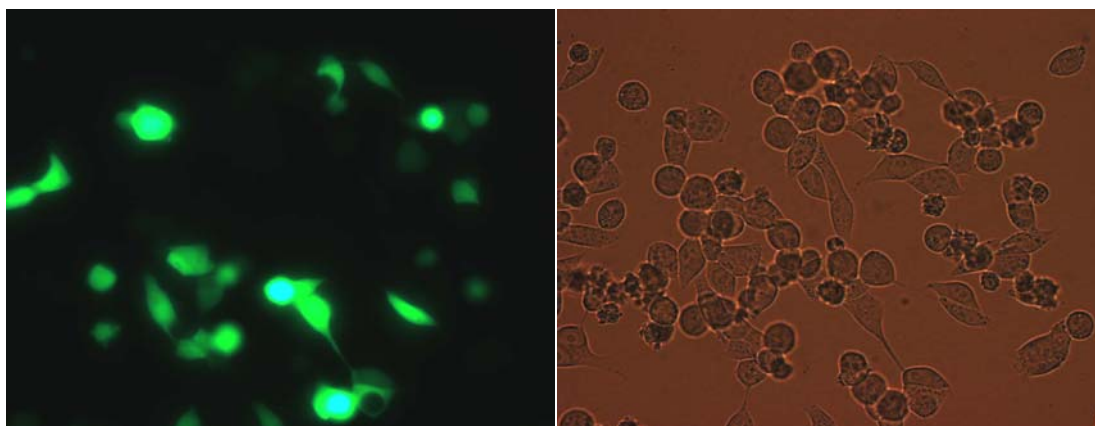


Fig 5.7 Images of L194N/S86D in HeLa cells 72 hrs after transfection with expression at 30 °C at 20x magnification with 200 ms exposure indicating fluorescence of this partial site that is as bright as EGFP.

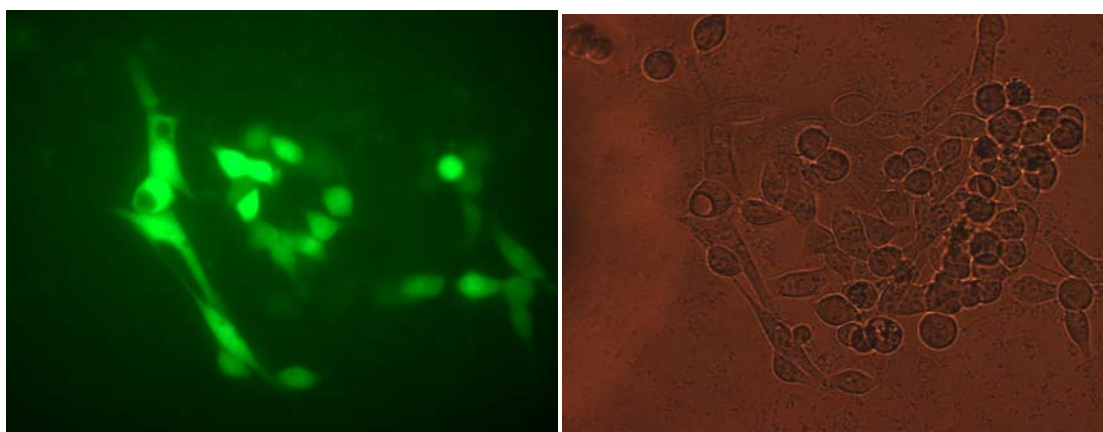


Fig 5.8 Images of Site 177 expressed in HeLa cells 72 hrs after transfection with expression at 30 °C at 40x magnification with 2 s exposure. The left image is with 488 nm excitation/510 emission, and the right image is transmitted light.

they do not exhibit fluorescence at 37 °C. In the past, calcium phosphate was the transfection protocol most largely followed, but with the advent of liposomal reagents, many researchers have moved away from calcium phosphate. We chose to pursue the liposome avenue.

Liposomes contain charged and hydrophobic portions. These molecules surround negatively charged DNA and allow the DNA to move across the hydrophobic cell membrane. There are many liposomes available from many companies, and the choice depends upon the cell type. Lipofectamine₂₀₀₀ was initially chosen for two reasons: 1) Invitrogen recommended this reagent for use with HeLa cells and had available literature indicating the use of this reagent with HeLa cells, and 2) Our collaborators on this project who taught us the mammalian protocols had previously indicated great success with this reagent. Once decided upon, the transfection reagent ratio must be optimized along with the amount of DNA to be applied per plate.

This optimization is two-fold, varying the amount of DNA and the ratio of DNA to liposome. For EGFP, 1 µg in a 1:1 ratio was more than sufficient to provide for very bright cells with high transfection efficiency (>80%). However, transfection of 177 with these conditions yielded very weakly fluorescent cells with low efficiency. The DNA amount was increased to 3 µg and the ratios from 1:1 to 1:5 were tested. It was found for HeLa cells that 3 µg with a 1:3 ratio worked very well providing fluorescent cells with >60% efficiency. The amount of DNA was then tested by keeping the DNA:liposome ratio at 1:3 and varying the amount of DNA from 2 µg to 5 µg. The increased amount of

DNA increased the fluorescence, but there were more dead/dying cells in the 4 and 5 μg dishes, likely due to the use of so much liposome during the transfection (Fig 5.9). Therefore, 3 μg of DNA in a 1:3 DNA:liposome ratio was employed for further experiments in HeLa cells with an observed transfection efficiency of 70-80%.

Initial studies on the transfection of Vero cells yielded very little fluorescence in only 10% of the cells. To improve the transfection efficiency and protein expression, different ratios of DNA and Lipofectamine₂₀₀₀ were investigated. It was found that the 1:4 ratio produced the best results with approximately 40% efficiency for EGFP expression (Fig 5.10). For sensor 177 using a 1:4 ratio, it was observed that 4 μg generated the largest number of fluorescent cells at approximately 50% efficiency, but the fluorescence was still quite weak for 177 with 2 and 4 s exposure times necessary to obtain fluorescence (Fig 5.11). However, fluorescence was observed after expression for 72 hrs, which is better than the initial studies produced.

Optimization of CHO cells proceeded as stated for the HeLa cells. A ratio of 1:3 with 3 μg of DNA produces a high efficiency (>80%) with fluorescent cells (Fig 5.12). However, one factor was discovered for CHO cells that changed the protocol for working with these cells. Transfection studies were normally performed on plastic dishes with images taken through a long working distance, plastic corrected objective. After the best conditions were established, dishes were prepared for calcium response studies. It was found that CHO cells, unlike HeLa, do not adhere to glass cover slips. The cells would initially adhere, but would separate from the coverslip after 24-48 hrs

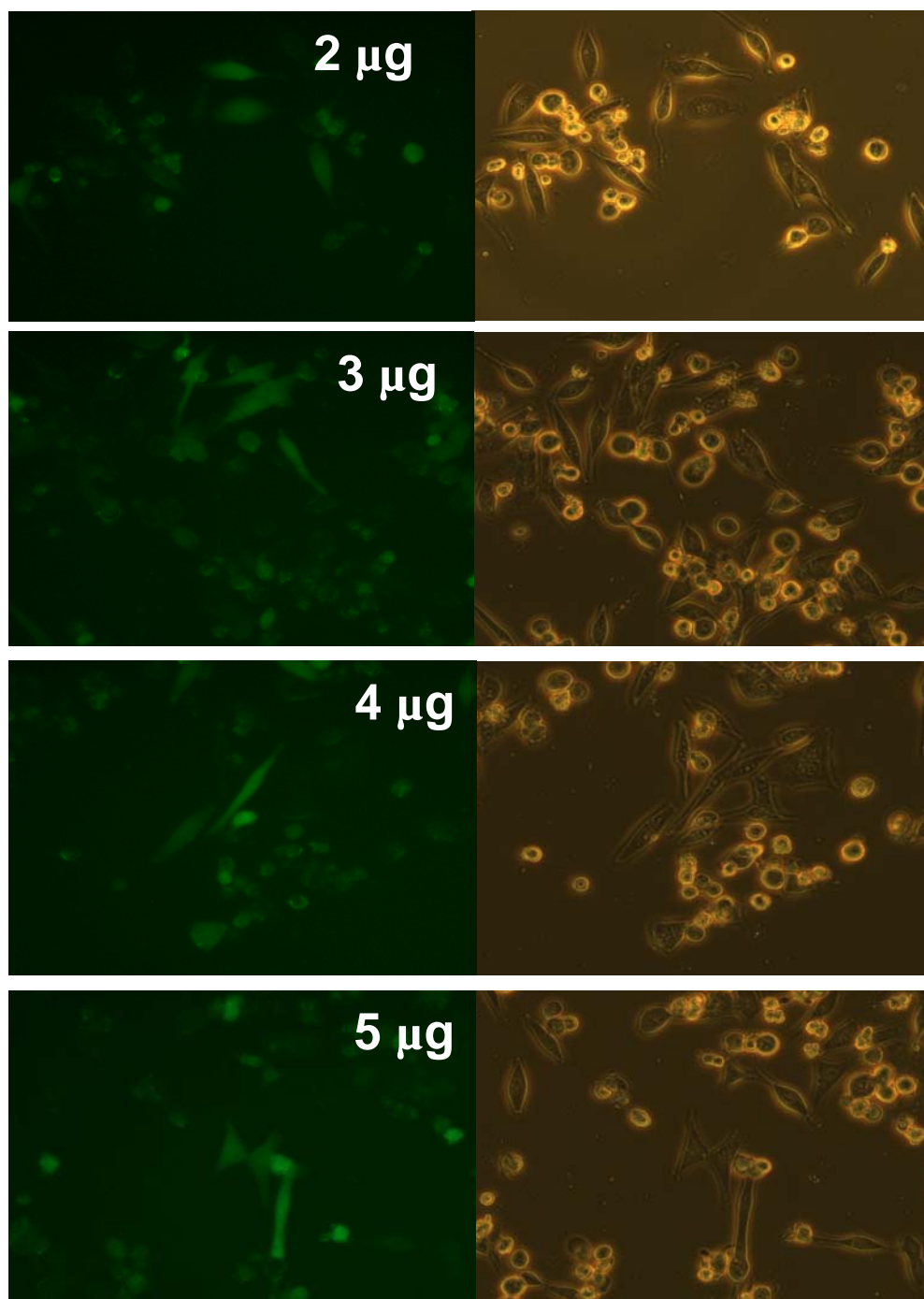


Fig 5.9 Site 177 with different amounts of DNA transfected into HeLa cells in a 1:3 DNA:lipofectamine2000 ratio 72 hrs after transfection at 20x magnification with 2 s exposure.

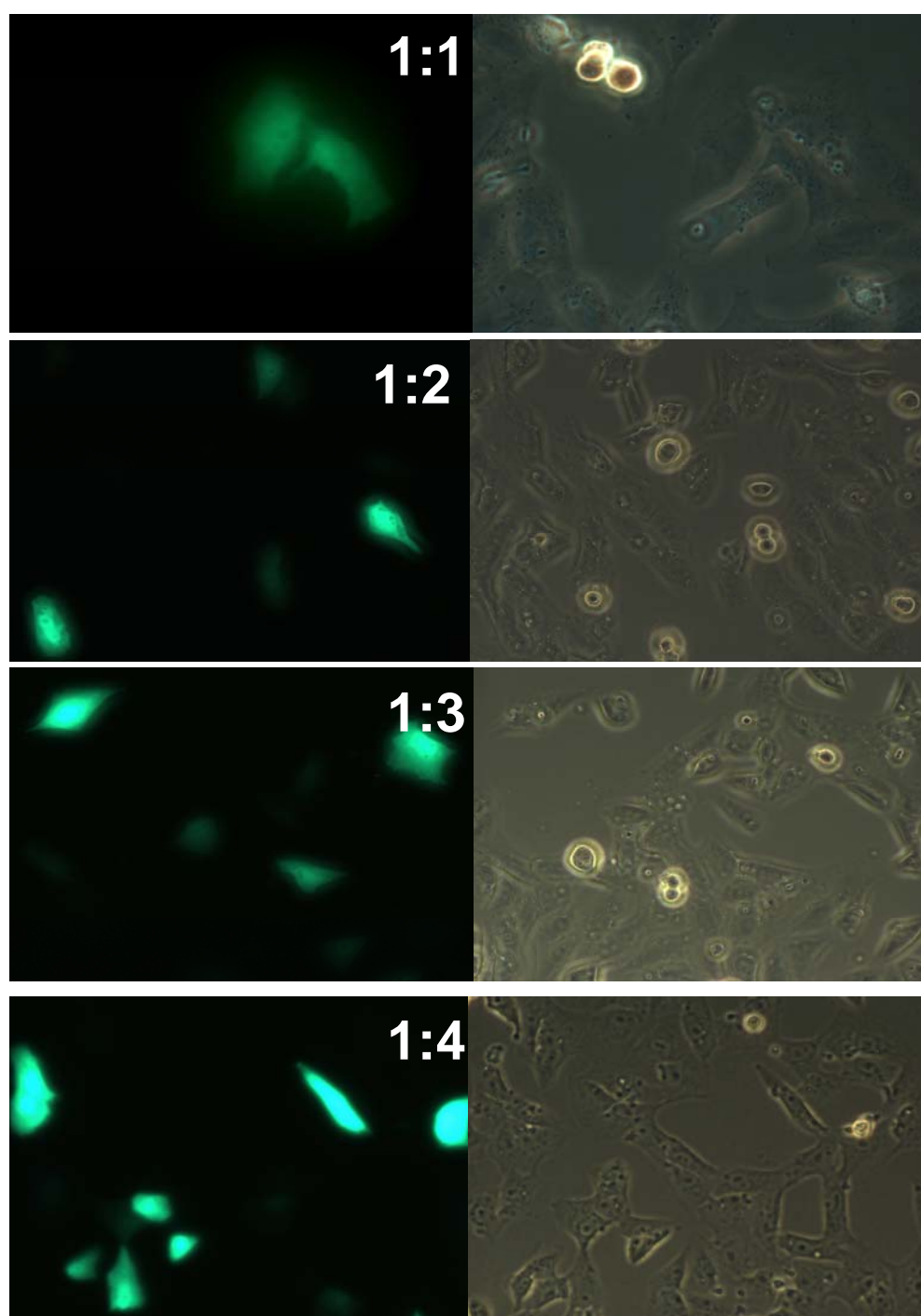


Fig 5.10 Images of EGFP transfected into Vero cells at different DNA:liposome ratios with 1 μ g of DNA 48 hrs after transfection at 20x magnification with 1 s exposure.

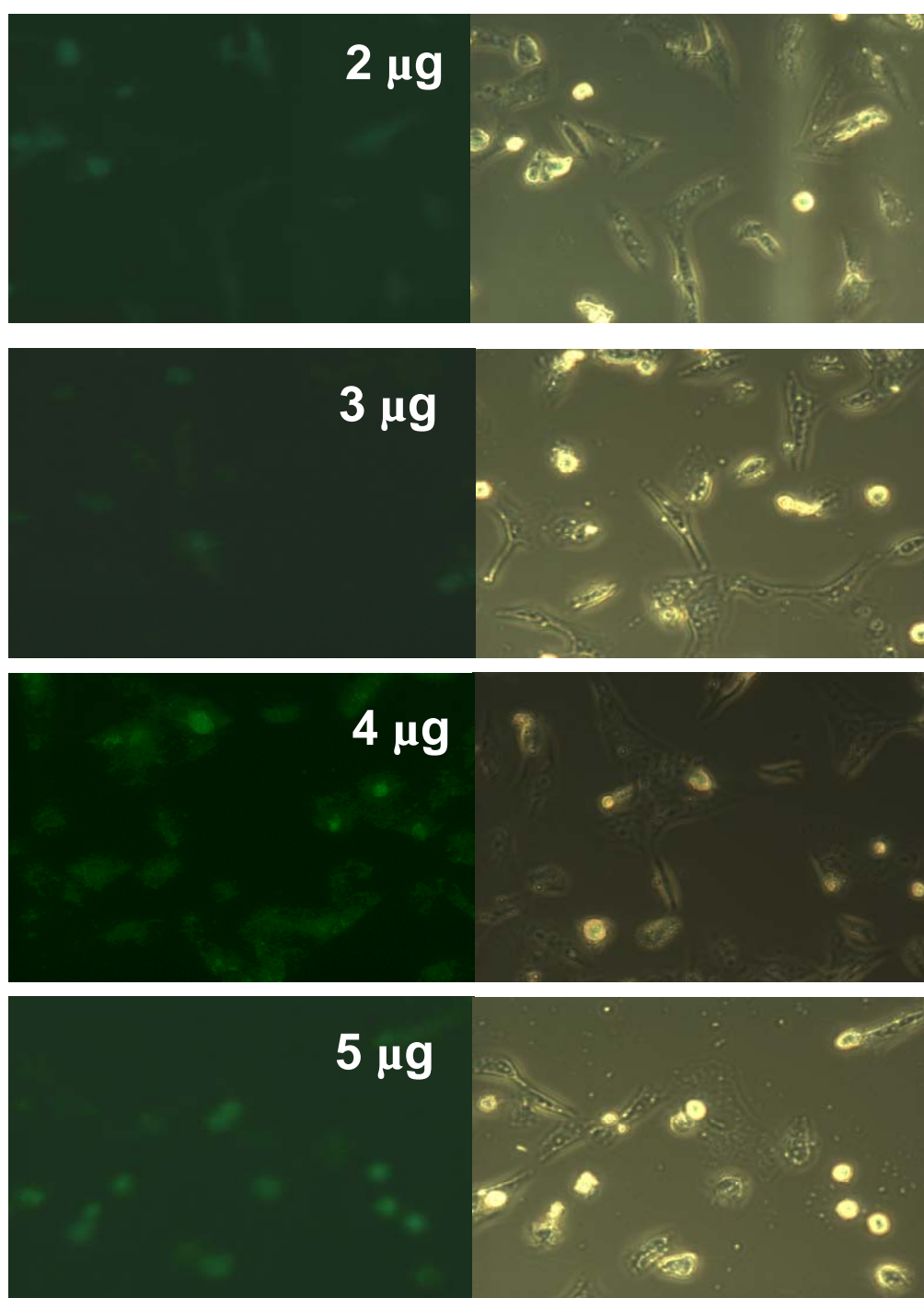


Fig 5.11 Images of Site 177 expressed in Vero cells at different DNA concentrations in a 1:4 DNA:liposome ratio 72 hrs after transfection at 20x magnification with 2 s exposure.

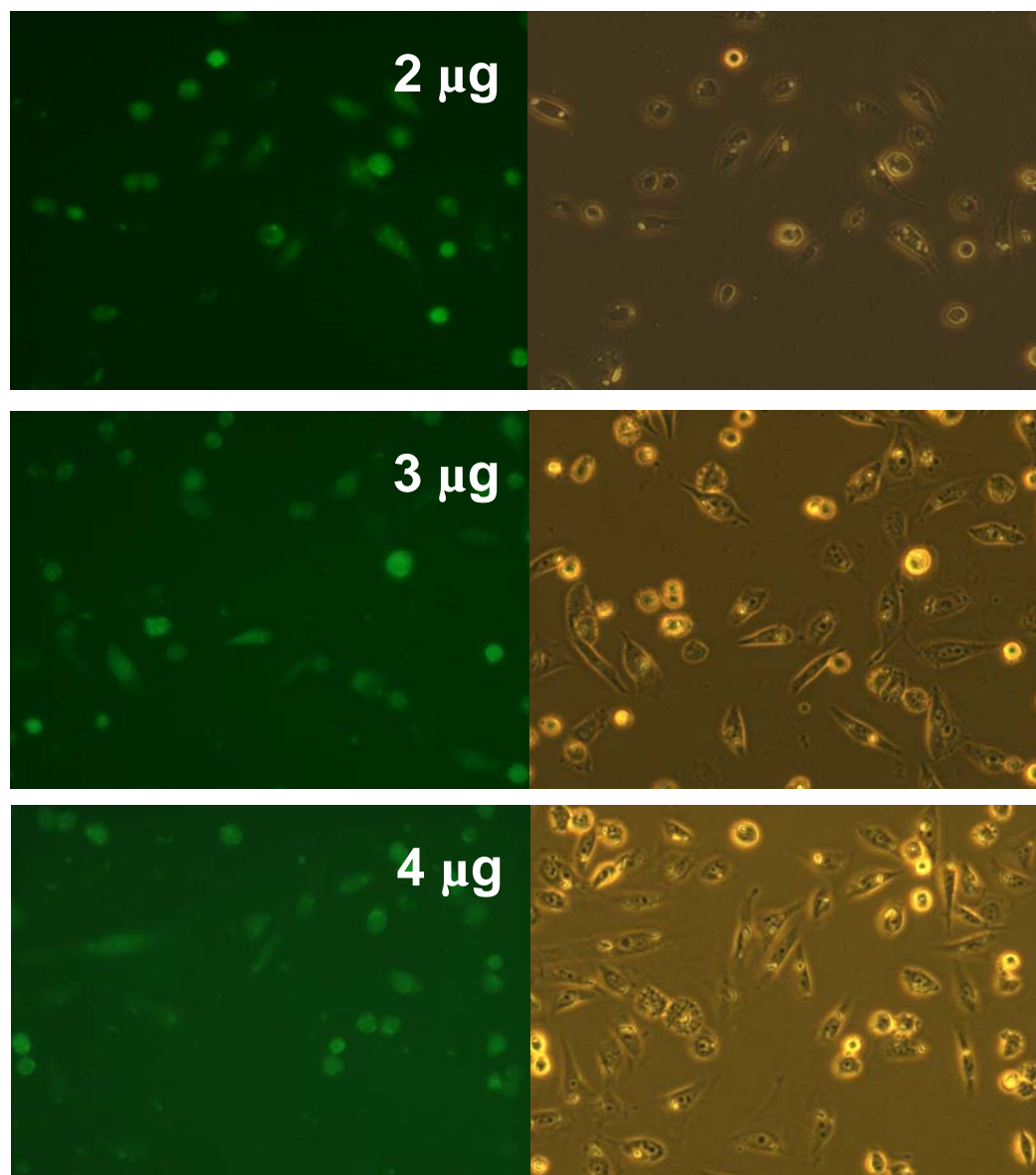


Fig 5.12 Images of Site 177 expressed in CHO cells at different DNA concentrations with a 1:3 DNA:liposome ratio 72 hrs after transfection at 20x magnification with 2 s exposure.

and within 16 hrs after transfection. Coating the glass coverslips with fibronectin and collagen eliminated this problem by giving the cells attachment points. Fortunately, fibronectin and collagen do not interfere with fluorescence studies of our sensors so coated cover slips were employed in further experiments by growth of the cells on coated plates.

For HeLa, CHO, and Vero cells, Lipofectamine₂₀₀₀ was utilized with great success. The transfection efficiency of this liposome is >70%, which is quite a bit higher than most other transfection means. However, when Lipofectamine₂₀₀₀ was utilized to transfect Hek293 cells, the cells repeatedly died 24-48 hrs after transfection. The cells round up, lifted from the plate, and could not be resuspended. Although the liposomes manufacturer stated that the liposome could be used with Hek293 cells, a search of the literature revealed that no one had published transfection of Hek293 cells with Lipofectamine₂₀₀₀. In general, Lipofectin was utilized. Transfection of Hek293 cells with Lipofectin yielded live, healthy cells, but the transfection efficiency is much lower than the harsher Lipofectamine₂₀₀₀. A ratio of 1:4 was necessary for transfection with 2 to 3 μ g of DNA, but the efficiency was ~30%, much less than Lipofectamine₂₀₀₀.

5.3 Engineering a Brighter Sensor: incorporation of the cycle 3 mutations

5.3.1 Rationale for further modifying the designed proteins

Extensive work has been reported in the literature to try to increase the expression temperature of GFP with some success. Cycle 3 GFP with the mutations F99S, M153T, and V163A has been observed to increase the folding of the protein at

37 °C, allowing for the chromophore to demonstrate fluorescence when expressed at 37 °C (139, 140). In addition, these mutations increase the fluorescence efficiency when the protein is expressed at 30 °C. Cycle 3 GFP is estimated to be 30,000 times more fluorescent than wild type GFP. A computational study by Zimmer et. al. indicated that the three mutations in cycle 3, F99S, M153T, and V163A play a role in the maturation of the chromophore (141). They propose that these mutations decrease the distance between the Gly67 amide nitrogen and the Ser65 carbonyl carbon of the immature protein when compared to GFP-S65T, which allows for more efficient nucleophilic attack by the amide nitrogen of Gly67. Since there are multiple steps involved in the folding of the protein, it is likely that these mutations allow for better arrangement of the sidechains, which decreases the distance for the reaction. It is doubtful that the increased thermostability of chromophore formation is only due to the distance decrease, but likely involves many steps that lead to the decreased distance. Although there have been copious efforts in fully understanding the chromophore formation and the factors that affect the formation, no conclusive results have yet been obtained. However, there is consensus that the cycle 3 mutations aid in the formation of the chromophore, increasing the brightness and thermostability. In light of this, the cycle 3 mutations were added to Sites 177, 120, and 194a to increase the brightness at 30 °C and to try to obtain fluorescence when expressed at 37 °C (Fig 5.13).

5.3.2 Incorporation of mutations F99S, M153T, and V163A

F99S was first engineered into the variants, and then M153T and V163A were engineered together. The forward primer for the F99S mutation was

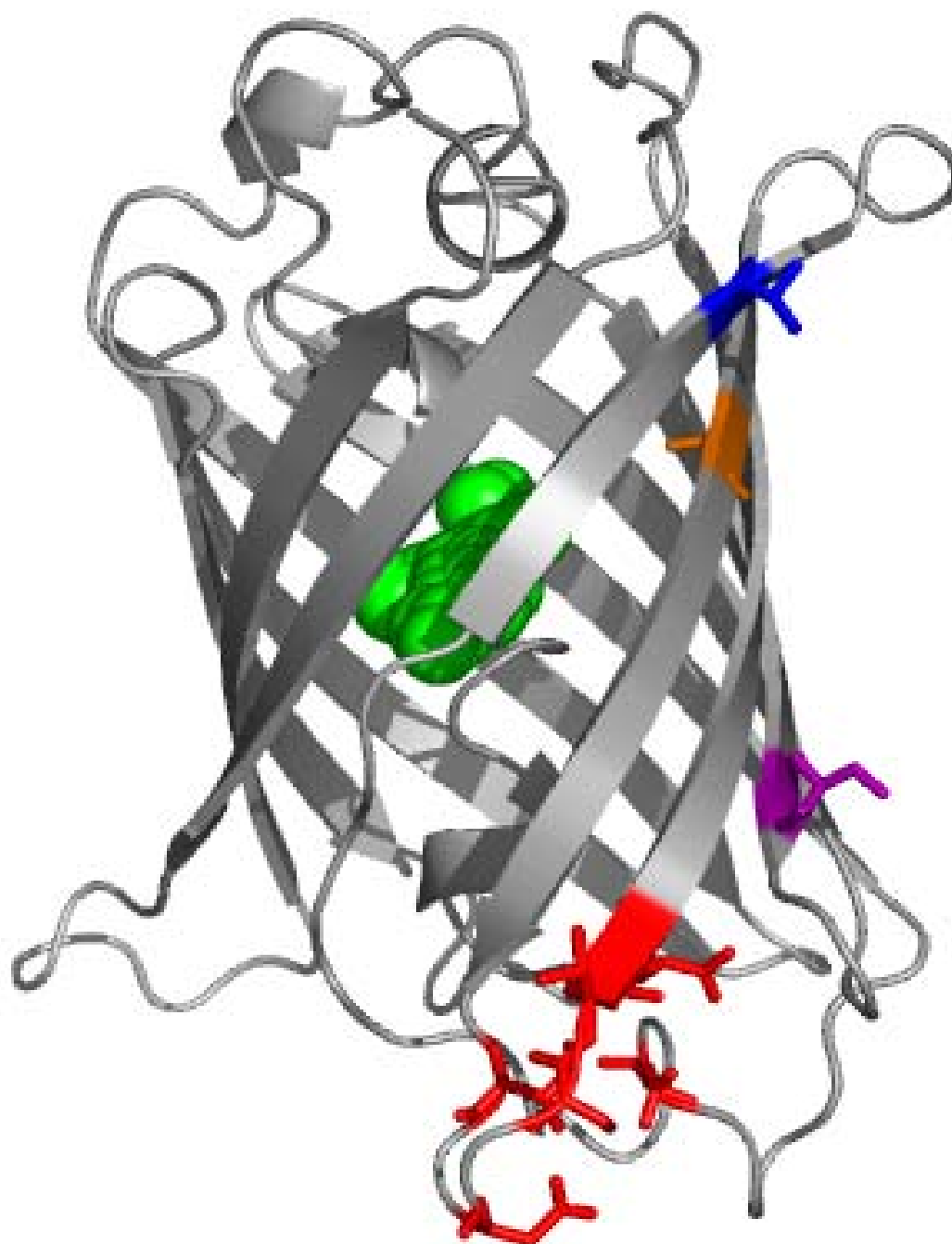


Fig 5.13 EGFP with Site 177 ligands in red and the cycle 3 mutations (F99S, M153T, V163A) in various colors to illustrate the location of these mutations in comparison to the chromophore and the designed site.

5'-CGCACCATCT**TC**CTTCAAGGACG-3', and the reverse primer was 5'- CTCCTGGACGTAGCCTTCCC-3'. The F99S mutation was obtained after several attempts at PCR. The reaction was optimized by utilizing only distilled water, not deionized water, and by adjusting the primer and DNA concentrations until the appropriate conditions were discovered for the reaction to generate product with the correct mutation. The forward primer for the M153T/V163A mutations was 5'-GAACGGCATCAAG**GCG**AACTTCAA-3', and the reverse primer was 5'-TTCTGCTTGTCGG**CGT**GATATAGA-3'. The M153T mutation is incorporated into the reverse primer, and the V163A mutation is incorporated into the forward primer. In this way, both of the mutations could be engineered with one PCR. The initial reaction for M153T and V163A yielded DNA with a single base deletion at the junction of the two primers for the 153 and 163 mutations. The PCR was repeated on the DNA that contained the correct 153 and 163 mutations to reinsert the deleted base, which was successful.

5.3.3 Mammalian cell expression and tests of cycle 3 designed proteins

Sites 120 and 194a with the cycle 3 mutations, termed 120c3 and 194-c3, were transfected into HeLa cells. Neither of these variants exhibited fluorescence 72 hrs after transfection. Much of the work in the literature suggests that expression of GFP variants for longer periods of time, up to 10 days in some reports (50), allows for eventual chromophore formation. Sites 120c3 and 194a-c3 were expressed in CHO cells for 7 days, but no fluorescence was observed (Fig 5.14). Apparently, the incorporation of the mutations for these designed sites disrupts the protein packing

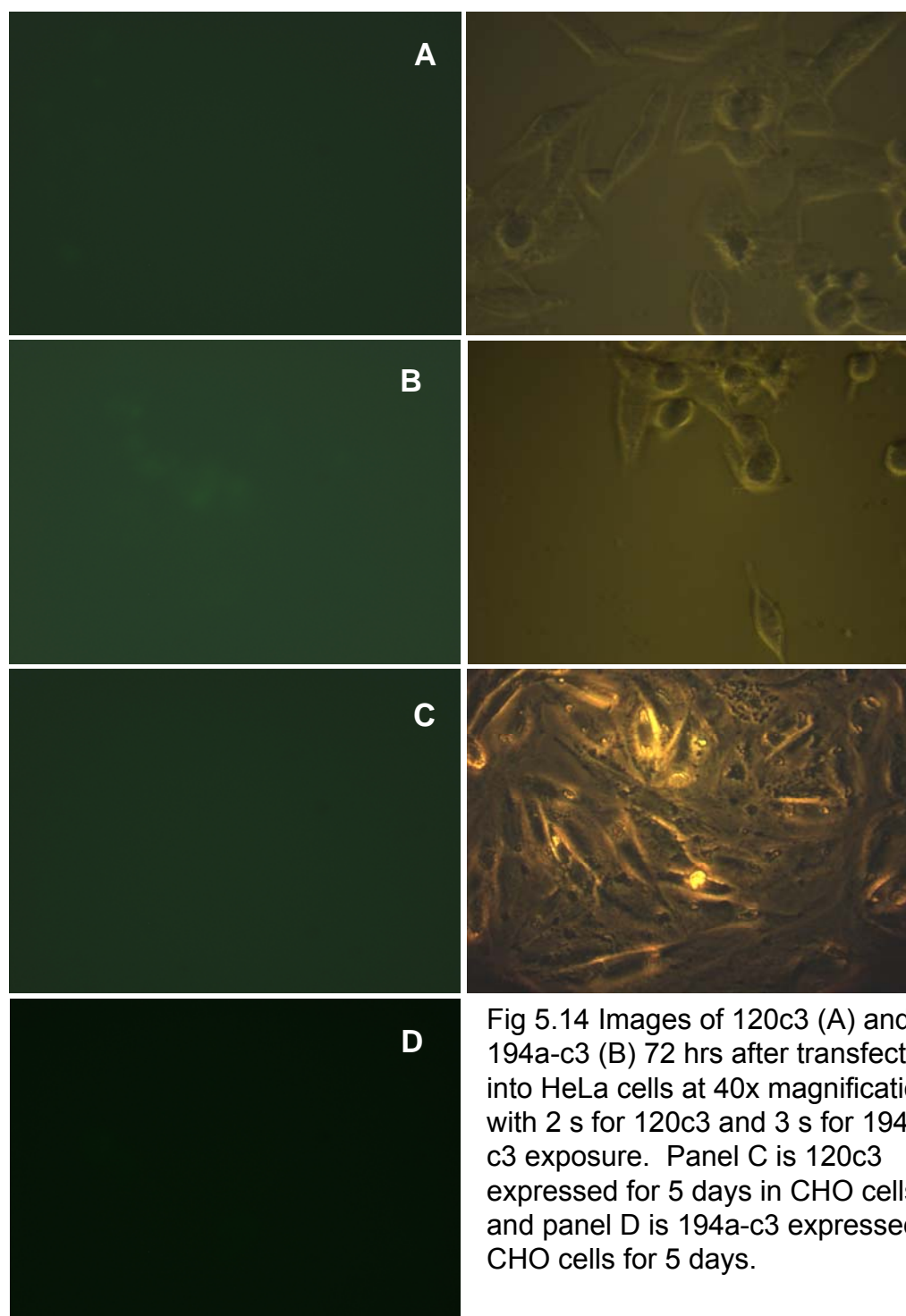


Fig 5.14 Images of 120c3 (A) and 194a-c3 (B) 72 hrs after transfection into HeLa cells at 40x magnification with 2 s for 120c3 and 3 s for 194a-c3 exposure. Panel C is 120c3 expressed for 5 days in CHO cells and panel D is 194a-c3 expressed in CHO cells for 5 days.

enough so that the chromophore does not form, even with the aid of the cycle 3 mutations. Since Site 120 is located in the middle of the β -barrel, the introduction of the two negative charges, especially at location 120 feasibly disrupts the β -strands so the residues involved in forming the chromophore can not come into close enough contact to begin the formation reaction. This result is more surprising for 194a since this site is located at the end of the barrel, relatively far away from the chromophore. One possibility is that the mutations, especially at K79 and/or K85, disrupts the H-bond network inside the barrel of the protein. With the mutations from positive to negative charges, perhaps there is electrostatic repulsion and a disruption in H-bonds so that the two together do not allow the protein to form the chromophore even with the cycle 3 mutations.

5.3.4 Optimization of time and temperature for expression

The expression time and temperature are largely protein dependent, although the cell line does play a role, so these two factors were initially tested in HeLa and CHO cells for Site 177 and 177c3. After transfection, the cells were incubated for 48 and 72 hrs, and images were taken at these times. After 48 hrs, Site 177 exhibited very weak fluorescence that required very long exposure times to capture (>2 s). After 72 hrs, Site 177 exhibited fluorescence that was easily captured by the camera without extensive exposure times (<2 s) (Figs 5.15 and 5.16).

Site 177c3 was expressed after transfection into HeLa cells with Site 177 as a comparison control. The cells were examined after 48 and 72 hrs of growth at 30 °C (Fig 5.17) with the DAPI, FITC, and TexasRed filter sets. Site 177c3 is approximately

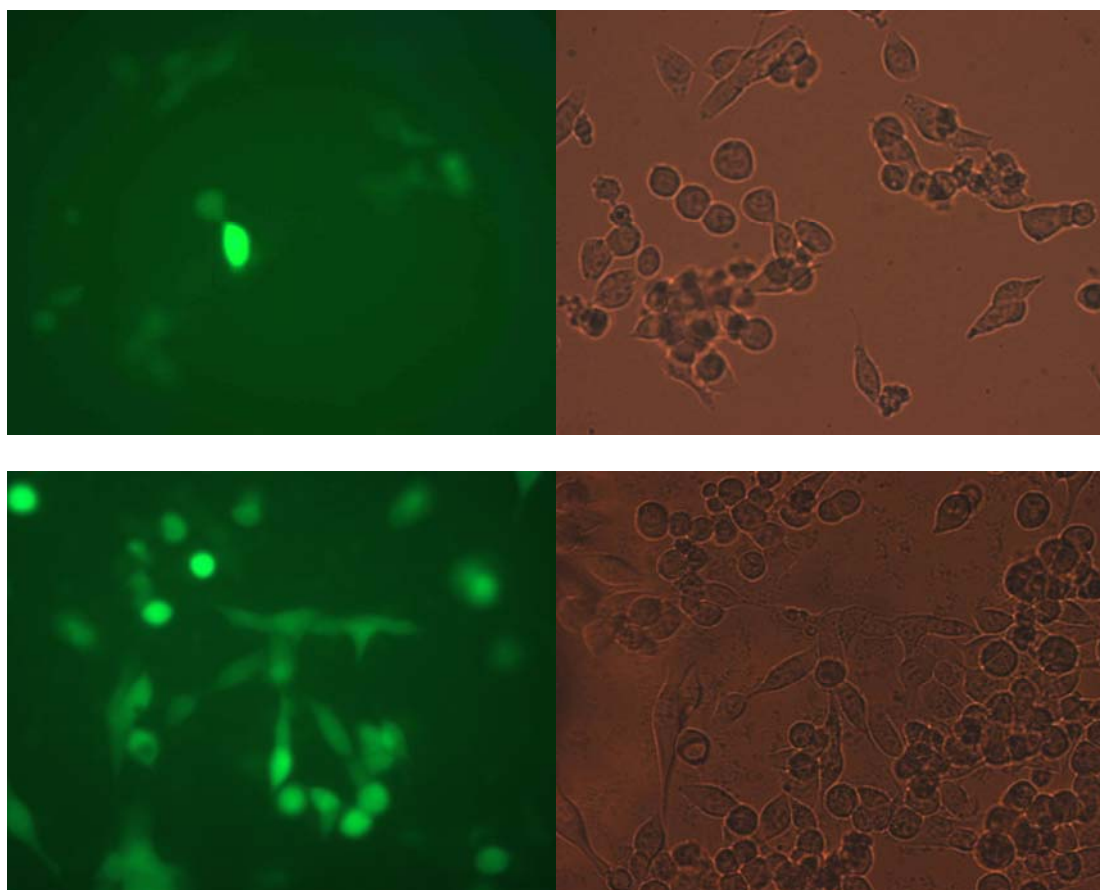


Fig 5.15 Images of site 177 in HeLa cells 48 hrs (top) and 72 hrs (bottom) after transfection at 40x magnification with 2 s exposure. Transmitted images are on the right.

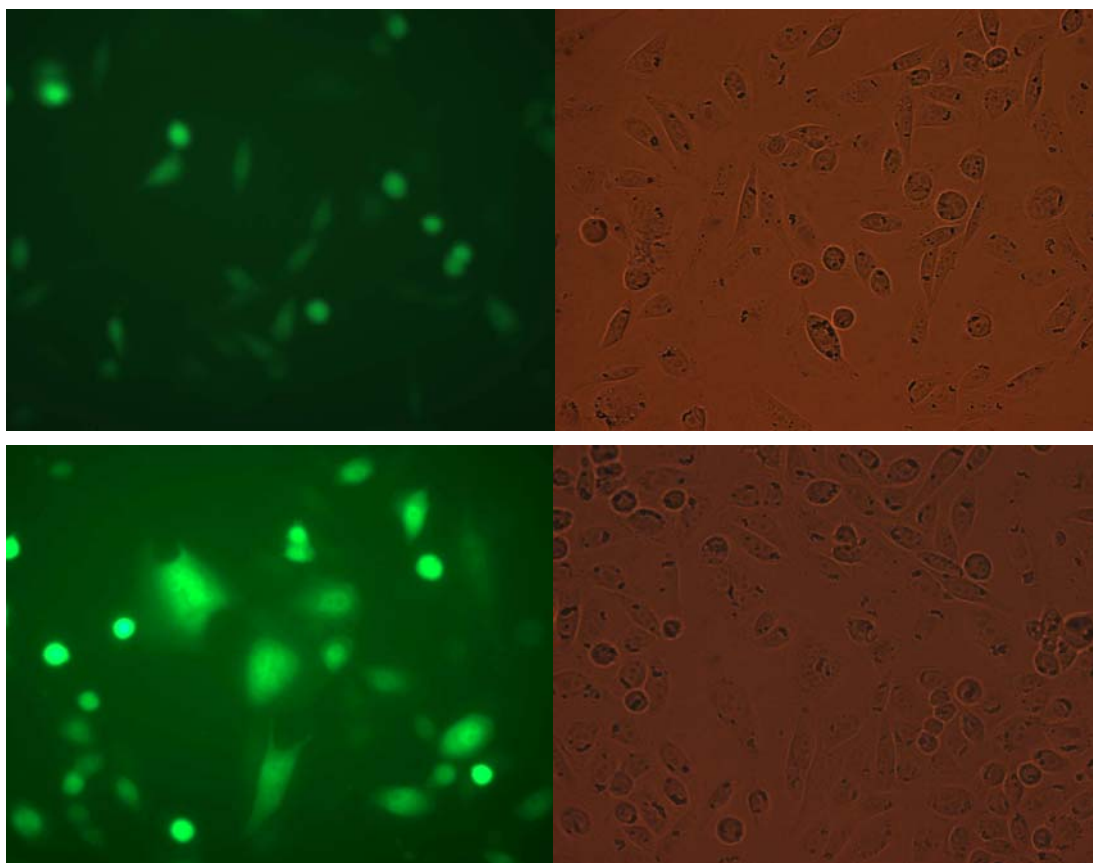


Fig 5.16 Images of Site 177 in CHO cells 48 hrs (top) and 72 hrs (bottom) after transfection with the transmitted light images on the right. The images were taken with 2 s exposure at 40x magnification.

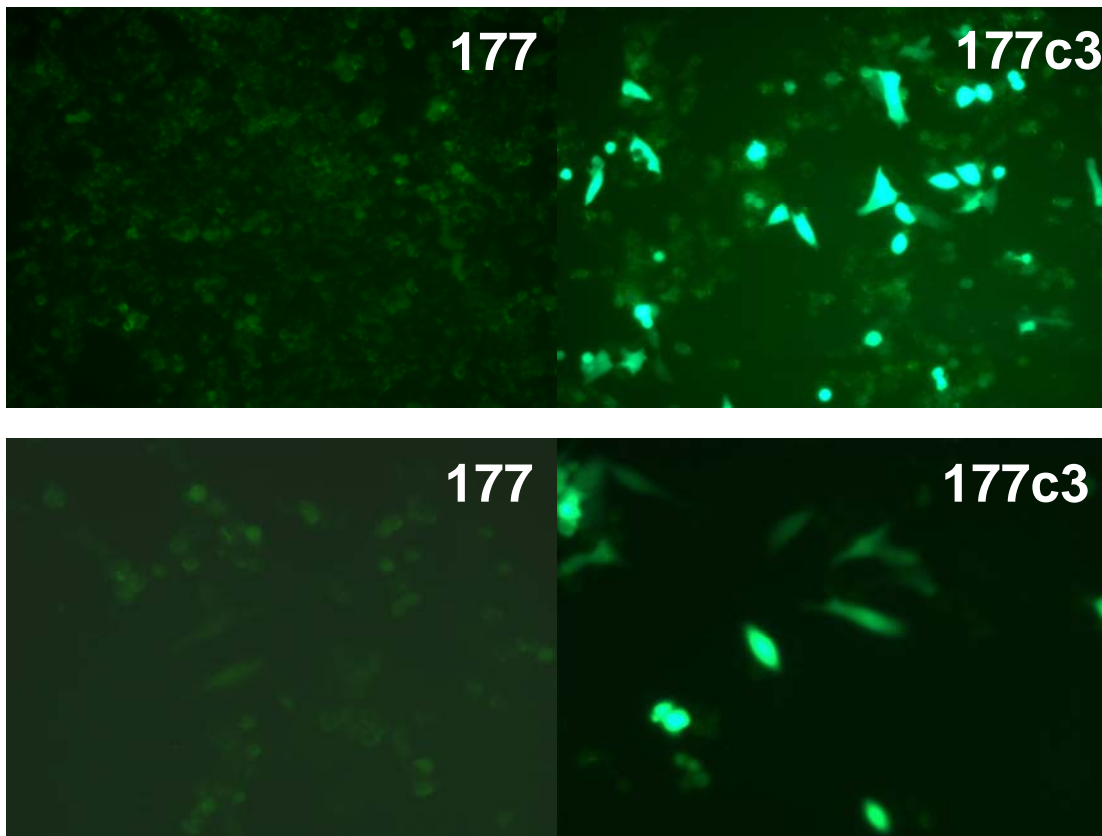


Fig 5.17 Expression of 177 and 177c3 in HeLa cells 48 hrs (top) and 72 hrs (bottom) after transfection with expression at 30 °C. Images were taken at 20x magnification with 2 s exposure.

ten times brighter than 177 when expressed at 30 °C as observed with the FITC filter set and the 40x oil objective. To test the temperature, the proteins 177 and 177c3 were expressed for 72 hrs at 30 °C and 37 °C. No fluorescence with the three filter sets (DAPI, FITC, TexasRed) was observed for the expression of 177 at 37 °C, but fluorescence was observed for expression at 30 °C. As shown in figure 5.18, when expressed at 37 °C, weak fluorescence is observed for 177c3 with the FITC filter set although none is observed for 177. It is likely that the introduction of the binding site with three negative charges negates a small part of the cycle 3 amino acids' effect on the chromophore formation so there is only a weak fluorescence at 37 °C. However, with a robust imaging system, 177c3 could be expressed at 37 °C and imaged. A strong light source coupled with little light loss from optimized arrangement of the equipment, such as a camera in direct line with the objective, could allow for imaging of 177c3 with expression at 37 °C. This work also suggests that it is possible to incorporate other “stable mutants” to increase the optical properties of GFP variants at 37 °C.

The wild type GFP has been reported to need many days to “mature” and become fluorescent. Also, EGFP does not exhibit fluorescence at 37 °C. GFP was isolated from cold water jellyfish so its gene was adapted for the temperatures experienced by the jellyfish. Since the designed protein obviously disrupts the fold to some extent—as observed by the expression in bacteria—it is not surprising that several days are needed for the designed protein to exhibit fluorescence. In addition, HeLa cells require about 16 hrs after transfection to begin to produce protein.

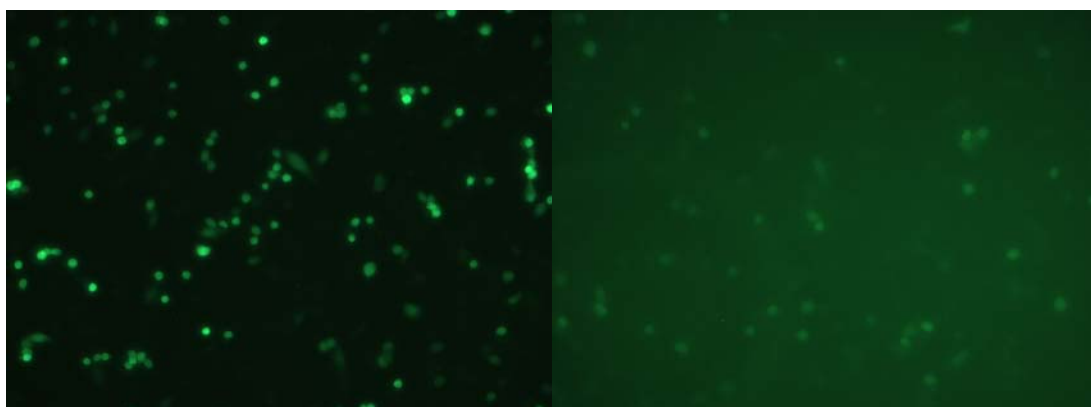


Fig 5.18 Images of 177c3 expressed in HeLa cells 72 hrs after transfection at 30 °C (left) and 37 °C (right). Images were taken at 10x magnification with 2 s exposure.

Expression of the protein for longer than 72 hrs was tested, but HeLa cells do not grow well without passaging for longer than 72 hrs. The cells begin to pile up and form plaques, eventually rounding up and detaching from the plate. It is possible that the protein would be more fluorescent with longer expression time as many articles have reported expression of their particular variant for up to 10 days, but comparisons among cell lines should include expression for the same amount of time.

Although the sensors are most fluorescent with expression at 30 °C, the temperature sensitivity of the chromophore formation is not detrimental to further testing in animal models since there are organisms that live at 30 °C, such as *C. elegans* and zebrafish. The expression at lower than physiological temperatures is consistent with other reported GFP sensors, such as the pericam and cameleon series (51). In addition, measuring the temporal and spatial changes of calcium in living cells is not hindered by growth at 30 °C. One of the eventual goals of this project is to understand the changes of calcium at the cellular level and to ascertain the differences in calcium changes for different cell types, such as between cancer and normal cells. These experiments can be performed at room temperature or at physiological temperature after expressing the protein at lower temperatures since EGFP does not lose its fluorescence at 37 °C once the chromophore is formed due to its relatively high melting temperature of 78 °C. Further improvements could be formulated by incorporating other mutations that have been reported to improve the chromophore formation or by carrying out random mutagenesis and selecting for brighter clones. The drawback to random mutagenesis would be loss of the calcium binding site that would need to be

reincorporated and tested for calcium response. In addition, folding chaperones could be coexpressed with the sensor to aid in the folding if the correct chaperones could be ascertained for GFP folding.

5.4 Calcium response of 177 and 177c3 in the cytosol

Once the expression conditions were optimized, the *in vivo* calcium response was tested for 177 and the brighter 177c3. There are many ways to test calcium response, as detailed in Chapter 1, but the easiest to perform and monitor is through the use of ionomycin. Ionomycin is a calcium ionophore that exchanges protons for calcium across the plasma membrane. This process can theoretically change the pH of the cytosol, which has been observed in BHK fibroblasts. However, studies by Dr. Louis and Dr. Lurtz of UC Riverside (private communication) using pH indicators demonstrated that the pH of HeLa cells does not change upon introduction of ionomycin and calcium. Ionomycin is easier to monitor calcium induced changes because increasing the outside calcium in the bathing medium can further increase the calcium in the cytosol. Although, the calcium pumps are continuously working to remove the calcium from the cytosol in order to keep the cell healthy so high concentrations of calcium do not remain in the cell, a quick increase in the outside calcium allows for the cytosolic calcium concentration to be artificially raised enough to monitor calcium response of new sensors (142, 143). The use of physiological responses, such as binding of an agonist (ATP or histamine) and causing IP3 production does not raise the calcium concentration as high as can be accomplished with ionomycin. Therefore, if the

designed sensor does not respond to small calcium changes, the IP3 pathway would not be useful.

Sites 177 and 177c3 were tested for calcium response initially in HeLa cells. Our collaborators, Dr. Monica Lurtz and Dr. Charles Louis, first tested 177 on a Nikon inverted epifluorescence microscope with standard FITC filters with excitation centered at 490 nm and emission at 520 nm as detailed in Chapter 2, section 2.21. The initial results were promising with increases in fluorescence observed for the designed sensors that were not observed for the wild type protein, EGFP (Fig 5.19), when the outside calcium was increased after ionomycin addition. As shown in figure 5.20, the addition of 2 μ M ionomycin does not alter the baseline fluorescence of the cells but fluorescence increases are observed by addition of 20 mM calcium, which continue until the addition of 60 mM calcium. The calcium pumps removing calcium from the cell are highly efficient and do not allow the cytosolic calcium to become very large so large calcium concentrations are need in the bathing medium to overwhelm the calcium pumps. Removal of the extracellular calcium by buffer exchange indicates a reduction in the fluorescence, suggesting that the process is reversible. Further addition of ionomycin and calcium again indicates a fluorescence increase. Figure 5.21 indicates the averaged and normalized fluorescence changes observed for 177 as detailed in figure 5.20. The data was evaluated for statistical relevance by Kristy Welshhans in Dr. Vincent Rehder's laboratory as shown in figure 5.22. The t-test indicated that the data were statistically valid.

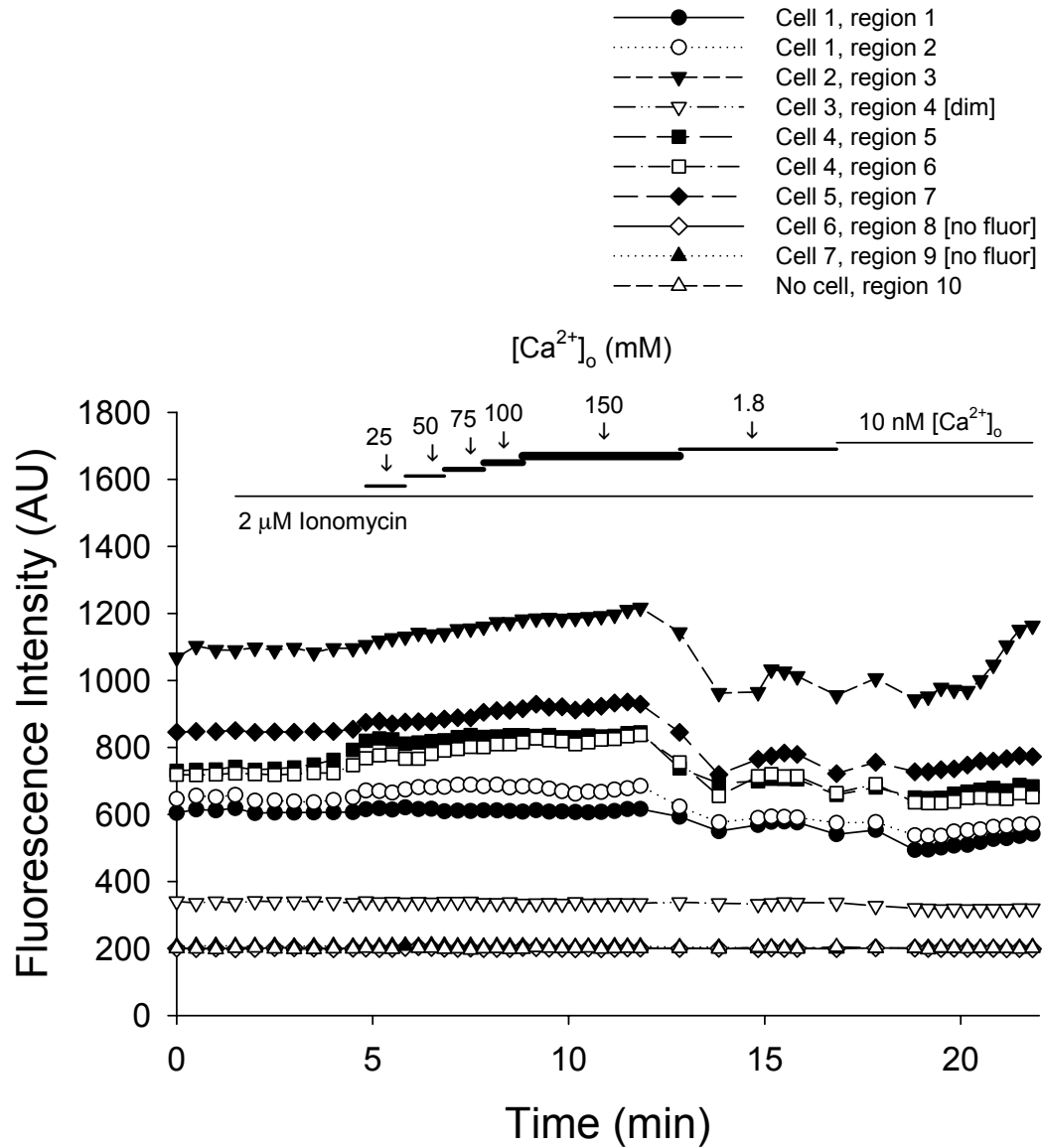


Fig 5.19 Imaging on the inverted Nikon microscope of EGFP expressed in HeLa cells at 30 °C. No calcium response is observed with addition of ionomycin and extracellular calcium for the wild type protein.

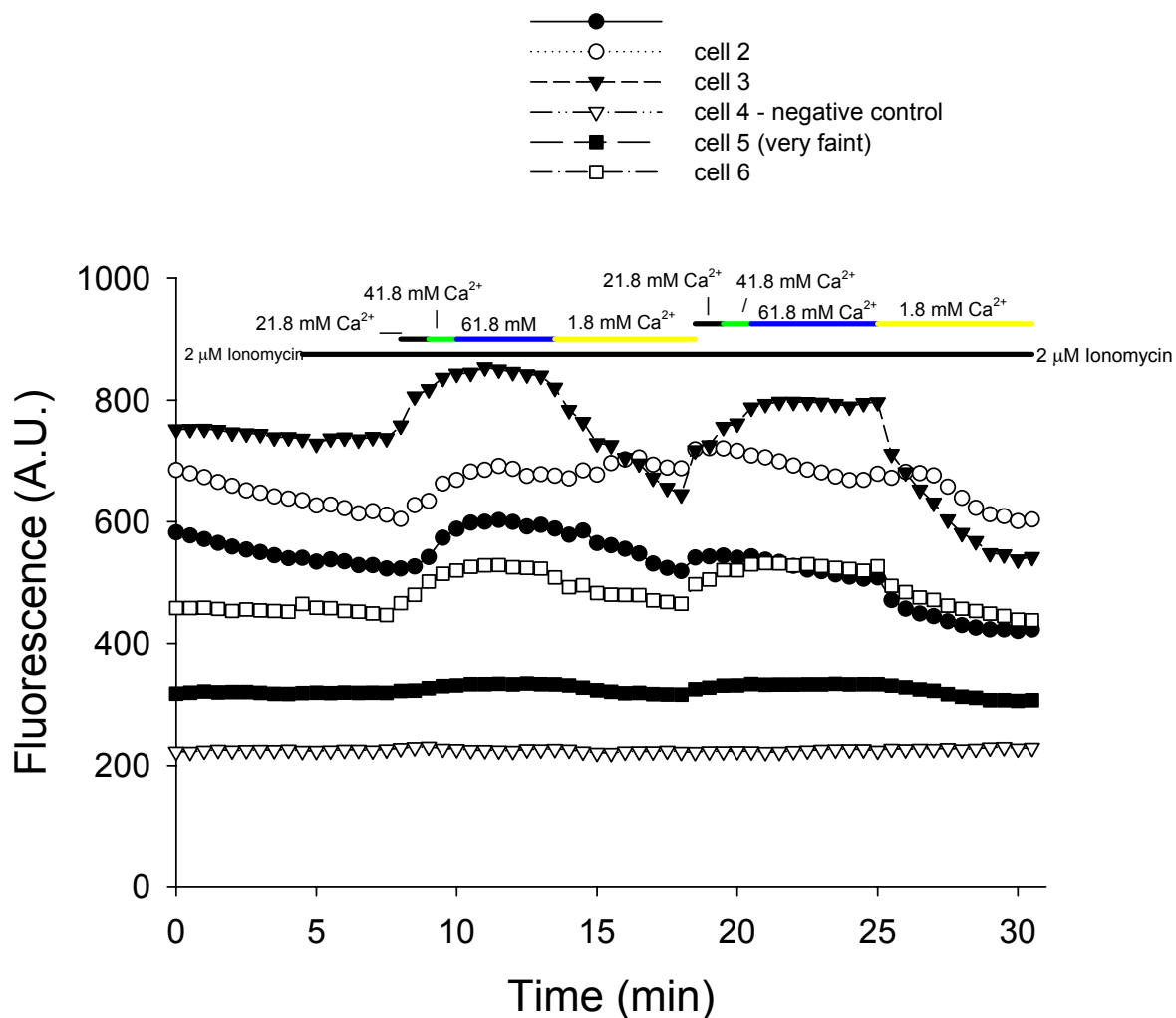


Fig 5.20 Calcium response of Sensor 177 expressed in the cytosol of HeLa cells as generated by addition of ionomycin and calcium to the bathing medium. The reduction in sensor fluorescence when the outside calcium is washed away indicates the reversible response of the sensor. This measurement was performed on an inverted Nikon microscope by Dr. Monica Lurtz.

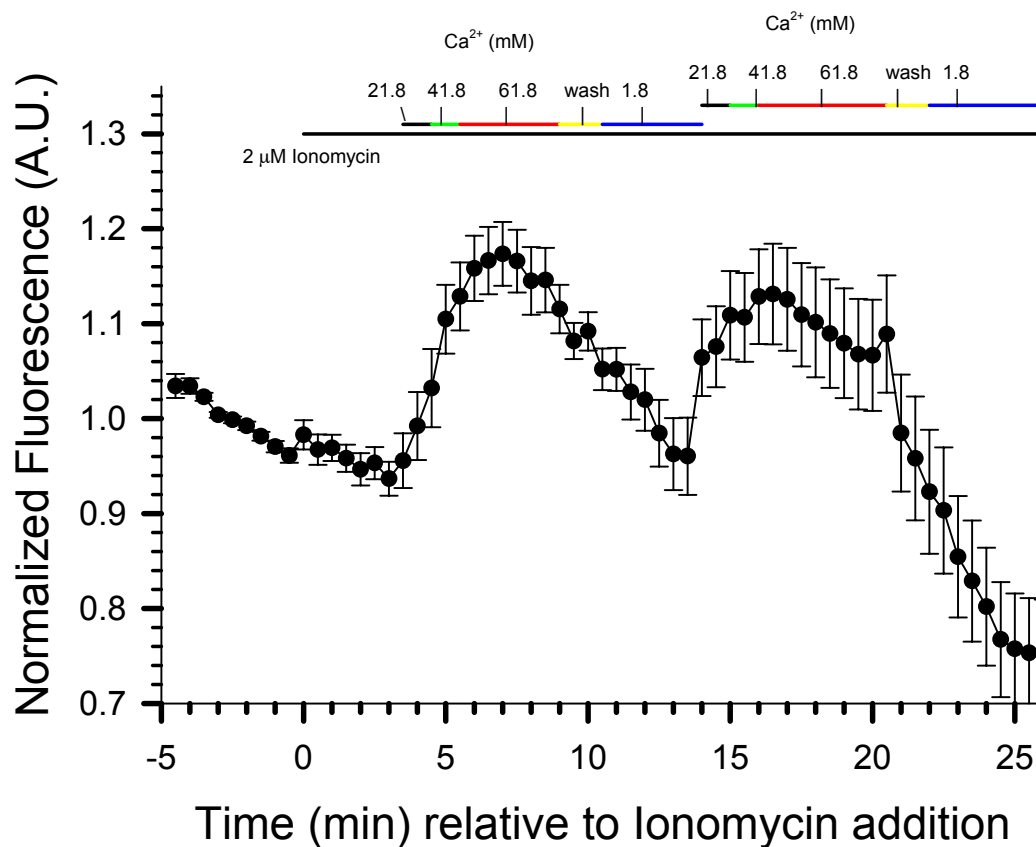


Fig 5.21 Averaged and normalized data for the previously shown calcium response of Sensor 177 expressed in the cytosol of HeLa cells as generated by addition of ionomycin and calcium to the bathing medium. Increases in the fluorescence are observed beginning with 20 mM outside calcium and continue with additional calcium up to 60 mM. This measurement was performed on an inverted Nikon microscope by Dr. Monica Lurtz.

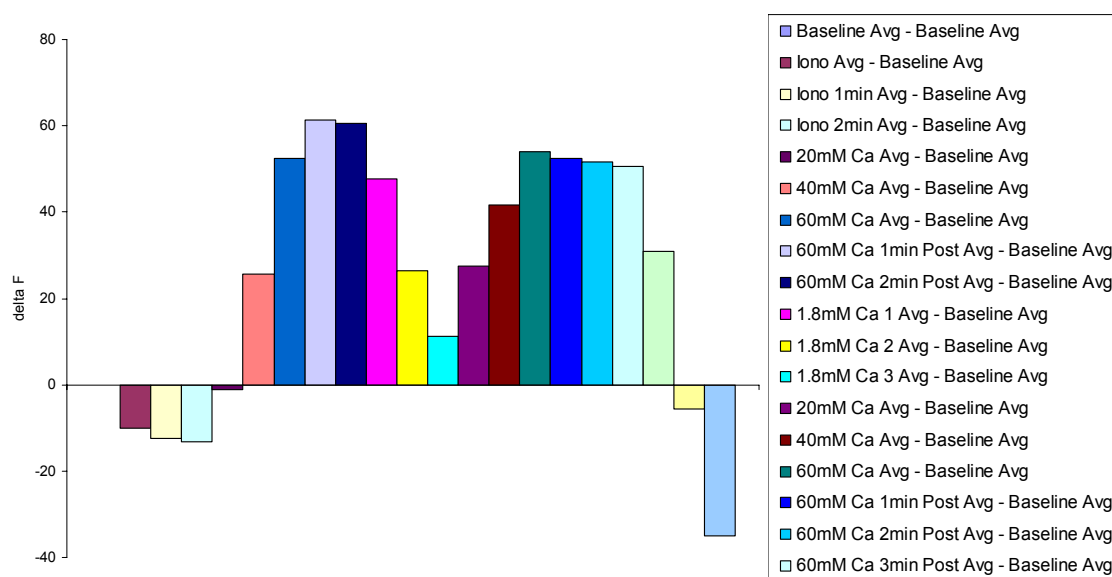


Fig 5.22 Statistical evaluation of the calcium response imaging of cytosolically expressed 177 in HeLa cells on the inverted Nikon microscope. The evaluation was performed with the student t-test by a collaborator, Kristy Welshhans. The results indicate that the calcium response observed for 177 is statistically valid.

Sensor 177 was also evaluated for physiologically response by addition of 50 μ M ATP to induce calcium release from the ER through the IP3 pathway, as shown in figure 5.23. The fluorescence response reaches a plateau that is not further changed by addition of more ATP, but a decrease is observed when the ATP is removed so that calcium is no longer being released from the ER into the cytosol. The increase in fluorescence observed for the cytosolically expressed sensor indicates that the calcium release from the ER can be monitored by this protein for physiological processes.

Another experiment was performed with sensor 177 expressed in the cytosol with addition of thapsigargin to block the calcium reuptake pumps in the ER allowing for a slow leak of calcium and calmidazolium to inhibit the calcium exchangers in the plasma membrane. This experiment should result in an increase in fluorescence for sensor 177 over time as calcium leaks from the ER and can not be taken back up. However, as shown in figure 5.24, the calcium released is not a large enough concentration to cause an increase in 177's fluorescence. Addition of ionomycin and calcium at the end of the experiments indicates that the sensor is functioning and responding to calcium.

Calcium response of sensor 177 was also tested on the Zeiss Axiovert 200 at GSU. As shown in figure 5.25, EGFP expressed in HeLa cells does not indicate a fluorescence response to calcium. However, as shown in figure 5.26, sensor 177 indicates a fluorescence increase with addition of ionomycin and calcium. Fluorescence response is observed with 20 mM extracellular calcium that continues up to 60 mM

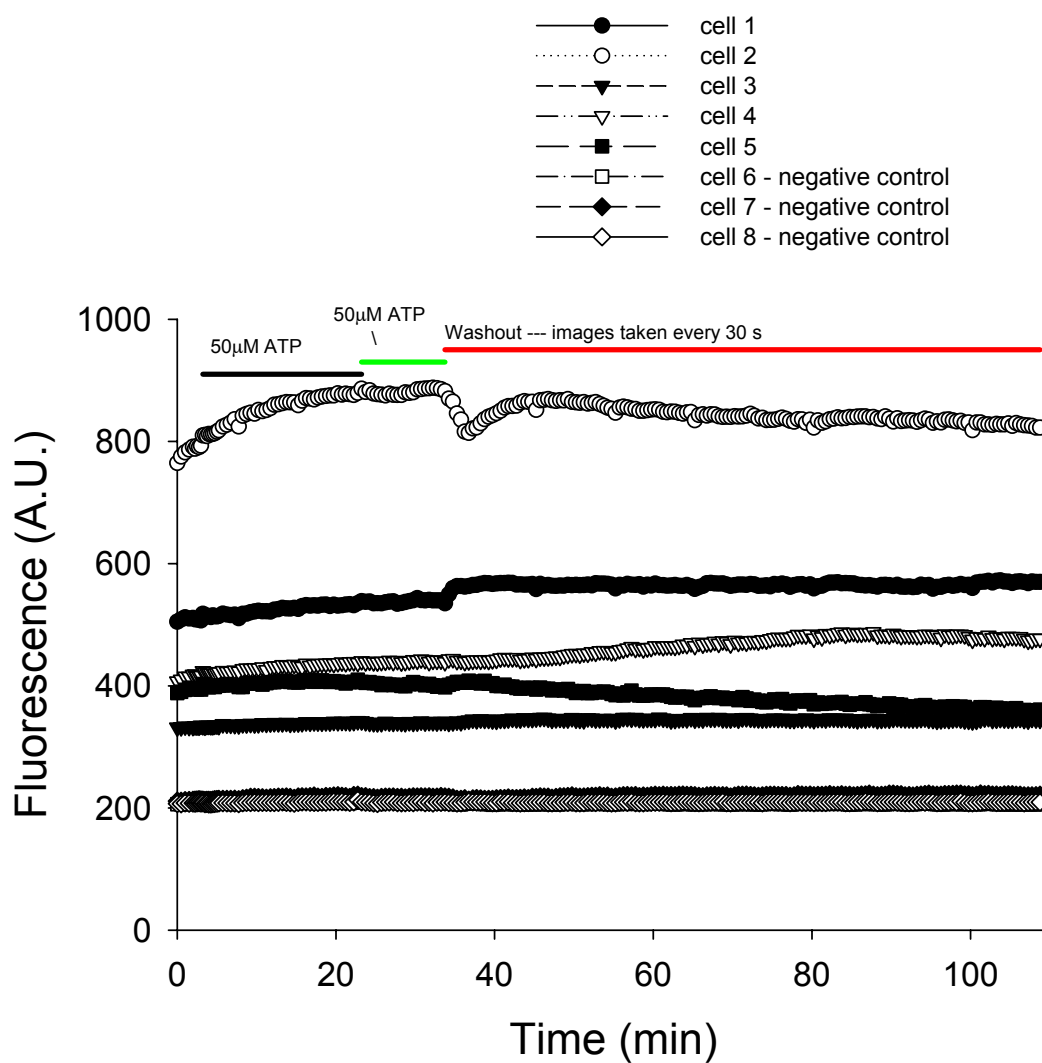


Fig 5.23 Imaging of cytosolically expressed 177 in HeLa cells. Addition of 50 μ M ATP induces calcium release from the ER by the IP3 pathway, which can be observed by the increase in fluorescence for 177 as it binds the calcium released into the cytosol.

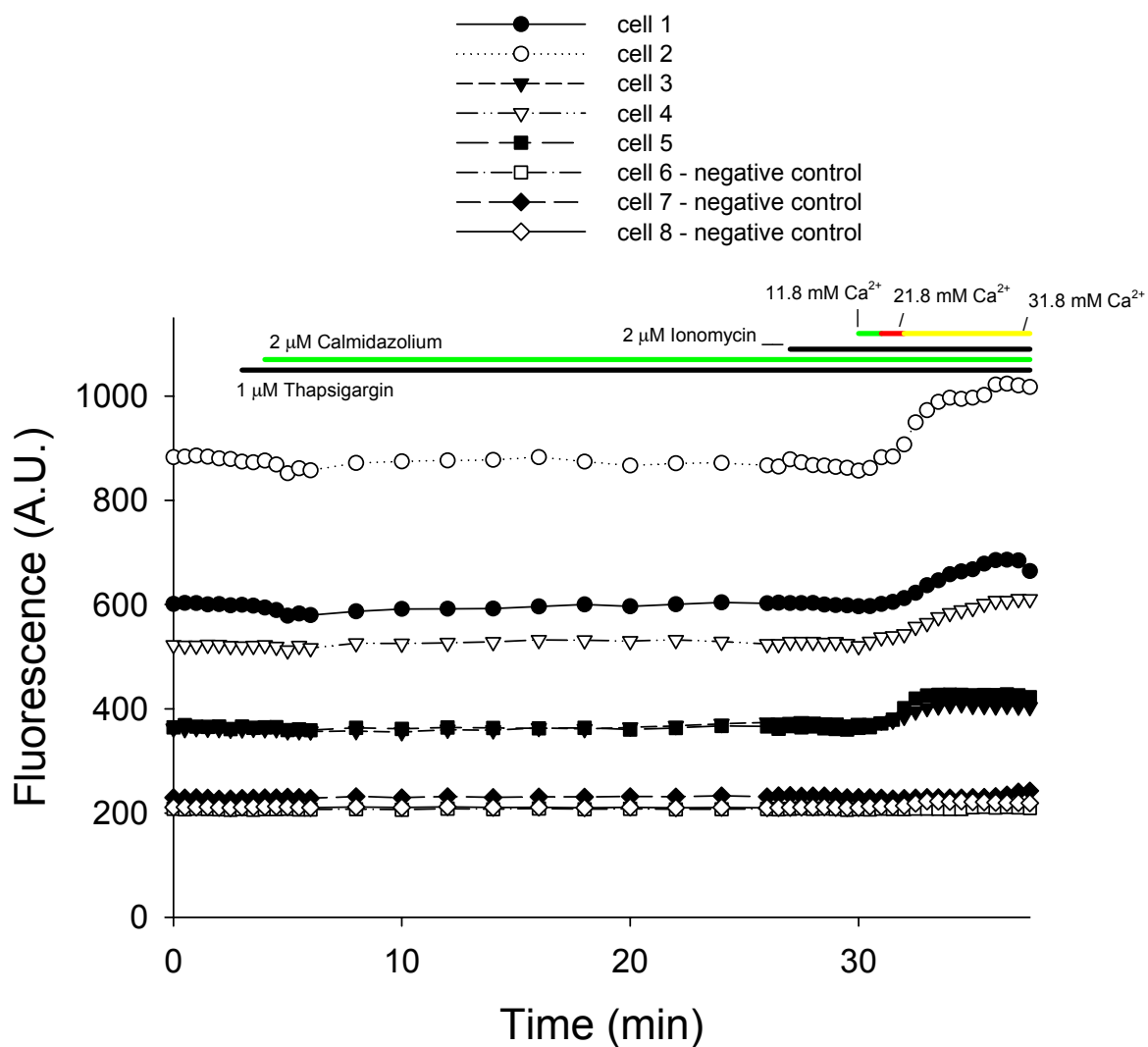


Fig 5.24 Imaging of cytosolically expressed 177 in HeLa cells on the inverted Nikon microscope. Addition of thapsigargin empties ER calcium while calmidazolium blocks the reuptake calcium pumps in the ER. This process should allow for a fluorescence increase of 177 to be monitored, but the calcium released by this pathway is very low concentration and is likely out of the sensing range for 177.

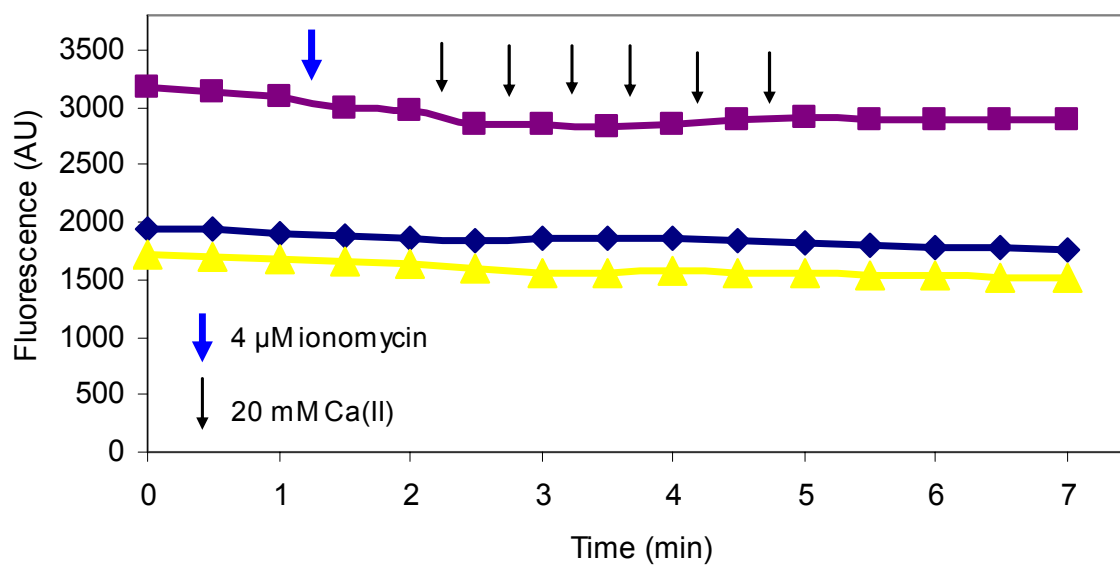


Fig 5.25 Traces of the imaging of cytosolically expressed EGFP in HeLa cells on the Zeiss Axiovert 200 microscope with the 40x dry objective, 100 ms exposure, and the FITC filter set. Addition of ionomycin and calcium does not indicate a fluorescence change for the wild type protein, as it should not since the protein does not bind calcium.

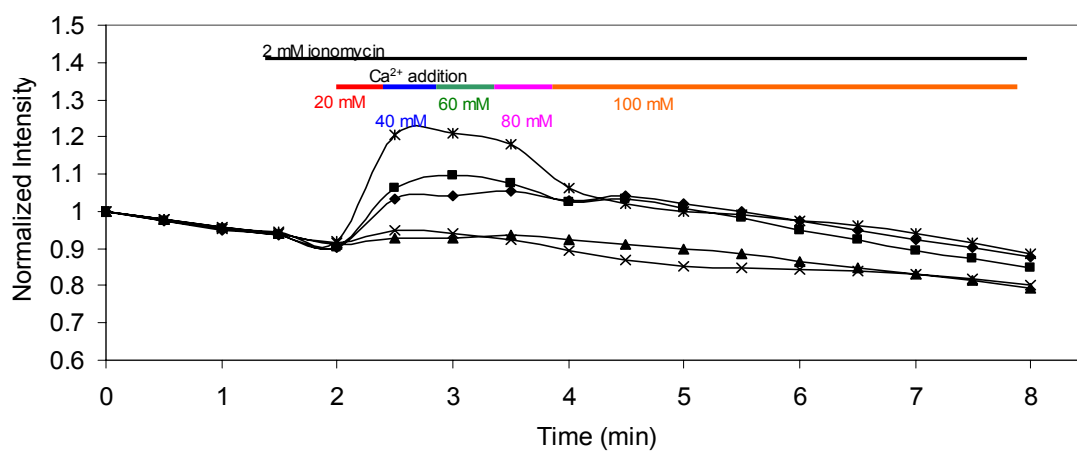


Fig 5.26 In vivo calcium response of 177 as imaged by the Zeiss Axiovert 200 inverted epifluorescence microscope at 40x magnification (oil objective) and 300 ms exposure with the FITC filter set.

calcium. Over time, bleaching is observed for the protein, which can likely be remedied by exposure for less time and reducing the power on the Fluoarc light box.

The data obtained with the confocal instrument indicates the same increase, but the wild type protein, EGFP, also indicates some increase in fluorescence upon addition of calcium. This is likely due to some cell shape changes or swelling of the cell due to the calcium. Since confocal is confined to one very small plane in the Z-axis, any cell swelling and shape changes could indicate a change in the fluorescence that is artificial. The change for EGFP is not as large as for the designed sensors with EGFP indicating 10-20% fluorescence increase and the designed sensors exhibiting 20-30% fluorescence increase. However, further tests must be performed to find the correct conditions for imaging of calcium changes on the confocal instrument so that the wild type protein does not indicate change but the designed proteins do. Trials of taking stacks at each time point and opening the pinhole up completely did not solve this dilemma.

In addition, real further testing by Dr. Aldebaran Hofer at Harvard University of this sensor expressed in BHK fibroblasts cells confirmed that the sensor was indeed responding to calcium. With the same results from three labs on four instruments, we can definitively say that our sensor is successful. Repeated experiments indicated the same calcium dependent increase, therefore, our designed sensor responds to calcium! Control experiments were performed by adding only calcium without ionomycin and no fluorescence increase was observed indicating that the sensor indeed responds to the increase calcium in the cytosol caused by ionomycin. This is the first instance of a

designed sensor with the calcium binding site incorporated into the frame of the host protein by site directed mutagenesis that responds to calcium changes *in vivo*.

The brighter sensor 177c3 was also monitored for calcium response *in vivo*. It was expressed in the cytosol of HeLa cells and observed with inverted epifluorescence at 40x magnification on both the Nikon inverted epifluorescence microscope and on the Zeiss Axiovert 200 inverted epifluorescence microscope, as shown in figures 5.27 and 5.28. An increase in the fluorescence is observed upon addition of ionomycin and calcium with both microscope setups. Up to 100 mM calcium was added to the bathing medium to test how large the outside calcium concentration needed to be to no longer see additional changes. From the data, 60 mM outside calcium is sufficient. After removal of calcium from the bathing medium, the sensor indicates a decrease in fluorescence. This result suggests that the fluorescence response to calcium is reversible. The calcium stimulated fluorescence increase is comparable or better in percent change to 177, but much less exposure time is necessary since the protein is much brighter. The shortest exposure time possible is desirable to monitor quick calcium changes in the cell and to reduce photobleaching as much as possible.

To ascertain if the non-fluorescent calcium-binding mutants would become fluorescent upon binding calcium, Sites 120 and 194a were expressed in HeLa cells and tested for calcium response. Ionomycin and calcium were added to the bathing medium and images were obtained. After addition of 60 mM outside calcium, no fluorescence was observed with the FITC or TexasRed filters. Unfortunately, binding to calcium did not induce chromophore formation of these proteins.

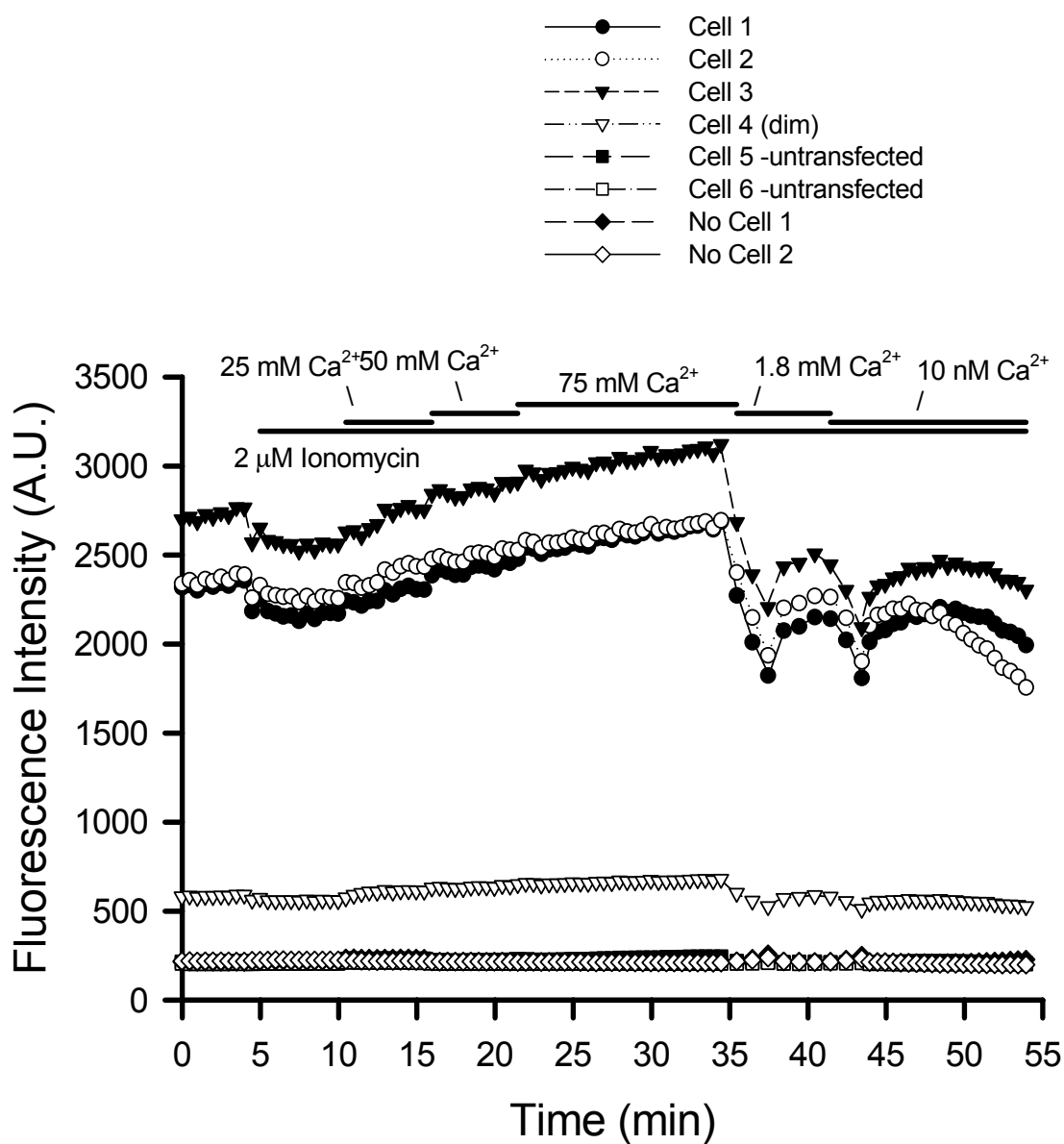


Fig 5.27 *In vivo* calcium response of 177c3 as imaged by inverted epifluorescence on the Nikon microscope, performed by Dr. Monica Lurtz, at 40x magnification.

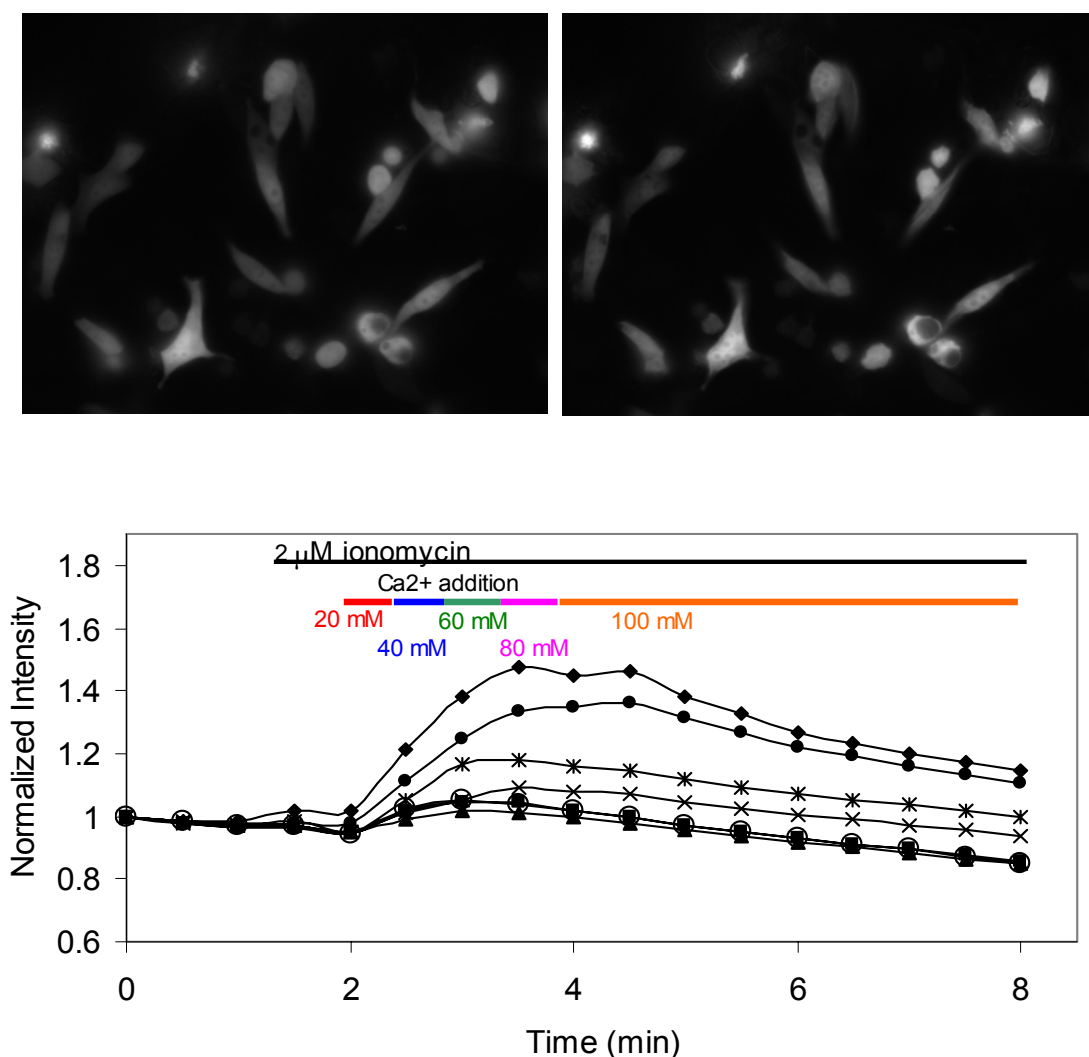


Fig 5.28 *In vivo* calcium response of 177c3 in HeLa cells as imaged on the Zeiss Axiovert inverted epifluorescence microscope at 40x magnification (oil objective) with 50 ms exposure. The top images are before and after calcium addition. The different traces are different cells in the region being monitored with the regions of interest being drawn around the entire cell for the best average fluorescence. The data was normalized by dividing each start point by itself so that the beginning would be 1. The remaining data was divided by the same number.

5.5 Calcium Response of Sensors 177 and 177c3 when Expressed in the ER

5.5.1 Addition of ER targeting signal peptides

In order to express the designed sensor in the ER of mammalian cells, two tags were added to the gene encoding 177 and 177c3. The N-terminal tag is a peptide from calreticulin, MLLSVPLLLGLLGLAAAD, which directs the expression of the gene to commence in the ER. The C-terminal tag, KDEL, is a retention sequence that retains the expressed protein in the ER and does not allow it to be shuffled to the Golgi. The use of these two tags has been demonstrated by Tsien, Miyawaki, and others in the literature (50, 62). The C-term tag was added by PCR utilizing primers that contained the DNA sequence for the KDEL tag and matched the GFP sequence (Table 5.2). In this way, the polymerase will incorporate the insert during the PCR. The tag was added between the last amino acid codon and the stop codon. After this was confirmed through automated sequencing at the core facility at GSU, the calreticulin signal sequence was initially added by PCR in the same manner as the KDEL. A vector containing the calreticulin sequence was later engineered for ease of multiple insertions. Inserting the calreticulin sequence by PCR required two rounds of PCR, but product was not always obtained due to the large insert. The experiment was repeated until the correct sequence was verified.

To target 177c3 to the ER, the same signal peptides were used as those used for 177. The C-terminal KDEL sequence was inserted by PCR between the last amino acid and the stop codon. However, addition of the calreticulin signal sequence was performed by a subclone rather than PCR into a modified pcDNA3.1+ vector. The

Table 5.2 Primers to insert the ER signal tags into EGFP variants.

Insertion for Calreticulin sequence is:

**ATG CTG CTA TCC GTG CCG TTG CTG CTC GGC CTC CTC GGC CTG
GCC GCT GCA GAC**

Primer Name	Sequence
----------------	----------

Cal1	CTG GCC GCT GCA GAC GGATCC ACT AGT CCA GTG TGG T
------	---

Cal2	CAC GGA TAG CAG CAT GAG CTC GGT ACC AAG CTT AAG TT
------	---

Cal3	GGC CTC CTC GGC CTG GCC GCT GCA GAC GGA TC
------	---

Cal4	GAG CAG CAA CGG CAC GGA TAG CAG CAT GGATCC G
------	---

Insertion for KDEL sequence is:

AAG GAC GAG CTG

KDEL1	GAG CTG TAA GAATTC TGC AGA TAT CCA GCC AC
-------	--

KDEL2	GTC CTT CTT GTA CAG CTC GTC CAT GCC G
-------	--

vector was modified by PCR to include the calreticulin signal sequence before the BamH1 site. In this way, any gene will have the calreticulin sequence included by a simple subclone with BamH1 and EcoR1 restriction enzymes, which is a much quicker and easier method than insertion by PCR. The primers and DNA base insertions are shown in table 5.2. The modified vector is termed pcDNA-CalR.

5.5.2 ER localization of sensors 177-ER and 177c3-ER

The ER tagged constructs of Site 177 and 177c3 were termed 177-ER and 177c3-ER. To test if the construct indeed localizes to the ER, double transfection of it and a purchased vector DsRed2-ER was performed. DsRed2-ER from Clontech has been shown to localize to the ER through immunohistochemistry (personal communication). If the 177-ER and 177c3-ER constructs' fluorescence perfectly overlays the fluorescence of DsRed2-ER, then it can be concluded that the two localize in the ER. Previous work in our laboratory demonstrated the necessity of the calreticulin sequence and the KDEL sequence in localizing to the ER (144). As shown in figures 5.29 and 5.30, when 177-ER and 177c3-ER were expressed with DsRed2-ER, it was observed that the two fluorophores completely overlapped forming an orange color in the image with no lone red or green observed. The green fluorescence is measured by excitation with the 488 nm Argon laser line, and the red fluorescence is measured by excitation with the 543 nm line of the He/Ne laser. The filters are set to only encompass the appropriate fluorescence, i.e. the green fluorescence is obtained with the BP 505-530 nm filter. This result indicates that both constructs indeed localize in the ER.

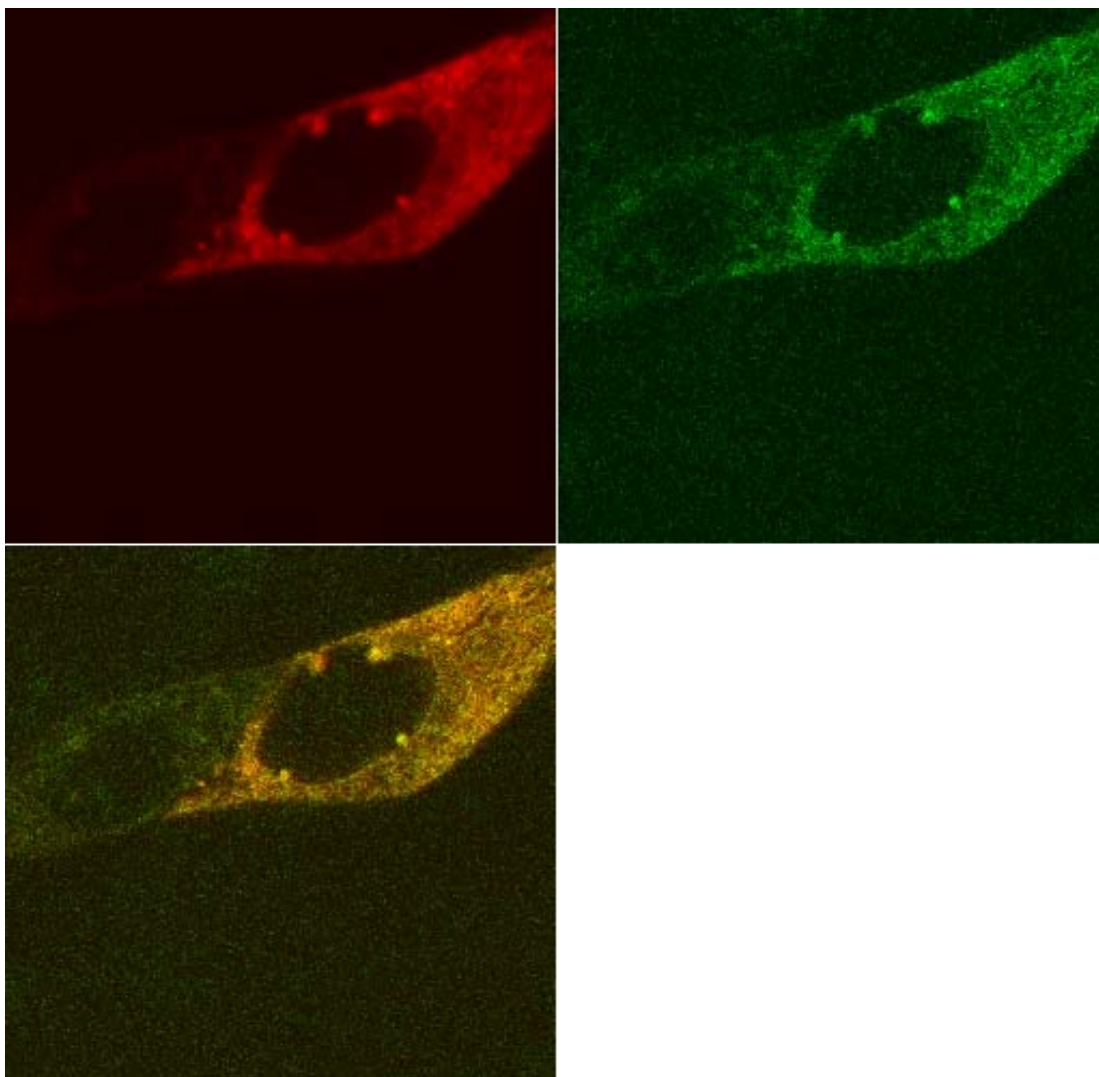


Fig 5.29 Confocal images of Sensor 177-ER cotransfected with DsRed2-ER in HeLa cells 72 hrs after transfection at 100x magnification. The overlay image on the bottom indicates that 177-ER is indeed localizing to the ER.

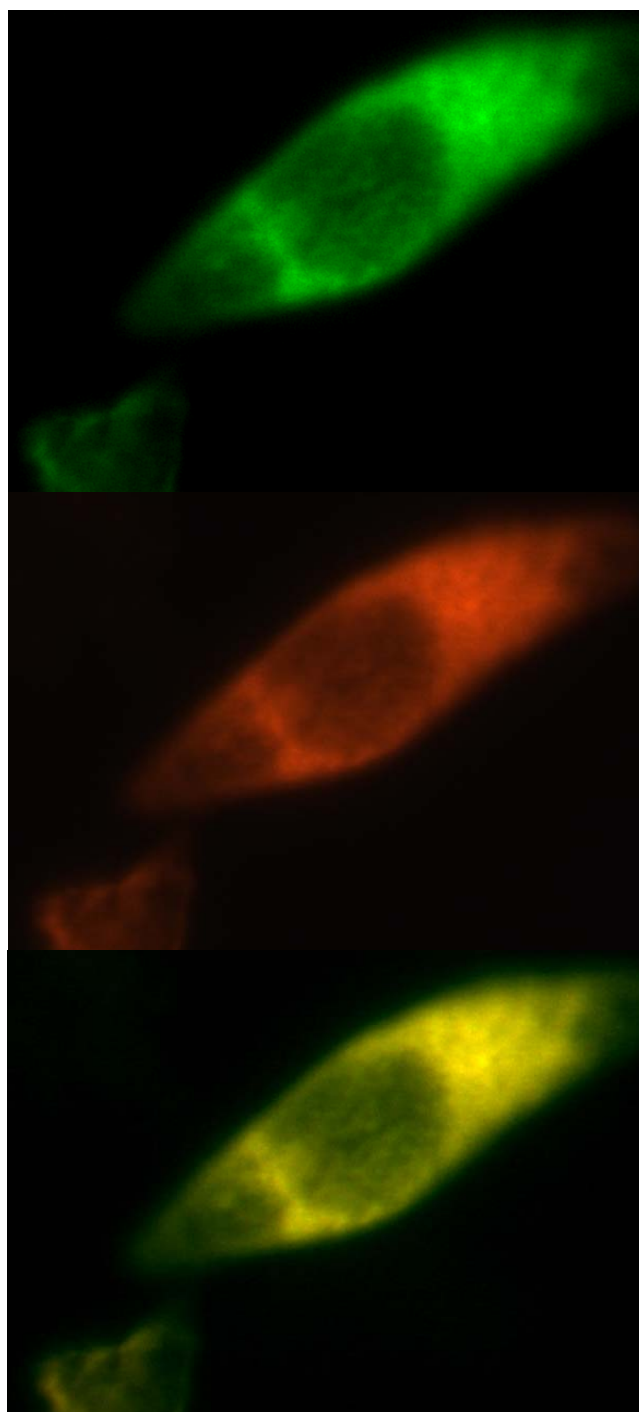


Fig 5.30 Colocalization of 177c3-ER and DsRed2-eR in HeLa cells 72 hrs after transfection as imaged by inverted epifluorescence with the FITC and TexasRed filters and automatic exposure.

5.5.3 Calcium response in the ER

To test the calcium response of 177-ER and 177c3-ER, the protein was expressed for 72 hrs at 30 °C in HeLa cells. ATP and/or histamine (100 μ M final concentration each) were added to the bathing medium. The addition of these two agonists should cause a large decrease in the ER fluorescence as the calcium stores are dumped. Small changes were observed when ATP was added, but the percent change is quite small (Fig 5.31). The experiments for 177c3-ER were performed on the laser scanning confocal instrument at GSU at 100x magnification. When 177c3 was tested for calcium response, a small reduction in chromophore fluorescence due to calcium release was observed but bleaching was also observed for this construct as shown in figure 5.32. The changes detected were small, similar to those detected for 177. This could be due to several factors. First, the fluorescence of 177-ER is weak in comparison to EGFP and Dr. Zou's sensors. This may contribute to the small change observed since a decrease when the fluorescence is already weak is difficult to accurately observe and requires more intense excitation light to be applied to obtain images in the dynamic range. This sensor does indicate some photobleaching during experiments, which may be overwhelming the calcium induced response. Second, ATP generated IP3 calcium release is a relatively small response. Third, the *in vitro* binding affinity of 177 is 59.7 μ M. Since the calcium concentration has been estimated to be 0.5 to 1 mM, such a strong binding constant in comparison may not be able to sense the relatively small change in calcium concentration through IP3 action. Evidence of this

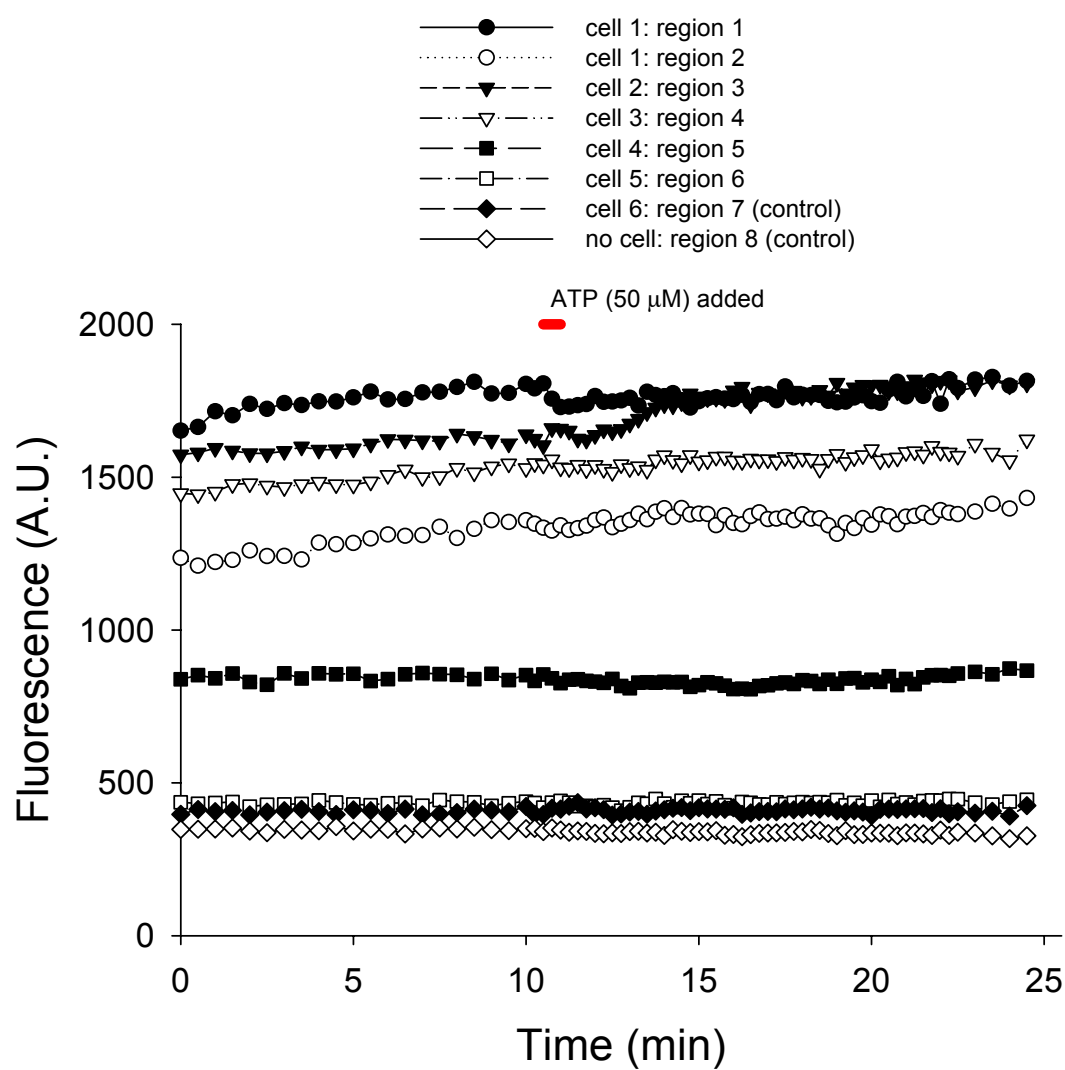


Fig 5.31 Calcium response of 177-ER with the addition of ATP. This experiment was performed by Dr. Lurtz on the Nikon inverted microscope at 40x magnification.

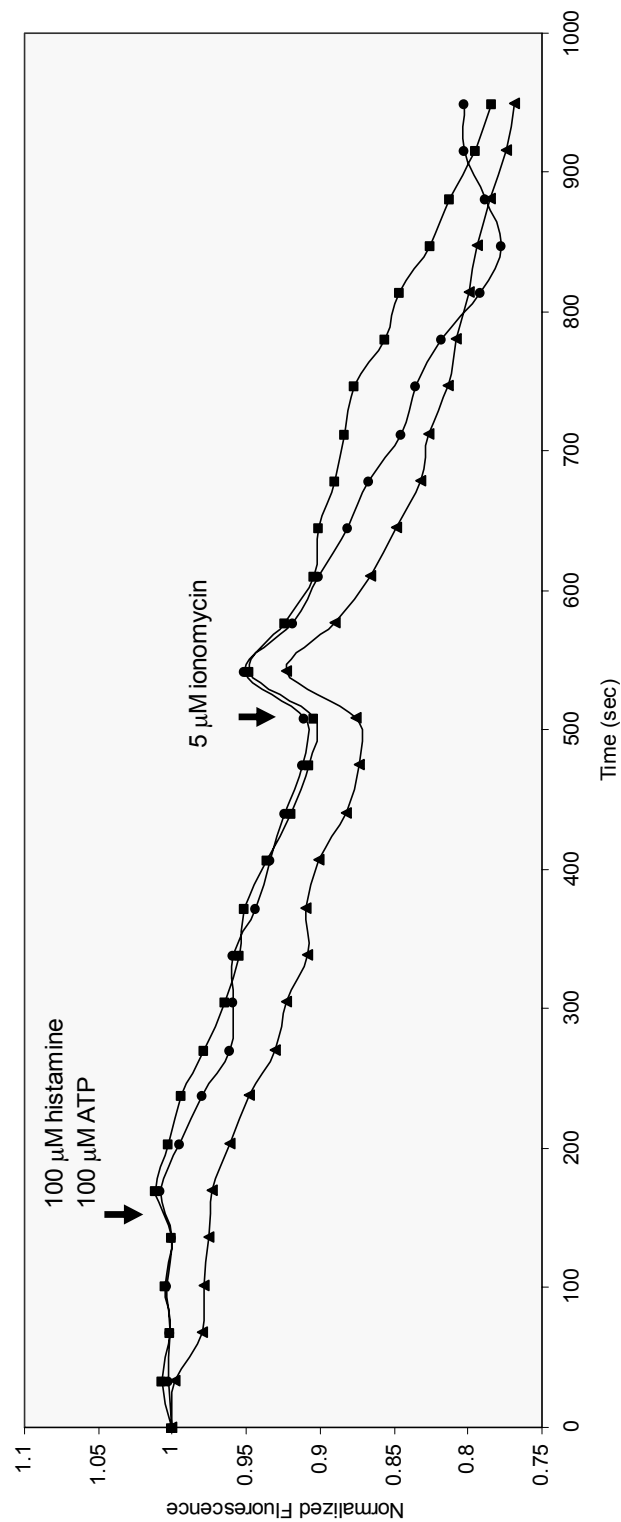


Fig 5.32 Response of 177c3-ER as imaged by confocal microscopy at 100x magnification, expressed in HeLa cells for 72 hrs at 30 °C.

has been observed in our laboratory by Dr. Jin Zou, whose grafted sensors exhibit response when expressed in the ER. The binding affinities of the grafted sensors are 100 to 300 μM , in a much better range for the higher ER calcium concentration. Hofer's work on ER calcium release using Mag-Fura-2, which has a calcium binding affinity of 53 μM , indicates very little response with ATP but a large response with other methods, such as soaponin and IP3 addition (30). In addition, the K_d for calcium may be stronger when the protein is expressed in HeLa cells. The protein is definitely better folded since it is fluorescent, which was not observed for bacterially expressed protein, so the binding affinity may be stronger than that measured for bacterially expressed protein. This idea is supported by the cytosolic response observed for 177 and 177c3, where the calcium concentration reaches 10-20 μM . In this case, another method to measure the ER calcium changes with 177c3 is to express the sensor in the cytosol, where the binding affinity is more adept for the calcium concentration range, and cause a calcium release from the ER as was performed for sensor 177. The calcium increase in the cytosol can then be correlated to the ER release activation.

5.6 Calcium response of 177c3 in vitro

5.6.1 Expression of 177c3 in HeLa suspension

In order to obtain enough folded, fluorescent protein for *in vitro* characterization of 177c3, it was expressed in HeLa cells in suspension. The DNA was first transfected into attached HeLa cells, as detailed in section 2.23, the cells were harvested, and they were placed in suspension for growth. In this way, a much larger number of cells can

be obtained without needing to grow on many plates or flasks, and, therefore, much more protein can be acquired. In addition, suspension growth was optimized so that the cells could be expressed for 4-6 days without cell death so that more protein could be obtained (section 2.23). This was accomplished by the use of a 1 L MantaRay bottle, which creates a constant stirring when placed on a stir plate so that the cells can not attach to the sides of the bottle, and by suspending the harvested cells in only 400 mL of media. The reasons for this are several fold. First, HeLa cells need to be a certain cell density to produce enough CO₂ for survival without growth in a CO₂ incubator. The initial use of a smaller amount of media allowed for a high enough cell density for CO₂ production. If 1 L of media was initially employed, more plates (atleast 14) and much more DNA would have needed to be transfected to reach the needed cell density. Second, simply adding media each day without separating the cells and media and removing the old media reduces the possibility for contamination and cell destruction. Also, the addition of the media allows for more space for the cells to grow, which is needed as the cells double every 28 hrs.

After 4-6 days, the cells were harvested and sonicated to break the cell membrane, releasing the designed protein into the supernatant. The designed protein was then measured with fluorescence spectroscopy to ascertain the chromophore spectrum and for calcium response. The fluorescence excitation spectrum of 177c3 is highly similar to EGFP except that the peak at 398 nm is not evident (Fig 5.33). Fluorescence at 510 nm is produced by excitation at 450 nm, 469 nm, and 483 nm but only a small peak is produced by excitation at 398 nm (Fig 5.34). EGFP produces

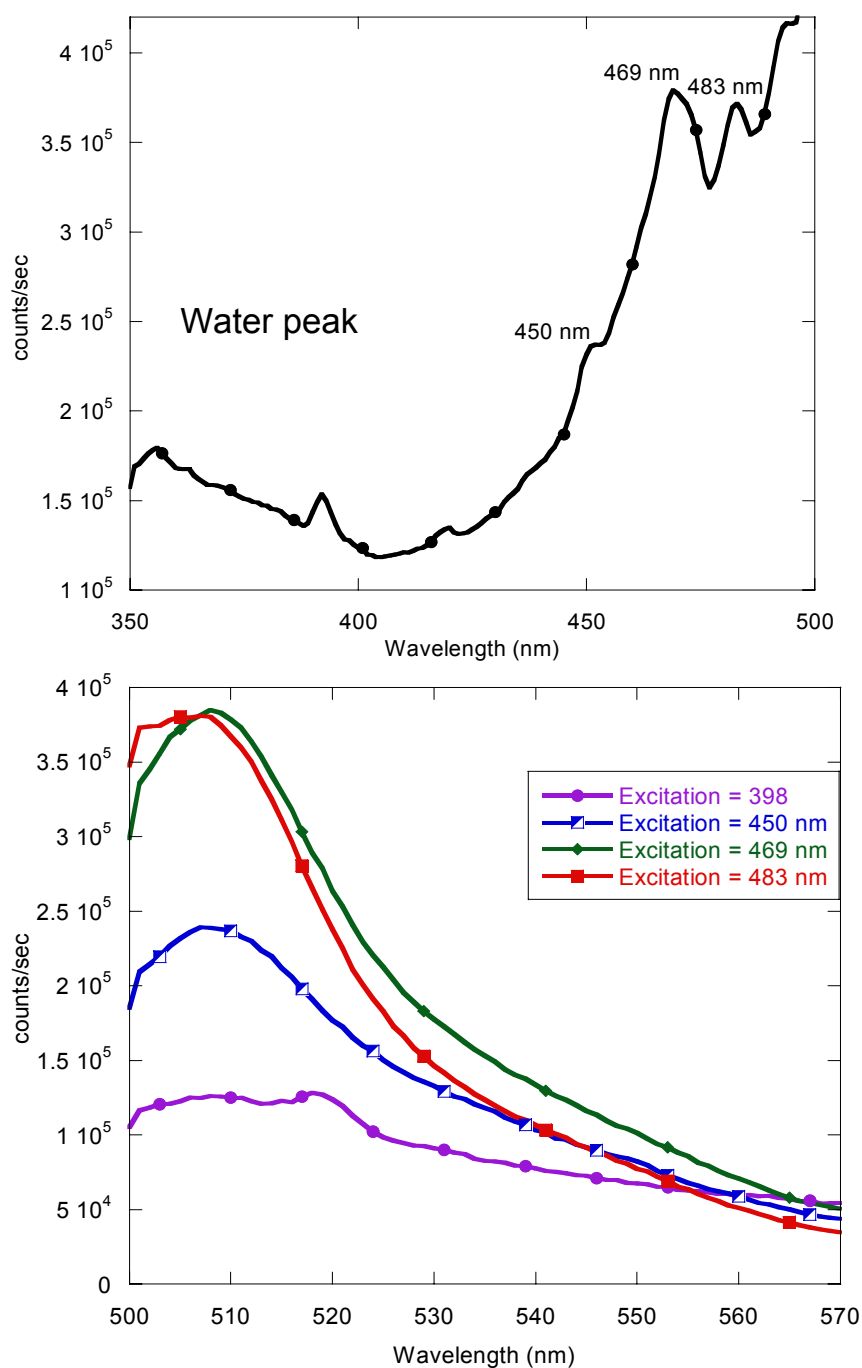


Fig 5.33 Excitation with emission at 510 nm and emission spectra of 177c3 in cell supernatant after sonication of cells with the protein expression in suspended HeLa cells. The various excitation wavelengths were examined to ascertain the emission for each excitation.

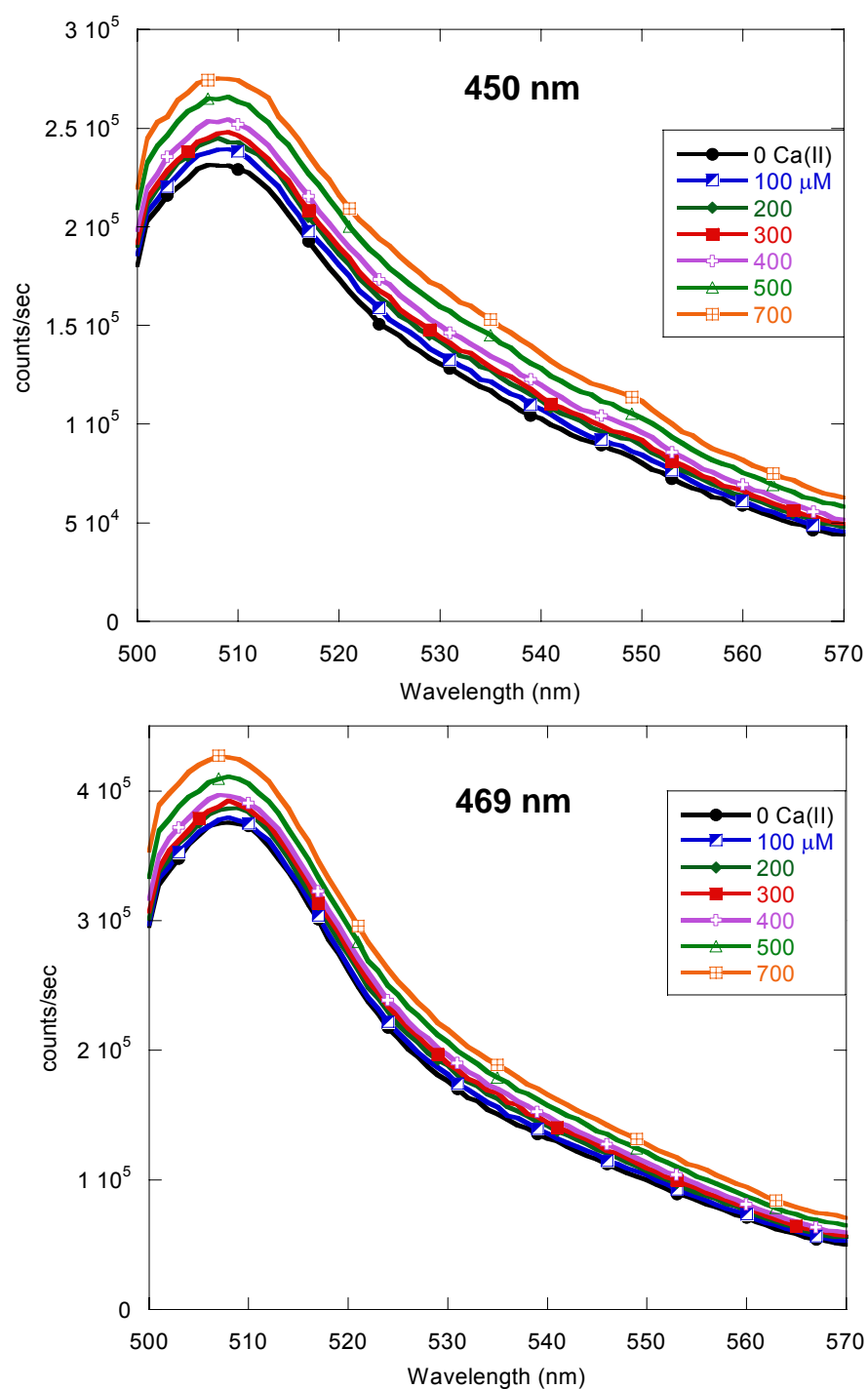
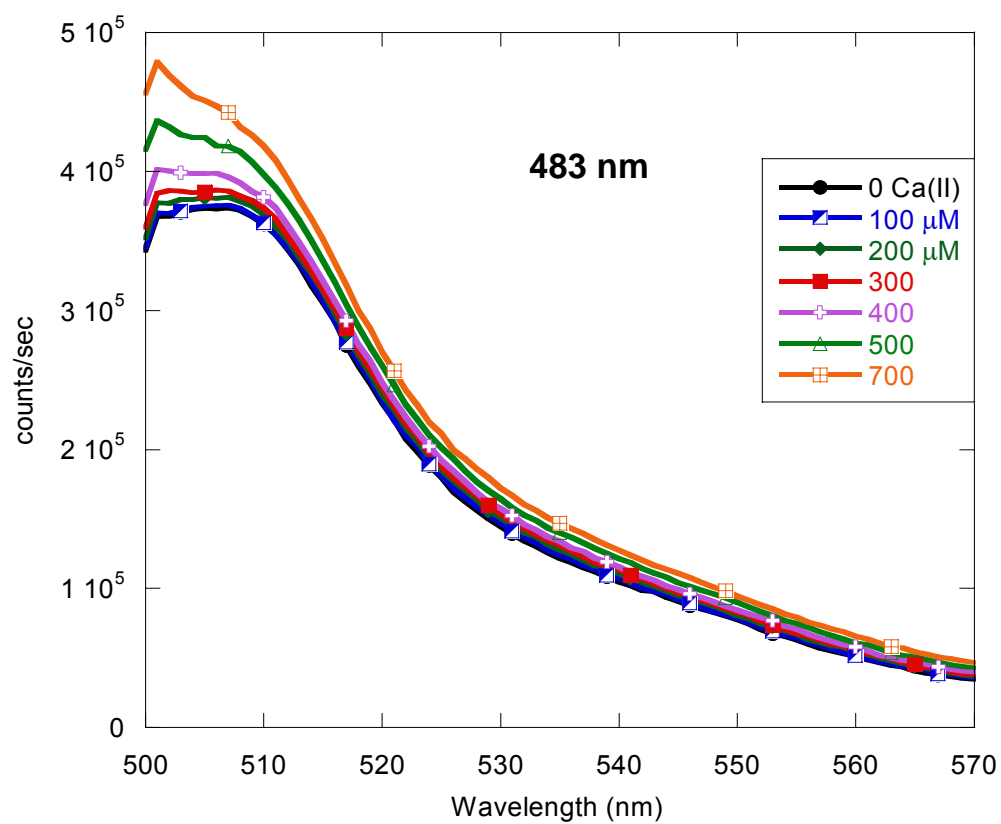


Fig 5.34 Emission spectra of 177c3 lysate with increasing calcium at 3 different excitation wavelengths (3rd on next page). The largest increase in fluorescence is observed for excitation at 450 nm.



fluorescence at 510 nm with excitation at 398 nm due to excitation of the neutral state of the chromophore with much more intensity than 177c3. This result indicates that 177c3's chromophore is shifted nearly entirely to the anionic state. This shift could be the cause for the change in chromophore fluorescence upon calcium binding. Emission spectra were obtained for excitation at 450 nm, 469 nm, and 483 nm with the addition of calcium in 100 μ M increments up to 700 μ M. At 700 μ M calcium, precipitation was observed (Fig 5.34). Excitation at 450 nm indicates the largest calcium change with only 100 μ M calcium needed to induce a response whereas excitation at the other wavelengths requires 200 μ M or more to indicate a change. EGFP does not exhibit these calcium induced changes in chromophore fluorescence (Fig 5.35), suggesting that the change is unique to the designed calcium sensor. Since this protein mixture was not pretreated with EGTA, the protein may have contained some calcium since only small changes were observed with 100-300 μ M. The binding affinity of this designed site is 59 μ M when expressed in bacteria. The affinity may be different with expression in mammalian cells, but it is more likely that the effect on the chromophore fluorescence is slightly different than the true binding affinity. Binding events at low concentrations may not produce a measurable fluorescence change so that the apparent affinity measured by the fluorescence change is not the same as the true binding affinity. With *in vitro* and *in vivo* calcium induced changes observed for this protein, it is apparent that a calcium sensor has been engineered.

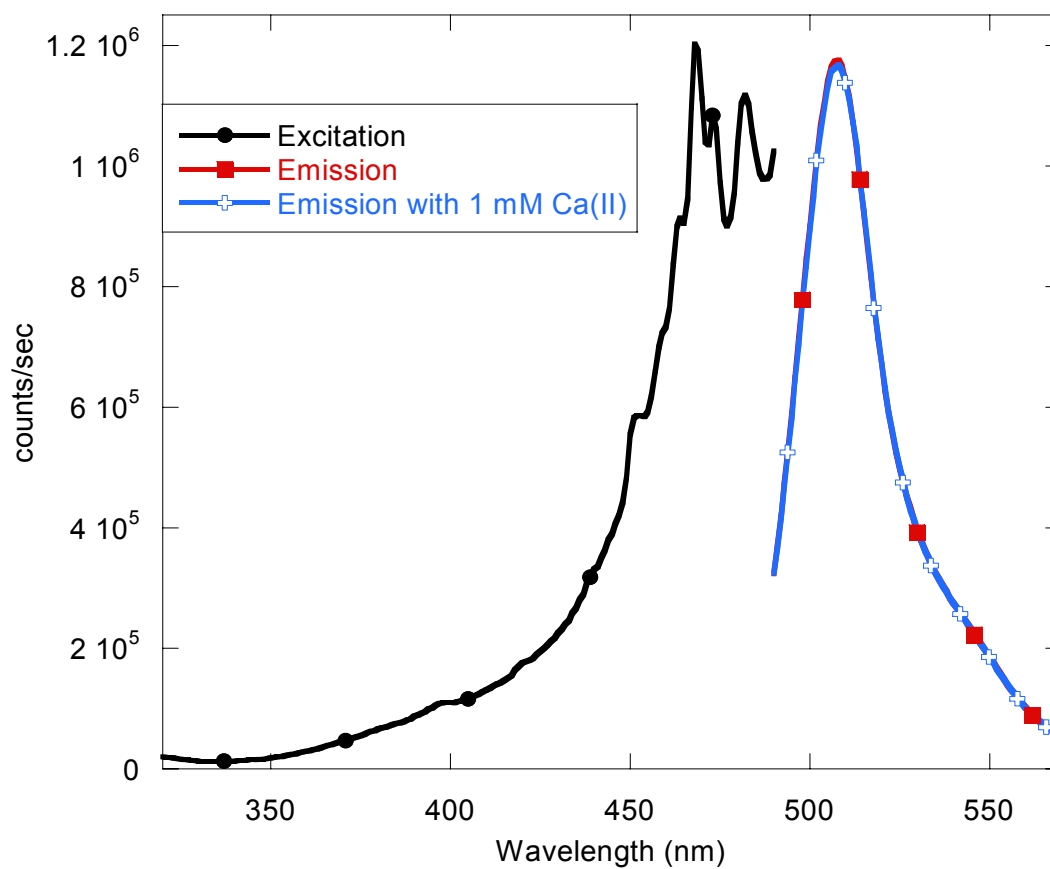


Fig 5.35 Excitation (with emission at 510 nm) and emission (with excitation at 482 nm) spectra of EGFP in 10 mM Tris, 1 mM DTT, 1% glycerol, pH 7.4. The emission was measured with and without calcium to ensure there were no changes in the chromophore's emission with calcium.

5.7 Major Findings

Designed proteins 229, 120, 194a, and 177 were expressed in mammalian cells in which fluorescence was indicated for sensor 177. Addition of the cycle 3 mutations, F99S/M153T/V163A, increased the brightness of sensor 177 approximately 10 times but did not indicate fluorescence for sensor 120 and 194a. Sensor 177c3 indicates weak fluorescence when expressed at 37 °C in HeLa cells that is not observed for sensor 177. Sensors 177 and 177c3, when expressed in the cytosol of HeLa cells, indicate an increase in fluorescence signal upon an increase in calcium concentration through ionomycin action with increased extracellular calcium and through addition of ATP to release calcium from the ER. Including the calreticulin and KDEL tags in the 177 and 177c3 constructs produced protein that localized in the ER of HeLa cells. Measurements of calcium response of 177 and 177c3 expressed in the ER did not yield fluorescence signal change, likely due to a binding affinity that is too strong to sense the small calcium changes when release is induced by ATP or histamine. Expression of 177c3 in suspended HeLa cells allowed for in vitro fluorescence measurements of the protein and observed calcium changes upon introduction of calcium.

Chapter 6 Second Generation of Designed Sensors

6.1 Lessons Learned: design of a second generation of sensors

6.1.1 New criteria in the design of the second generation

In an effort to create better, brighter sensors with a larger calcium response, the initial 10,000 sites from the computer algorithm research for possible calcium-binding sites were reexamined. The possible sites were grouped by location in the protein, and the various residues (usually 8-10) in each location were considered. The previously studied mutations that caused fluorescence loss (K79D, K85D, and H81D) were removed from consideration. During the inspection of the possible sites, it was noticed that many sites were located in similar places as the first generation with a few different ligands. These sites were further contemplated since binding sites in those locations in the first generation proved to be fluorescent in mammalian cells and/or demonstrated calcium sensitivity. In this search, the idea of stabilizing the protein with surrounding positive sidechains was taken into account. Since introduction of several negative charges disrupts the chromophore formation, balancing the negative charges with surrounding positive charges to form salt bridges when not bound to calcium should aid in chromophore formation. When deciding upon which residues should be the final amino acids, each pocket was closely examined and distances were measure to ascertain the size of the sidechain that would fit into the location without causing steric clash with other sidechains. In addition, lysines and histidines were avoided altogether since those mutations have proved detrimental in our work, K79D for example, and in the literature. The final sites chosen for study are listed in table 6.1. Models of the sites

Table 6.1 The second generation designed proteins are detailed with the calcium-binding pocket ligands, the charges introduced by mutation to the binding ligands, and the similar first generation sites.

Design Site	Ligands	Charges Introduced	1st generation similar site
Site 1	L194E, S86D, D82, E5, S2D	-5	194b with L194N/S86D/K79D
Site 2	L15D, R122E, V120S, E17, E115	-4	120 with L15N/R122D,V120N
Site 3	F83D, I161D, A154D, I152E, L194E	-5	None except a.a. 194
Site 4	T59D, L141N, Q177E, F100E, I136S	-3	None except a.a. 177
Site 5	L7D, V12N, M88S, F114D, L119E	-3	None
Site 6	L7D, V12N, M88T, F114D, L119E	-3	None

are illustrated in figure 6.1. Two of the sites, 1 and 2, are based on the 1st generation of designed proteins with residue changes to allow for proper chromophore formation. Sites 3 and 4 are more aggressive sites than in the past with the hopes that a large calcium response would be observed. Sites 5 and 6 are the same amino acid locations, but the ligand types are different.

Site 1 is very similar to site 194b from the first generation but with a change in one of the ligands to avoid fluorescence loss but still obtain a calcium response. K79D caused a complete fluorescence loss in the protein so S2D was included in this generation. Also, 194 was mutated to E instead of N to increase the binding affinity for calcium with an additional negative charge incorporated into the site.

Site 2 is similar to site 120 but V120 was changed to a serine because the valine is on the outside but buried inside the other residues. Mutating 120 to an asparagine in the first generation disrupted the chromophore formation so it was mutated to a serine, which is also a less frequently used calcium ligand, to reduce the clash from the surrounding residues. L15 was mutated to aspartate and R122 was mutated to glutamate to better form the correct calcium binding geometry and to increase the binding affinity.

Sites 3, 4, and 5 are entirely new sites that were suggested by Dezymer but were modified by this researcher and Dr. Wei Yang to better form the calcium binding pocket. Site 3 is contained in the upper portion of the barrel with several ligands in the loop regions. The M153T mutation of the cycle 3 variant is near this site so it was thought

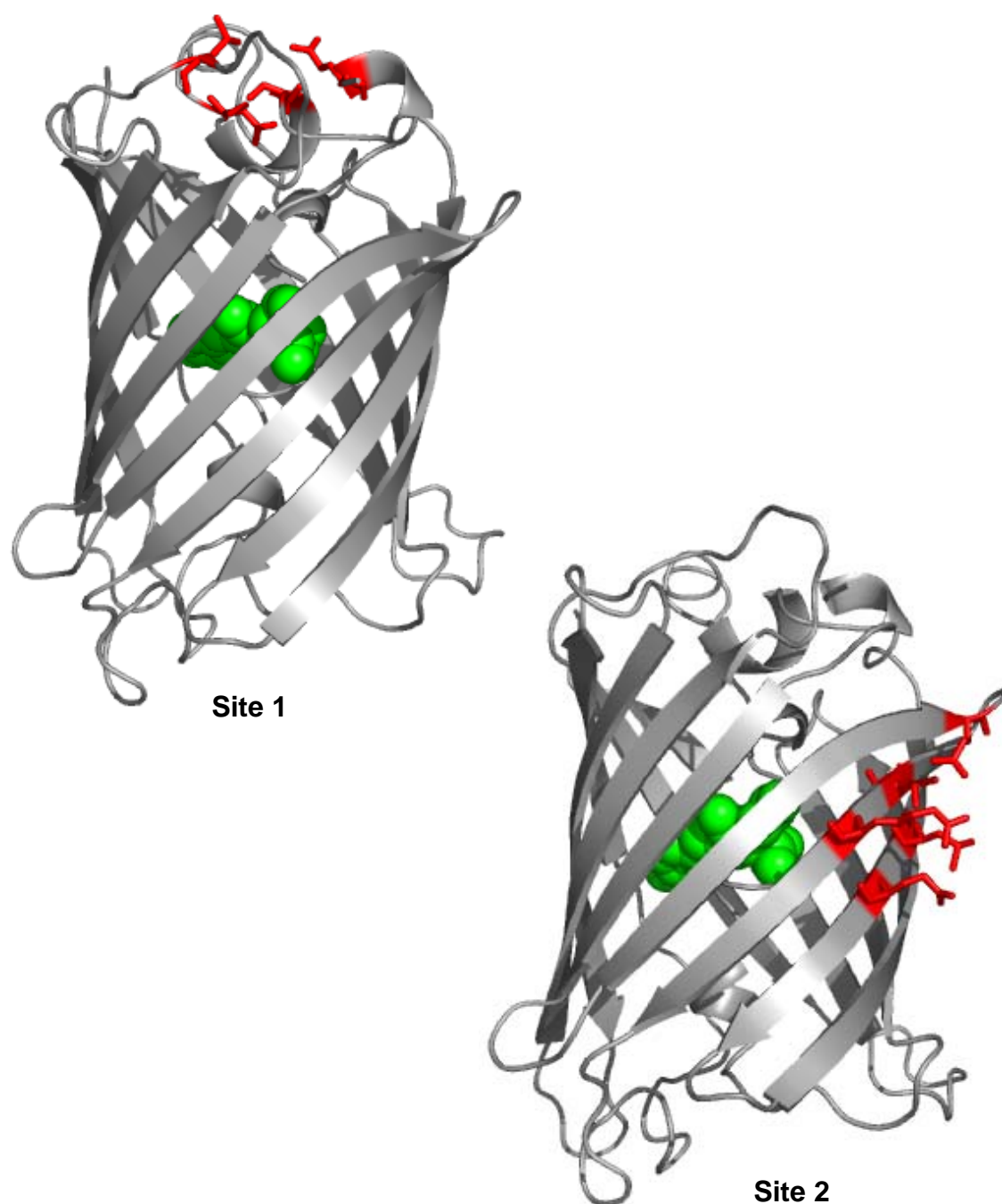
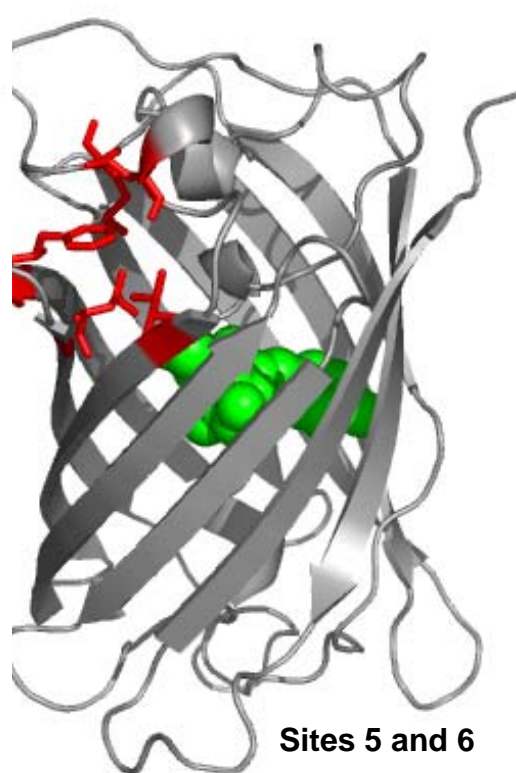
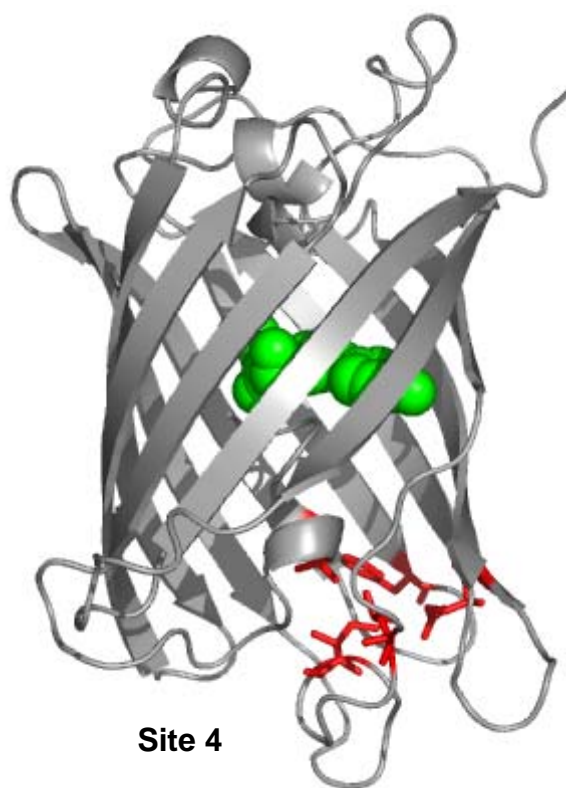
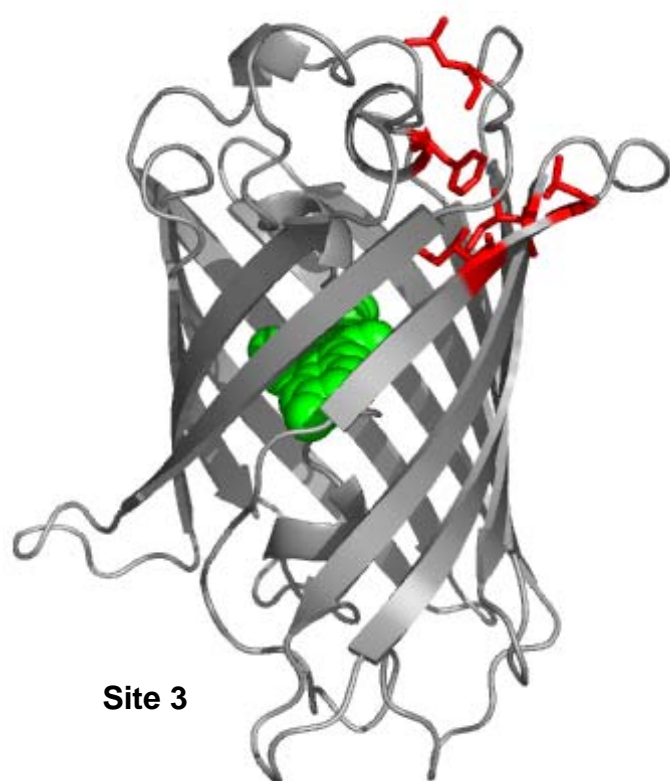


Fig 6.1 Pymol models of the second generation of designed calcium-binding green fluorescent proteins illustrating the different locations of each site with the ligands shown in red and the chromophore in green.



that binding calcium in this location would likely lead to a large signal change upon calcium binding.

Site 4 is near the site 177 region and contains residue 177. This site is slightly more inside the barrel than site 177 with the idea that a site closer to the chromophore would cause a larger change in fluorescence. Many of the residues are located in the loops so they should be flexible enough to form the correct calcium-binding geometry. However, this site does contain a residue that is quite close to the chromophore, T59D, which could perturb the chromophore.

Sites 5 and 6 are located in an open portion of the barrel with three of the residues (12, 114, and 119) at the end of β -strands. This pocket provides a direct line to the chromophore so closing the conformation by calcium binding should cause an increase in chromophore fluorescence due to decreased solvent accessibility. The concern for this site was mutating the phenylalanine since it is a large, bulky residue and could possibly be involved in π stacking, but there were no other residues in close enough proximity that could form the binding pocket. Therefore, the site was kept to a -3 charge to reduce the electrostatic repulsion.

6.2 Protein Engineering of Calcium Sensors

The second generation variant mutations were performed by site-directed mutagenesis directly on the pcDNA3.1+ construct of EGFP so no subclone was necessary for mammalian expression. Table 6.2 details the order in which the mutations were completed. Some of the mutations were carried out in tandem to

Table 6.2 The order of the mutagenesis performed for the second generation. The proteins that exhibited green fluorescence when expressed in HeLa cells are highlighted in green.

Design Site	Ligands	Order of Mutations
Site 1	L194E, S86D, D82, E5, S2D	L194E/S86D +S2D
Site 2	L15D, R122E, V120S, E17, E115	R122E/V120S +L15D
Site 3	F83D, I161D, A154D, I152E, L194E	I161D/A154D/I152E +F83D +L194E
Site 4	T59D, L141N, Q177E, F100E, I136S	T59D +L141N/I136S +F100E +Q177E
Site 5	L7D, V12N, M88S, F114D, L119E	L7D/V12N +F114D/L119E +M88S
Site 6	L7D, V12N, M88T, F114D, L119E	Site 5 + M88T

reduce the number of PCR to be performed. For site 1, the L194N/S86D DNA was utilized as the template so that L194N was mutated to E without needing to purchase primers and carry out the reaction for S86D. To engineer site 3, EGFP with the cycle 3 mutations was utilized since the binding site mutations were located at 152 and 154. Sites 5 and 6 were only separated in the last round of PCR when M88 was mutated to either S or T.

Initially, a new polymerase KOD was utilized to engineer the new sites. After the PCR, very large, bright bands were observed in the agarose gel. Once the samples were prepped and received back from automated sequencing, it was realized that only one out of 10 samples was correct. The other samples either did not contain the mutations incorporated into the primers or they contained deletions and/or insertions in the DNA sequence. After conferring with other laboratory members, the conclusion was drawn that KOD was not as high fidelity as the manufacturer states since only a few reactions out of ~40 were correct. As a note of caution, new reagents should be tested stringently before being widely utilized. Due to these results, *turbo pfu* was utilized for all of the second generation mutations since it has been used for years in our laboratory with success.

6.3 Mammalian Expression of the Second Generation

To efficiently identify correctly folded GFP variants, each round of mutations was screened for fluorescence by expression in HeLa cells rather than expression in bacteria. In this way, if some mutations caused fluorescence loss, it could be more easily identified if there were 1 to 3 mutations in the construct than if it were a full site

with 5 or 6 mutations. The DNA, after being verified through automated sequencing, was transfected into HeLa cells and allowed to express at 30 °C for 72 hrs. Each construct was inspected with the three available, standard filters in the inverted epifluorescence microscope, DAPI, FITC, and Texas Red.

Site 1 with mutations L194E/S86D indicated green fluorescence when expressed in HeLa cells at 30 °C for 48 and 72 hrs after transfection with both the UV/DAPI filter and the FITC filter (Fig 6.2). EGFP does not indicate strong fluorescence with the UV filter since the UV excitation peak for EGFP is very weak. This result may indicate some shift in the chromophore's ionic state so that the UV excitation peak is stronger than for EGFP. The full site with L194E/S86D/S2D also indicated fluorescence after expression in HeLa cells (Fig 6.3). The transfection efficiency was approximately 70 to 80%.

Site 2 with mutations R122E/V120S indicated green fluorescence in a few cells, but the transfection efficiency was not very high, <20% (Fig 6.4). Further tests of increasing the amount of DNA and varying the DNA:liposome ratio were performed to increase the efficiency and obtain more fluorescent cells. These results are encouraging because previous mutations of V120 caused loss of fluorescence of EGFP. The mutation to serine should be able to bind calcium but is not disrupting the fold as drastically as the mutation to asparagine. Unfortunately, the addition of the L15D mutation caused fluorescence loss. Likely this additional mutation brought about too much electrostatic repulsion or steric clash so that the short distance between Gly67 and Ser65 could not be achieved. Since this site is very close to the chromophore and



Fig 6.2 Images of the first round of mutations for Site 1, L194E/S86D, expressed in HeLa cells taken with the FITC (top left) and DAPI (top right) filter and transmitted light (bottom) at 100 ms exposure with the 40x dry objective. The fluorescence observed with the DAPI filter is not evident with EGFP, suggesting some change in the spectral profile of Site 1.

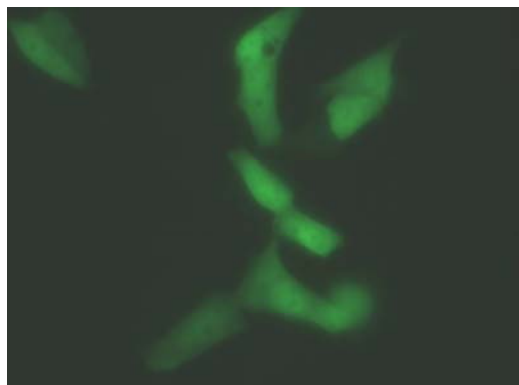


Fig 6.3 Images of Site 1 expressed in HeLa cells with all three mutations, indicating fluorescence with the FITC filter and 1 s exposure imaged with the 40x dry objective. These cells were grown at 30 °C for 72 hrs after transfection.

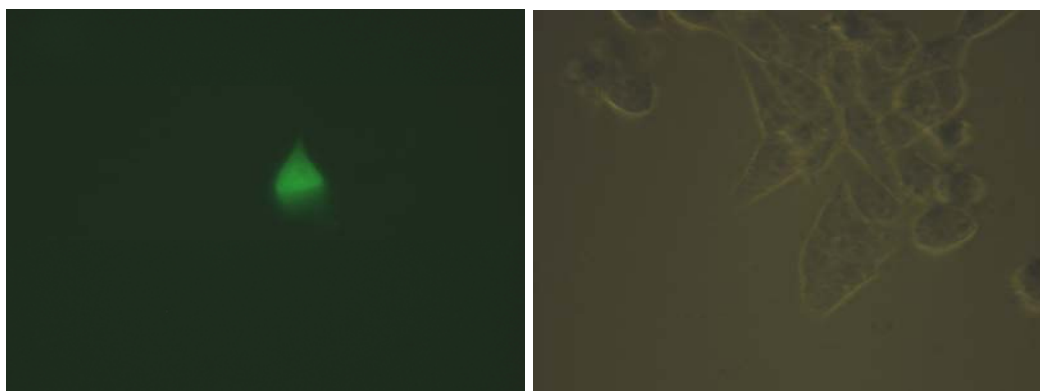


Fig 6.4 Site 2 partial mutations of R122E/V120S expressed in HeLa cells with fluorescence observed in one cell. Other regions were similar with one or two fluorescent cells out of ~10 cells. Images were taken with 1 s exposure and a 40x dry objective.

contained in the β -sheets, any repulsion or interference that causes a greater distance between the chromophore forming amino acids could prevent the chromophore from forming the initial cyclization. It is likely that the addition of the negative charge from L15D was too much for the protein to compensate.

The first three mutations in Site 3, I152E/A154D/I161D, were screened in HeLa cells as well with expression at 30 °C for 72 hrs. This variant did not display fluorescence. The cycle 3 mutations were first incorporated into the gene before these three mutations were generated. Apparently, these three mutations disrupt the fold of the protein more than the better folding of the cycle 3 mutations can overcome. Possibly, the three mutations from hydrophobic residues to charged residues were too drastic of a change. Further mutation of F83D did not yield fluorescent protein.

Site 4 with the single mutation T59D did not indicate fluorescence with expression in HeLa cells at 30 °C for 72 hrs after transfection. Since this mutation is close to the chromophore, it may have disrupted the fold of the protein or may have disturbed the chromophore formation. Since T59D is located at the end of the central helix, mutation of it to a negatively charged residue may have initiated repulsion that distorts the α -helix so that the initial cyclization can not ensue. Further mutation of this site to include all of the designed residues did not yield fluorescent protein.

Site 5 (and 6) with mutations L7D/V12N indicated fluorescence in HeLa cells with the FITC filter as shown in figure 6.5. However, the fluorescence is weaker than EGFP, about 10 times reduced, with a longer exposure time necessary, at least 2 s. Since

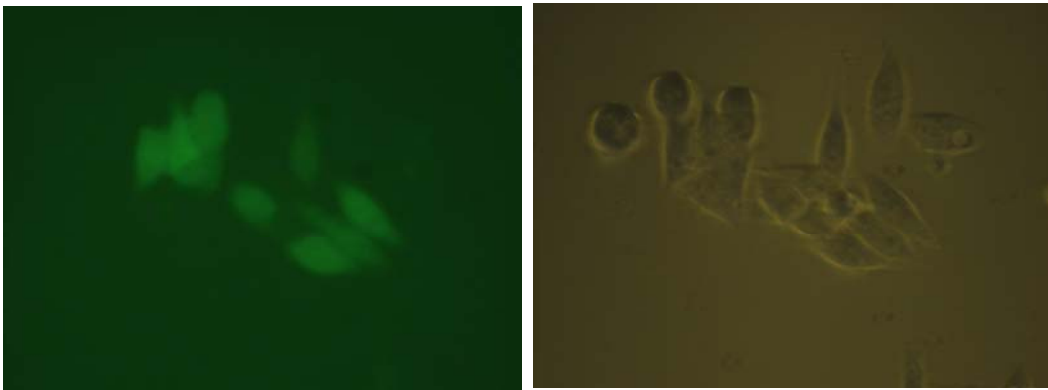


Fig 6.5 Site 5 with mutations L7D/V12N expressed in HeLa cells for 72 hrs indicating fluorescence with the FITC filter (left) with 2 s exposure and the 40x dry objective.

these two mutations are somewhat precarious due to the change from hydrophobic residues to polar residues, the reduced fluorescence is not unexpected. Further mutation to include F114D and L119E failed to produce fluorescent protein. The M88S and M88T mutations were completed as well, but no fluorescence was observed.

As indicated in table 6.2, one of the second generation sites indicated fluorescence with all of the mutations completed, Site 1. Site 2 indicated fluorescence with the initial two mutations, R122E/V120S, but no fluorescence was observed with the addition of the final mutation, L15D. The first three mutations in Site 3 did not indicate fluorescence. The first mutation, T59D, in Site 4 abolished chromophore fluorescence. For Sites 5 and 6, the first mutations, L7D/V12N, indicated fluorescence, but addition of F114D and L119E eliminated fluorescence. Due to Site 1's fluorescence in HeLa cells, it was further studied for calcium response.

6.4 Site 1 Calcium Response *in Vivo*

6.4.1 Cytosolic calcium response of Site 1

Since Site 1 indicated fluorescence brighter than 177 and on par with 177c3, it was tested for calcium response in HeLa cells. After transfection optimization, as detailed for Site 177 in Chapter 5, it was found that less DNA (1 μ g for Site 1 versus 3 μ g for 177) in a 1:3 DNA:Lipofectamine₂₀₀₀ ratio produced fluorescent cells with 60-80% transfection efficiency when expressed at 30 °C. In addition, it was possible to obtain fluorescent cells 48 hrs after transfection rather than waiting until 72 hrs. Site 1 is about

ten times less bright than EGFP under the same condition. Under these conditions, the cytosolic calcium response was tested.

To test the cytosolic calcium response, the confocal instrument at GSU was utilized with the 488 nm line of the Argon laser. Ionomycin and calcium were added to the bathing medium, and images were obtained before and after the additions at regular intervals (Fig 6.6). The cells were monitored for any shape change during the experiment. No fluorescence change was observed when ionomycin was added, but a 20% increase in fluorescence was observed with addition of 10 mM calcium. Concomitant increases were observed with addition of calcium to 20 and 30 mM in the bathing medium. The fluorescence decreased to baseline when the outside calcium was removed. This change is larger than the 177c3 change and occurs at lower outside calcium concentrations, promising and exciting results for the second generation of designed sensors.

The calcium response was also tested by Dr. Monica Lurtz at UC Riverside with the inverted Nikon microscope, as shown in figure 6.7. The fluorescence increases with increasing calcium after ionomycin addition very similar to the confocal data obtained at GSU. The fluorescence decreases with removal of the high extracellular calcium.

6.4.2 Direction of Site 1 to the ER

The ER signal peptides were incorporated into Site 1 through the use of PCR for the C-terminal KDEL sequence and subcloned into the modified pcDNA3.1+ vector for the N-terminal calreticulin sequence. This vector was discussed in section 5.5 of Chapter 5. In brief, it includes the calreticulin signal peptide at the N-terminal before the

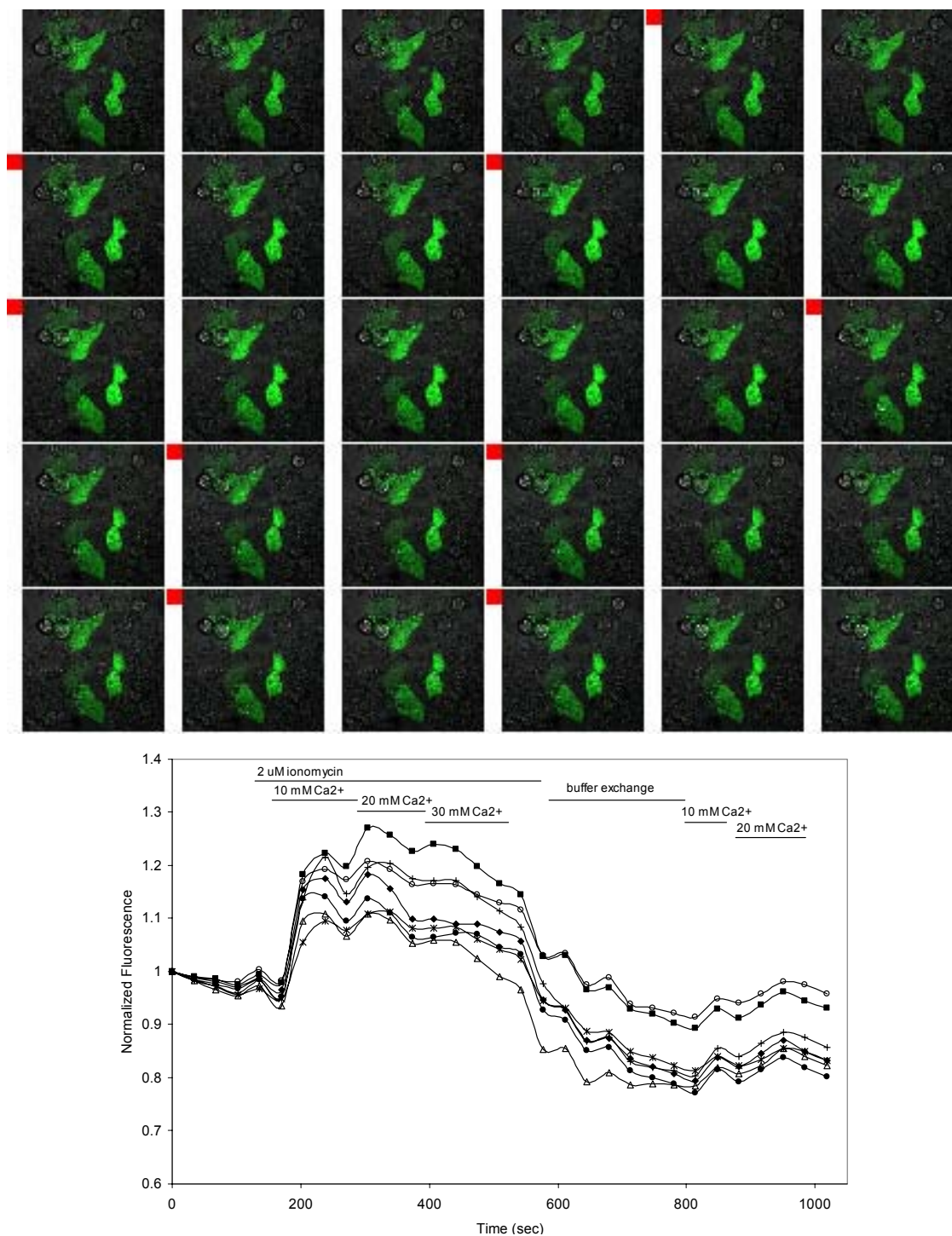


Fig 6.6 Site 1 calcium response in HeLa cells with addition of ionomycin and calcium to the bathing medium, removal of the calcium, and two more additions as indicated by the red squares in the image set. The data in the graph was normalized to 1 at the first point for ease of viewing.

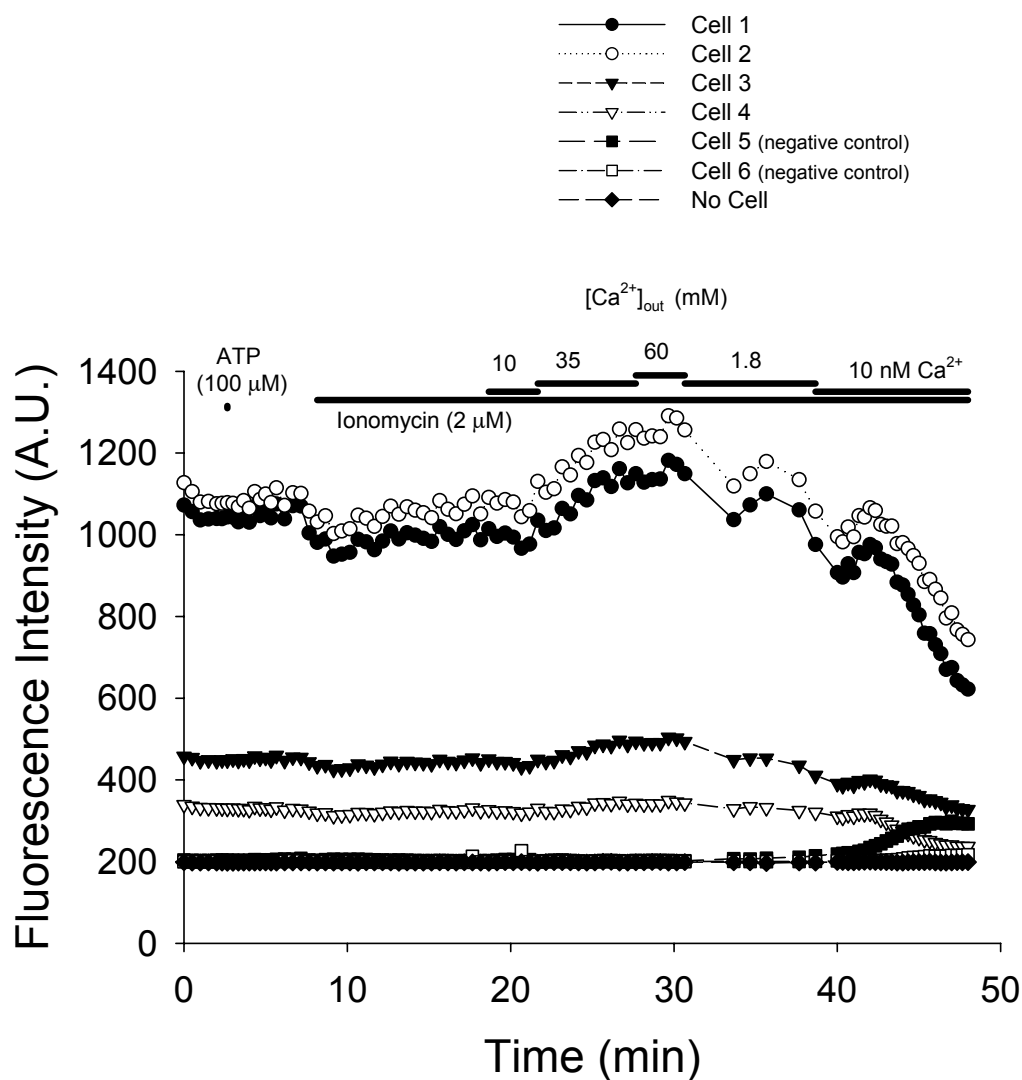


Fig 6.7 Calcium response of Site 1 expressed in HeLa cells at 30 °C for 72 hrs after transfection obtained on the Nikon inverted epifluorescence microscope at UC Riverside by Dr. Monica Lurtz. The fluorescence signal increase of Site 1 indicates that the protein is responding to calcium changes in the cells.

BamH1 site so that the gene was simply subcloned into the vector to add the calreticulin sequence.

After this process was complete, the targeting was tested by cotransfection with DsRed2-ER (Clontech). Imaging of the two proteins revealed complete colocalization, implying that the sensor was successfully targeted to the ER (Fig 6.8).

6.4.3 Response of Site 1 to ER calcium release

When the ER was stimulated to release calcium by ATP and histamine addition, no appreciable change due to the calcium release was observed (Fig 6.8). Site 1 illustrated photobleaching that was stronger than the calcium release response. The confocal instrument, due to the use of lasers, is a very strong illuminator so the construct was also tested by inverted epifluorescence at UC Riverside. As shown in figure 6.9, the control experiment of EGFP-ER does not indicate a calcium response with no appreciable changes in the fluorescence signal upon introduction of high ionomycin, utilized to permeate the ER membrane and allow calcium release. The changes observed with an increase in extracellular calcium concentration also occur with the baseline cells not expressing EGFP-ER, signifying that the changes are an artifact. As shown in figure 6.10, Site 1-ER responds to calcium changes in the cell by exhibiting a decrease in fluorescence signal with ER calcium release. The fluorescence signal then increases with an increase in extracellular calcium, which refills the ER stores and likely causes more calcium to enter the ER since the ionomycin permeates the ER membrane. This data strongly suggests that Site 1-ER responds to intracellular calcium changes in both the cytosol and in the ER. In comparison to 177-ER, it is likely

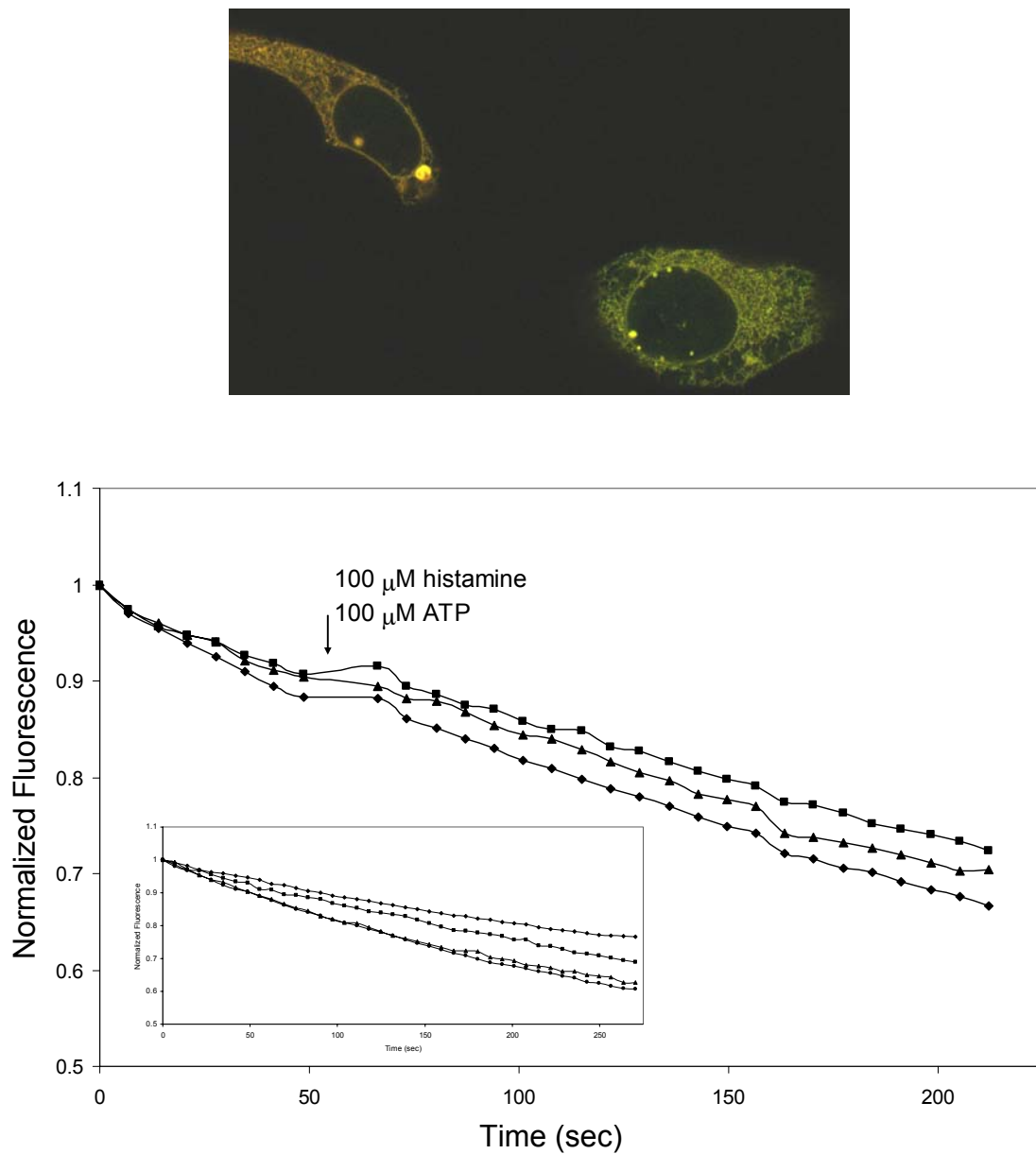


Fig 6.8 ER targeted Site 1 cotransfected with DsRed2-ER (top). The intensities of the two proteins are not the same in both cells so one of the cells appears more green than orange. The graph illustrates the imaging from calcium release experiments with ATP and histamine. The inset graph is a bleaching control with no additions or induced calcium release.

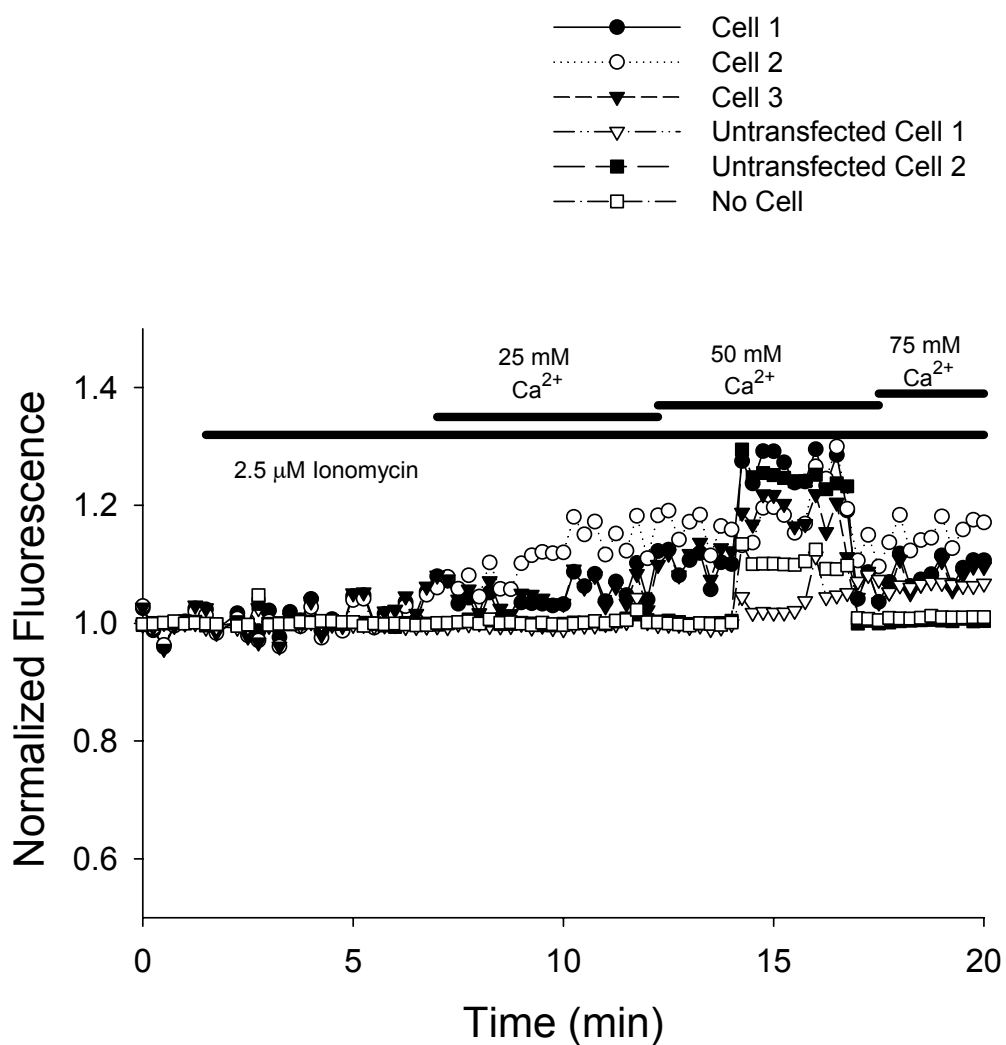


Fig 6.9 Control experiments of EGFP-ER expressed in HeLa cells at 30 °C for 48 hrs after transfection. The only fluorescence signal changes observed for this protein are artifacts, as suggested by the changes observed for the baseline traces. Addition of a high concentration of ionomycin should permeate the ER membrane and allow calcium release, but EGFP does not respond to calcium changes in the cell.

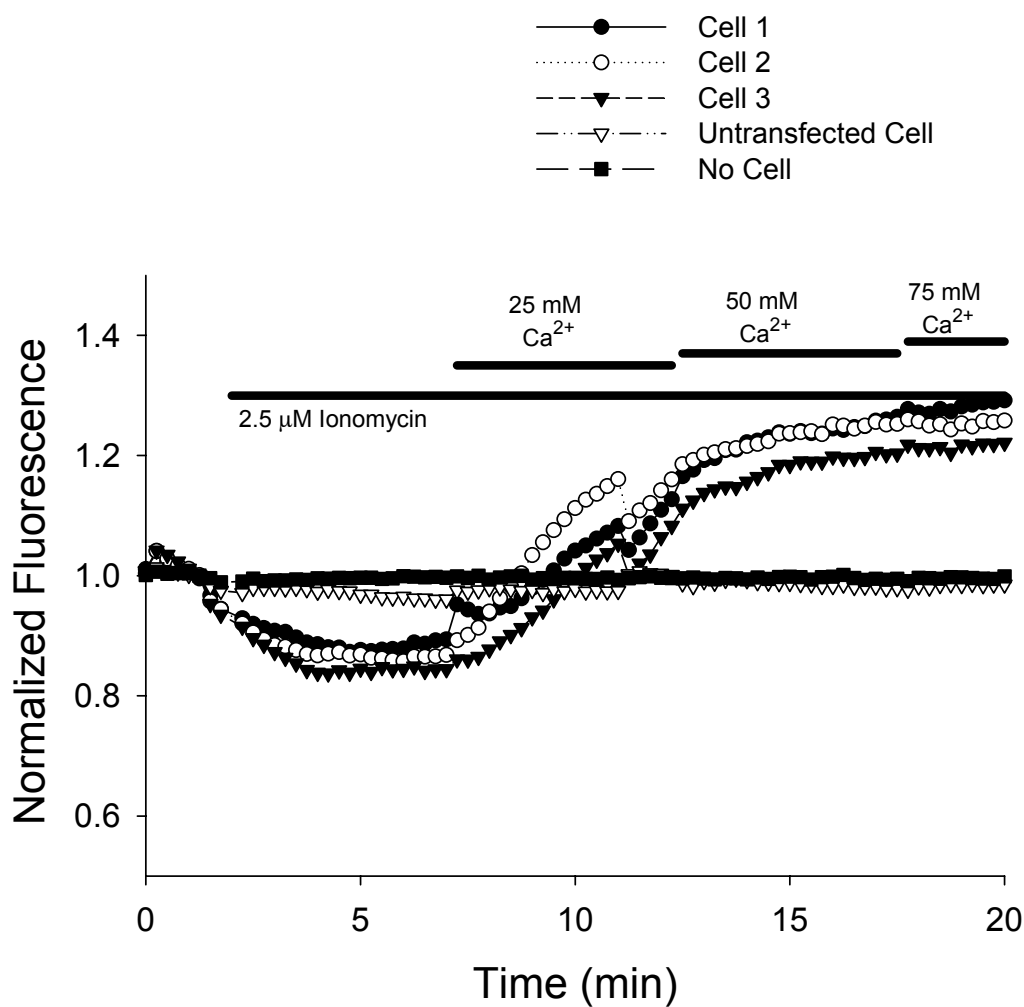


Fig 6.10 Fluorescence imaging for calcium response of Site1-ER expressed in HeLa cells at 30 °C for 72 hrs after transfection. Addition of a high concentration of ionomycin should permeate the ER membrane and allow calcium release, which is observed with a decrease in fluorescence signal. Addition of high extracellular calcium should refill the calcium stores in the ER and likely cause a higher concentration of calcium to enter the ER, which is indicated by a fluorescence increase of Site 1-ER.

that Site 1 has a weaker binding affinity since it is able to indicate calcium response in the ER whereas 177 does not display a fluorescence change when expressed in the ER.

6.5 Site 1 in Vitro Profile and Calcium Response

6.5.1 Preparation, expression and purification from HeLa cells

To express Site 1 in mammalian cells for purification, another vector His/pcDNA4 was utilized. This vector is very similar to pcDNA3.1+ but it encodes a 6x histidine tag at the N-terminal of the protein for ease of purification. Since the histidine tag purification protocols were well established in our laboratory, this vector and means of purification were chosen. Site 1 in the His/pcDNA4 vector was expressed in HeLa cells for 6 days after transfection in suspension culture after harvesting from a 175 cm² T-flask at 30 °C to obtain enough protein for *in vitro* characterization. In normal circumstances, it would be best to express in bacteria because bacteria will produce a large amount of protein, but, since these designed sensors are not fluorescent in bacteria, it is best to use mammalian cells for the expression. In addition, the folding in bacteria is different so the characterization needed to be performed with the same protein that was being tested by microscopy. Expression in mammalian cells does not yield a large amount of protein, but these sensors are bright enough that small amounts are measurable. EGFP can saturate the fluorimeter linear range at 1 μ M.

After expression, the cells were harvested from the dish by trypsinization and sonicated to break the cell membrane and release the protein. Protein purification was

attempted by binding to the nickel chelating column with the protocol utilized for bacterial expressed protein (Chapter 4), as shown in figure 6.11. Elution of the protein did not yield pure protein as all of the HeLa proteins had also remained in the column and eluted with Site 1, as shown in figure 6.11. The protein was then bound to the Hitrap Q anion exchange column (Chapter 4) with the same results as for the nickel chelating column with many contaminant proteins evident in each of the fractions.

Another approach was then taken to try to purify the protein by partitioning the samples by molecular weight. Initially, a 10 KDa centricon was utilized to remove salt from the sample along with any small molecule proteins or peptides. The sample was exchanged in this manner with buffer (10 mM Tris, 1% glycerol, pH 7.4) numerous times, approximately 10-15, until it was certain that all small molecules were removed. Then, a 50 KDa centricon was utilized to allow Site 1 to pass through the membrane but keep the larger proteins, such as albumin, in the original sample. After half of the sample was exchanged in this way, it was collected and concentrated to 1 mL with the 10 KDa centricon. A gel of this process is shown in figure 6.12. The lack of protein observed in the sample after concentration of the 50 KDa exchange indicates that Site 1 did not pass through the membrane as was expected. Some precipitation was observed during the exchange process, which may have been due to Site 1. The sample was then dialyzed overnight against 2 L of 10 mM Tris, 1 mM DTT, 1% glycerol, pH 7.4 to try to remove any contaminants that may have been causing the precipitation. The protein appeared to have precipitated in the bag during dialysis, which would have allowed for separation by centrifugation and refolding with urea. However, when the

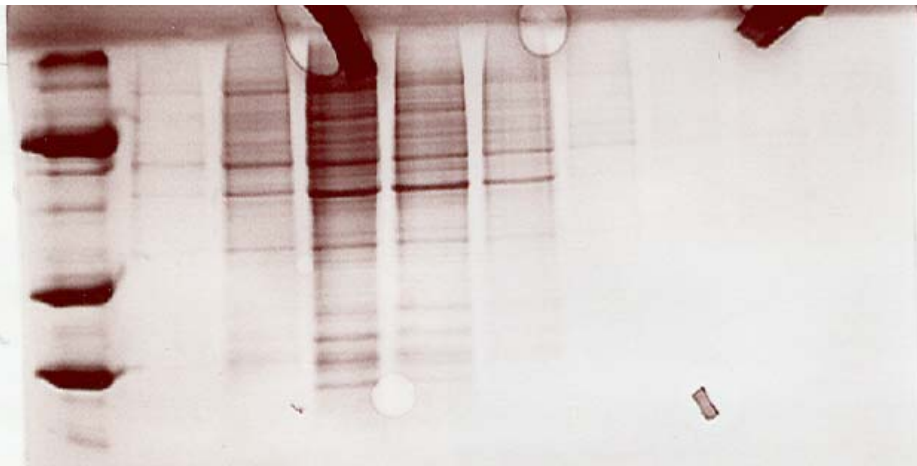


Fig 6.11 SDS-PAGE gels of the purification of Site 1-His/pcDNA expressed in suspended HeLa cells. The top gel is the fractions during the binding of Site 1 to the column. Initially, much of the protein did not bind to the column. The bottom gel is the elution from the nickel chelating column, indicating that the protein is not pure. In addition, distinguishing the Site 1 band is difficult since it is not overexpressed as it would be in bacteria and there is no distinct band at 30 KDa.

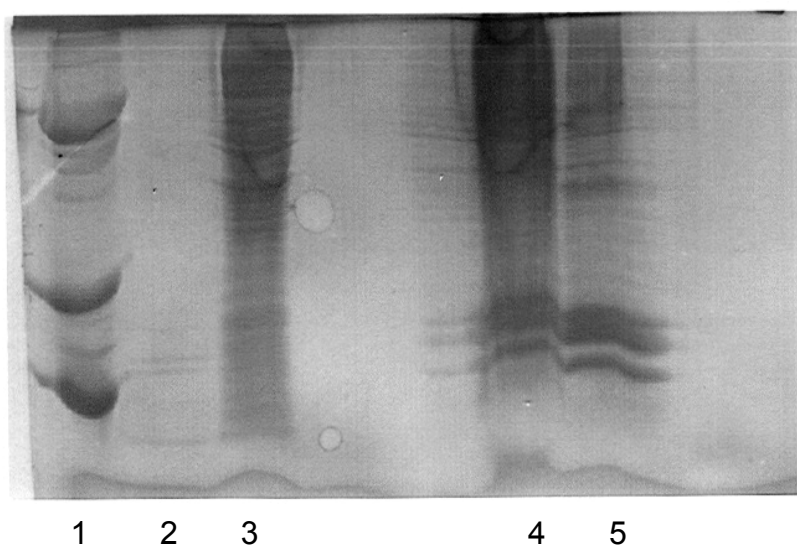


Fig 6.12 SDS-PAGE gel of the partitioning by molecular weight of Site 1 expressed in HeLa cells. Lane 1 is the marker, lane 2 is the concentrated sample after exchange with the 10 and 50 KDa centricones, lane 3 is the exchange with the 10 KDa centricon, lane 4 is the cell pellet before sonication, lane 5 is the cell pellet after sonication. The lack of protein observed in lane 1 indicates that Site 1 did not pass through the membrane as was expected.

protein was transferred to a falcon tube, the protein resolubilized. Repeated attempts at purifying this protein were not successful.

6.5.2 Fluorescence profile of Site 1

Since the protein could not be purified, a fluorescence profile was obtained with the cell lysate after sonication. Since HeLa cells do not normally express fluorescent proteins, any fluorescence observed with the mixture should be due to Site 1. The excitation and emission profiles were obtained as shown in figure 6.13. Initially, the emission was set to 510 nm and the excitation profile was obtained. A large peak at 398 nm was observed but no peak at 482 nm, as is normal for EGFP. The excitation was then set to 398 nm and an emission scan was performed from 420 nm to 580 nm. It was observed that the emission of Site 1 expressed in HeLa cells occurred at 465 nm, between the two peaks (450 nm and 510 nm) normally observed for EGFP. Excitation at several wavelengths did not result in a wavelength shift in the emission indicating that the peak was not an artifact or due to some water scattering as occurs for excitation at 320 nm and 357 nm. The likely explanation for the emission difference is that the mutations made to form the binding site shifted the equilibrium of the neutral and anionic states more towards the neutral since excitation occurs at 398 nm, the neutral peak. The emission of the neutral peak at low pH is at 450 nm. Perhaps the chromophore environment was changed by the introduction of the binding site so that emission of the neutral peak is red shifted to 465 nm and the chromophore does not undergo excited state proton transfer as EGFP does so the primary emission is not observed at 510 nm.

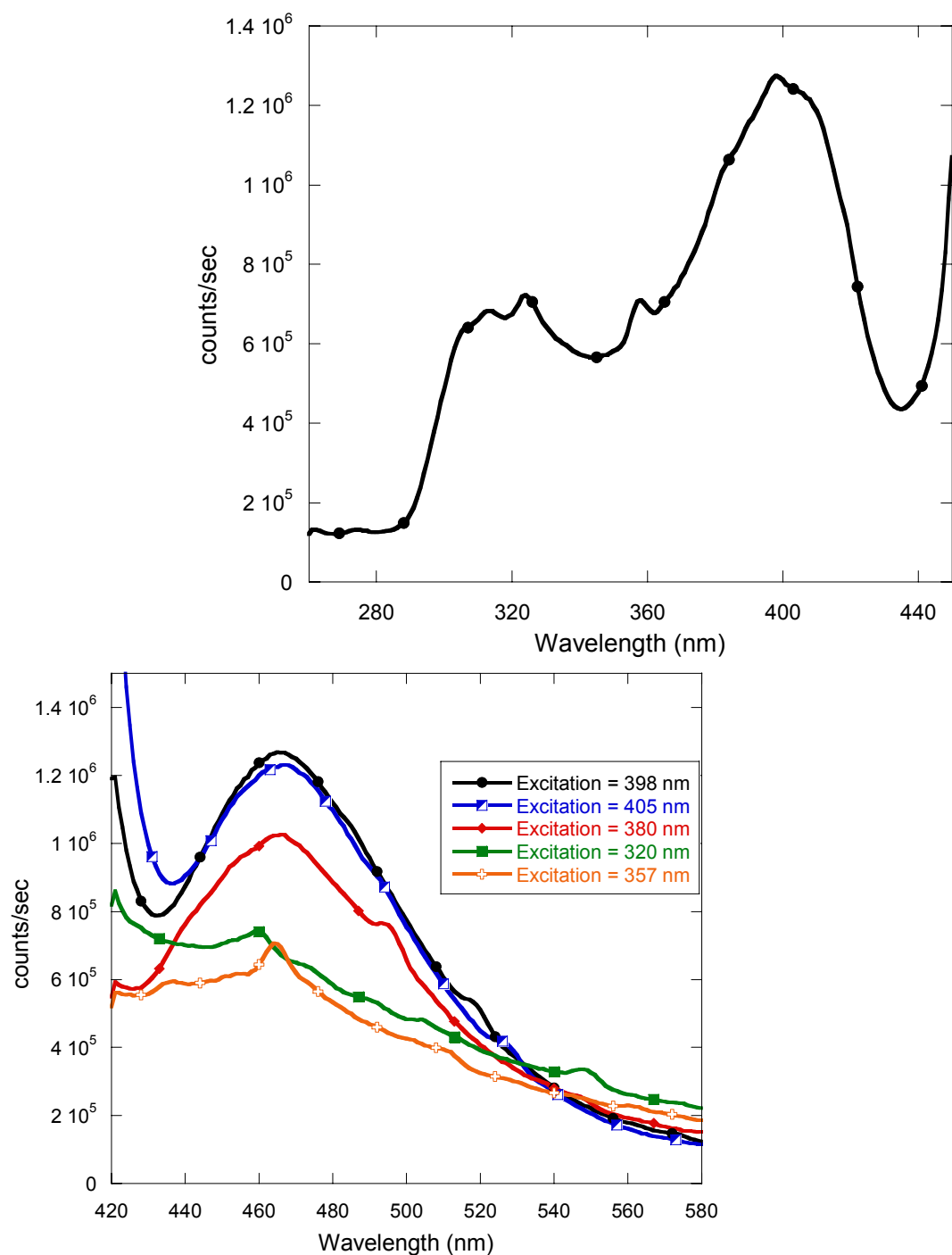


Fig 6.13 Excitation (top) spectrum with emission at 465 nm and emission (bottom) spectra at various excitations for Site 1 cell lysate (in 10 mM Tris, 1 mM DTT, 1% glycerol, pH 7.4) after expression in HeLa cells. The excitation and emission profiles differ from EGFP.

6.5.3 Calcium response of Site 1 *in vitro*

The calcium induced change to Site 1's spectra was measured by addition of calcium in 100 μ M increments and the excitation and emission spectra were monitored as shown in figure 6.14. The excitation with emission at 465 nm was observed to increase with increasing calcium concentration until the signal saturated at 600 μ M calcium. The emission intensity at 465 nm, with excitation at 398 nm, also increased with calcium until saturation was reached at 600 μ M. This result suggests that the increase in fluorescence signal observed *in vivo* is due to calcium response. The data could not be fit to a 1:1 binding equation.

6.6 Creation of Site 1 cycle 3

Although Site 1 was bright enough to measure, it consistently photobleached during experiments. Since the ER calcium release could not be measured due to the photobleaching, the cycle 3 mutations were added to improve the fold of the protein and to allow for a brighter sensor. Brighter sensors do not demonstrate photobleaching as drastically as the more weakly fluorescent sensors, as observed by Dr. Jin Zou's results on our laboratory. The mutations, F99S, M153T, and V163A, were added as detailed in Chapter 5 with M153T/V163A completed in one PCR round by Angela Holder, a M.S. student in our laboratory. The F99S mutation was then included, also performed by Angela Holder.

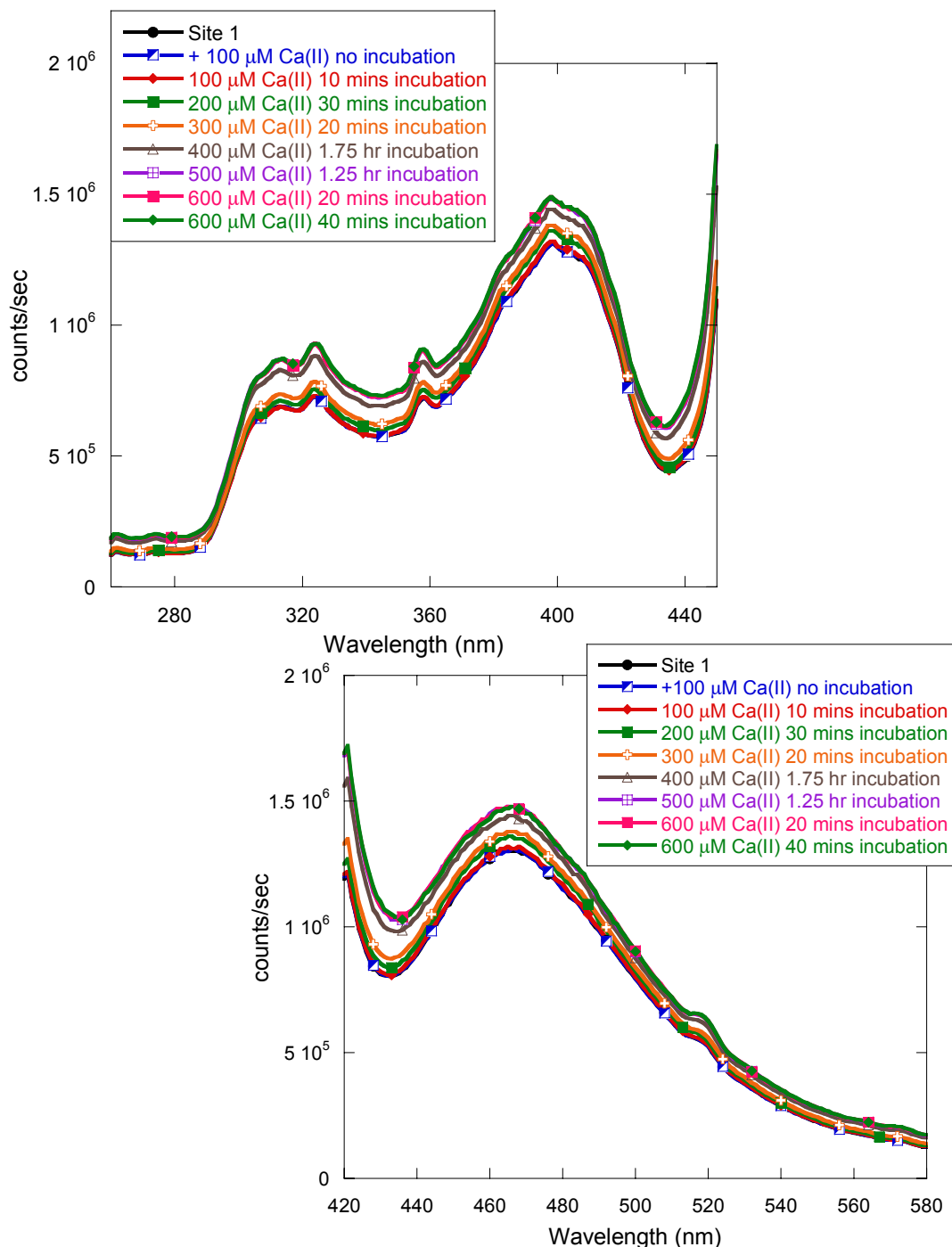


Fig 6.14 Excitation (top) spectra with emission at 465 nm and emission (bottom) spectra with excitation at 398 nm of Site 1 cell lysate (in 10 mM Tris, 1 mM DTT, 1% glycerol, pH 7.4) after expression in HeLa cells. The fluorescence signal increases with increasing calcium until saturation is reached at 600 μM .

6.6.1 Comparison of Site 1 and Site 1-M153T/V163A

The original Site 1 was compared to Site 1-M153T/V163A in fluorescence intensity and chromophore formation by expression in HeLa cells for 48 and 72 hrs after transfection at 30 °C and 37 °C. As shown in figure 6.15, Site 1 produces fluorescence when expressed in HeLa cells at 30 °C and 37 °C, but the intensity with expression at 30 °C is on average 8 times brighter than that of expression at 37 °C when the data is normalized for exposure time. Expression of Site 1-M153T/V163A at 30 °C and 37 °C in HeLa cells both yield brighter fluorescence than expression of Site 1 in HeLa cells as shown in figure 6.16. At 30 °C, Site 1-M153T/V163A is twice as bright as Site 1 and 1.5 times as bright as Site 1-M153T/V163A expressed at 37 °C. At 37 °C, Site 1-M153T/V163A is 10 times brighter than Site 1. The addition of these two mutations to the designed calcium binding sensor allows for expression of the protein at physiological temperatures, an advancement in the design of our sensors. Interestingly, EGFP does not produce fluorescence when expressed at 37 °C, but Site 1 does. This may be due to the S2D mutation since the L194N/S86D mutations of site 194b (Chapter 4) did not produce fluorescence at 37 °C.

Figures 6.17 and 6.18 are examples of Site 1 and Site 1-M153T/V163A expressed in HeLa cells for 72 hrs at both 30 °C and 37 °C. Site 1-M153T/V163A is 6 times brighter than Site 1 when expressed at 37 °C, but they begin to display the same average intensity with expression at 30 °C. However, there are a greater number of very bright cells for Site 1-M153T/V163A at 30 °C than for Site 1. The saturated cells are not normally included in calculating the average intensity of a region of interest;

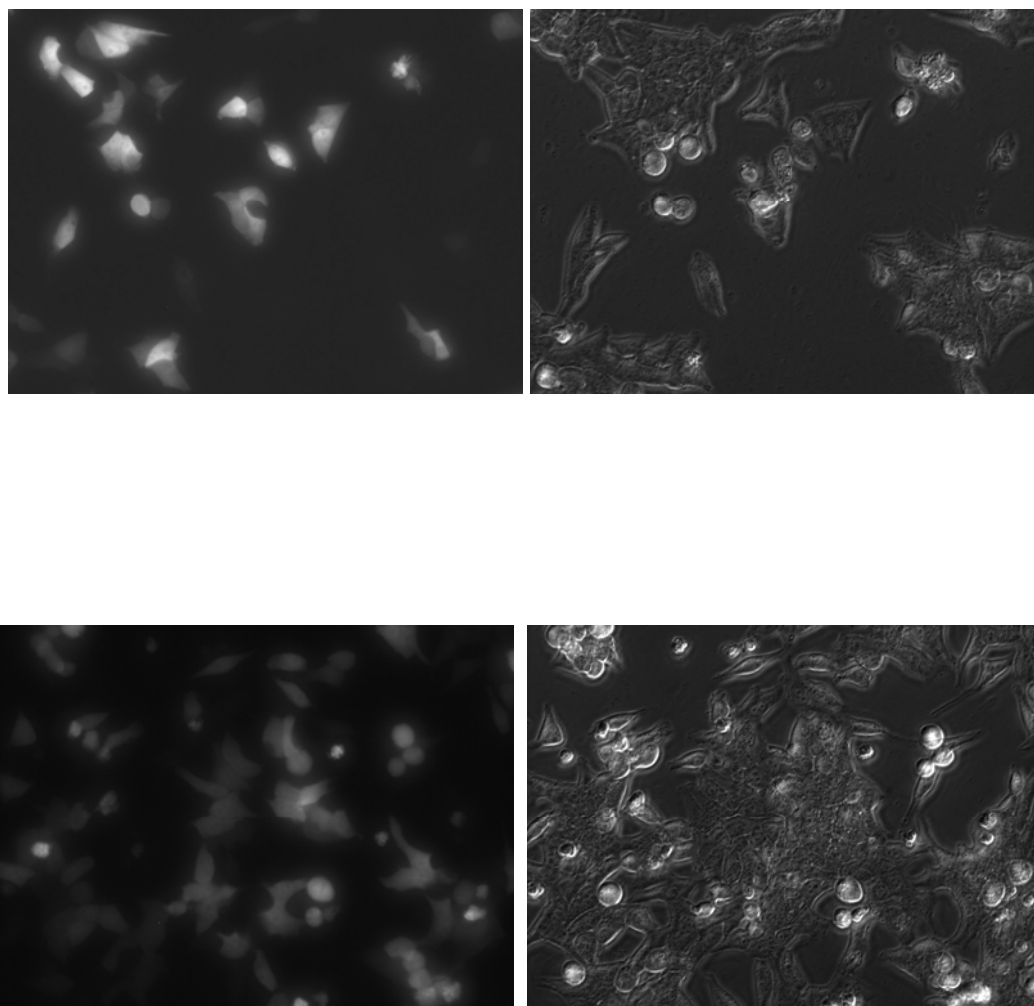


Fig 6.15 Images at 20x magnification of Site 1 expressed in HeLa cells at 30 °C (top) and 37 °C (bottom) for 48 hr after transfection. The left images are fluorescence with the FITC filter (top is 500 ms, bottom is 2000 ms), and the right images are transmitted light.

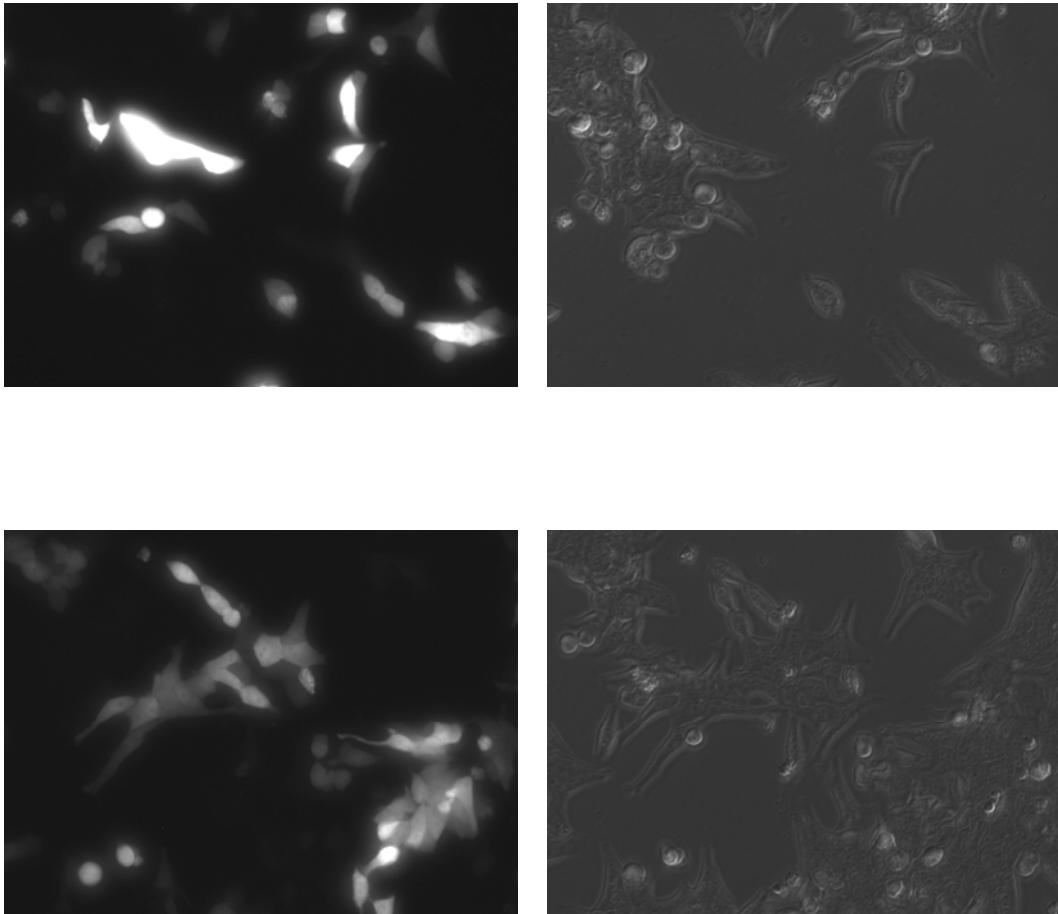


Fig 6.16 Images at 20x magnification of Site 1-M153T/V163A expressed in HeLa cells at 30 °C (top) and 37 °C (bottom) for 48 hr after transfection. The left images are fluorescence with the FITC filter and 500 ms exposure, and the right images are transmitted light.

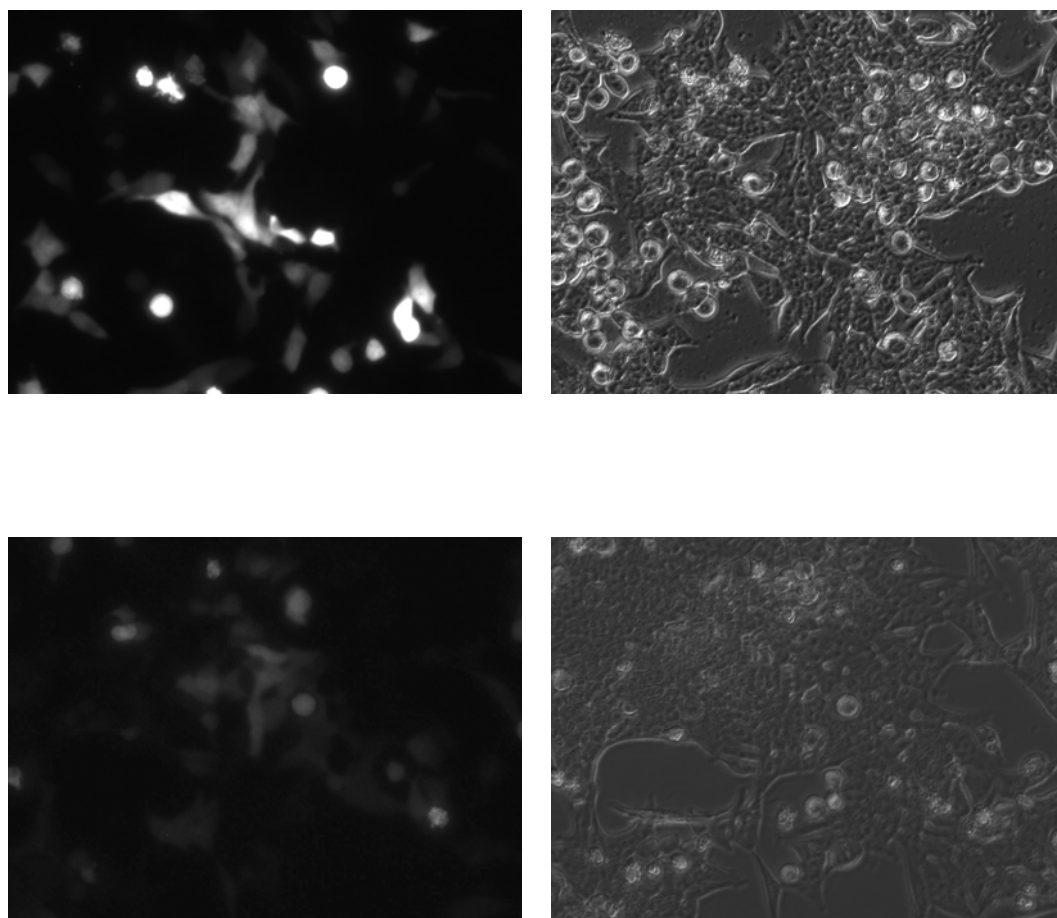


Fig 6.17 Images at 20x magnification of Site 1 expressed in HeLa cells at 30 °C (top) and 37 °C (bottom) for 72 hr after transfection. The left images are fluorescence with the FITC filter (top is 500 ms, bottom is 1000 ms), and the right images are transmitted light.

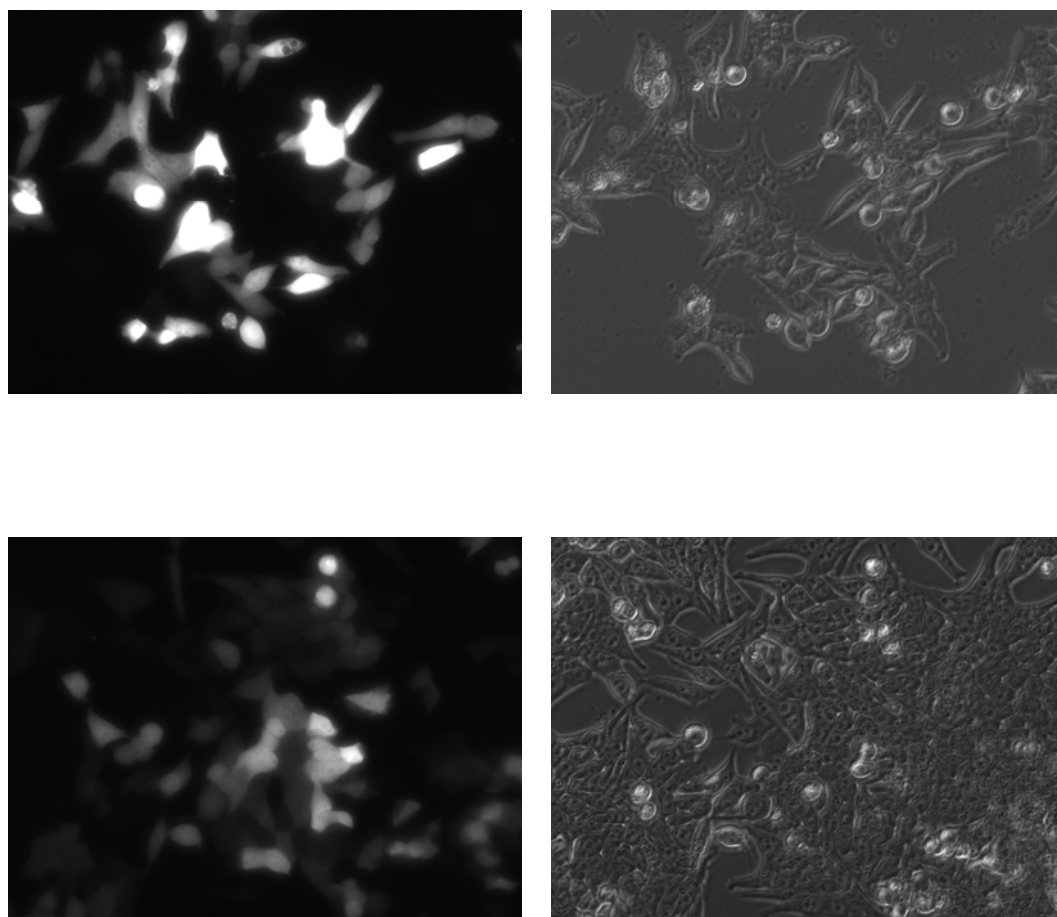


Fig 6.18 Images at 20x magnification of Site 1-M153T/V163A expressed in HeLa cells at 30 °C (top) and 37 °C (bottom) for 72 hr after transfection. The left images are fluorescence with the FITC filter with 500 ms exposure, and the right images are transmitted light.

therefore, the average intensity is the same but the number of saturated cells for Site 1-M153T/V163A is greater than Site 1. From this data, there is no doubt that the mutations M153T and V163A are quite useful in engineering brighter sensors so that less excitation light may be used with shorter exposure times.

6.6.2 Bacterial expression and purification of Site 1-M153T/V163A

Since Site 1-M153T/V163A indicated very bright fluorescence in mammalian cells even when expressed at 37 °C, it was expressed in bacteria by Angela Holder to produce enough protein to obtain a K_d by both chromophore fluorescence change and by the dye competition assay with Rhodamin-5N (Chapter 4). The temperature was reduced to 30 °C after induction and the cells were incubated overnight with agitation to allow the protein enough time to produce a mature chromophore. Fluostar results of the expression indicated that the protein was fluorescent, as shown in figure 6.19. The high expression yield of the protein is indicated by SDS-PAGE with a large band observed at 33 KDa, as shown in figure 6.20.

After expression, the protein was then purified in conjunction with Angela Holder with the nickel chelating column and the Hitrap Q anion exchange column on the FPLC. The expression yield was so high that the purification had to be repeated twice to produce >95% pure protein. The protein was dialyzed in 10 mM Tris, 1 mM DTT, 1% glycerol, p 7.4 after the anion exchange column to remove the excess salt.

6.6.3 Fluorescence of Site 1-M153T/V163A

The fluorescence of Site 1-M153T/V163A was examined on a PTI lifetime fluorimeter, as detailed in chapter 2. The excitation spectrum was obtained with

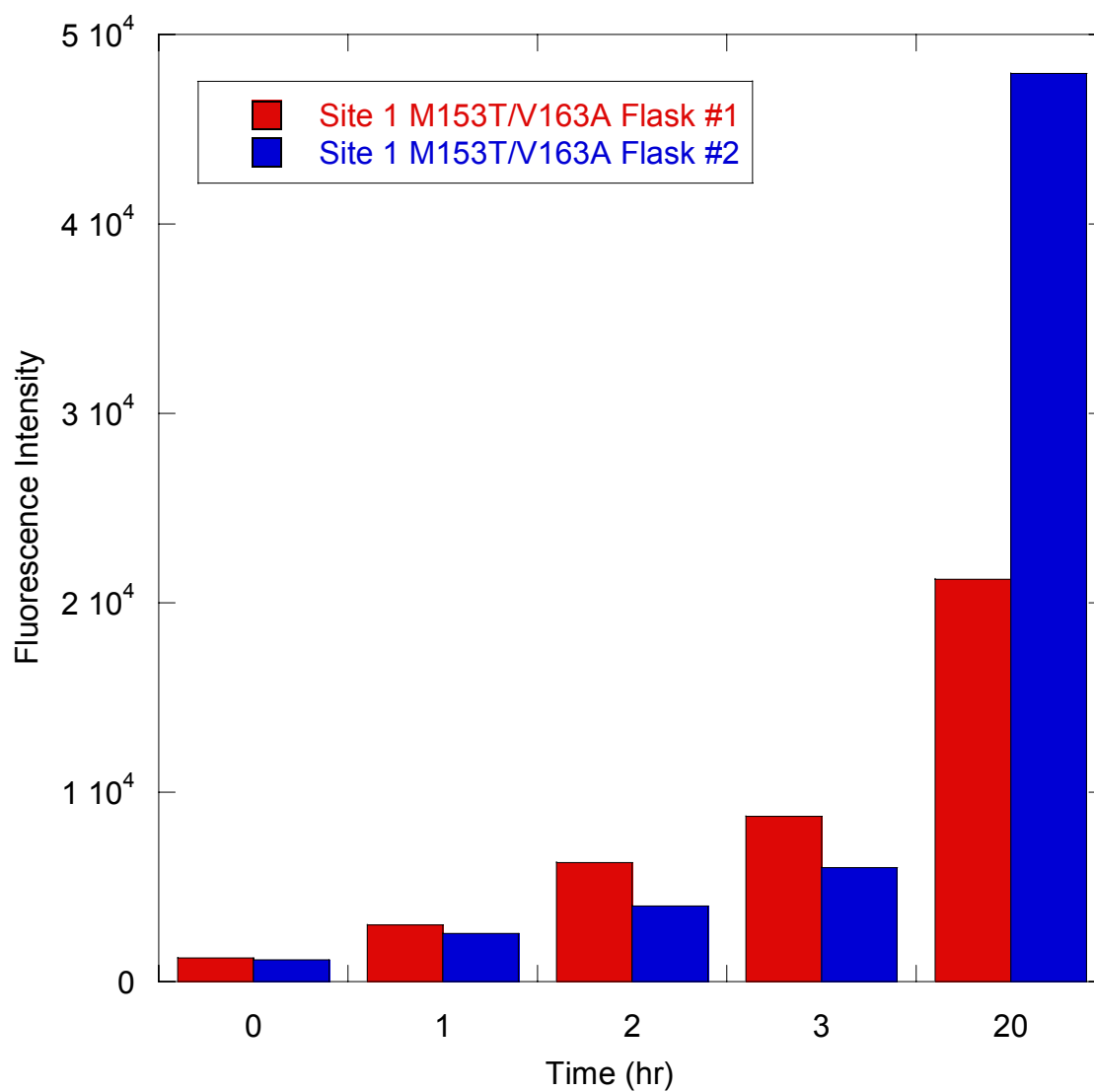


Fig 6.19 Fluostar microarray results of the expression of Site 1-M153T/V163A indicating that the protein is fluorescent when expressed in bacteria overnight at 30 °C.

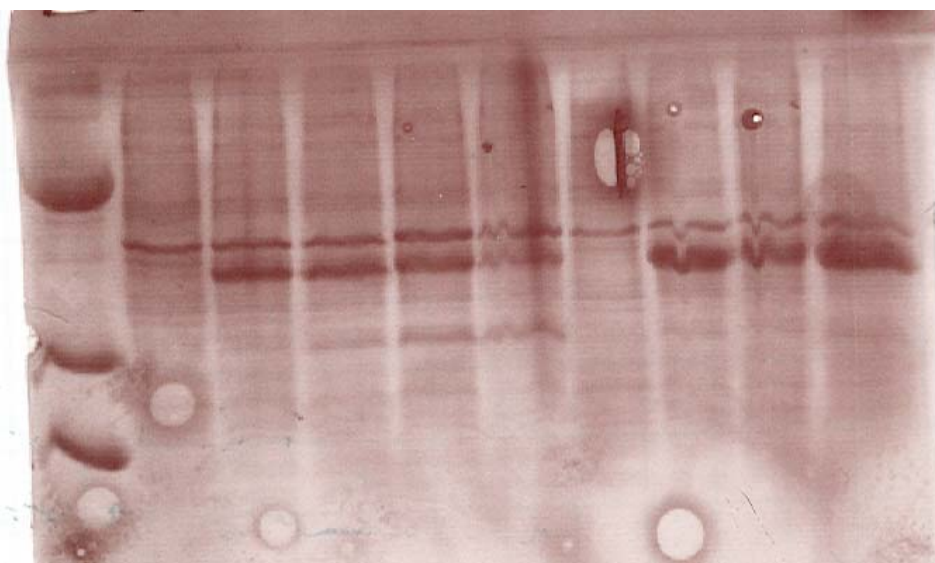


Fig 6.20 SDS-PAGE gel of the expression of Site 1-M153T/V163A in *E. coli* indicating the high expression yield of the protein.

emission at 510 nm as shown in figure 6.21. The emission spectra were obtained with excitation at 398 nm (Fig 6.21) and 482 nm (Fig 6.22). The fluorescence of the protein is highly similar to EGFP, suggesting that the two mutations allow for proper chromophore formation of the designed protein when expressed in bacteria.

6.6.4 Calcium response of Site 1-M153T/V163A

Site 1-M153T/V163A was tested for calcium response by addition of calcium and measurement of the excitation and emission spectra after each calcium addition (Figs 6.21 and 6.22). The 510 nm emission with excitation at 482 nm was observed to decrease with increasing calcium while the 510 emission with excitation at 398 nm did not change with calcium. A fit of the decrease at 510 nm with excitation at 482 nm with the 1:1 binding equation (Eq 2.3) supplied an average K_d of $107 \pm 13 \mu\text{M}$. This binding affinity is similar to the first generation of designed sites, which displayed binding affinities of 50-100 μM by dye competition. However, measurement of 177c3 calcium induced changes *in vitro* did not yield as strong an effect on the chromophore as Site 1-M153T/V163A exhibits. This finding represents great progress towards our goal of designing intrinsically fluorescent calcium sensors with calcium induced changes in the chromophore at low concentrations of calcium.

6.6.5 Competition assay with Rhodamine-5N and Site 1-M153TV163A

To measure the intrinsic binding affinity of the designed site rather than the binding affinity obtained by the binding event's effect on the chromophore, a dye competition assay was utilized as detailed in Chapter 4. Site 1-M153T/V163A and

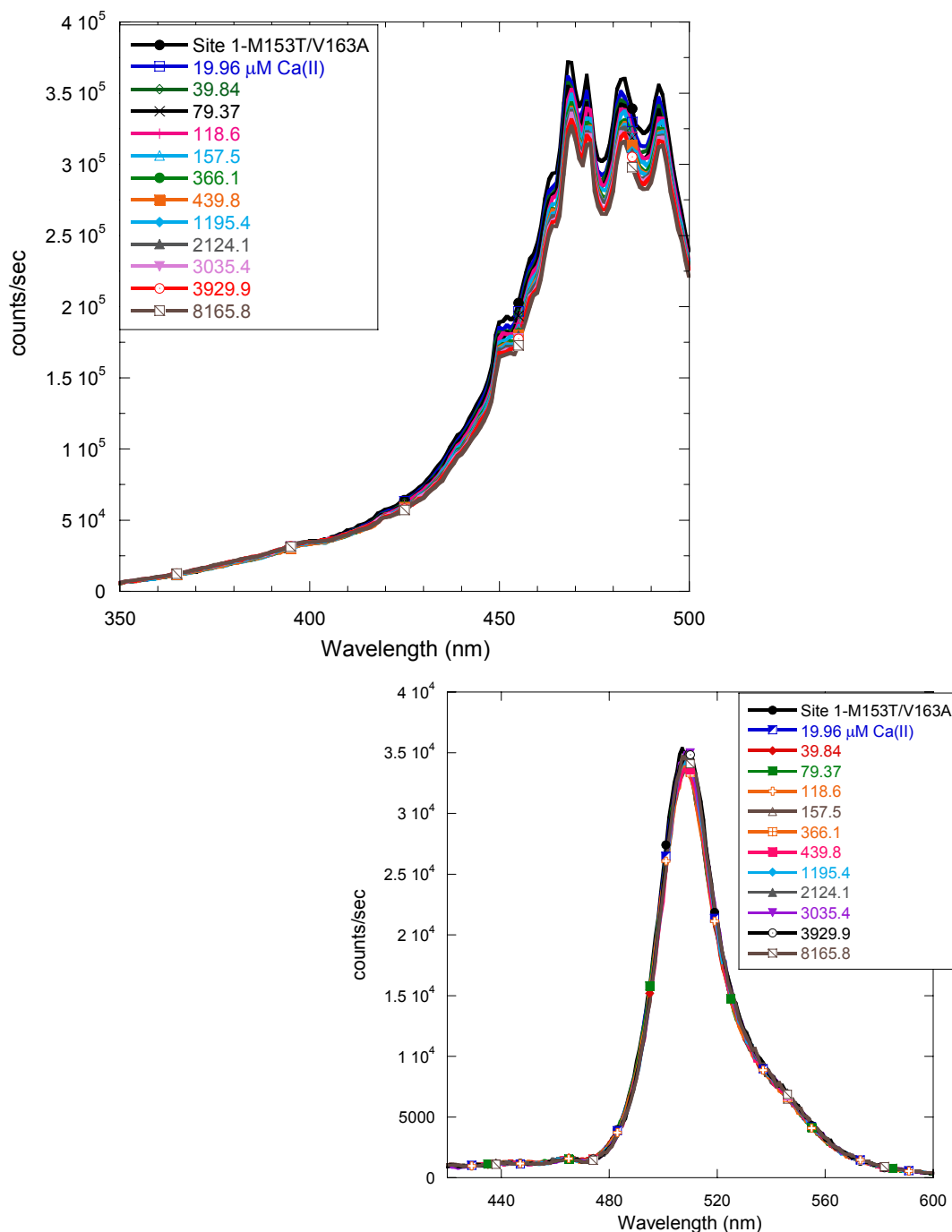


Fig 6.21 Excitation with emission at 510 nm (top) and emission with excitation at 398 nm (bottom) spectra of Site 1-M153T/V163A with calcium after expression in *E. coli*. The excitation and emission are highly similar to EGFP. The experiments were performed in 10 mM Tris, 1 mM DTT, 1% glycerol, pH 7.4. The excitation spectrum changes with increasing calcium, but the emission at 510 nm with excitation at 398 nm does not.

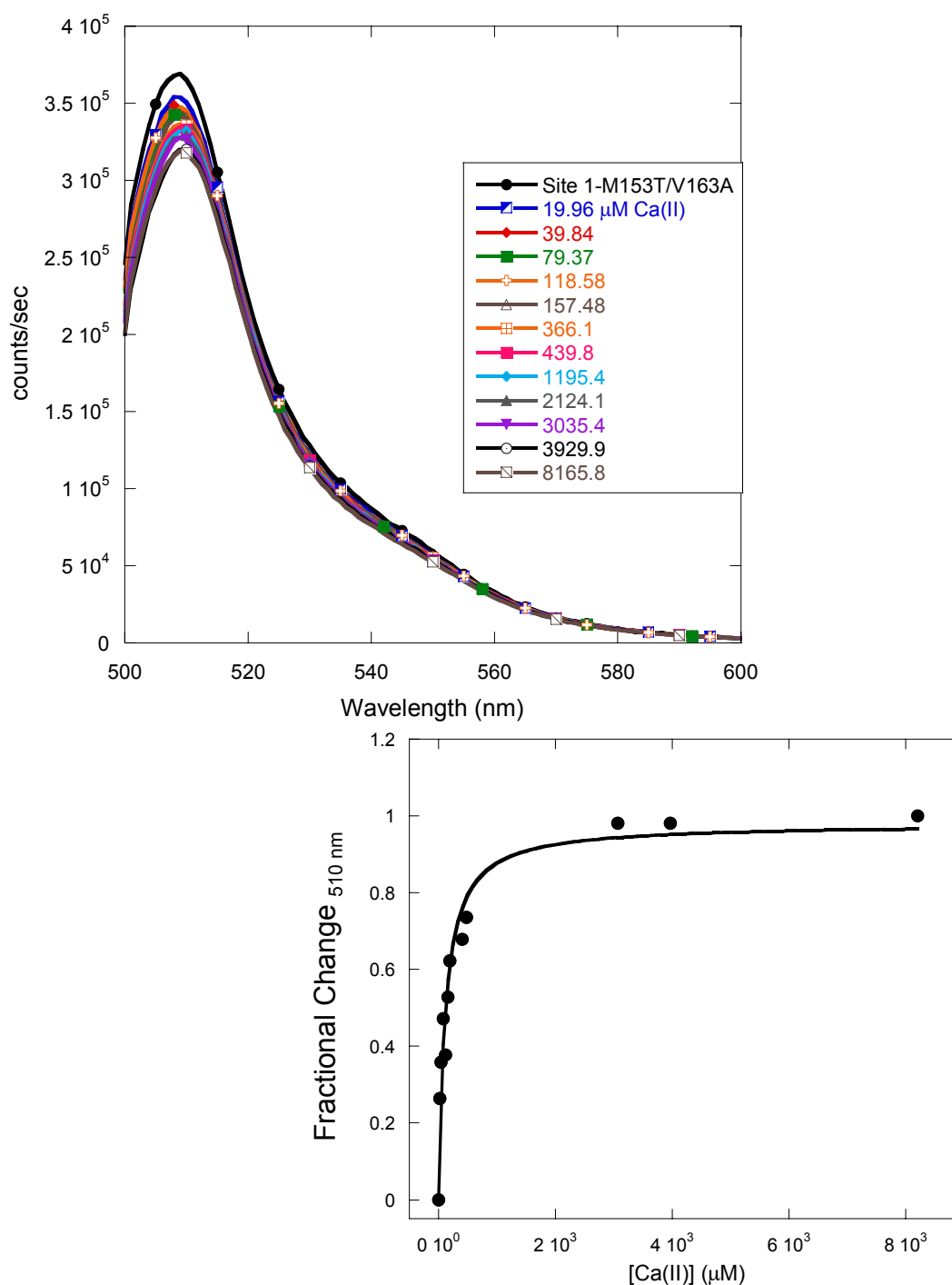


Fig 6.22 Calcium induced chromophore emission change for Site 1-M153T/V163A expressed in *E. coli* with excitation at 482 nm in 10 mM Tris, 1 mM DTT, 1% glycerol, pH 7.4. The fit of the data with the 1:1 binding equation (Eq 2.3) is shown (bottom) and produces a K_d of 107 μM .

Rhodamine-5N were titrated with calcium and the Rhodamine-5N fluorescence at 578 nm was measured with excitation at 552 nm as shown in figure 6.23. The buffer for this experiment was 10 mM Tris, 1 mM DTT, 20% glycerol, pH 7.4. The higher glycerol was utilized because the stock protein was stored in 20% glycerol and the concentration was only 31 μ M, which was the concentration needed for the competition. A control of Rhodamine-5N in the same conditions as the competition samples was performed to ensure that the binding affinity was not affected by the addition of 20% glycerol and to measure the binding affinity in these conditions. Rhodamine-5N exhibited a K_d of 61.3 μ M. After the titration, the data was fit as shown in figure 6.24 using Specfit/32 to obtain the protein's K_d , which was 107 μ M for one sample and 21 μ M for the second sample. The data fit of the second sample is not good, but the fit for the first sample is flawless so the K_d is likely \sim 100 μ M. In addition, the binding affinity obtained by calcium's effect on the chromophore is in agreement with the 100 μ M binding affinity. Repetition of this result will be completed by Angela Holder to be included in her Master's thesis.

6.7 Major Findings

The major findings of the second generation endeavor are several fold. First, there are several mutations that disrupt chromophore formation so that GFP is not fluorescent as detailed in table 6.2. Second, changing one residue in a non-fluorescent design site, such as 194b, can yield fluorescent protein, Site 1, that responds to calcium both *in vivo* and *in vitro*. This particular residue change, from using K79D to using S2D, seems to have yielded some ability for the protein to be fluorescent when expressed at

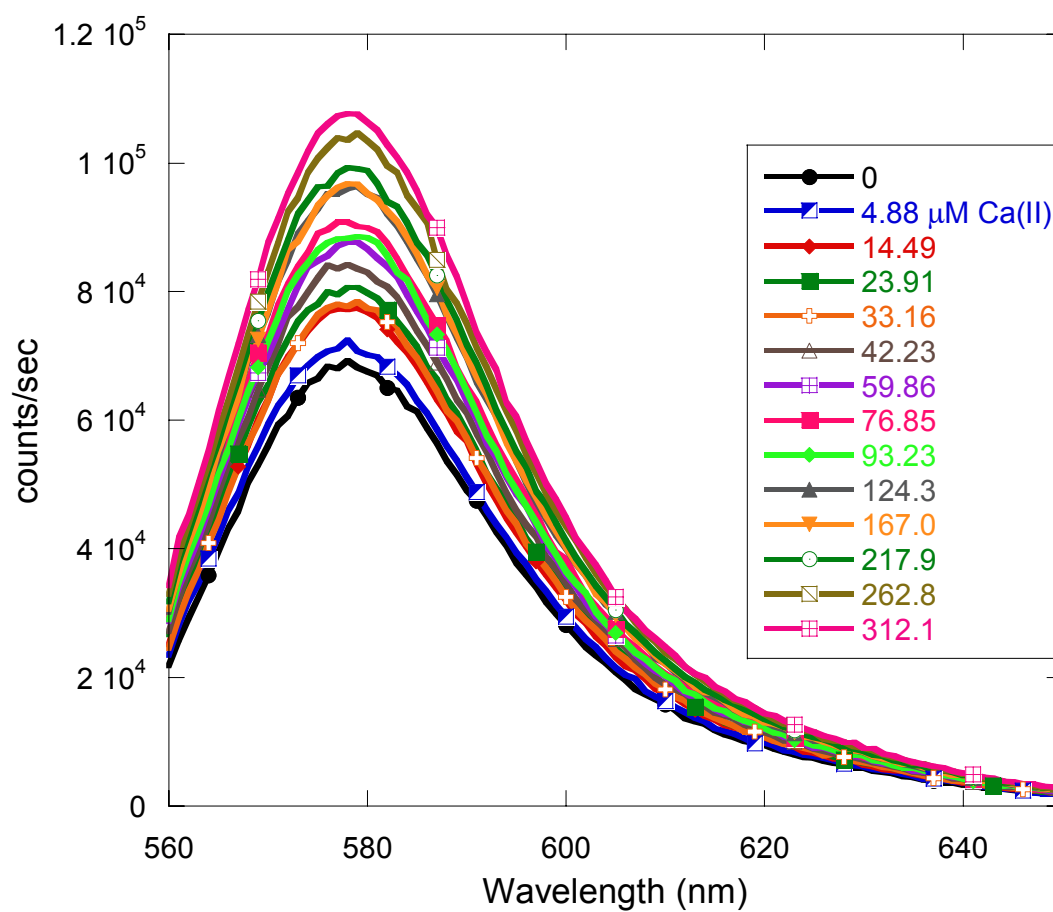


Fig 6.23 Rhodamine-5N competition with Site 1-M153T/V163A for calcium binding fluorescence emission with excitation at 552 nm. The experiment was performed in 10 mM Tris, 1 mM DTT, 20% glycerol, pH 7.4.

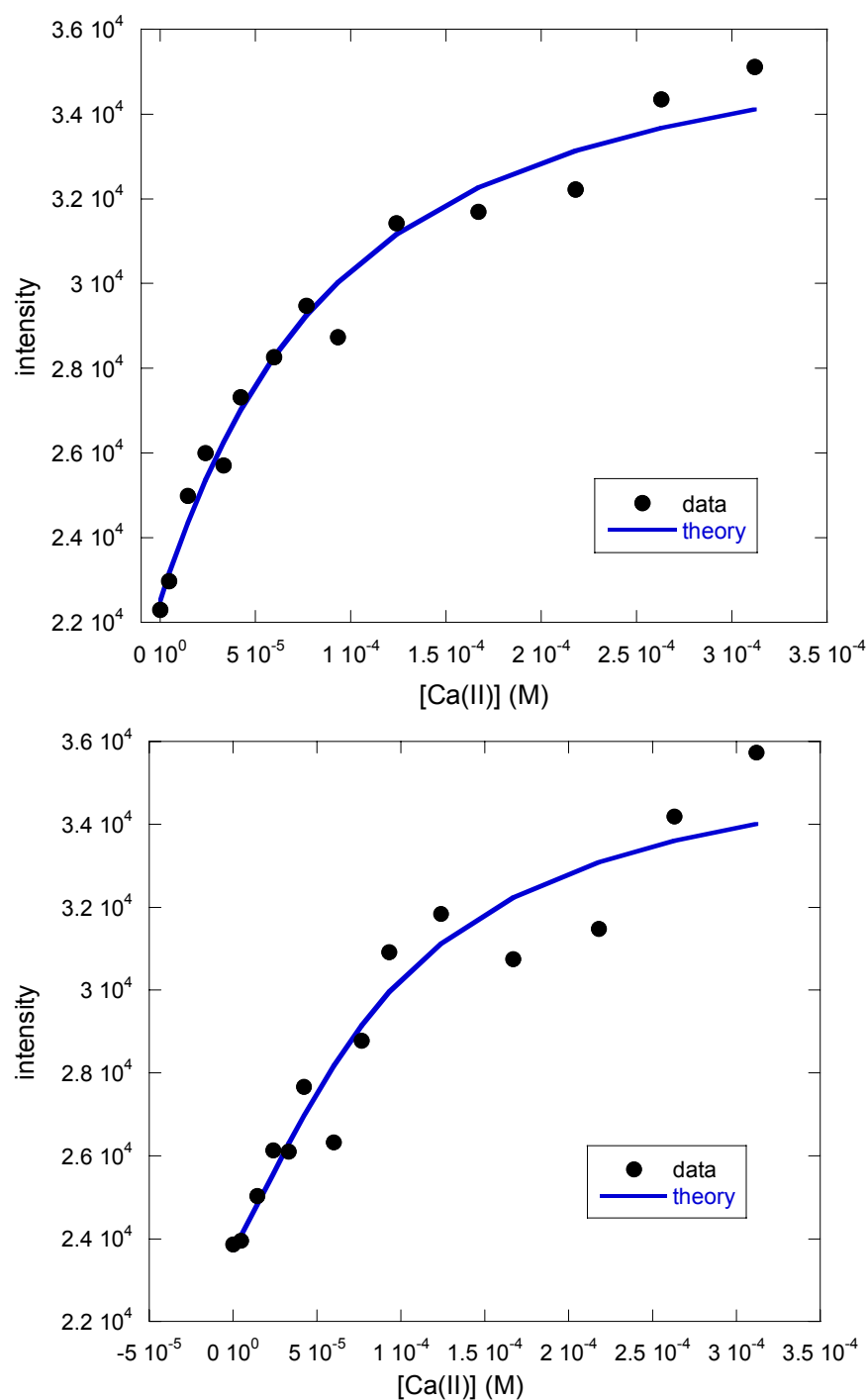


Fig 6.24 The two Specfit results of the competition between Site 1-M153T/V163A and Rhodamine-5N is shown. The top is the one sample that yields a very good fit with a K_d of $107 \mu\text{M}$ while the bottom graph is the sample with a poor fit and a K_d of $21 \mu\text{M}$.

physiological temperatures. Site 1 responds to calcium with a fluorescence signal enhancement both *in vivo* and *in vitro*, although the emission maximum seems to be shifted from that of EGFP. Since the filters in use on the microscopes have a wide bandwidth, the fluorescence can still be observed but efficient use of this protein would require special filters. The partial cycle 3 mutations, M153T and V163A, confer much more brightness to Site 1 and allow for protein expression at 37 °C in HeLa cells. These mutations also allow for fluorescent protein to be formed when expressed in bacteria. The spectral profile of Site 1 with these mutations is highly similar to EGFP, suggesting that the chromophore is the same and that the mutations do allow for the correct distances for chromophore formation as suggested by Zimmer (141). Site 1-M153T/V163A indicates chromophore fluorescence response to calcium with an average binding affinity of 107 μ M and an intrinsic calcium binding affinity of 100 μ M by dye competition. The brightness of this protein and the calcium response indicated by this protein will allow Site 1-M153T/V163A to be a useful and productive designed calcium sensor for future studies.

Chapter 7 Conclusions and Major Findings

7.1 Major Findings of the Designed Calcium-binding Proteins

Calcium binding green fluorescent proteins were rationally designed based on the ideal geometry of pentagonal bipyramid using the computer algorithm Dezymer to identify possible sites. Six sites, detailed in chapter 4, were selected for protein engineering based on the criteria discussed in chapter 4, such as flexibility of the site and the surrounding environment. A method of bacterial expression of the proteins with an attached 6x histidine tag, and purification using a nickel chelating column has been developed. The attached histidine tag does not interfere with calcium binding measurements with no change observed in the fluorescence on a non-calcium binding GFP with or without calcium. The histidine tag does, however, exhibit binding to nickel, zinc, copper, cadmium, and cobalt with a range of binding affinities from 6 μM to 50 μM .

The design sites 120, 177, 194a, and 194b all exhibit metal binding capability for calcium and terbium, which demonstrates the generality of our design approach when coupled with the CD2 work performed by others in our laboratory. The terbium binding affinities for bacterially expressed protein with the titrations performed in 20 mM PIPES, 10 mM KCl, 1 mM DTT, 1% glycerol, pH 6.8 are $4.9 \pm 0.2 \mu\text{M}$ for 120, $1.9 \pm 0.4 \mu\text{M}$ for 177, and $31.6 \pm 12.9 \mu\text{M}$ for 194a. Site 194b exhibits a terbium binding affinity of $2.9 \pm 0.3 \mu\text{M}$ when titrated in 10 mM Tris, 1 mM DTT, 1% glycerol, pH 7.4. The calcium binding affinities measured by Rhodamine-5N competition in 10 mM Tris, 1 mM DTT, 1% glycerol, pH 7.4 are $57.2 \pm 1.6 \mu\text{M}$ for 120, $59.7 \pm 4.8 \mu\text{M}$ for 177, $95.5 \pm 6.6 \mu\text{M}$ for 194a, and $37.7 \pm 4.5 \mu\text{M}$ for 194b. The difference in affinities for the calcium analog,

terbium, and for calcium likely result from the location of the binding sites, the ligand types involved in binding, and the local environment of the sites. Further modification of the binding sites could allow for tuning of the affinities to suit various needs, such as calcium measurement in cellular subcompartments.

Examination of the secondary structure of these proteins revealed native-like secondary β -sheet formation with negative maxima observed at 216 nm in the Far-UV CD. This data suggests that the proteins contain the backbone conformation necessary for β -sheet indication by CD. On the other hand, upon assessment of the optical properties of these proteins, it was observed that the chromophore native to GFP did not form during the designed protein expression in *E. coli*. Absorbance measurements of the designed proteins produced only a peak at 280 nm, corresponding to the aromatic absorbance, with no peak observed for the chromophore. Fluorescence measurements of these proteins with excitation at 482 nm and emission at 510 nm did not produce fluorescence signal. This result is likely due to decreased tertiary packing so that the initial cyclization step of the chromophore formation could not occur. The necessary distance between the amide nitrogen of G67 and the S65 carbonyl carbon has been shown to be $\sim 3 \text{ \AA}$, with increasing distances observed concurrent with less fluorescent protein (141). Small rearrangements of the sidechains induced by repulsion of the negative charges of the binding site could lengthen the distance between the amide nitrogen and the carbonyl carbon, resulting in no chromophore formation. Examination of the partial sites of the designed calcium binding variants suggests that

the mutations V120N and K79D are fatal to chromophore formation. These two mutations made alone in EGFP cause complete fluorescence loss.

Measurement of the pK_a of EGFP and the variants L15N and L194N by absorbance and fluorescence were performed. EGFP exhibits an average pK_a of 5.99 by absorbance and of 5.69 by fluorescence at 510 nm for excitation at both 398 nm and 582 nm. The pK_a at 450 nm was 6.11 for EGFP, which differs from the other pK_a values, likely due to excited state proton transfer of the neutral form of the chromophore. L15N exhibits an average pK_a by absorbance of 5.87 and of 5.65 by fluorescence with emission at 510 nm for both 398 nm excitation and 482 nm excitation. L15N exhibits a pK_a of 6.10 for the 450 nm emission, again not the same as emission at 510 nm for likely the same reason as EGFP. L194N exhibits a pK_a of 5.83 for emission at 510 nm with excitation at 482 nm. These pK_a values are very close and little difference is observed for the two mutants when compared to EGFP.

The quantum yields of EGFP, L15N, and L194N were also measured in this laboratory by examination of several concentrations of protein with both absorbance and fluorescence. EGFP exhibits a quantum yield of 0.603. L15N and L194N exhibit slightly lowered quantum yields of 0.44 and 0.43, respectively. The two mutations cause some reduction in the quantum yield of the chromophore but not so much as to be detrimental to measurements of the proteins.

7.2 Expression of Designed Proteins in Mammalian Cells

The designed proteins that were not fluorescent when expressed in bacteria were tested in mammalian cells to observe if the folding machinery of the mammalian

cells could allow for chromophore formation. Sites 120 and 194a were not fluorescent when expressed in HeLa or CHO cells. Site 177 exhibited fluorescence when expressed in HeLa, CHO, Vero, and HEK293 cells. This outcome suggests that chromophore formation of GFP variants is dependent upon the cellular protein synthesis machinery, but, also, that particular mutations lead to fluorescence loss. The mutations V120N and K79D disrupt chromophore formation, even in mammalian cells.

Further modification of Site 177 by addition of the cycle 3 mutations (F99S, M153T, V163A) increased the brightness of the protein when expressed at 30 °C and indicated weak fluorescence when expressed at 37 °C. These mutations were also added to site 120 and 194a, but fluorescence was not observed. Coupled with Zimmer's observations on the distance changes caused by the cycle 3 mutations, it is apparent that chromophore formation is dependent upon several factors, i.e. the distance between Gly67 and Ser65 and the folding trajectory of the protein. The increased fluorescence of 177c3 allows for shorter exposure times during imaging experiments and measurements of quick calcium response.

7.3 Major Findings from In Vivo Imaging of Calcium Response

Site 177 and 177c3 indicate calcium response when expressed in the cytosol of HeLa cells. Induced calcium concentration changes by addition of ionomycin and calcium to the bathing medium indicated an increase in fluorescence of 177 and 177c3 with decreases observed concomitant with reduction of calcium in the bathing medium. These results indicate that the designed proteins 177 and 177c3 are able to sense calcium changes in the cytosolic environment.

When the designed proteins 177 and 177c3 were targeted to the ER through the use of signal peptides, they were observed to colocalize in the ER with a purchased DsRed-ER construct. When calcium release was stimulated with addition of histamine and ATP, no release was apparent by measuring the fluorescence. This result could be due to three factors. The binding affinity measured by bacterially expressed protein may not be the same as the binding affinity for the protein expressed in HeLa cells. Since the tertiary structure of the protein is apparently better packed in HeLa cells, as observed by the chromophore formation, the binding site could be in a different conformation, which may change the binding affinity. In addition, the effect of calcium binding on the chromophore is related to the binding affinity but will not necessarily be in accordance with the K_d since it is a secondary process caused by a change in the chromophore environment. Considering the fluorescence increase observed when the cytosolic calcium concentration is raised, likely up to 10 μM , and the lack of fluorescence change in the ER observed when calcium is released, it is likely that the binding affinity for calcium is stronger than that measured from bacterially expressed protein. Modification of the binding site to weaken the affinity would likely result in an observable fluorescence change upon calcium release from the ER. The binding affinity of the protein expressed in HeLa cells will be measured before publication of this work. Also, the fluorescence of 177 is quite weak when expressed in the ER due to the reduced volume and possibly the environment. For this reason, the sensing ability of the protein may be reduced since this protein decreases in fluorescence when calcium is removed and measuring a decrease in an already weak signal is difficult.

7.4 Major Findings of the Second Generation of Designed Proteins

In the second generation, one full site was observed to maintain fluorescence after all mutations were made, Site 1 with mutations L194E, S86D, and S2D. The other 5 sites in the design included aggressive mutations that likely disrupted the tertiary structure of the protein. For Site 2, the combination of the mutations results in fluorescence loss although each of the individual mutations does not. The introduction of the clustered negative charges likely is the cause. For sites 3 and 4, the mutations of Ile and Phe to Asp or Glu possibly cause the fluorescence loss. For sites 5 and 6, the L7D and V12N mutations were fluorescent, but the addition of F114D and L119E resulted in no fluorescence. This could be due to the incorporation of clustered negative charges and/or the mutation of Phe to Asp. Since Sites 2-6 were not fluorescent, they were not pursued as calcium sensors.

Inclusion of the mutations M153T and V163A in the Site 1 construct allowed for expression of the protein at 37 °C in HeLa cells with bright fluorescence observed. In addition, Site 1-M153T/V163A was expressed in bacteria with fluorescence observed. Measurement of the calcium affinity of this construct through in vitro fluorescence changes of the chromophore upon calcium addition produced a K_d of 107 μM . Dye competition measurements of the intrinsic binding affinity of Site 1-M153T/V163A yielded a K_d of 100 μM , which is in good agreement with the chromophore fluorescence binding affinity. This protein will likely prove to be a useful sensor.

7.5 Major Findings of the *in Vivo* Calcium Measurements of Site 1

Site 1 exhibits calcium response when expressed in the cytosol of HeLa cells with an increase in fluorescence that is removed when calcium is removed from the bathing medium. When Site 1 was targeted to the ER, it was observed to colocalize with the purchased DsRed-ER. Calcium release caused by addition of larger concentrations of ionomycin to permeate the ER membrane resulted in a 20% fluorescence decrease, indicating that this designed protein responds to calcium release from the ER. Addition of calcium to the bathing medium to force the ER to reuptake calcium resulted in fluorescence increase 25% greater than the resting fluorescence for a total of approximately 56% from calcium free to calcium loaded. This large change in fluorescence from calcium free to calcium loaded suggests that the binding affinity for Site 1 is quite different than that for 177. When calcium is released from the ER, the equilibrium of the protein-calcium binding shifts to free protein if the K_d is weak enough. A stronger binding affinity shifts the equilibrium more to the metal-protein complex so that removal of free metal would not greatly affect the fluorescence. Possibly Site 177 has a stronger binding affinity than Site 1 so that ER calcium changes can not be observed because 177 does not release calcium as readily as Site 1. The cytosolic fluorescence response observed by these two sensors, with calcium concentration of 10-20 μM , is still in the observable range of these sensors if the binding affinities are low micromolar to 100 μM . The binding affinity of Site 1 will be measured from bacterially expressed and HeLa expressed protein before this work is published in a journal.

References

1. Clapham, D. E. (1995) *Cell* 80, 259-268.
2. Carafoli, E., and Penniston, J. T. (1985) *Sci Am* 253, 70-8.
3. Murakami, K., Yumoto, F., Ohki, S. Y., Yasunaga, T., Tanokura, M., and Wakabayashi, T. (2005) *J Mol Biol* 352, 178-201.
4. Barnes, S., and Kelly, M. E. (2002) *Adv Exp Med Biol* 514, 465-76.
5. Palczewski, K., Verlinde, C. L., and Haeseleer, F. (1999) *Novartis Found Symp* 224, 191-204; discussion 204-7.
6. Konur, S., and Ghosh, A. (2005) *Neuron* 46, 401-5.
7. Rakhilin, S. V., Olson, P. A., Nishi, A., Starkova, N. N., Fienberg, A. A., Nairn, A. C., Surmeier, D. J., and Greengard, P. (2004) *Science* 306, 698-701.
8. Bootman, M. D., and Berridge, M. J. (1995) *Cell* 83, 675-8.
9. Berridge, M. J. (1994) *Mol Cell Endocrinol* 98, 119-24.
10. Gunter, T. E., Yule, D. I., Gunter, K. K., Eliseev, R. A., and Salter, J. D. (2004) *FEBS Lett* 567, 96-102.
11. Malviya, A. N., and Rogue, P. J. (1998) *Cell* 92, 17-23.
12. Duchen, M. R. (2000) *J Physiol* 529 Pt 1, 57-68.
13. Kohlmeier, L., Gasner, C., and Marcus, R. (1993) *American Journal of Medicine* 95, 568-572.
14. Sigel, H. (1984) in *Calcium and Its Biological Role* (Sigel, H., Ed.), Marcel Dekker, Inc., New York.

15. Louis, C. F., Balog, E. M., and Fruen, B. R. (2001) *Biosci Rep* 21, 155-68.
16. Balog, E. M., Fruen, B. R., Shomer, N. H., and Louis, C. F. (2001) *Biophys J* 81, 2050-8.
17. Zhao, F., Li, P., Chen, S. R., Louis, C. F., and Fruen, B. R. (2001) *J Biol Chem* 276, 13810-6.
18. Mickelson, J. R., and Louis, C. F. (1996) *Physiol Rev* 76, 537-92.
19. Shomer, N. H., Mickelson, J. R., and Louis, C. F. (1995) *Muscle Nerve* 18, 1167-76.
20. Kretsinger, R. H., Rudnick, S. E., and Weissman, L. J. (1986) *J Inorg Biochem* 28, 289-302.
21. Vinogradova, M. V., Reddy, V. S., Reddy, A. S., Sablin, E. P., and Fletterick, R. J. (2004) *J Biol Chem* 279, 23504-9.
22. Chou, J. J., Li, S., Klee, C. B., and Bax, A. (2001) *Nat Struct Biol* 8, 990-7.
23. Fajmut, A., Brumen, M., and Schuster, S. (2005) *FEBS Lett* 579, 4361-6.
24. Taylor, C. W., and Laude, A. J. (2002) *Cell Calcium* 32, 321-34.
25. Kahl, C. R., and Means, A. R. (2003) *Endocr Rev* 24, 719-36.
26. Herzberg, O., Moulton, J., and James, M. N. (1986) *Ciba Found Symp* 122, 120-44.
27. Heim, N., and Griesbeck, O. (2004) *J Biol Chem* 279, 14280-6.
28. Menaldino, D. S., Bushnev, A., Sun, A., Liotta, D. C., Symolon, H., Desai, K., Dillehay, D. L., Peng, Q., Wang, E., Allegood, J., Trotman-Pruett, S., Sullards, M. C., and Merrill, A. H., Jr. (2003) *Pharmacol Res* 47, 373-81.

29. Merrill, A. H., Jr., Schmelz, E. M., Dillehay, D. L., Spiegel, S., Shayman, J. A., Schroeder, J. J., Riley, R. T., Voss, K. A., and Wang, E. (1997) *Toxicol Appl Pharmacol* 142, 208-25.
30. Hofer, A. M. (2001) in *Calcium Signalling* (Tepikin, A. V., Ed.) pp 111-123, Oxford University Press, Oxford.
31. Probes, M. (2005), Molecular Probes.
32. Richard P. Haugland, P. D. (1996), Molecular Probes, Inc., Eugene.
33. Richard P. Haugland, P. D. (2001), Molecular Probes, Inc., Eugene.
34. Takita, M., Puka-Sundvall, M., Miyakawa, A., and Hagberg, H. (2004) *Neurosci Res* 48, 169-73.
35. Rusakov, D. A., and Fine, A. (2003) *Neuron* 37, 287-97.
36. Landolfi, B., Curci, S., Debellis, L., Pozzan, T., and Hofer, A. M. (1998) *J Cell Biol* 142, 1235-43.
37. Wang, Z., Tymianski, M., Jones, O. T., and Nedergaard, M. (1997) *J Neurosci* 17, 7359-71.
38. Inouye, S. (2001) *Tanpakushitsu Kakusan Koso* 46, 220-7.
39. Robert, V., Pinton, P., Tosello, V., Rizzuto, R., and Pozzan, T. (2000) *Methods Enzymol* 327, 440-56.
40. Missiaen, L., Van Acker, K., Van Baelen, K., Raeymaekers, L., Wuytack, F., Parys, J. B., De Smedt, H., Vanoevelen, J., Dode, L., Rizzuto, R., and Callewaert, G. (2004) *Cell Calcium* 36, 479-87.

41. George, S. E., Schaeffer, M. T., Cully, D., Beer, M. S., and McAllister, G. (2000) *Anal Biochem* 286, 231-7.
42. Torrecilla, I., Leganes, F., Bonilla, I., and Fernandez-Pinas, F. (2000) *Plant Physiol* 123, 161-76.
43. Tepikin, A. (2001), Oxford University Press, New York.
44. Magalhaes, P. J., Pinton, P., Filippin, L., and Pozzan, T. (2001) in *Calcium Signalling* (Tepikin, A., Ed.), Oxford University Press, Oxford.
45. Stables, J., Mattheakis, L. C., Chang, R., and Rees, S. (2000) *Methods Enzymol* 327, 456-71.
46. Persechini, A. (2002) *Methods Mol Biol* 173, 365-82.
47. Romoser, V. A., Hinkle, P. M., and Persechini, A. (1997) *J Biol Chem* 272, 13270-4.
48. Persechini, A., Lynch, J. A., and Romoser, V. A. (1997) *Cell Calcium* 22, 209-16.
49. Delano, W. L. (2002), Delano Scientific, San Carlos, CA.
50. Miyawaki, A., Llopis, J., Heim, R., McCaffery, J. M., Adams, J. A., Ikura, M., and Tsien, R. Y. (1997) *Nature* 388, 882-7.
51. Baird, G. S., Zacharias, D. A., and Tsien, R. Y. (1999) *Proc Natl Acad Sci U S A* 96, 11241-6.
52. Miyawaki, A., Griesbeck, O., Heim, R., and Tsien, R. Y. (1999) *Proc Natl Acad Sci U S A* 96, 2135-40.
53. Allen, G. J., Kwak, J. M., Chu, S. P., Llopis, J., Tsien, R. Y., Harper, J. F., and Schroeder, J. I. (1999) *Plant J* 19, 735-47.

54. Nagai, T., Sawano, A., Park, E. S., and Miyawaki, A. (2001) *Proc Natl Acad Sci U S A* 98, 3197-202.
55. Kaprielian, R., del Monte, F., and Hajjar, R. J. (2002) *Basic Res Cardiol* 97 Suppl 1, I136-45.
56. Pogwizd, S. M., and Bers, D. M. (2002) *Ann N Y Acad Sci* 976, 454-65.
57. Pieske, B., Maier, L. S., and Schmidt-Schweda, S. (2002) *Basic Res Cardiol* 97 Suppl 1, I63-71.
58. Hempel, P., Hoch, B., Bartel, S., and Karczewski, P. (2002) *Basic Res Cardiol* 97 Suppl 1, I96-101.
59. Schuhmeier, R. P., Dietze, B., Ursu, D., Lehmann-Horn, F., and Melzer, W. (2003) *Biophys J* 84, 1065-78.
60. Linse, S., and Forsen, S. (1995) *Adv Second Messenger Phosphoprotein Res* 30, 89-151.
61. Forsen, S., Linse, S., Thulin, E., Lindegard, B., Martin, S. R., Bayley, P. M., Brodin, P., and Grundstrom, T. (1988) *Eur J Biochem* 177, 47-52.
62. Palmer, A. E., Jin, C., Reed, J. C., and Tsien, R. Y. (2004) *Proc Natl Acad Sci U S A* 101, 17404-9.
63. Tsien, R. Y. (1998) *Annual Review of Biochemistry* 67, 509-544.
64. Yang, F., Moss, L. G., and G. N. Phillips, J. (1996) *Nat. Biotechnol.* 14, 1246-1251.
65. Remington, S. J. (2000) *Methods Enzymol* 305, 196-211.

66. Baird, G. S., Zacharias, D. A., and Tsien, R. Y. (1999) *Proceedings of the National Academy of Science* 96, 11241-11246.
67. Angelis, D. A. D., Miesenbock, G., Zemelman, B. V., and Rothman, J. E. (1998) *Proceeding of the National Academy of Science* 95, 12312-12316.
68. Richmond, T. A., Takahashi, T. T., Shimkhada, R., and Bernsdorf, J. (2000) *Biochemical and Biophysical Research Communications* 268, 462-465.
69. Jensen, K. K., Martini, L., and Schwartz, T. W. (2001) *Biochemistry* 40, 938-945.
70. Miyawaki, A., Griesbeck, O., Heim, R., and Tsien, R. Y. (1999) *Proc. Natl. Aca. Sci.* 96, 2135-2140.
71. Liao, B., Paschal, B. M., and Luby-Phelps, K. (1999) *Proc. Natl. Acad. Sci.* 96, 6217-6222.
72. Nagai, T., Sawano, A., Park, E. S., and Miyawaki, A. (2001) *Proc. Natl. Acad. Sci.* 98, 3197-3202.
73. Bajorath, J., Hinrichs, W., and Saenger, W. (1988) *Eur J Biochem* 176, 441-7.
74. McPhalen, C. A., Strynadka, N. C., and James, M. N. (1991) *Adv Protein Chem* 42, 77-144.
75. Kretsinger, R. H. (1976) *Int Rev Cytol* 46, 323-93.
76. Kretsinger, R. H. (1976) *Annu Rev Biochem* 45, 239-66.
77. Kawasaki, H., and Kretsinger, R. H. (1995) *Protein Profile* 2, 297-490.
78. Kawasaki, H., and Kretsinger, R. H. (1994) *Protein Profile* 1, 343-517.
79. Babu, Y. S., Sack, J. S., Greenhough, T. J., Bugg, C. E., Means, A. R., and Cook, W. J. (1985) *Nature* 315, 37-40.

80. Swain, A. L., Kretsinger, R. H., and Amma, E. L. (1989) *J Biol Chem* 264, 16620-8.
81. Nagar, B., Overduin, M., Ikura, M., and Rini, J. M. (1996) *Nature* 380, 360-4.
82. Linse, S., Johansson, C., Brodin, P., Grundstrom, T., Drakenberg, T., and Forsen, S. (1991) *Biochemistry* 30, 154-62.
83. Linse, S., Brodin, P., Johansson, C., Thulin, E., Grundstrom, T., and Forsen, S. (1988) *Nature* 335, 651-2.
84. Ye, Y., Lee, H. W., Yang, W., and Yang, J. J. (2005) *J Inorg Biochem* 99, 1376-83.
85. Ye, Y., Lee, H. W., Yang, W., Shealy, S., and Yang, J. J. (2005) *J Am Chem Soc* 127, 3743-50.
86. Yang, W., Wilkins, A. L., Ye, Y., Liu, Z. R., Li, S. Y., Urbauer, J. L., Hellinga, H. W., Kearney, A., van der Merwe, P. A., and Yang, J. J. (2005) *J Am Chem Soc* 127, 2085-93.
87. Yang, W., Jones, L. M., Isley, L., Ye, Y., Lee, H. W., Wilkins, A., Liu, Z. R., Hellinga, H. W., Malchow, R., Ghazi, M., and Yang, J. J. (2003) *J Am Chem Soc* 125, 6165-71.
88. Wilkins, A. L., Ye, Y., Yang, W., Lee, H. W., Liu, Z. R., and Yang, J. J. (2002) *Protein Eng* 15, 571-4.
89. Yang, W., Lee, H. W., Hellinga, H., and Yang, J. J. (2002) *Proteins* 47, 344-56.
90. Minta, A., and Tsien, R. Y. (1989) *The Journal of Biological Chemistry* 264, 19449-19457.

91. Harootunian, A. T., Kao, J. P. Y., Eckert, B. K., and Tsien, R. Y. (1989) *The Journal of Biological Chemistry* 264, 19458-19467.
92. Gryniewicz, G., Poenie, M., and Tsien, R. Y. (1985) *Journal of Biological Chemistry* 260, 3440-3450.
93. Kawanishi, T., Blank, L. M., Harootunian, A. T., Smith, M. T., and Tsien, R. Y. (1989) *Journal of Biological Chemistry* 264, 12859-12866.
94. Ozmen, B., and Akkaya, E. U. (2000) *Tetrahedron Letters* 41, 9185-9188.
95. Akkaya, E. U., and Turkyilmaz, S. (1997) *Tetrahedron Letters* 38, 4513-4516.
96. Liu, Y., Zhang, H.-Y., Bai, Z.-P., Wada, T., and Inoue, Y. (2000) *Journal of Organic Chemistry* 65, 7105-7109.
97. Nakatsuji, Y., Nakamura, T., Yonetani, M., Yuya, H., and Okahara, M. (1988) *Journal of the American Chemical Society* 110, 531-538.
98. Barbour, L. J., Wall, S. L. D., Meadows, E. S., and Gokel, G. W. (2000) *Industrial and Engineering Chemistry Research* 39, 3436-3441.
99. Wong, A., and Wu, G. (2000) *The Journal of Physical Chemistry A* Web, A-I.
100. Pederson, C. J. (1967) *Journal of the American Chemical Society* 89, 7017-7036.
101. Erk, C. (2000) *Industrial and Engineering Chemistry Research* 39, 3582-3588.
102. Hay, B. P., and Rustad, J. R. (1994) *Journal of the American Chemical Society* 116, 6316-6326.
103. Boulatov, R., Du, B., Meyers, E. A., and Shore, S. G. (1999) *Inorganic Chemistry* 1999, 4554-4558.

104. Feller, D., Thompson, M. A., and Kendall, R. A. (1997) *Journal of Physical Chemistry* 101, 7292-7298.
105. Erk, C., and Gocmen, A. (2000) *Talanta* 53, 137-140.
106. Atwood, J. L., and Junk, P. C. (2000) *Polyhedron* 19, 85-91.
107. Bradshaw, J. S., and Izatt, R. M. (1997) *Accounts of Chemical Research* 30, 338-345.
108. Prodi, L., Bolletta, F., Montalti, M., Zaccheroni, M., Savage, P. B., Bradshaw, J. S., and Izatt, R. M. (1998) *Tetrahedron Letters* 39, 5451-5454.
109. Bordunov, A. B., Bradshaw, J. S., Zhang, X. X., Dalley, N. K., Kou, X., and Izatt, R. M. (1996) *Inorganic Chemistry* 35, 7229-7240.
110. Strekowski, L., Lipowska, M., and Patonay, G. (1992) *Journal of Organic Chemistry* 57, 4578-4580.
111. Gorecki, T., Patonay, G., Strekowski, L., Chin, R., and Salazar, N. (1996) *Journal of Heterocyclic Chemistry* 33, 1871-1876.
112. Yang, W., Tsai, T., Kats, M., and Yang, J. J. (2000) *Journal of Peptide Research* 55, 203-215.
113. Bagshaw, C. R., and Harris, D. A. (1987) (Bagshaw, C. R., and Harris, D. A., Eds.) pp 91-113, IRL Press, Washington.
114. Lipowska, M., Patterson, S. E., Patonay, G., and Strekowski, L. (1993) *Journal of Heterocyclic Chemistry* 30, 1177-1180.
115. Valet, G., Raffael, A., and Russmann, L. (1985) *Naturwissenschaften* 72, 600-602.

116. Murphy, E., Freudenrich, C. C., Levy, L. A., London, R. E., and Lieberman, M. (1989) *Proceedings of the National Academy of Science* 86, 2981-2984.
117. Scheenen, W. J. J. M., Makings, L. T., Gross, L. R., Pozzan, T., and Tsien, R. Y. (1996) *Chemistry & Biology* 3, 765-774.
118. Strekowski, L., Lipowska, M., Gorecki, T., Mason, J. C., and Patonay, G. (1996) *Journal of Heterocyclic Chemistry* 33, 1685-1688.
119. Linse, S., and Forsen, S. (1995) *Adv Second Messenger Phosphoprotein Res* 30, 89-151.
120. Falke, J. J., Drake, S. K., Hazard, A. L., and Peersen, O. B. (1994) *Q. Rev. Biophys.* 27, 219-90.
121. Battistutta, R., Negro, A., and Zanotti, G. (2000) *Proteins* 41, 429-37.
122. Palm, G. J., Zdanov, A., Gaitanaris, G. A., Stauber, R., Pavlakis, G. N., and Wlodawer, A. (1997) *Nat Struct Biol* 4, 361-5.
123. Yang, F., Moss, L. G., and Phillips, G. N., Jr. (1996) *Nat Biotechnol* 14, 1246-51.
124. Zhu, H., Oezguen, N., Soman, K., Fraczekiewicz, R., and Braun, W. (1996).
125. King, J., and Betts, S. (1999) *Nat Biotechnol* 17, 637-8.
126. Waldo, G. S., Standish, B. M., Berendzen, J., and Terwilliger, T. C. (1999) *Nat Biotechnol* 17, 691-5.
127. Suzuki, M., Ito, Y., Savage, H. E., Husimi, Y., and Douglas, K. T. (2004) *Biochim Biophys Acta* 1679, 222-9.
128. Mohanty, A. K., and Wiener, M. C. (2004) *Protein. Expr. Purif.* 33, 311-25.

129. Spiga, O., Scarselli, M., Bernini, A., Ciutti, A., Giovannoni, L., Laschi, F., Bracci, L., and Niccolai, N. (2002) *Biophys. Chem.* 97, 79-86.
130. Ghanem, M., and Gadda, G. (2005) *Biochemistry* 44, 893-904.
131. Hanson, G. T., McAnaney, T. B., Park, E. S., Rendell, M. E., Yarbrough, D. K., Chu, S., Xi, L., Boxer, S. G., Montrose, M. H., and Remington, S. J. (2002) *Biochemistry* 41, 15477-88.
132. McAnaney, T. B., Park, E. S., Hanson, G. T., Remington, S. J., and Boxer, S. G. (2002) *Biochemistry* 41, 15489-94.
133. McAnaney, T. B., Shi, X., Abbyad, P., Jung, H., Remington, S. J., and Boxer, S. G. (2005) *Biochemistry* 44, 8701-11.
134. Jain, R. K., Joyce, P. B., Molinete, M., Halban, P. A., and Gorr, S. U. (2001) *Biochem J* 360, 645-9.
135. Ostergaard, H., Henriksen, A., Hansen, F. G., and Winther, J. R. (2001) *Embo J* 20, 5853-62.
136. Sacchetti, A., Cappetti, V., Marra, P., Dell'Arciprete, R., El Sewedy, T., Crescenzi, C., and Alberti, S. (2001) *J Cell Biochem* 81, 117-128.
137. Sakikawa, C., Taguchi, H., Makino, Y., and Yoshida, M. (1999) *J Biol Chem* 274, 21251-6.
138. Foecking, M. K., and Hofstetter, H. (1986) *Gene* 45, 101-5.
139. Vessoni Penna, T. C., and Ishii, M. (2002) *BMC Biotechnol* 2, 7.
140. Vessoni Penna, T. C., Ishii, M., Cholewa, O., and de Souza, L. C. (2004) *Lett Appl Microbiol* 38, 135-9.

141. Baffour-Awuah, N. Y., Fedeles, F., and Zimmer, M. (2005) *Chemical Physics* 310, 25-31.
142. Churchill, G. C., Lurtz, M. M., and Louis, C. F. (2001) *Am J Physiol Cell Physiol* 281, C972-81.
143. Lurtz, M. M., and Louis, C. F. (2003) *Am J Physiol Cell Physiol* 285, C1475-82.
144. Zou, J., Ye, Y., Welshhans, K., Lurtz, M., Ellis, A. L., Louis, C., Rehder, V., and Yang, J. J. (2005) *J Biotechnol* 119, 368-78.